NONLINEAR FINITE ELEMENT TREATMENT OF BIFURCATION IN THE POST-BUCKLING ANALYSIS OF THIN ELASTIC PLATES AND SHELLS

A Thesis Submitted for the Degree of Doctor of Philosophy

by

Tim Richard Bangemann

Department of Mathematics & Statistics, Brunel University

April 1995

Acknowledgements

I would like to express my deepest gratitude to Professor L. S. D. Morley FRS for introducing me into and teaching me about the field of finite elements and its engineering applications. Many thanks for the superb guidance, continuous encouragement and optimistic attitude which I enjoyed throughout the course of research work as well as the huge amount of freedom I was given in order to lead it to a successful completion.

My deep appreciation is directed to Professor J. R. Whiteman for making all necessary arrangements for the completion of this thesis.

Special acknowledgements are directed to Dr D. J. Allman of the Defence Research Agency in his role as a technical co-ordinator and for the interesting discussions and his helpful co-operation.

Thanks to Dr M. K. Warby and Dr S. Shaw as well as other colleagues at BICOM for the time, companionship and help they have given me.

Also, I would like to thank Dr N. Herrmann from the University of Hanover for enabling my trip to the UK in the first place and Dr S. A. Matar for giving me the idea and convincing me to do a PhD.

A thousand thanks for the support I have received from Jack, Michael, Giovanni and other friends over the last few years. A special thank you goes to Roshi.

A simple thank you is not sufficient for expressing my gratitude towards my family who always stood behind me and without whose support it would never have been possible for me to accomplish this work.

The Procurement Executive of the Ministry of Defence under Strategic Research Programme AS011D02 is specially acknowledged for providing the financial support.

Abstract

The geometrically nonlinear constant moment triangle based on the von Kármán theory of thin plates is first described. This finite element, which is believed to be the simplest possible element to pass the totality of the von Kármán patch test, is employed throughout the present work. It possesses the special characteristic of providing a tangent stiffness matrix which is accurate and without approximation.

The stability of equilibrium of discrete conservative systems is discussed. The criteria which identify the critical points (limit and bifurcation), and the method of determination of the stability coefficients are presented in a simple matrix formulation which is suitable for computation. An alternative formulation which makes direct use of higher order directional derivatives of the total potential energy is also presented.

Continuation along the stable equilibrium solution path is achieved by using a recently developed Newton method specially modified so that stable points are points of attraction. In conjunction with this solution technique, a branch switching method is introduced which directly computes any intersecting branches. Bifurcational buckling often exhibits huge structural changes and it is believed that the computation of the required switch procedure is performed here, and for the first time, in a satisfactory manner. Hence, both limit *and* bifurcation points can be treated without difficulty and with continuation into the post buckling regime. In this way, the ability to compute the stable equilibrium path throughout the load - deformation history is accomplished.

Two numerical examples which exhibit bifurcational buckling are treated in detail and provide numerical evidence as to the ability of the employed techniques to handle even the most complex problems. Although only relatively coarse finite element meshes are used it is evident that the technique provides a powerful tool for any kind of thin elastic plate and shell problem.

The thesis concludes with a proposal for an algorithm to automate the computation of the unknown parameter in the branch switching method.

Contents

Chapter 1

Introduction

1.1 Background and motivation

Many problems in engineering are concerned with the calculation of stresses and displacements in thin elastic plates and shells which are flat and curved structures, respectively, for which the thicknesses are much smaller than the remaining dimensions.

These kinds of thin-walled structural components are used *e.g.* in high-performance flight-vehicle structures and pose difficult problems for the structural analyst. In many applications, service loads cause the structure to operate in the geometrically nonlinear regime, and even when load levels vary slowly, dynamic events such as snap-through or buckling can occur.

Hence, there are situations where nonlinear effects must be incorporated for a realistic assessment of structural response. In general, it is possible to identify five areas where nonlinear stress analysis may be necessary, *c.f.* Hinton [He92]:

1. direct use in *design* for both ultimate load and serviceability limit states (high technology industry requires high performance and efficient components, *e.g.* in aerospace, automobile or nuclear industries);

2. use in the *assessment of existing structures* whose integrity may be in doubt due to visible damage (cracking etc), special loadings not envisaged at the design state or concern over corrosion or general ageing;

3. use to help to *establish the causes of a structural failure*;

4. use in *research* to help establish simple 'code-based' methods of analysis and design, to help understand basic structural behaviour and to test the validity of proposed 'material models';

5. use in the *simulation of materials processing and manufacturing*, *e.g.* metal forming, glass forming and casting process.

Note that in the present work nonlinearity always means geometrical nonlinearity; material nonlinearities are not discussed.

Analytical solutions for nonlinear problems are scarcely obtainable and are restricted to essentially one-dimensional problems. Thus, the need to develop approximating numerical techniques in order to solve the governing differential equations becomes imperative. The *Rayleigh-Ritz energy method* and the *finite difference method* were the first methods to be employed for this purpose but since the advent of powerful computers, the solution cost is no longer such an obstacle and the *finite element method* has overshadowed all other approximating numerical methods for the solution of nonlinear thin plate and shell problems.

Modern finite element methods of computational structural mechanics employ discrete idealizations, based on appropriate physical laws, to characterize real continuous systems for numerical calculation. In particular, a discrete system for the prediction of the static equilibrium paths of elastic structures under varying loads is generally derived using the principle of conservation of energy. The behaviour of such a system is governed by nonlinear equilibrium equations, formulated in terms of the nodal finite element variables, with an imbedded parameter corresponding to a physical quantity such as the intensity of the applied loading. Solutions of these equations, for varying values of the parameter, represent points on the static equilibrium paths of a discrete system.

While a rigorous analysis of the complex phenomena of nonlinear thin plate and shell problems must account for dynamic effects, the desire to apply existing static analysis methods to general structural configurations has led to the development of techniques for following equilibrium solution paths past critical stability points and through regimes of unstable equilibrium. A number of these techniques are discussed

by Riks [Rik84a]. By tracing equilibrium solution paths through regimes of stable and unstable equilibrium, a qualitative understanding of transient dynamic events can often be obtained.

Now it is well known that points of stable equilibrium paths of a conservative system are the local minima of a continuously differentiable potential energy function; other stationary points correspond to states of unstable equilibrium. The transition from stable to unstable equilibrium occurs at a singular point where the Hessian matrix of second derivatives of the potential energy has a zero eigenvalue. These points signify bifurcation or limit point behaviour of an equilibrium path, and this has important implications for the subsequent physical behaviour of a system. An essential requirement of a satisfactory solution technique, therefore, is to locate and identify singular points on a stable equilibrium path.

A very extensive literature on the numerical solution of nonlinear equations with singular points is available in mathematical publications, as shown by the reviews of Mittelmann and Weber [MW80], Allgower [All81] and Allgower and Georg [AG92]. But numerical methods for nonlinear problems in engineering applications have developed independently. In the field of structural mechanics a common approach for calculating solution paths of nonlinear equilibrium equations has evidently evolved, *cf.* Riks [Rik79], [Rik84a], Crisfield [Cri91] and Hinton [He92]. The system of equations is augmented by an extra equation incorporating a new parameter, usually taken as an approximation to the arc length of the solution path; the original natural parameter of the equations is treated as an unknown variable to be determined. At limit points this procedure leads to an augmented set of equations whose Hessian matrix is nonsingular and so the standard Newton-Raphson method may be used to calculate local solution points. The Hessian matrix of the augmented equations used in the arc length method remains singular at bifurcation points, however, and difficulties of convergence then arise in the numerical solution of the equations. Special techniques for accurate location of limit points and bifurcation points are, hence, of great importance.

1.2 Aims and objectives

Keeping all the above in mind and being aware of the problems one can encounter by employing the standard Newton-Raphson method - convergence is often very slow or the method fails due to numerical errors in computation - a basic methodology is now sought for efficient calculation of the stable equilibrium paths of discrete conservative systems with singular points. A first step in this direction has been made by Allman [All89a]. In his paper, the governing system of nonlinear equations is not augmented by an extra equation, as in the popular arc length method, so that intrinsic properties of symmetry or bandedness of the associated Hessian matrix may be readily exploited in a numerical solution. Points on stable equilibrium paths are located reliably by a generalization of Newton's method, *cf.* Allman [All84], which converges only to minima in applications to find stationary points of a function of several variables; stable equilibrium paths are therefore preferentially followed. This simulates the behaviour of a real continuous system, with a varying natural parameter such as an applied load, where unstable equilibrium states are unattainable.

As discussed earlier, most finite element codes are capable of computing nonlinear deformation paths as long as the path is sufficiently smooth. In case of bifurcations, however, there are difficulties in the direct computation of intersecting branches. The reason for this is that, although the underlying theory is reasonably well established, the switch procedures which enable these computations have not yet been implemented into the finite element codes in a satisfactory manner.

Therefore, the general objective is to provide a careful finite element implementation of the works by Koiter [Koi45] and Allman [All84] , [All89b] , [All89a] by following the stable equilibrium path throughout the load-deformation history, *i.e.* to be able to perform the following four steps with repetition:

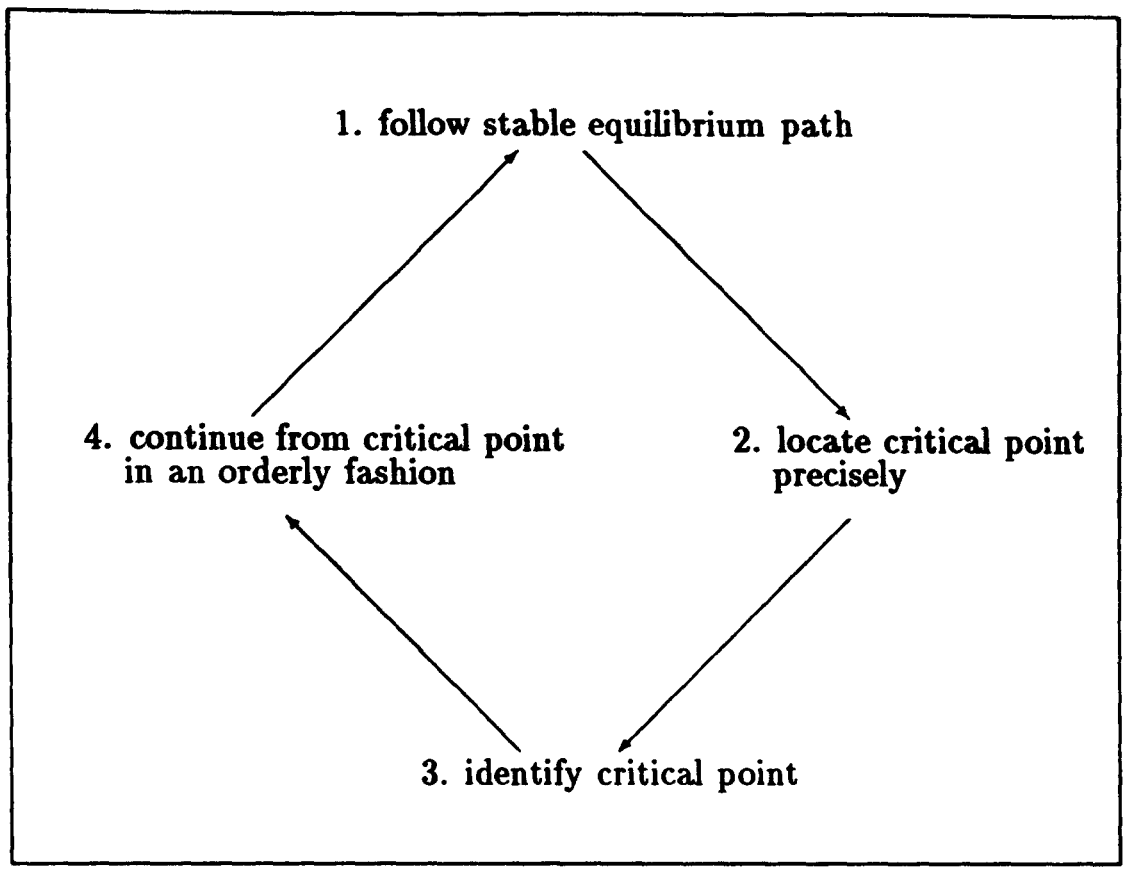

The emphasis in the present work is given to the continuation from bifurcation points since no generally valid method has been developed for this. Limit points can be handled without difficulty by employing the arc length technique as mentioned earlier.

1.3 Strategy

In order to make it feasible to follow the above mentioned steps, use is made of:

1. *Allman's solution technique*;
   this is the generalized Newton-Raphson method by Allman [All89a], as mentioned earlier, which is discussed in detail in Chapter 6.

2. *Adaptive step size criteria*;
   the critical point is located precisely with help of a step size adaption technique which decreases the step size whenever the tangent stiffness matrix is no longer positive definite.

3. *Rederivation of Koiter's work by Allman*;
   the rederivation of the classical criteria by Koiter [Koi45] in a computationally simple form is also due to Allman [All89b]. These criteria precisely define the

nature of the critical point, *i.e.* a clear distinction is made between a limit point, a symmetric bifurcation point and an asymmetric bifurcation point. Further criteria are available to assess the stability of equilibrium. Since then, Allman's work has been rewritten by Bangemann [Ban92] into a more convenient matrix form for computation which is presented in Chapter 5. The proper evaluation of critical points requires higher order derivatives of the potential energy function. Currently, this presents a formidable task since for most finite elements even the tangent stiffness matrix consisting of the second derivatives of the potential energy function is an approximation, *i.e.* there are serious doubts about the sensibility of even attempting to calculate higher derivatives.

4. *Development of the geometrically nonlinear constant moment triangle finite element by Morley*;
   the problem of calculating higher order derivatives of the potential energy function is overcome by making use of the *geometrically nonlinear constant moment triangle* finite element by Morley, *c.f.* [Mor91], which is discussed in more detail in Chapter 4. The triangle is based on the Hu-Washizu variational principle and has constant strains and constant moments within each element. It is a fundamental element which passes the von Kármán geometrically nonlinear patch test. Most importantly for the present work, the geometrically nonlinear constant moment triangle allows a ready and accurate calculation of all directional derivatives of the potential energy function and, thus, enables determining the type of critical points exactly.

5. *Branch switching method*;
   once the critical point has been identified, a branch switching method as presented in Chapter 6 can be employed to enable entering the post critical regime.

It should be mentioned here that the intention of the present work is not to derive the most accurate results for a particular problem or problems. Rather, the emphasis is on developing a methodology and the numerical examples are used to exhibit this.

For setting the scene, in Chapter 2 relevant plate and shell theories are discussed with the introduction of tensor notation. Of special interest here is the von Kármán nonlinear plate theory. The concept of practical components which enables the conversion of curvilinear tensor connectors into physically realistic orthogonal displacement components is made extensive use of in the current work and is therefore drawn attention to. The finite element method both in the linear and nonlinear theory is presented in Chapter 3 with a more detailed examination of the geometrically nonlinear constant moment triangle finite element, which is used throughout the thesis, following in Chapter 4. Chapter 5 investigates the stability of equilibrium of discrete conservative systems and provides a rewrite of Koiter's [Koi45] and Allman's [All89b] works in a convenient matrix form suitable for finite element computation whereby the stability of critical points is determined by so-called stability coefficients. An equivalent formulation for determining the stability coefficients is based on a report by Morley [Mor94] and makes direct use of higher order directional derivatives. The various calculations required are discussed in Chapter 6. Here, Allman's solution technique is described and some computational aspects such as *e.g.* step length adaption are considered. For the continuation from bifurcation points a branch switching method is presented which has been developed during the course of the current research work. This method has been applied successfully at bifurcation points in order to enter the post buckling regime on the stable equilibrium path. Numerical applications follow in Chapter 7 where two problems are examined in detail with concluding discussions: firstly, a square flat plate under uniaxial compression and, secondly, a cylindrical panel under biaxial compression. Chapter 8 concludes the thesis by summarizing the achievements of the present work and also gives some thought regarding future developments.

Chapter 2

Thin elastic shell and plate theories

2.1 Introduction

There exist many thin shell theories. Plates are shells with zero curvature and, therefore, plate theories can easily be derived from shell theories. Most of the shell theories are based on the well-known Love-Kirchhoff hypothesis which states that the entire deformation of the structure is described by the deformation of its middle surface. In this chapter, first equations regarding the geometry and deformation of the middle surface are looked at with the introduction of some basic concepts of tensor analysis. Then, Love's first approximation of the strain energy and Koiter's relevant results are given. Details are presented of Marguerre's theory for thin shallow shells and the von Kármán nonlinear theory for thin plates which is of special importance to the present work. Finally, the concept of practical components is introduced. With the help of this notation, curvilinear tensor connectors which are not immediately useful in engineering applications, are converted into physically realistic orthogonal displacement components. The presented thesis carries on from the work by Providas [Pro90] and, thus, makes use of the same theoretical background. Due to this, similarities to [Pro90] may be found.

2.2 Geometry of the undeformed middle surface

Let x^i , $i = 1,2,3$ describe a fixed, right-handed Cartesian coordinate system in three-dimensional space with $\mathbf{e}_i$ being the corresponding unit vectors. Also, consider ξ^α , $\alpha = 1,2$ to represent an arbitrary curvilinear coordinate system on the undeformed middle surface. Then the undeformed middle surface is completely described by the position vector

$$\mathbf{r} = x^i \mathbf{e}_i \ , \ x^i = x^i(\xi^\alpha) \ . \tag{2.2.1}$$

The base vectors which are tangent to the coordinate curves ξ^α are

$$\mathbf{r}_{,\alpha} = \frac{\partial \mathbf{r}}{\partial \xi^\alpha} \ . \tag{2.2.2}$$

The above summation convention which is employed throughout the current work makes use of the following:

- Latin indices have range 3 and the summation convention applies to repeated indices in any position;
- Greek indices have range 2 and the summation convention applies to repeated indices in mixed positions;
- Primed Greek indices have range $2'$ and the summation convention applies to repeated indices in any position.

Commas preceding a subscript indicate partial differentiation with respect to coordinates x^i or ξ^α, as specified at the time.

The distance between two neighbouring points is defined by

$$(ds)^2 = a_{\alpha\beta} \, d\xi^\alpha \, d\xi^\beta \tag{2.2.3}$$

with

$$a_{\alpha\beta} = \mathbf{r}_{,\alpha} \cdot \mathbf{r}_{,\beta} \tag{2.2.4}$$

being the covariant or first fundamental tensor of the undeformed middle surface. Here, the vector dot-product is applied in the usual way. The contravariant components of the metric tensor are defined by

$$a^{\alpha\lambda} \, a_{\lambda\beta} = \delta^\alpha_\beta \tag{2.2.5}$$

where δ^{α}_{β} is the Kronecker-delta. The normal vector n to the undeformed middle surface is

$$\mathbf{n} = \frac{1}{2}\,\varepsilon^{\alpha\beta}\,\mathbf{r}_{,\alpha} \times \mathbf{r}_{,\beta} \tag{2.2.6}$$

where $\times$ denotes the vector cross-product and the right-hand screw rule is employed. $\varepsilon_{\alpha\beta}$ and $\varepsilon^{\alpha\beta}$ are respectively the covariant and contravariant components of the two-dimensional permutation tensor where

$$\begin{aligned} \varepsilon_{11} = \varepsilon_{22} = \varepsilon^{11} = \varepsilon^{22} &= 0 \quad , \\ \varepsilon_{12} = -\varepsilon_{21} &= \sqrt{a} \quad , \\ \varepsilon^{12} = -\varepsilon^{21} &= \tfrac{1}{\sqrt{a}} \quad , \end{aligned} \tag{2.2.7}$$

and $a = |a_{\alpha\beta}|$ is the determinant of the metric tensor. The curvature or second fundamental tensor $b_{\alpha\beta}$ is defined by

$$b_{\alpha\beta} = -\,\mathbf{n} \cdot \mathbf{r}_{,\alpha\beta} \tag{2.2.8}$$

where the sign convention is adopted from Sanders [San63], *i.e.* giving positive curvature to a sphere when the surface normal n points outwards. Contravariant and mixed variant components of the symmetric tensor $b_{\alpha\beta}$ are then

$$\begin{aligned} b^{\alpha\beta} &= b_{\lambda\mu} a^{\lambda\alpha}\, a^{\mu\beta} \quad , \\ b^{\alpha}_{\beta} = b_{\lambda\beta}\, a^{\lambda\alpha} &= b^{\alpha\lambda}\, a_{\lambda\beta} \quad . \end{aligned} \tag{2.2.9}$$

These ways of raising or lowering indices are standard procedures in tensor theory. The invariant quantity, *i.e.* a quantity which remains invariant against coordinate transformations, related to $b_{\alpha\beta}$ is the Gaussian curvature

$$K = \frac{b}{a} = \frac{1}{2}\,(b^{\alpha}_{\alpha} b^{\lambda}_{\lambda} - b^{\alpha}_{\lambda} b^{\lambda}_{\alpha}) \tag{2.2.10}$$

where $b = |b_{\alpha\beta}|$ is the determinant of the curvature tensor.

The Christoffel symbols have proved useful in tensor analysis. The Christoffel symbols of the first and second kind are defined respectively by

$$\Gamma_{\alpha\beta\gamma} = \frac{1}{2}\,(\,a_{\beta\gamma,\alpha} + a_{\gamma\alpha,\beta} - a_{\alpha\beta,\gamma}\,) \tag{2.2.11}$$

and

$$\Gamma^{\gamma}_{\alpha\beta} = \Gamma_{\alpha\beta\lambda}\, a^{\lambda\gamma} \quad . \tag{2.2.12}$$

Christoffel symbols are used for covariant differentiation. It is prudent to note here that they do not form tensors. They are symmetric with respect to the first two subscripts and only the third index can be raised or lowered as with tensors.

Covariant derivatives of two-dimensional vectors and tensors, *e.g.* $\mathbf{v} = v^\alpha \mathbf{r}_{,\alpha}$ and $b_{\alpha\beta}$, with reference to ξ^α coordinates are

$$\begin{aligned} \mathbf{v}_{,\beta} &= v^\alpha\,|_\beta\, \mathbf{r}_{,\alpha} - v^\gamma b_{\gamma\beta}\mathbf{n}\ ,\ v^\alpha\,|_\beta = v^\alpha_{,\beta} + v^\lambda \Gamma^\alpha_{\lambda\beta}\ . \\ b_{\alpha\beta}\,|_\gamma &= b_{\alpha\beta,\gamma} - b_{\lambda\beta}\Gamma^\lambda_{\alpha\gamma} - b_{\alpha\lambda}\Gamma^\lambda_{\beta\gamma}\ . \end{aligned} \tag{2.2.13}$$

Note that there exist similar expressions for contravariant and mixed variant and higher order tensors, *c.f. e.g.* Niordson [Nio85]. It is evident that when considering a scalar quantity, the ordinary and covariant differentiations are identical, *e.g.* $w_{,\alpha} = w\,|_\alpha$.

Two well-known formulae should be stated here, the Gauss formula

$$\mathbf{r}_{,\alpha\beta} = \Gamma^\lambda_{\alpha\beta}\mathbf{r}_{,\lambda} - b_{\alpha\beta}\mathbf{n} \tag{2.2.14}$$

and the Weingarten formula

$$\mathbf{n}_{,\alpha} = b^\lambda_\alpha \mathbf{r}_{,\lambda}\ . \tag{2.2.15}$$

Hence, the geometry of the undeformed middle surface is specified completely by its first and second fundamental tensors. These two tensors should satisfy the Gauss equation and the Mainardi-Codazzi equation which entail the integrability conditions for the above mentioned equations (2.2.14) and (2.2.15). The Gauss equation states that

$$R_{\alpha\beta\gamma\mu} = b_{\alpha\lambda}b_{\beta\mu} - b_{\alpha\mu}b_{\beta\lambda} = K\,\varepsilon_{\alpha\beta}\,\varepsilon_{\lambda\mu} \tag{2.2.16}$$

where $R_{\alpha\beta\gamma\mu}$ is the Riemann-Christoffel tensor, and the Mainardi-Codazzi equation is

$$b_{\alpha\beta}\,|_\gamma = b_{\alpha\gamma}\,|_\beta\ . \tag{2.2.17}$$

2.3 Deformation of the middle surface

Under the deformation of a shell we understand that a material point of the undeformed middle surface with coordinates ξ^α moves to a position on the middle surface of the deformed shell. Here we assume that the curvilinear coordinate net deforms

with the body and, hence, the new position can be specified with the same ξ^α. The new position vector is given by

$$\tilde{\mathbf{r}} = \mathbf{r} + \mathbf{u} \tag{2.3.18}$$

where

$$\mathbf{u} = u^\alpha \mathbf{r}_{,\alpha} + w\mathbf{n} \tag{2.3.19}$$

is resolved with respect to $\mathbf{r}_{,\alpha}$ and $\mathbf{n}$ of the undeformed middle surface. Here, the u^α denote the in-plane displacements and w is the deflection or normal displacement. Partial differentiation of $\tilde{\mathbf{r}}$ in equation (2.3.18) gives (with help of the Weingarten formula, equation (2.2.13), and equation (2.3.19)) base vectors, tangent to the deformed coordinate curve ξ^α, as

$$\tilde{\mathbf{r}}_{,\alpha} = (\delta^\lambda_\alpha + u^\lambda |_\alpha + w b^\lambda_\alpha) \mathbf{r}_{,\lambda} + (w_{,\alpha} - u^\beta b_{\alpha\beta}) \mathbf{n} . \tag{2.3.20}$$

The metric / first fundamental tensor of the deformed middle surface is

$$\tilde{a}_{\alpha\beta} = \tilde{\mathbf{r}}_{,\alpha} \cdot \tilde{\mathbf{r}}_{,\beta} \tag{2.3.21}$$

and the unit normal vector

$$\tilde{\mathbf{n}} = \frac{1}{2} \tilde{\varepsilon}^{\alpha\beta} \tilde{\mathbf{r}}_{,\alpha} \times \tilde{\mathbf{r}}_{,\beta} . \tag{2.3.22}$$

The curvature / second fundamental tensor of the deformed middle surface is

$$\tilde{b}_{\alpha\beta} = -\tilde{\mathbf{n}} \cdot \tilde{\mathbf{r}}_{,\alpha\beta} . \tag{2.3.23}$$

Recalling the equations for the geometry of the shell it can thus be said that the deformed middle surface has its equivalent equations to those given for the undeformed middle surface. Components corresponding to the deformed geometry are denoted with a tilde.

Equation (2.3.20) can be used for establishing various quantities. These include the surface vector ϕ_α describing rotations in the undeformed directions ξ^α of the normal to the middle surface (sign convention as in [San63])

$$\phi_\alpha = - \mathbf{n} \cdot \tilde{\mathbf{r}}_{,\alpha} = -w_{,\alpha} + b_{\alpha\beta} u^\beta = -w_{,\alpha} + b^\beta_\alpha u_\beta . \tag{2.3.24}$$

The asymmetric surface tensor is

$$1_{\alpha\beta} = \tilde{\mathbf{r}}_{,\alpha} \cdot \mathbf{r}_{,\beta} = a_{\alpha\beta} + u_\beta |_\alpha + w b_{\alpha\beta} . \tag{2.3.25}$$

The skew-symmetric part $\omega_{\alpha\beta}$ is called the rotation tensor in the middle surface and is defined by

$$\omega_{\alpha\beta} = \frac{1}{2}\left(1_{\beta\alpha} - 1_{\alpha\beta} \right) = \frac{1}{2}\left(u_\beta \,|_\alpha - u_\alpha \,|_\beta \right) . \tag{2.3.26}$$

The invariant

$$\phi = \frac{1}{2}\varepsilon^{\alpha\beta}\omega_{\alpha\beta} = \frac{1}{2}\varepsilon^{\alpha\beta}u_\beta \,|_\alpha \tag{2.3.27}$$

is called the rotation about the normal to the middle surface.

For the deformation of the middle surface there exist two measures. Firstly, the strain tensor

$$\gamma_{\alpha\beta} = \frac{1}{2}\left(\tilde{a}_{\alpha\beta} - a_{\alpha\beta} \right) \tag{2.3.28}$$

and, secondly, the curvature change tensor

$$\kappa_{\alpha\beta} = \tilde{b}_{\alpha\beta} - b_{\alpha\beta} . \tag{2.3.29}$$

Note that $\gamma_{\alpha\beta}$, $\kappa_{\alpha\beta}$ can be expressed in terms of u^α, w, ϕ_α and ϕ and covariant derivates with respect to the undeformed middle surface. These are, however, usually simplified by neglecting various terms. For alternative definitions of $\kappa_{\alpha\beta}$ see Koiter [Koi66] and Pietraszkiewicz [Pie84].

2.4 First approximation shell theories

Many existing shell theories are based on the Love-Kirchhoff assumptions which state that

1. the transverse normal stress component can be neglected in comparison with the other stress components;

2. normals to the undeformed middle surface move to normals on the deformed middle surface and suffer no extensions.

Therefore, under these assumptions it is evident that the deformed state of a shell is determined entirely by the deformed configuration of its middle surface and, hence, an initially three dimensional problem is reduced to a two dimensional problem. If it is additionally assumed that the strains are small then the equations describing the

deformation of the middle surface simplify considerably. In this category of small-strain theories there are several subclasses. There is no generally accepted shell theory for each subclass. Also, as there is no agreement on the best approximation form for $\kappa_{\alpha\beta}$, many different theories exist and are employed.

Koiter [Koi60] makes use of the assumptions that

1. the shell is elastic, homogeneous and of an isotropic material;
2. the thickness h is constant with $\frac{h}{R} \ll 1$, where R is the smallest principal radius of curvature of the undeformed configuration;
3. $\eta \ll 1$ where η is the largest principal strain (strains small everywhere in the shell).

Under these assumptions the strain energy per unit area (strain energy density) equals approximately the sum of the extensional and bending energies per unit area, *i.e.*

$$V = V_\gamma + V_\kappa = \frac{1}{2} H^{\alpha\beta\gamma\mu} \left(\gamma_{\alpha\beta}\gamma_{\lambda\mu} + \frac{h^2}{12}\kappa_{\alpha\beta}\kappa_{\lambda\mu} \right) \tag{2.4.30}$$

where

$$\begin{aligned} H^{\alpha\beta\lambda\mu} &= \frac{Eh}{1-\nu^2}\left(\nu a^{\alpha\beta}a^{\lambda\mu} + \frac{1-\nu}{2}\left(a^{\alpha\lambda}a^{\beta\mu} + a^{\alpha\mu}a^{\beta\lambda} \right) \right), \\ H^{\alpha\beta\lambda\mu} &= H^{\beta\alpha\lambda\mu} = H^{\alpha\beta\mu\lambda} = H^{\lambda\mu\alpha\beta} = H^{\beta\alpha\mu\lambda}. \end{aligned} \tag{2.4.31}$$

Here, $H^{\alpha\beta\lambda\mu}$ is the elastic moduli tensor, E is Young's modulus and ν is Poisson's ratio. Equation (2.4.30) is known as Love's first approximation. From this the symmetric contravariant strain resultant tensor

$$N^{\alpha\beta} = \frac{\partial V}{\partial \gamma_{\alpha\beta}} = H^{\alpha\beta\lambda\mu}\gamma_{\lambda\mu} \tag{2.4.32}$$

and the symmetric contravariant strain couple tensor

$$M^{\alpha\beta} = \frac{\partial V}{\partial \kappa_{\alpha\beta}} = \frac{h^2}{12} H^{\alpha\beta\lambda\mu}\kappa_{\lambda\mu} \tag{2.4.33}$$

are obtained. Equations (2.4.32) and (2.4.33) form the linear constitutive equations.

In his work Koiter [Koi60] states that ".. the Love's so-called first approximation for the strain energy, as the sum of stretching or extensional energy and bending or flexural energy, is a consistent first approximation, and that no refinement of this

first approximation is justified, in general, if the basic Love-Kirchhoff assumptions (or equivalent assumptions) are retained..", and in another place ".. the relative error in this approximation does not exceed $\frac{h^2}{L^2}$ or $\frac{h}{R}$ whichever of these may be critical." Here L is the smallest wavelength of the deformation pattern of the middle surface.

Interpreting these results it becomes clear that they are valid for both geometrically linear and nonlinear shell theories and that it is permitted to add terms of the type $b^{\lambda}_{\alpha}\gamma_{\lambda\beta}$ to $\kappa_{\alpha\beta}$ without affecting Love's first approximation's accuracy. By defining

$$\theta \;=\; max\,(\frac{h}{L}, \frac{h}{d}, \frac{\sqrt{h}}{\sqrt{R}}, \sqrt{\eta}\,) \tag{2.4.34}$$

where d is the distance of a point from the lateral shell boundary it can be stated that the error in the first approximation of strain energy is of order θ^2, *i.e.* $O(\theta^2)$.

2.5 Marguerre's theory for thin shallow shells

Geometrically nonlinear theories in the presence of finite rotations are associated with many complexities and are, thus, usually avoided. The shallow shell theories are the members of the simplest possible category of small strain theories. Marguerre's theory underlies the following assumptions:

1. u_α small compared to w;

2. ϕ_α (bending rotations) moderate;

3. ϕ (rotation about the normal to the surface) small such that

$$\begin{aligned} \gamma_{\alpha\beta} &= \frac{1}{2}\,(\,u_\alpha\,|_\beta \,+\, u_\beta\,|_\alpha\,) \,+\, b_{\alpha\beta}w \,+\, \frac{1}{2}w_{,\alpha}w_{,\beta}\ , \\ \kappa_{\alpha\beta} &= -w\,|_{\alpha\beta}\ . \end{aligned} \tag{2.5.35}$$

If the shell is nearly flat and parallel to the x^α-plane then the approximations by Sanders [San63] can be used, where

$$\begin{aligned} b_{\alpha\beta} &\approx -z\,|_{\alpha\beta}\ , \\ u_\alpha &\approx U_\alpha \,+\, z_{,\alpha}w\ , \\ w &\approx U_3\ . \end{aligned} \tag{2.5.36}$$

Here, $z = x^3$, U_α are the in-plane displacements (in the directions of ξ^α projected on the x^α-plane) and U_3 the normal displacement (in the direction x^3) such that

$$\begin{aligned} \gamma_{\alpha\beta} &= \frac{1}{2}\left(U_\alpha|_\beta + U_\beta|_\alpha + z_{,\alpha}w_{,\beta} + z_{,\beta}w_{,\alpha} + w_{,\alpha}w_{,\beta} \right) , \\ \kappa_{\alpha\beta} &= -w|_{\alpha\beta} \ . \end{aligned} \tag{2.5.37}$$

The differential equations of equilibrium in the horizontal and vertical directions are then given by

$$\begin{aligned} N^{\alpha\beta}|_\beta + p^\alpha &= 0 , \\ Q^\alpha|_\alpha + \left(z|_{\alpha\beta} + w|_{\alpha\beta} \right) N^{\alpha\beta} & \\ + \left(z_{,\alpha} + w_{,\alpha} \right) N^{\alpha\beta}|_\beta + p &= 0 , \\ M^{\alpha\beta}|_\beta - Q^\alpha &= 0 , \end{aligned} \tag{2.5.38}$$

where Q^α denotes the transverse shear stress resultants, whereas p^α and p are the intensities of horizontal and vertical surface loads, respectively. The third equation in (2.5.38) can be used to substitute Q^α into the second equation in (2.5.38), thereby reducing the number of equations from three to two.

If it is now assumed that the boundary of the undeformed middle surface is a smooth curve C with no corner points (and hence no concentrated forces), then the boundary conditions to be applied become

$$\begin{aligned} & & N^{\alpha\beta}\tilde{n}_\beta \ \text{ or } \ U_\alpha , \\ \{ Q^\beta + \left(z_{,\alpha} + w_{,\alpha} \right) N^{\alpha\beta} \}\tilde{n}_\beta + \frac{d}{ds}\left(M^{\alpha\beta}t_\alpha\tilde{n}_\beta \right) & \text{ or } & w , \\ & & M^{\alpha\beta}\tilde{n}_\alpha\tilde{n}_\beta \ \text{ or } \ \phi_\alpha\tilde{n}^\alpha , \end{aligned} \tag{2.5.39}$$

where use is made of

$$\begin{aligned} \mathbf{t} = \frac{d\mathbf{r}}{ds} = t^\alpha \mathbf{r}_{,\alpha} \ , \ t_\alpha = t^\lambda a_{\alpha\lambda} , \\ \tilde{\mathbf{n}} = \mathbf{t} \times \mathbf{n} = \tilde{n}^\alpha \mathbf{r}_{,\alpha} \ , \ \tilde{n}_\alpha = \tilde{n}^\lambda a_{\alpha\lambda} , \end{aligned} \tag{2.5.40}$$

in which $\mathbf{t}$ and $\tilde{\mathbf{n}}$ are the unit tangent and unit normal to C, respectively, and s is a length parameter taken positive in the anticlockwise sense. All the above equations agree with those of Washizu [Was82] when transformed into Cartesian coordinates x^i.

2.6 The von Kármán nonlinear theory for thin plates

Plates are shells with zero curvature. Therefore, they have flat middle surfaces when undeformed. If a plate is considered with small thickness compared to its other dimensions and if the x^α-plane coincides with the undeformed middle surface, then putting $b_{\alpha\beta} = 0$ gives rise to von Kármán's theory derived as a special case of Marguerre's theory. Again, the usual assumptions apply, *i.e.* the Love-Kirchhoff hypothesis is presumed to be valid, also the strains are assumed to be small, the ϕ_α are moderate. The term ϕ is small and w is allowed to be several times larger than the thickness but small compared to other dimensions.

The strain tensor in the von Kármán theory is hence defined by

$$\gamma_{\alpha\beta} = \frac{1}{2}\left(u_\alpha |_\beta + u_\beta |_\alpha + w_{,\alpha} w_{,\beta} \right) , \tag{2.6.41}$$

and the curvature change tensor is

$$\kappa_{\alpha\beta} = -w |_{\alpha\beta} \ . \tag{2.6.42}$$

Thus, the differential equations of equilibrium reduce to

$$\begin{aligned} N^{\alpha\beta} |_\beta + p^\alpha &= 0 \ , \\ M^{\alpha\beta} |_{\beta\alpha} + w |_{\alpha\beta} N^{\alpha\beta} + w_{,\alpha} N^{\alpha\beta} |_\beta + p &= 0 \ . \end{aligned} \tag{2.6.43}$$

The boundary conditions on C, assuming that C has continuously turning tangent, to be applied become

$$\begin{aligned} & N^{\alpha\beta} n_\beta \quad \text{or} \quad u_\alpha \ , \\ \left(Q^\beta + w_{,\alpha} N^{\alpha\beta} \right) n_\beta + \frac{d}{ds}\left(M^{\alpha\beta} t_\alpha n_\beta \right) & \quad \text{or} \quad w \ , \\ & M^{\alpha\beta} n_\alpha n_\beta \quad \text{or} \quad \phi_\alpha n^\alpha \ . \end{aligned} \tag{2.6.44}$$

In the original paper of Theodore von Kármán [vK10] the equilibrium equations are given in terms of w and a stress function for the middle surface stresses, see also Timoshenko and Woinowsky-Krieger [TWK59], Timoshenko and Gere [TG61], Novozhilov [Nov53] and Niordson [Nio85] for works from the point of view of mechanics and *e.g.* Berger [Ber77] for a thorough mathematical treatment. For the purpose of the current work (nonlinear constant moment triangle) a displacement

formulation of equilibrium equations is more appropriate. Ciarlet [Cia80] gives a mathematical justification of von Kármán's two-dimensional approximation in relation to three-dimensional elasticity equations and also proves the equivalence of the original derivation to the displacement formulation presented here. In the case of $\xi^\alpha = x^\alpha$, the covariant differentiation in equations (2.6.41), (2.6.42) and (2.6.43) is substituted with ordinary differentiation as in Washizu [Was82]. For the present work it is of importance to know that, for sufficiently large compressive forces along the lateral surface of the plate, the von Kármán equations and, indeed, the Marguerre equations may possess several distinct solutions, which correspond to the experimentally observed buckling phenomenon, *c.f.* [Ber77].

2.7 Practical components of surface vectors and tensors

Vector and tensor components with respect to arbitrary curvilinear coordinates ξ^α are not useful in engineering applications as they represent quantities not capable of physical measurement. Morley [Mor87] introduces so-called practical components which are a useful and more versatile alternative to the traditional concept of physical components originally defined by McConnell [McC31] and Truesdell [Tru53]. The symbols developed $h^\alpha_{\alpha'}$, $h^{\alpha'}_\alpha$ have the property that, in products with surface vectors and tensors referred to the coordinates ξ^α, they give at once physically significant components measured in the directions of an orthogonal set of unit vectors $\mathbf{t}_{\alpha'}$ which is orientated as required with respect to the coordinates ξ^α.

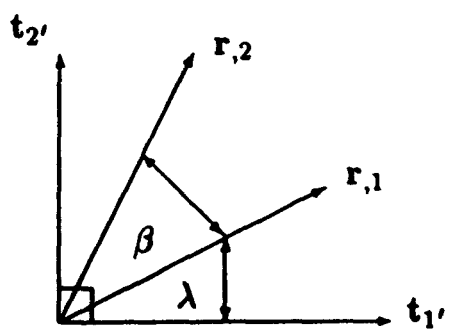

Figure 2.1. Base and unit orthogonal tangent vectors at a point of the surface.

Consider, here, β to be the angle between the base vectors $\mathbf{r}_{,1}$ and $\mathbf{r}_{,2}$ and λ the angle between the arbitrarily orientated vectors $\mathbf{t}_{,1'}$ and $\mathbf{r}_{,1}$. With $\alpha_\alpha = |\,\mathbf{r}_{,\alpha}\,|$ denoting the magnitude of the vector $\mathbf{r}_{,\alpha}$, it can then be shown that

$$\mathbf{t}_{,\alpha'} = h^{\alpha}_{\alpha'}\,\mathbf{r}_{,\alpha}, \tag{2.7.45}$$

where

$$\begin{aligned} h^{1}_{1'} &= \frac{\sin(\beta+\lambda)}{\alpha_1 \sin\beta} \quad , \quad h^{2}_{1'} = -\frac{\sin\lambda}{\alpha_2 \sin\beta}\,, \\ h^{1}_{2'} &= -\frac{\cos(\beta+\lambda)}{\alpha_1 \sin\beta} \quad , \quad h^{2}_{2'} = \frac{\cos\lambda}{\alpha_2 \sin\beta}\,. \end{aligned} \tag{2.7.46}$$

Similarly,

$$\mathbf{r}_{,\alpha} = h^{\alpha'}_{\alpha}\,\mathbf{t}_{\alpha'} \tag{2.7.47}$$

where

$$\begin{aligned} h^{1'}_{1} &= \alpha_1 \cos\lambda \quad , \quad h^{2'}_{1} = \alpha_1 \sin\lambda \\ h^{1'}_{2} &= \alpha_2 \cos(\beta+\lambda) \quad , \quad h^{2'}_{2} = \alpha_2 \sin(\beta+\lambda)\,. \end{aligned} \tag{2.7.48}$$

The symbols $h^{\alpha}_{\alpha'}$ and $h^{\alpha'}_{\alpha}$ exhibit an ordered algebra which is a natural extension to that of tensor theory. Some of their properties are

$$\begin{aligned} h^{\alpha'}_{\alpha} &= a_{\alpha\beta}\,h^{\beta'}_{\alpha'} \quad , \quad h^{\alpha}_{\alpha'} = a^{\alpha\beta}\,h^{\alpha'}_{\beta}\,, \\ h^{\alpha'}_{\alpha}\,h^{\alpha}_{\beta'} &= \delta^{\alpha'}_{\beta'} \quad , \quad h^{\alpha'}_{\alpha}\,h^{\beta}_{\alpha'} = \delta^{\alpha}_{\beta}\,, \\ a_{\alpha\beta} &= h^{\alpha'}_{\alpha}\,h^{\alpha'}_{\beta} \quad , \quad a^{\alpha\beta} = h^{\alpha}_{\alpha'}\,h^{\beta}_{\alpha'}\,. \end{aligned} \tag{2.7.49}$$

Practical components of vectors and tensors referred to the undeformed middle surface of a shell or plate readily follow. For example,

$$\begin{aligned} &u_{\alpha'} = h^{\alpha}_{\alpha'}\,u_{\alpha}\,,\ \gamma_{\alpha'\beta'} = h^{\alpha}_{\alpha'}\,h^{\beta}_{\beta'}\,\gamma_{\alpha\beta}\,,\ \kappa_{\alpha'\beta'} = h^{\alpha}_{\alpha'}\,h^{\beta}_{\beta'}\,\kappa_{\alpha\beta}\,, \\ &N_{\alpha'\beta'} = h^{\alpha'}_{\alpha}\,h^{\beta'}_{\beta}\,N^{\alpha\beta}\,,\ M_{\alpha'\beta'} = h^{\alpha'}_{\alpha}\,h^{\beta'}_{\beta}\,M^{\alpha\beta}\,, \end{aligned} \tag{2.7.50}$$

with inverses

$$\begin{aligned} &u_{\alpha} = h^{\alpha'}_{\alpha}\,u_{\alpha'}\,,\ \gamma_{\alpha\beta} = h^{\alpha'}_{\alpha}\,h^{\beta'}_{\beta}\,\gamma_{\alpha'\beta'}\,,\ \kappa_{\alpha\beta} = h^{\alpha'}_{\alpha}\,h^{\beta'}_{\beta}\,\kappa_{\alpha'\beta'}\,, \\ &N^{\alpha\beta} = h^{\alpha}_{\alpha'}\,h^{\beta}_{\beta'}\,N_{\alpha'\beta'}\,,\ M^{\alpha\beta} = h^{\alpha}_{\alpha'}\,h^{\beta}_{\beta'}\,M_{\alpha'\beta'}\,. \end{aligned} \tag{2.7.51}$$

The contravariant elasticity moduli tensor in equation (2.4.31) may be written

$$H^{\alpha\beta\lambda\mu} = h^{\alpha}_{\alpha'}\,h^{\alpha}_{\beta'}\,h^{\lambda}_{\lambda'}\,h^{\mu}_{\mu'}\,H_{\alpha'\beta'\lambda'\mu'}\,, \tag{2.7.52}$$

where

$$H_{\alpha'\beta'\lambda'\mu'} = \frac{Eh}{1-\nu^2}\{\nu\,\delta_{\alpha'\beta'}\,\delta_{\lambda'\mu'} + \frac{1-\nu}{2}(\delta_{\alpha'\lambda'}\,\delta_{\beta'\mu'} + \delta_{\alpha'\mu'}\,\delta_{\beta'\lambda'})\} \qquad (2.7.53)$$

with $\delta_{\alpha'\beta'}$ being an alternative form of the Kronecker delta. The $H_{\alpha'\beta'\lambda'\mu'}$ defines the elasticity tensor for an isotropic plate with reference to a pair of middle surface Cartesian coordinates.

On the boundary C of the middle surface of an undeformed shell or plate it is feasible to orientate the orthogonal unit vectors $\mathbf{t}_{1'}$ and $\mathbf{t}_{2'}$ such that they coincide with the normal $\tilde{\mathbf{n}}$ and tangent $\mathbf{t}$ vectors, respectively. In accordance with this, the third equation in (2.5.39), for example, may be written

$$M_{1'1'} = h^{1'}_{\alpha}\,h^{1'}_{\beta}\,M^{\alpha\beta} = M^{\alpha\beta}\,\tilde{n}_{\alpha}\,\tilde{n}_{\beta} \text{ or } \phi_{1'} = h^{\alpha}_{1'}\,\phi_{\alpha} = \phi_{\alpha}\,\tilde{n}^{\alpha}\ . \qquad (2.7.54)$$

In general, the widely used convention for suffices n and t (or s) to denote quantities referred to normal and tangential directions at the boundary is directly equivalent with the use of suffices $1'$ and $2'$, *e.g.*

$$\begin{aligned} u_{1'} &= u_n\ , \\ u_{2'} &= u_t\ , \\ N_{1'\alpha'}\,u_{\alpha'} &= N_n\,u_n + N_{nt}\,u_t\ . \end{aligned} \qquad (2.7.55)$$

Chapter 3

Linear and nonlinear finite element analyses

3.1 Introduction

In Chapter 2 some classical differential equations were presented. Solving these equations analytically has not been possible except for very simple cases with specific boundary conditions and/or simple geometry. The simplest examples of all are the plane stress and bending problems in the linear theory, *c.f.* Timoshenko and Woinowsky-Krieger [TWK59]. The first approximation theory allows independent and accurate reductions of linear shell differential equations. In this way, differential equations describing membrane or inextensional bending actions are obtained without mixing them. Analytical solutions of such reduced equations for cylinders and spheres can be found in Flügge [Flü73]. Exact inextensional bending solutions for real shells whose surfaces are described by an arbitrary polynomial are given by Morley and Mould [MM87] with additional numerical results presented by Bangemann [Ban92].

Nonlinear plate and shell differential equations are very complicated. Thus, analytical solutions are restricted to essentially one-dimensional plate problems, *e.g.* uniformly loaded circular plates and infinitely long strips, *c.f.* Mansfield [Man89].

In engineering applications the solutions of the above mentioned equations are a prerequisite for further work in which a non-analytical course of proceedings is

sought. This leads to the need to develop approximating numerical methods for the solution of thin plate and shell differential equations. The two methods used in the early stages for this purpose were the *Rayleigh-Ritz energy method* and the *finite difference method.* Since the advent of powerful computers, however, the *finite element method* (FEM) has overshadowed all the other numerical techniques. All these applicable numerical methods possess the common feature of replacing the original problem, described in terms of differential equations in the unknown continuous functions, by a suitable formulation including algebraic equations in the discrete values of the unknowns at a finite number of points, *i.e.* the continuum model is approximated by a discrete model. In the beginning the finite element method was for a long time used for mainly solving linear problems in structural mechanics and few worked on the finite element analysis of thin plates and shells with material and/or geometric nonlinearities. This then changed and in the last two decades the finite element method has been extended and used widely for nonlinear problems.

In this chapter the finite element method is presented. First, a general introduction to the FEM is given. Then, different finite elements are discussed. Implications of the method's application in the geometrically nonlinear analysis of thin plates and shells follow and the chapter concludes with a short note on convergence and the patch test.

3.2 The finite element method

A common problem occurring in continuum mechanics is that of solving a set of differential equations

$$\mathbf{A}(\mathbf{v}) = \begin{Bmatrix} A_1(\mathbf{v}) \\ A_2(\mathbf{v}) \\ \cdot \\ \cdot \end{Bmatrix} = \mathbf{0} \quad \text{in } \Omega \tag{3.2.1}$$

with boundary conditions

$$\mathbf{B}(\mathbf{v}) = \left\{ \begin{array}{c} B_1(\mathbf{v}) \\ B_2(\mathbf{v}) \\ \cdot \\ \cdot \end{array} \right\} = \mathbf{0} \quad \text{on } \partial\Omega \tag{3.2.2}$$

where Ω represents the space occupied by the continuous body, $\partial\Omega$ is the boundary of this continuous body, **A** and **B** denote specific differential operators and **v** is the unknown function. Normally, a reformulation of the above problem is possible and leads to that of finding the unknown function **v** that minimizes the integral functional

$$\Pi = \int_{\Omega} F(\mathbf{v}\ ,\ \mathbf{v}_{,1}\ ,\ ...)d\Omega + \int_{\partial\Omega} E(\mathbf{v}\ ,\ \mathbf{v}_{,1}\ ,\ ...)d\partial\Omega \tag{3.2.3}$$

where F and E are appropriate operators. The subscript preceeded by a comma indicates differentiation with respect to independent variables, *e.g.* Cartesian coordinates x^i. Integral functionals of the above form can be derived directly from the principle of minimum potential energy, the principle of minimum complementary energy and other variational principles, *c.f.* Washizu [Was82] for a complete treatment.

In the finite element analysis, which was first developed in the 1950's, *c.f.* Turner *et al.* [MJTT56], the continuous body is divided into a number of fictitious elements of finite magnitude (finite elements). Each element has a domain Ω^e and a boundary $\partial\Omega^e$, part of which may coincide with a part of $\partial\Omega$. The use of the superscript ^{e} is introduced here to represent the local element level and for distinguishing between local and global levels. In each element the unknown function **v** is approximated by

$$\mathbf{v} \approx \tilde{\mathbf{v}} = \sum_r \mathbf{N}_r \mathbf{a}_r^e = \mathbf{N}\mathbf{a}^e \tag{3.2.4}$$

where $\mathbf{N}_r$ are so-called shape functions prescribed in terms of the independent variables and $\mathbf{a}^e$ represents the vector with the unknown element nodal connector quantities (element degrees of freedom). If the assumption is made that the $\mathbf{N}_r$ are chosen such that $\tilde{\mathbf{v}}$ satisfies the minimum continuity requirements in each element and across interelement boundaries as well as boundary conditions, then the func-

tional in equation (3.2.3) can be approximated by

$$\Pi = \sum_{e=1}^{M} \left(\int_{\Omega} F(\mathbf{N}\mathbf{a}^e, ...) d\Omega + \int_{\partial\Omega} E(\mathbf{N}\mathbf{a}^e, ...) d\partial\Omega \right) \tag{3.2.5}$$

where M is the total number of elements used to model the continuum. The only unknown quantities here are the nodal connectors in the whole model denoted by $\mathbf{a}$, say, which make up the total degrees of freedom. Therefore, the problem of finding $\mathbf{v}$ that minimizes equation (3.2.3) is transferred to the problem of finding $\tilde{\mathbf{v}}$ that minimizes equation (3.2.5) with respect to $\mathbf{a}$.

The functional Π attains a minimum/stationary value where

$$\delta\Pi = 0 \, . \tag{3.2.6}$$

The fundamental lemma of the calculus of variations, *c.f.* Courant and Hilbert [CH53], applied on this then leads to a discrete form of equilibrium equations

$$\mathbf{K}\,\mathbf{a} = \mathbf{p} \tag{3.2.7}$$

where

$$\mathbf{K} = \sum_{e=1}^{M} \mathbf{K}^e \quad , \quad \mathbf{p} = \sum_{e=1}^{M} \mathbf{p}^e \, . \tag{3.2.8}$$

Here, $\mathbf{K}$ denotes the coefficient matrix and $\mathbf{p}$ is the right hand side column vector.

Therefore, we can summarize that the finite element method can be described by the following step-by-step procedure:

1. Discretization of the problem into elements in such a way that the body is separated into a number of finite elements using imaginary lines by stipulating that element connections can be found at a discrete number of nodal points on the element boundaries.

2. Forming the element coefficient matrices $\mathbf{K}^e$, which can be derived directly through the various energy theorems.

3. Assemblage of the global coefficient matrix $\mathbf{K}$ using the element coefficient matrices already calculated.

4. Assemblage of the right hand side column vector $\mathbf{p}$.

5. Solving the global coefficient equation $\mathbf{Ka} = \mathbf{p}$ with boundary conditions for unknown $\mathbf{a}$.

6. Use of the solution for $\mathbf{a}$ in order to find secondary variables if required.

The most popular finite elements in structural analysis are based on a *displacement formulation* where $\tilde{\mathbf{v}}$ represents the assumed displacement field, $\mathbf{a}$ is the nodal displacement connection vector, $\mathbf{K}$ the stiffness matrix and $\mathbf{p}$ is the loads vector. For linear problems $\mathbf{K}$ is always constant and should be symmetric and positive definite. Equation (3.2.7) can then be solved uniquely by employing a numerical technique such as Gaussian elimination or Cholesky factorization. For nonlinear problems $\mathbf{K}$ depends on $\mathbf{a}$ and is in general not symmetric. Equation (3.2.7) must then normally be solved through the use of a numerical iterative technique. Here, the tangent stiffness matrix $\mathbf{K}_T$ obtained from the second variation of Π with respect to $\mathbf{a}$ (Hessian matrix) is required. It is prudent to note that $\mathbf{K}_T$ is in general symmetric and depends on $\mathbf{a}$. In the current work a lot of attention is given to the definiteness of $\mathbf{K}_T$ as it is of great importance in the structural stability analysis. Also it is noted that $\mathbf{p}$ is independent of $\mathbf{a}$ in both linear and nonlinear problems, *i.e.* conservative problems are treated.

Other finite elements in common use include elements derived by using the principle of minimum complementary energy or *equilibrium models*. Here, $\tilde{\mathbf{v}}$ represents the assumed stress field over each element and $\mathbf{a}$ is the unknown generalized force connector. Approximate solutions tend to be overflexible (overstiff solutions with conforming displacement models based on minimum potential energy principle). *Mixed finite elements* are usually derived through generalized variational principles. $\tilde{\mathbf{v}}$ may represent both stress and displacement fields and $\mathbf{a}$ may consist of both force and displacement connectors. The elements may be overstiff or overflexible. One drawback is that the coefficient matrix may be indefinite and, hence, they are not preferred for nonlinear problems. Each of these models has its own advantages and disadvantages but a displacement formulation is preferred, *c.f.* Zienkiewicz [Zie77] and Cook [Coo81].

3.3 Plate and shell finite elements

Finite elements exist in various shapes. They can lie flat on a plane or be curved. If flat they can have straight or curved sides. They can be one-dimensional, two-dimensional or three-dimensional. The best choice of element depends, on preference, on the geometry of the structure, the physical behaviour of the structure and the resources available. In Chapter 2 the Love-Kirchhoff hypothesis was stated and explained. With help of this the reduction of an initially three-dimensional problem to a two-dimensional problem was achieved. Thus, it allows the use of two-dimensional elements to model the middle surface of thin plates and shells. Although not of direct relevance to the present work, it is worth noting that the relaxation of the Love-Kichhoff assumption that normals remain normal to the middle plane after deformation extends the applicability to thick plates. Finite elements derived using this theory are known as Reissner-Mindlin elements.

Common finite elements to be used for thin plate problems are *common flat elements* which are either triangles or rectangles, or *isoparametric elements*, *i.e.* elements in which the displacements and geometry are interpolated to the same order, usually curvilinear triangles or quadrilaterals. In the linear theory, these elements are either membrane elements (for the solution of plate stretching problems) or bending elements (for the solution of plate bending problems).

Four thin plate elements are relevant to the present work. The *constant strain triangle* by Turner *et al.* [MJTT56], which is the first finite element ever developed. It is a membrane triangle with linearly varying in-plane displacements. The *constant moment triangle* by Hellan [Hel67] and Herrmann [Her67] is an element that corresponds to the constant strain triangle in the bending analysis of plates. It is a mixed finite element model and has a constant bending moment field with a linear representation of the deflection within each element. The degrees of freedom are taken as the nodal deflection at the vertices and the normal bending moment at the midpoints of each side. The main drawback of the element is the indefiniteness of its stiffness matrix. The *displacement version of the constant moment triangle* by Morley [Mor71] is an equilibrium element and provides an alternative derivation based on the theorem of minimum potential energy. In this way, a positive definite

stiffness matrix is obtained. The deflections vary quadratically and are expressed in terms of the nodal deflections at the vertices and the rotations at the midpoints of each side. No definite agreement has been found in rating the performance of this element. Irons and Loikkanen [IL83] and Kikuchi [Kik86], following on from the work of Dawe [Daw72], classify it as over-flexible in the linear thin plate analysis, whereas Morley and Mould [MM87] find it to perform extremely well for linear thin shell problems. The *geometrically nonlinear constant moment triangle* possesses connectors which are identical to those obtained by the superposition of the constant strain triangle and the displacement version of the constant moment triangle as described above. This element is used throughout the present work and is discussed in detail in Chapter 4.

Shells are curved structures and, therefore, no effective separation of membrane and bending actions is possible in both linear and nonlinear theories. There are various options for modelling thin shells. *Curved elements* based on either a shallow or deep shell theory possess the advantages that it may be possible to represent the actual curvature of the middle surface exactly and that the desired coupling of membrane and flexural actions is attained within each element. On the other hand, their derivation is formidable and their use is very expensive. Additionally they are, in general, not able to reproduce rigid body movements without straining. *Curved degenerated elements* obtained through the use of the isoparametric concept are the elements most widely used today. They are solid three-dimensional elements but there is the danger that the large number of simultaneous equations may become ill-conditioned. The coupling between membrane and bending actions is accomplished through inter-element continuity, *c.f.* Cook [Coo81]. The lower-order displacement elements are prone to membrane locking and, hence, overstiff solutions and slow convergence might be the consequence. Higher order elements can be derived so as to exclude membrane locking but the formulation is expensive. Therefore, they are not suitable for the nonlinear analysis since the recomputation of the stiffness matrices may be very expensive. *Flat facet elements* are simple to formulate and capable of rigid body movements without straining. They require a minimum of input data and are easy to mix with other types of elements. For the purposes of the present work they are preferred because their use in the nonlinear analysis

is cheap due to the simplicity of their stiffness matrices. In general, however, their performance is poor and, thus, a fine mesh is required for accurate results when shells with significant membrane actions are analysed. Most flat facet elements utilize a constant strain field to represent the actual membrane strains. If the geometry is not simple, a large number of elements is needed to reduce physical idealization errors. If displacement based elements are used, displacement compatibility between adjacent elements which do not lie in the same plane is violated (often true for a planar array of elements). This arises because of the different orders of the displacement fields in available membrane and bending elements.

3.4 Developments in the geometrically nonlinear analysis

Thin elastic plates are highly flexible in bending and thin elastic shells undergo deflections which are often larger than their thickness. If accuracy is required and the study of post buckling behaviour is of interest then geometrically nonlinear effects must be considered in the finite element formulation. Geometrical nonlinearities enter into the analysis because of extra nonlinear terms added into the strain-displacement relations and the effect of deformation on the equilibrium equations. The earliest nonlinear finite element formulations were simple extensions of linear analyses developed for specific applications on an intuitive basis. Today there are three well-known finite element approaches for the solution of geometrically nonlinear thin plate and shell problems, *c.f.* Mattiasson [Mat83] for a comprehensive review:

1. total Lagrangian formulation;
2. updated Lagrangian formulation;
3. co-rotational formulation.

In the total Lagrangian formulation, all static and kinematic finite element variables are referred to the initial, stress-free state of the structure, whereas in the updated Lagrangian formulation all variables are referred to the last calculated deformed configuration. The co-rotational formulation was developed independently

by many. It has also been given various names, *e.g.* 'natural approach', *c.f.* Argyris *et al.* [JHAS79], or 'convected coordinate formulation', *c.f.* Hinton [He92]. This is a geometrically nonlinear formulation in which a local Cartesian coordinate system is attached to the element and is allowed to rotate continuously with the element as the deformation proceeds. The main characteristic, hence, is the separation of the element rigid body movements from the local deformations which occur within the finite element itself. This approach entails the separation of large nonlinearities (associated with the connectors) from the smaller local nonlinearities appearing within the element. The equilibrium equations are derived by considering the deformation of the element relative to the current position of the moving Cartesian system in its undeformed shape prior to the transformation to global coordinates. In the case of small strains local nonlinearities are often ignored and geometrical nonlinearities are introduced solely through the transformation from local to global coordinates.

It should be mentioned here that the total and updated Lagrangian formulations are based on the corresponding well-established theories from nonlinear continuum mechanics, *c.f.* Bathe *et al.* [KJBW75], and should, therefore, yield the same numerical results as they are theoretically equivalent (provided that the transformation from local to global level is performed correctly in the updated Lagrangian formulation). The advantage of the updated Lagrangian formulation and the co-rotational formulation over the total Lagrangian formulation is that, in case of small strains, there is increased difficulty in solving geometrically nonlinear problems as rotations are allowed to become larger. This is because finite rotations are nonaccumulative quantities, *i.e.* they do not comply with vector addition as is explained *e.g.* by Malvern [Mal69]. The motion of individual elements for thin plates and shells consists to a large extent of rigid body movements. Therefore, rigid body rotations may be eliminated and deformation rotations relative to local coordinates become smaller quantities.

3.5 Convergence and patch test

Validation of the approximate computed results is accomplished by proving that the results converge towards the exact solution of the problem when the mesh is

refined. Most of the finite elements employed today do not satisfy the inter-element continuity requirement for convergence as the minimum C^1 continuity demands a high-order displacement polynomial representation and many degrees of freedom. Elements violating this condition are called *nonconforming elements* as opposed to *conforming elements.* Experience has shown, unexpectedly, that nonconforming elements can perform even better than their conforming counterparts.

The patch test, first introduced by Irons *et al.* [BCIZ65], provides a means to check whether the solution obtained in using a given element converges to the correct answer, when the mesh is arbitrarily refined. Considering a patch of finite elements containing at least one internal node, *i.e.* a node completely surrounded by elements, the element then passes the patch test if the computed results for the internal point coincide with the exact theoretical values. For simple finite elements already known to pass the patch test, the patch test is usually employed as an aid to verify the computer program or code.

A finite element based on a nonlinear theory should ideally be capable of reproducing exactly the following physical actions:

- three translational rigid body movements;
- three rotational rigid body movements;
- three independent constant states of membrane strain $\gamma_{\alpha\beta}$;
- two independent constant states of curvature $\kappa_{\alpha\alpha}$ and a constant curvature state κ_{12} satisfying the integrability condition $(\kappa_{12})^2 = \kappa_{11}\kappa_{22}$;
- all the above actions in any possible combination.

It is prudent to note that the geometrically nonlinear constant moment triangle, which is used throughout the present work and discussed in more detail in Chapter 4, is based on the von Kármán nonlinear plate theory as described in Chapter 2 and passes the totality of the nonlinear von Kármán patch tests for constant strain and curvature, *c.f.* Providas [Pro90].

Chapter 4

The geometrically nonlinear constant moment triangle

4.1 Introduction

A great number of finite elements suitable for solution of geometrically nonlinear problems of thin plate and shells are based on either the *updated Lagrangian formulation* or the *co-rotational formulation*. When the local nonlinearities are ignored, linear equations are obtained on the local level which makes the formulation easier. Therefore, the introduction of geometrical nonlinearities through transformation from element to system level extends the applicability. Evidently, there is a restriction upon the size of the finite elements and that, in case local nonlinearities are disregarded, patch test solutions cannot be covered exactly.

Therefore, the *geometrically nonlinear constant moment triangle*, which is a flat triangular element and is itself based on a geometrically nonlinear theory, has been developed by Morley [Mor91] with the hope that in this way no restrictions upon mesh size exist anymore and that more reliable solutions are obtained for a coarser mesh. This flat triangular element, derived through the *total Lagrangian method*, is based on the von Kármán geometrically nonlinear theory, which was discussed in Chapter 2, and passes the totality of the nonlinear von Kármán patch tests for constant strain and curvature, *c.f.* [Pro90]. It is the simplest possible geometrically nonlinear finite element which is accurate for the solution of general problems for

thin plates and shells (moderate ϕ_α and small ϕ). The element has constant stresses and constant moments and its connection properties are identical to those of the element obtained by the superposition of the constant strain triangle by Turner *et al.* [MJTT56] and the displacement version of the constant moment triangle by Morley [Mor71] in the linear analysis. It is an equilibrium element which in its displacement formulation is a nonconforming finite element, *i.e.* interelement continuity is violated, but is believed to be equally important as the constant strain triangle and the constant moment triangle in the linear finite element analysis. In particular, from the mathematical viewpoint, existence of the nonlinear triangle introduces a new basis from which to consider convergence and accuracy of approximate solutions when using nonconforming finite elements.

In this chapter the geometry of the triangle is described first of all. Then, equations from the von Kármán theory are stated, followed by the finite element derivation of the geometrically nonlinear constant moment triangle for which, in the concluding section, a matrix formulation suitable for finite element computation is presented.

4.2 Geometry of the flat triangle

The undeformed middle surface of the flat triangle is described by the position vector

$$\mathbf{r} = x^i(\xi^\alpha)\,\mathbf{e}_i \tag{4.2.1}$$

where x^i denote the Cartesian coordinates in the space with reference frame of unit vectors $\mathbf{e}_i$ and the ξ^α are oblique rectilinear coordinates aligning with sides 1 and 2 of the triangle, *c.f.* Figure 4.1.

In the sequel use is made of ξ^i such that

$$x^i = x^i_j\,\xi^j \tag{4.2.2}$$

where x^i_j gives the magnitude of x^i at vertex j. The natural base vectors along ξ^α are

$$\mathbf{r}_{,\alpha} = x^i_{,\alpha}\,\mathbf{e}_i \tag{4.2.3}$$

where

$$x^i_{,1} = x^i_1 - x^i_3 \quad , \quad x^i_{,2} = x^i_2 - x^i_3 \; . \tag{4.2.4}$$

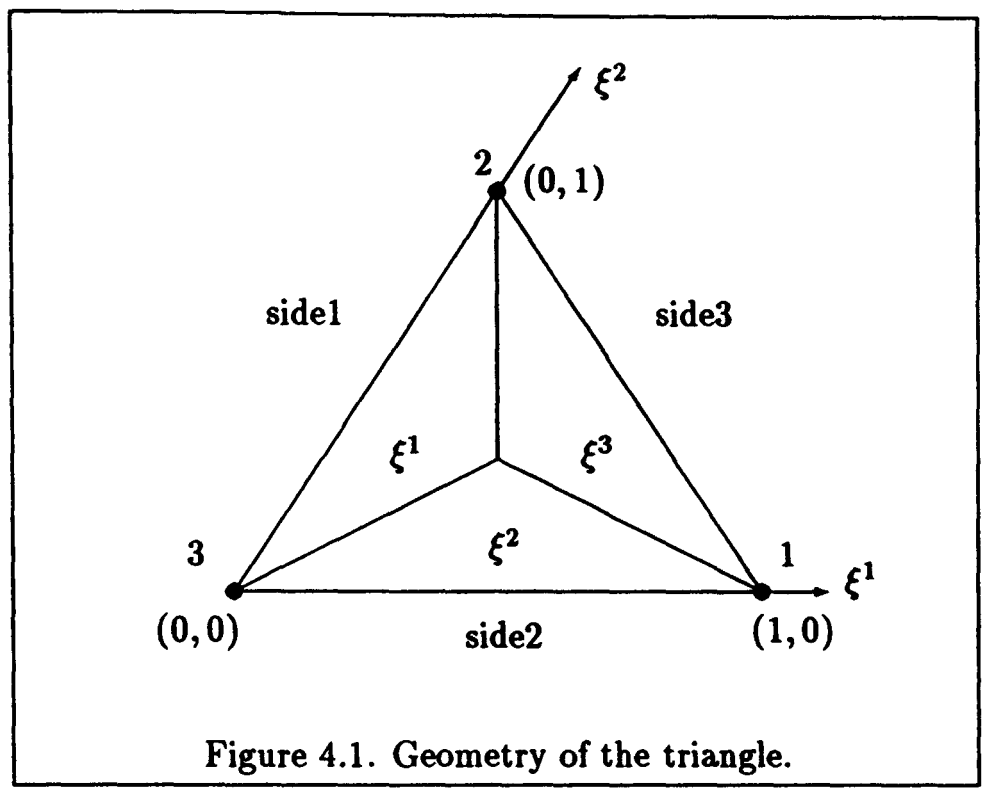

Figure 4.1. Geometry of the triangle.

Covariant components defined as in Chapter 2 are

$$a_{11} = (l_2)^2 \ , \ a_{22} = (l_1)^2 \ , \ a_{12} = \frac{1}{2} l_{12} \tag{4.2.5}$$

where l_i is the length of side i and

$$\begin{aligned} l_{12} &= (l_1)^2 + (l_2)^2 - (l_3)^2 \ , \\ l_{23} &= (l_2)^2 + (l_3)^2 - (l_1)^2 \ , \\ l_{31} &= (l_3)^2 + (l_1)^2 - (l_2)^2 \ . \end{aligned} \tag{4.2.6}$$

The determinant of $a_{\alpha\beta}$ is

$$a = det\,(a_{\alpha\beta}) = 4\,A^2 \tag{4.2.7}$$

where A denotes the area of the triangle. Alternatively, A can be calculated from

$$16\,A^2 = l_{12}l_{23} + l_{23}l_{31} + l_{31}l_{12} \ . \tag{4.2.8}$$

The unit vector orthogonal to the undeformed middle surface defined as in Chapter 2 is

$$\mathbf{n} = n^i\,\mathbf{e}_i \tag{4.2.9}$$

where

$$n^1 = \frac{1}{2A}\,(\,x^2_{,1}x^3_{,2} - x^2_{,2}x^3_{,1}\,) \tag{4.2.10}$$

and the remaining components follow by cyclic permutation of the superscripts. The triangle is enclosed by the boundary C consisting of straight lines (sides of the triangle). Tedious algebra yields values of $h^{\alpha}_{\alpha'}$ and $h^{\alpha'}_{\alpha}$ important for computation as in Table 4.1.

	side 1	side 2	side 3		side 1	side 2	side 3
$h^1_{1'}$	$-\frac{l_1}{2A}$	$\frac{l_{12}}{4Al_2}$	$\frac{l_{31}}{4Al_3}$	$h^{1'}_1$	$-\frac{2A}{l_1}$	0	$\frac{2A}{l_3}$
$h^2_{1'}$	$\frac{l_{12}}{4Al_1}$	$-\frac{l_2}{2A}$	$\frac{l_{23}}{4Al_3}$	$h^{1'}_2$	0	$-\frac{2A}{l_2}$	$\frac{2A}{l_3}$
$h^1_{2'}$	0	$\frac{1}{l_2}$	$-\frac{1}{l_3}$	$h^{2'}_1$	$-\frac{l_{12}}{2l_1}$	l_2	$-\frac{l_{23}}{2l_3}$
$h^2_{2'}$	$-\frac{1}{l_1}$	0	$\frac{1}{l_3}$	$h^{2'}_2$	$-l_1$	$\frac{l_{12}}{2l_2}$	$\frac{l_{31}}{2l_3}$

Table 4.1. $h^{\alpha}_{\alpha'}$ and $h^{\alpha'}_{\alpha}$ values along triangle sides.

4.3 Equations from the von Kármán nonlinear theory

Recalling the strain and curvature equations

$$\begin{aligned} \gamma_{\alpha\beta} &= \frac{1}{2}\left(u_{\alpha,\beta} + u_{\beta,\alpha} + w_{,\alpha} w_{,\beta} \right) , \\ \kappa_{\alpha\beta} &= -w_{,\alpha\beta} , \end{aligned} \tag{4.3.11}$$

with displacement vector

$$\mathbf{U} = U^i \mathbf{e}_i = u_\alpha \mathbf{a}^\alpha + w\mathbf{n} , \tag{4.3.12}$$

constant curvature states associated with inextensional bending prevail when $\gamma_{\alpha\beta} = 0$, leading to a system of three differential equations which upon elimination of the u_α reduces to a single differential equation

$$(\kappa_{12})^2 - \kappa_{11}\kappa_{22} = 0 . \tag{4.3.13}$$

Satisfaction of this equation guarantees that strains $\gamma_{\alpha\beta}$ are integrable.

For constant stress resultants $N^{\alpha\beta}$ and constant stress couples $M^{\alpha\beta}$ the von Kármán differential equations of equilibrium reduce to

$$\begin{aligned} p^\alpha &= 0 , \\ -\kappa_{\alpha\beta} N^{\alpha\beta} + p &= 0 , \end{aligned} \tag{4.3.14}$$

where p^α and p denote the surface and out-of-plane loads, respectively.

Consistent with the above, a Hu-Washizu functional Π_G for the energy can be set up as

$$\begin{aligned}
\Pi_G \quad &= \frac{1}{2}\int_A H^{\alpha\beta\lambda\mu}\left(\gamma_{\alpha\beta}\gamma_{\lambda\mu} + \frac{h^2}{12}\kappa_{\alpha\beta}\kappa_{\lambda\mu}\right) dA \\
&- \int_A \left(p^* w\right) dA \\
&- \int_A \left\{\gamma_{\alpha\beta} - \frac{1}{2}\left(u_{\alpha,\beta} + u_{\beta,\alpha} + w_{,\alpha}w_{,\beta}\right)\right\} N^{\alpha\beta}\, dA \\
&- \int_A \left(\kappa_{\alpha\beta} + w_{,\alpha\beta}\right) M^{\alpha\beta}\, dA \\
&- \int_{C_K} \left\{N_{1'\alpha'}\left(u_{\alpha'} - \tilde{u}_{\alpha'}\right) + R_i\left(w_n - \tilde{w}_i\right)\right. \\
&\qquad \left. + V_{1'}\left(w - \tilde{w}\right) + M_{1'1'}\left(\phi_{1'} - \tilde{\phi}_{1'}\right)\right\} ds \\
&- \int_{C_T} \left(N^*_{1'\alpha'}u_{\alpha'} + R^*_i w_i + V^*_{1'}w + M^*_{1'1'}\phi_{1'}\right) ds\,, \qquad (4.3.15)
\end{aligned}$$

c.f. [Was82]. Here, A denotes the area of the element, R_i is the concentrated normal force at the i'th corner $R_i = M^+_{1'2'} - M^-_{1'2'}$ where the superscripts $^+$ and $^-$ refer to values calculated at positions $s_i^+ = lim_{\epsilon\to 0}(s+\epsilon)$, $s_i^- = lim_{\epsilon\to 0}(s-\epsilon)$, with ϵ a small positive scalar and $V_{1'}$ is the Kirchhoff force which under the assumption of constant $N^{\alpha\beta}$ and $M^{\alpha\beta}$ becomes $V_{1'} = N_{1'\alpha'}w_{,\alpha'}$. The term $C = C_K + C_T$ describes the total element boundary with C_K being the part of the boundary where kinematic conditions are prescribed and C_T is the part of the boundary where tractions are prescribed. The only subsidiary condition to be satisfied is $\phi_{1'} \equiv -w_{,1'}$. All independent primary quantities u_α, w and $\kappa_{\alpha\beta}$ are subject to arbitrary variation as well as the Lagrange multipliers $N^{\alpha\beta}$, $M^{\alpha\beta}$, $N_{1'\alpha'}$, R_i, $V_{1'}$, $M_{1'1'}$. The $\tilde{u}_{\alpha'}(s)$, $\tilde{w}(s)$ and $\tilde{\phi}_{1'}(s)$ represent prescribed displacements and rotation quantities on C_K with w_i^* being the prescribed displacement w at vertex i. Analogously, $N^*_{1'\alpha'}$, $V^*_{1'}$ and $M^*_{1'1'}$ are the tractions prescribed on C_T with R_i^* being the prescribed concentrated load in direction of n at corner i.

Putting

$$\delta\Pi_G = 0 \qquad (4.3.16)$$

gives all fundamental equations which underlie the displacement formulation of the von Kármán theory. Note that the subsidiary condition

$$\phi_{1'} \equiv -w_{,1'} \qquad (4.3.17)$$

is determined from

$$\begin{aligned} \phi_\alpha &= -w_{,\alpha} \\ \phi_{\alpha'} &= -h^\alpha_{\alpha'} w_{,\alpha} \equiv -w_{,\alpha'} \ . \end{aligned} \tag{4.3.18}$$

The von Kármán patch test refers to displacements u_α and w which provide constant values for $\gamma_{\alpha\beta}$ and $\kappa_{\alpha\beta}$. This entails the requirements for displacements u_α to be complete cubic polynomials, whereas the displacement w has the form of a complete quadratic polynomial. The terms u_α and w can be written in either Cartesian coordinates, *c.f.* Allman [All82], or alternatively in oblique coordinates, *c.f.* Morley [Mor91] and Providas [Pro90].

4.4 The geometrically nonlinear constant moment triangle

The triangle has 12 connectors, *c.f.* Figure 4.2. These are recognizably identical with those from the linear analysis with the superposition of the constant strain triangle of Turner *et al.* [MJTT56] and the displacement version of the constant moment triangle of Morley [Mor71].

The geometrically nonlinear constant moment triangle passes the totality of the von Kármán patch tests for constant strain and constant curvature in the sense that recovery over the patch domain is achieved of displacement w with attendant curvatures $\kappa_{\alpha\beta} = -w_{,\alpha\beta}$ and bending rotations $\phi_\alpha = -w_{,\alpha}$, while recovery of displacements u_α is restricted to their connector positions with recovery of the constant strains $\tilde{\gamma}_{\alpha\beta}$ limited to integrated averages taken over the triangle.

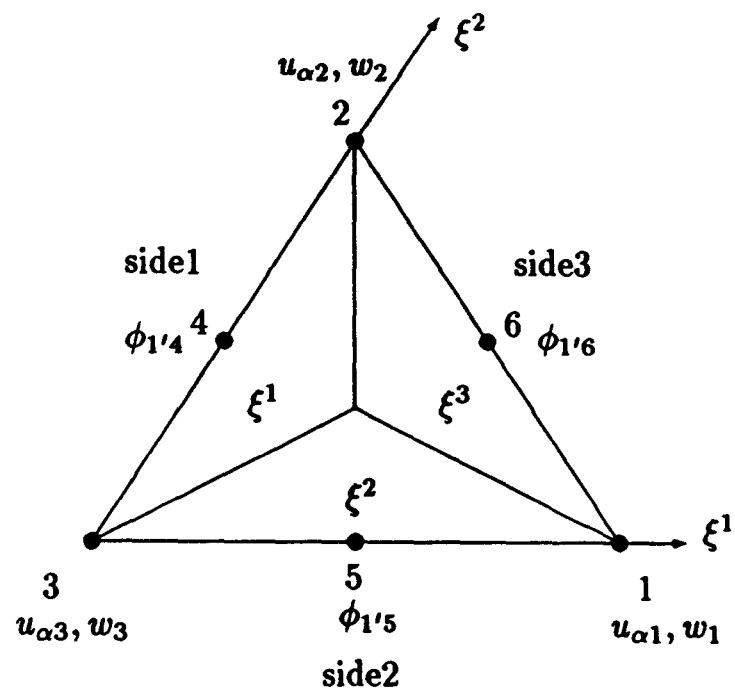

Figure 4.2 Connectors for the geometrically nonlinear constant moment triangle.

It is readily observed that for passing the patch test the u_α and w must be cubic and quadratic polynomials, respectively. On the interelement boundaries, the in-plane displacements $\tilde{u}_\alpha$ and the deflection $\tilde{w}$ vary linearly whereas the normal rotation $\tilde{\phi}_{1'}$ is assumed to be constant along each side. The modified generalized Hu-Washizu variational principle with the constant strain tensor $\tilde{\gamma}_{\alpha\beta}$ is defined by

$$\tilde{\gamma}_{\alpha\beta} = \frac{1}{A}\int_A \gamma_{\alpha\beta}\, dA = \frac{1}{A}\int_A \frac{1}{2}\left(u_{\alpha,\beta} + u_{\beta,\alpha} + w_{,\alpha} w_{,\beta} \right) dA \qquad (4.4.19)$$

where A is the element area. In the distributions for the assumed cubically varying u_α it is found that the terms $\xi^i\xi^j(\xi^i - \xi^j)$ (no sum) and $\xi^1\xi^2\xi^3$ are superfluous to the calculation of $\tilde{\gamma}_{\alpha\beta}$ and hence also to the design of the non-linear triangle which accordingly is proceeded on the basis that the distributions of u_α and w are all quadratically varying. These quadratically varying distributions of u_α and w when substituted into the weak form of the strain/displacement relations give constant strains $\tilde{\gamma}_{\alpha\beta}$ which are identical with those from equation (4.4.19). The first variation of the Hu-Washizu functional then reduces to a statement of virtual work and the remaining finite element formulation proceeds in conventional manner.

Considering the boundary conditions, if side1 coincides with part of the patch boundary, it is then appropriate to prescribe as contributions to the boundary con-

ditions at connectors 2, 4 and 3, *c.f.* . Figure 4.2, the quantities

$$\begin{aligned}
&\frac{1}{2}l_1 N^*_{1'1'} \quad \text{or} \quad u^*_{1'2} \ , \\
&\frac{1}{2}l_1 N^*_{1'2'} \quad \text{or} \quad u^*_{2'2} \ , \\
&\frac{1}{2}l_1 N^*_{1'1'} \quad \text{or} \quad u^*_{1'3} \ , \\
&\frac{1}{2}l_1 N^*_{1'2'} \quad \text{or} \quad u^*_{2'3} \ , \qquad (4.4.20) \\
M^*_{1'2'} - l_1 N^*_{1'1'}&(\frac{1}{2}\phi^*_{1'4} - \frac{1}{12}l_1\kappa^*_{1'2'}) \\
-l_1 N^*_{1'2'}&\{\frac{1}{2l_1}(w^*_2 - w^*_3) - \frac{1}{6}l_1\kappa^*_{2'2'}\} \quad \text{or} \quad w^*_2 \ , \\
-M^*_{1'2'} - l_1 N^*_{1'1'}&(\frac{1}{2}\phi^*_{1'4} + \frac{1}{12}l_1\kappa^*_{1'2'}) \\
-l_1 N^*_{1'2'}&\{\frac{1}{2l_1}(w^*_2 - w^*_3) + \frac{1}{6}l_1\kappa^*_{2'2'}\} \quad \text{or} \quad w^*_3 \ , \\
l_1&\{M^*_{1'1'} + \frac{1}{12}(l_1)^2\kappa^*_{2'2'}N^*_{1'1'}\} \quad \text{or} \quad \phi^*_{1'4'} \ ,
\end{aligned}$$

where an asterisk denotes magnitude at the solution or increment point depending on the case.

4.5 Matrix formulation

A matrix procedure which sets up the left hand side of the nonlinear equations of equilibrium as well as the tangent stiffness matrix is presented in a way convenient for finite element computing in Morley [Mor91] as in the following.

Let

$$\mathbf{a} = (\,\mathbf{u}^T\,\mathbf{w}^T\,\boldsymbol{\kappa}^T\,)^T \qquad (4.5.21)$$

with

$$\begin{aligned}
\mathbf{u} &= (\,u_{11}\,u_{21}\,u_{12}\,u_{22}\,u_{13}\,u_{23}\,)^T \ , \\
\mathbf{w} &= (\,w_1\,w_2\,w_3\,)^T \ , \qquad (4.5.22) \\
\boldsymbol{\kappa} &= (\,\kappa_1\,\kappa_2\,\kappa_3\,)^T \ ,
\end{aligned}$$

where the connectors of **u** are as in Figure 4.2. Also,

$$\boldsymbol{\gamma} = \begin{Bmatrix} \tilde{\gamma}_{11} \\ \tilde{\gamma}_{22} \\ \tilde{\gamma}_{12} \end{Bmatrix} \ ,$$

$$\mathbf{N} = \begin{Bmatrix} N^{11} \\ N^{22} \\ 2N^{12} \end{Bmatrix} , \qquad (4.5.23)$$

$$\mathbf{M} = \begin{Bmatrix} M^{11} \\ M^{22} \\ 2M^{12} \end{Bmatrix} .$$

The finite element derivation described in the prequel reveals that the $\tilde{\gamma}_{\alpha\beta}$ be expressed by

$$\begin{aligned} \tilde{\gamma}_{11} &= u_{11} - u_{13} + \frac{1}{2}(w_1 - w_3)^2 + \frac{1}{24}\{(\kappa_{11})^2 + 2\kappa_{11}\kappa_{22} - 2(\kappa_{12})^2\} , \\ \tilde{\gamma}_{22} &= u_{22} - u_{23} + \frac{1}{2}(w_2 - w_3)^2 + \frac{1}{24}\{(\kappa_{22})^2 + 2\kappa_{11}\kappa_{22} - 2(\kappa_{12})^2\} , \\ \tilde{\gamma}_{12} &= \frac{1}{2}(u_{12} - u_{13} + u_{21} - u_{23}) \\ &\quad + \frac{1}{2}(w_1 - w_3)(w_2 - w_3) + \frac{1}{24}(2\kappa_{11} + 2\kappa_{22} - 3\kappa_{12}) , \end{aligned} \qquad (4.5.24)$$

so that

$$\delta\gamma = \mathbf{B}\delta\mathbf{u} + \mathbf{B}_w\delta\mathbf{w} + \mathbf{B}_\kappa\delta\boldsymbol{\kappa} \qquad (4.5.25)$$

where

$$\mathbf{B} = \frac{1}{2}\begin{pmatrix} 2 & 0 & 0 & 0 & -2 & 0 \\ 0 & 0 & 0 & 2 & 0 & -2 \\ 0 & 1 & 1 & 0 & -1 & -1 \end{pmatrix} ,$$

$$\mathbf{B}_w = \frac{1}{2}\begin{bmatrix} 2(w_1 - w_3) & 0 & -2(w_1 - w_3) \\ 0 & 2(w_2 - w_3) & -2(w_2 - w_3) \\ w_2 - w_3 & w_1 - w_3 & -w_1 - w_2 + 2w_3 \end{bmatrix} , \qquad (4.5.26)$$

$$\mathbf{B}_\kappa = \frac{1}{12}\begin{bmatrix} \kappa_{11} + \kappa_{22} & \kappa_{11} & -2\kappa_{12} \\ \kappa_{22} & \kappa_{11} + \kappa_{22} & -2\kappa_{12} \\ \kappa_{12} & \kappa_{12} & \kappa_{11} + \kappa_{22} - 3\kappa_{12} \end{bmatrix} .$$

Since

$$\begin{aligned} \mathbf{B}_w\delta\mathbf{w} &= \delta\mathbf{B}_w\mathbf{w} , \\ \mathbf{B}_\kappa\delta\boldsymbol{\kappa} &= \delta\mathbf{B}_\kappa\boldsymbol{\kappa} , \end{aligned} \qquad (4.5.27)$$

it follows that

$$\boldsymbol{\gamma} = \mathbf{B}\mathbf{u} + \frac{1}{2}\mathbf{B}_w\mathbf{w} + \frac{1}{2}\mathbf{B}_\kappa\boldsymbol{\kappa} . \qquad (4.5.28)$$

The practical components for the strains and curvatures are as defined in Table 4.1 so that

$$\begin{aligned} \tilde{\gamma}_{\alpha'\beta'} &= h^{\alpha}_{\alpha'} h^{\beta}_{\beta'} \tilde{\gamma}_{\alpha\beta} \ , \\ \kappa_{\alpha'\beta'} &= h^{\alpha}_{\alpha'} h^{\beta}_{\beta'} \kappa_{\alpha\beta} \ . \end{aligned} \tag{4.5.29}$$

With

$$\begin{aligned} \gamma' &= \left\{ \begin{array}{c} \gamma_{1'1'} \\ \gamma_{2'2'} \\ \gamma_{1'2'} \end{array} \right\} \ , \\ \kappa' &= \left\{ \begin{array}{c} \kappa_{1'1'} \\ \kappa_{2'2'} \\ \kappa_{1'2'} \end{array} \right\} \ , \end{aligned} \tag{4.5.30}$$

this becomes in matrix notation

$$\begin{aligned} \gamma' &= \mathbf{H}\gamma \ , \\ \kappa' &= \mathbf{H}\kappa \ , \end{aligned} \tag{4.5.31}$$

where H is the matrix containing the practical components used for transformation between local oblique and global systems and is given by

$$\mathbf{H} = \left[\begin{array}{ccc} h^1_{1'} h^1_{1'} & h^2_{1'} h^2_{1'} & 2h^1_{1'} h^2_{1'} \\ h^1_{2'} h^1_{2'} & h^2_{2'} h^2_{2'} & 2h^1_{2'} h^2_{2'} \\ h^1_{1'} h^1_{2'} & h^2_{1'} h^2_{2'} & h^1_{1'} h^2_{2'} + h^2_{1'} h^1_{2'} \end{array} \right] \tag{4.5.32}$$

which has the inverse

$$\mathbf{H}^{-1} = \left[\begin{array}{ccc} h^{1'}_1 h^{1'}_1 & h^{2'}_1 h^{2'}_1 & 2h^{1'}_1 h^{2'}_1 \\ h^{1'}_2 h^{1'}_2 & h^{2'}_2 h^{2'}_2 & 2h^{1'}_2 h^{2'}_2 \\ h^{1'}_1 h^{1'}_2 & h^{2'}_1 h^{2'}_2 & h^{1'}_1 h^{2'}_2 + h^{1'}_2 h^{2'}_1 \end{array} \right] \ . \tag{4.5.33}$$

Introducing the further notations

$$\begin{aligned} \mathbf{N}' &= \left\{ \begin{array}{c} N_{1'1'} \\ N_{2'2'} \\ N_{1'2'} \end{array} \right\} \ , \\ \mathbf{M}' &= \left\{ \begin{array}{c} M_{1'1'} \\ M_{2'2'} \\ M_{1'2'} \end{array} \right\} \ , \end{aligned} \tag{4.5.34}$$

with

$$\mathbf{D}' = \frac{Eh}{1-\nu^2}\begin{bmatrix} 1 & \nu & 0 \\ & 1 & 0 \\ \text{sym} & & 2(1-\nu^2) \end{bmatrix} \tag{4.5.35}$$

appropriate to a triangle made of isotropic material with E the Young's modulus, ν the Poisson's ratio and h the thickness, it then follows that

$$\mathbf{N} = \mathbf{H}^T\mathbf{N}' \ , \ \mathbf{M} = \mathbf{H}^T\mathbf{M}' \tag{4.5.36}$$

with inverses

$$\mathbf{N}' = (\mathbf{H}^{-1})^T\mathbf{N} \ , \ \mathbf{M}' = (\mathbf{H}^{-1})^T\mathbf{M} \tag{4.5.37}$$

which allows the constitutive relations to be written as

$$\begin{aligned} \mathbf{N}' = \mathbf{D}'\boldsymbol{\gamma}' \quad , \quad \mathbf{M}' &= \frac{h^2}{12}\mathbf{D}'\boldsymbol{\kappa}' \\ \mathbf{N} = \mathbf{H}^T\mathbf{D}'\mathbf{H}\boldsymbol{\gamma} = \mathbf{D}\boldsymbol{\gamma} \quad , \quad \mathbf{M} &= \frac{h^2}{12}\mathbf{D}\boldsymbol{\kappa} \end{aligned} \tag{4.5.38}$$

where

$$\mathbf{D} = \mathbf{H}^T\mathbf{D}'\mathbf{H} \ . \tag{4.5.39}$$

Using the reduced Hu-Washizu functional, the total strain energy Π is written as

$$\begin{aligned} \Pi &= \frac{1}{2}\int_A\int (N^{\alpha\beta}\tilde{\gamma}_{\alpha\beta} + M^{\alpha\beta}\kappa_{\alpha\beta})\, dA \\ &= \frac{A}{2}(\boldsymbol{\gamma}^T\mathbf{D}\boldsymbol{\gamma} + \frac{h^2}{12}\boldsymbol{\kappa}^T\mathbf{D}\boldsymbol{\kappa}) \\ &= \frac{A}{2}[(\mathbf{u}^T\mathbf{B}^T + \frac{1}{2}\mathbf{w}^T\mathbf{B}_w^T + \frac{1}{2}\boldsymbol{\kappa}^T\mathbf{B}_\kappa^T)\mathbf{D}(\mathbf{B}\mathbf{u} + \frac{1}{2}\mathbf{B}_w\mathbf{w} + \frac{1}{2}\mathbf{B}_\kappa\boldsymbol{\kappa}) + \frac{h^2}{12}\boldsymbol{\kappa}^T\mathbf{D}\boldsymbol{\kappa}] \\ &= \mathbf{a}^T\mathbf{K}_{SE}\,\mathbf{a} \end{aligned} \tag{4.5.40}$$

where $\mathbf{K}_{SE}$ is the symmetrical matrix

$$\mathbf{K}_{SE} = A\begin{bmatrix} \mathbf{B}^T\mathbf{D}\mathbf{B} & \frac{1}{2}\mathbf{B}^T\mathbf{D}\mathbf{B}_w & \frac{1}{2}\mathbf{B}^T\mathbf{D}\mathbf{B}_\kappa \\ & \frac{1}{4}\mathbf{B}_w^T\mathbf{D}\mathbf{B}_w & \frac{1}{4}\mathbf{B}_w^T\mathbf{D}\mathbf{B}_\kappa \\ \text{sym} & & \frac{1}{4}\mathbf{B}_\kappa{}^T\mathbf{D}\mathbf{B}_\kappa + \frac{h^2}{12}\mathbf{D} \end{bmatrix} . \tag{4.5.41}$$

Taking a variation $\delta\Pi$ gives

$$\begin{aligned} \delta\Pi &= A(\delta\boldsymbol{\gamma}\mathbf{D}\boldsymbol{\gamma} + \frac{h^2}{12}\delta\boldsymbol{\kappa}^T\mathbf{D}\boldsymbol{\kappa}) \\ &= A\{(\delta\mathbf{u}^T\mathbf{B}^T + \delta\mathbf{w}^T\mathbf{B}_w^T + \delta\boldsymbol{\kappa}^T\mathbf{B}_\kappa^T)\mathbf{D}(\mathbf{B}\mathbf{u} + \frac{1}{2}\mathbf{B}_w\mathbf{w} + \frac{1}{2}\mathbf{B}_\kappa\boldsymbol{\kappa}) + \frac{h^2}{12}\delta\boldsymbol{\kappa}^T\mathbf{D}\boldsymbol{\kappa}\} \\ &= \delta\mathbf{a}^T\mathbf{K}\,\mathbf{a} \end{aligned} \tag{4.5.42}$$

where **K** is the asymmetrical stiffness matrix

$$\mathbf{K} = A \begin{bmatrix} \mathbf{B}^T\mathbf{D}\mathbf{B} & \frac{1}{2}\mathbf{B}^T\mathbf{D}\mathbf{B}_w & \frac{1}{2}\mathbf{B}^T\mathbf{D}\mathbf{B}_\kappa \\ \mathbf{B}_w^T\mathbf{D}\mathbf{B} & \frac{1}{2}\mathbf{B}_w^T\mathbf{D}\mathbf{B}_w & \frac{1}{2}\mathbf{B}_w^T\mathbf{D}\mathbf{B}_\kappa \\ \mathbf{B}_\kappa^T\mathbf{D}\mathbf{B} & \frac{1}{2}\mathbf{B}_\kappa^T\mathbf{D}\mathbf{B}_w & \frac{1}{2}\mathbf{B}_\kappa{}^T\mathbf{D}\mathbf{B}_\kappa + \frac{h^2}{12}\mathbf{D} \end{bmatrix} . \tag{4.5.43}$$

The column matrix **Ka** now gives the left hand side of the nonlinear equations of equilibrium, *i.e.* the generalized forces, taken with respect to the variations $\delta\mathbf{a}^T$ as

$$\mathbf{K}\mathbf{a} = A \begin{Bmatrix} \mathbf{B}^T\mathbf{N} \\ \mathbf{B}_w^T\mathbf{N} \\ \mathbf{B}_\kappa^T\mathbf{N} + \mathbf{M} \end{Bmatrix} \tag{4.5.44}$$

$$= A \begin{Bmatrix} N^{11} \\ N^{12} \\ N^{12} \\ N^{22} \\ -(N^{11} + N^{22}) \\ -(N^{22} + N^{12}) \\ (w_1 - w_3)N^{11} + (w_2 - w_3)N^{12} \\ (w_2 - w_3)N^{22} + (w_1 - w_3)N^{12} \\ -(w_1 - w_3)N^{11} - (w_2 - w_3)N^{22} - (w_1 + w_2 - 2w_3)N^{12} \\ \frac{1}{12}(N^{\alpha\beta}\kappa_{\alpha\beta} + N^{11}\kappa_{22}) + M^{11} \\ \frac{1}{12}(N^{\alpha\beta}\kappa_{\alpha\beta} + N^{22}\kappa_{11}) + M^{22} \\ \frac{1}{6}\{-N^{11}\kappa_{12} - N^{22}\kappa_{12} + N^{12}(\kappa_{11} + \kappa_{22} - 3\kappa_{12})\} + 2M^{12} \end{Bmatrix} .$$

The tangent stiffness matrix is derived by first writing

$$\begin{aligned} \mathbf{B}_w^T\mathbf{D}\boldsymbol{\gamma} &= \mathbf{B}_w^T\mathbf{N} = \mathbf{B}_{Gw}\mathbf{w} , \\ \mathbf{B}_\kappa^T\mathbf{D}\boldsymbol{\gamma} &= \mathbf{B}_\kappa^T\mathbf{N} = \mathbf{B}_{G\kappa}\boldsymbol{\kappa} , \end{aligned} \tag{4.5.45}$$

where $\mathbf{B}_{Gw}$ and $\mathbf{B}_{G\kappa}$ are the symmetric geometric stiffness matrices

$$\mathbf{B}_{Gw} = \begin{bmatrix} N^{11} & N^{12} & -(N^{11} + N^{12}) \\ & N^{22} & -(N^{22} + N^{12}) \\ \text{sym} & & N^{11} + N^{22} + 2N^{12} \end{bmatrix} ,$$

$$\mathbf{B}_{G\kappa} = \frac{1}{12} \begin{bmatrix} N^{11} & N^{11} + N^{12} & 2N^{12} \\ & N^{22} & 2N^{12} \\ \text{sym} & & -2(N^{11} + N^{22} + 3N^{12}) \end{bmatrix} . \tag{4.5.46}$$

Therefore

$$\begin{aligned} \delta \mathbf{B}_w^T \mathbf{N} &= \mathbf{B}_{Gw}\, \delta \mathbf{w} \ , \\ \delta \mathbf{B}_\kappa^T \mathbf{N} &= \mathbf{B}_{G\kappa}\, \delta \boldsymbol{\kappa} \ . \end{aligned} \tag{4.5.47}$$

The second variation $\delta^2 \Pi$ of equation (4.5.40) gives

$$\delta^2 \Pi = A\,(\delta^2 \boldsymbol{\gamma}^T \mathbf{D} \boldsymbol{\gamma} + \delta \boldsymbol{\gamma} \mathbf{D} \delta \boldsymbol{\gamma} + \frac{h^2}{12} \delta \boldsymbol{\kappa}^T \mathbf{D} \delta \boldsymbol{\kappa}) \tag{4.5.48}$$

which can be written as

$$\delta^2 \Pi = \delta \mathbf{a}^T \mathbf{K}_T\, \delta \mathbf{a} \tag{4.5.49}$$

where $\mathbf{K}_T$ is the symmetrical tangent stiffness matrix

$$\mathbf{K}_T = A \begin{bmatrix} \mathbf{B}^T \mathbf{D} \mathbf{B} & \mathbf{B}^T \mathbf{D} \mathbf{B}_w & \mathbf{B}^T \mathbf{D} \mathbf{B}_\kappa \\ & \mathbf{B}_w^T \mathbf{D} \mathbf{B}_w + \mathbf{B}_{Gw} & \mathbf{B}_w^T \mathbf{D} \mathbf{B}_\kappa \\ \text{sym} & & \mathbf{B}_\kappa^T \mathbf{D} \mathbf{B}_\kappa + \mathbf{B}_{G\kappa} + \frac{h^2}{12} \mathbf{D} \end{bmatrix} . \tag{4.5.50}$$

The connectors $u_{\alpha j}$, w_j, $\kappa_{\alpha\beta}$ in equations (4.5.21) and (4.5.22) are readily transformed to the global connectors U_j^i, $\phi_{1'4}$, $\phi_{1'5}$, $\phi_{1'6}$ of shell space first by noting equations (4.3.12) and (4.2.3) which give

$$u_{\alpha j} = x^i_{,\alpha}\, U_j^i \tag{4.5.51}$$

where the $x^i_{,\alpha}$ are defined in equations (4.2.4) and by noting equations (4.2.9) which give

$$w_j = n^i\, U_j^i \tag{4.5.52}$$

where the n^i are defined by equations (4.2.10). The $\kappa_{\alpha\beta}$ are then transformed by

$$\begin{aligned} \kappa_{11} &= \frac{4A}{l_1}\phi_{1'4} + \frac{4A}{l_3}\phi_{1'6} - \frac{l_{23}}{(l_3)^2} w_1 + \{\frac{l_{12}}{(l_1)^2} + \frac{l_{23}}{(l_3)^2}\} w_2 - \frac{l_{12}}{(l_1)^2} w_3 \ , \\ \kappa_{22} &= \frac{4A}{l_2}\phi_{1'5} + \frac{4A}{l_3}\phi_{1'6} + \{\frac{l_{12}}{(l_2)^2} + \frac{l_{31}}{(l_3)^2}\} w_1 - \frac{l_{31}}{(l_3)^2}\} w_2 - \frac{l_{12}}{(l_2)^2} w_3 \ , \\ \kappa_{12} &= \frac{4A}{l_3}\phi_{1'6} + \frac{l_{31}}{(l_3)^2} w_1 + \frac{l_{23}}{(l_3)^2} w_2 - 2 w_3 \ , \end{aligned} \tag{4.5.53}$$

where the relationships are obtained through the finite element derivation.

Chapter 5

On the general theory of the stability of equilibrium of discrete conservative systems

5.1 Introduction

The general theory of the stability of equilibrium of conservative systems was founded by Koiter in his now celebrated dissertation 'On the stability of elastic equilibrium' [Koi45]. The energy criterion for stability of equilibrium of a conservative system requires that the total potential energy, consisting of the sum of internal and external energy, has a local minimum. This forms the basis of Koiter's work. He assumes that the total potential energy can be expanded in a Taylor's series in ascending powers of the displacements (and their derivatives) of an elastic body and his analysis proceeds, by investigation of a sequence of minimum problems, to establish the basic results accepted today. While his early formulation relates specifically to continuous conservative systems, it is possible to adapt it to obtain a perturbation analysis of a discrete conservative system with a finite number of variables, as encountered in present computer techniques like the finite element method.

In contrast to the perturbation methods, there exists another class of solution techniques where the governing nonlinear equations of a discrete conservative system are solved iteratively at different values of the parameter to find points which define

equilibrium paths. For this type of iterative approach it is useful to have available a version of the theory which, from the outset, features a natural parameter of the system as the independent variable. Modern finite element methods generally employ solution techniques of this class.

The potential energy function of a discrete conservative system, like that resulting from the finite element analysis of elastic plates and shells, may be written

$$\Pi = \Pi(\mathbf{a}, \lambda) , \tag{5.1.1}$$

where the elements of the displacement vector $\mathbf{a}$ are taken as the generalized coordinates of the system which describe its state of deformation and λ represents the intensity of the applied loads. Equation (5.1.1) is a more general form of equation (3.2.5) where λ has a specified value. The equilibrium equations follow as usual from the stationary nature of Π and we may write

$$\mathbf{f}(\mathbf{a}, \lambda) = \mathbf{K}\,\mathbf{a} - \mathbf{p} = 0 , \tag{5.1.2}$$

where

$$f_i(\mathbf{a}, \lambda) = \Pi_{,i} = 0 \quad , \quad i = 1, .., n , \tag{5.1.3}$$

with n denoting the total number of degrees of freedom in the system and the subscript $_{,i}$ indicates partial differentiation with respect to the displacement parameter $\mathbf{a}_i$. In general, equation (5.1.2) is nonlinear in $\mathbf{a}$ and λ. For conservative proportional loading the load vector $\mathbf{p}$ may be expressed as

$$\mathbf{p} = \lambda \mathbf{p}^* , \tag{5.1.4}$$

where $\mathbf{p}^*$ is a constant vector of reference loads.

Every solution $\mathbf{a}$ of equation (5.1.2) for a given value of λ describes an equilibrium state which can be represented with the point $(\mathbf{a}, \lambda)$ in an $(n + 1)$ dimensional space spanned by the generalized coordinates and the load intensity. The set of all equilibrium points derived through continuous deformation from the undeformed state $(\mathbf{a} = 0, \lambda = 0)$ define a curve which is referred to as the *primary* or the *fundamental equilibrium path.* It is usual in the solution of nonlinear problems that for a given value of λ more than one equilibrium solution $\mathbf{a}$ may exist. This means that *secondary equilibrium paths* may exist and usually appear as branches to the fundamental equilibrium path at bifurcation points.

Equilibrium paths (or parts of an equilibrium path) can be stable or unstable. Stable equilibrium configurations are characterized by a positive definite tangent stiffness matrix (Hessian matrix),

$$\Pi_{,ij} = \mathbf{K}_T \quad , \quad i,j = 1,..,n \; . \tag{5.1.5}$$

Unstable equilibrium states are characterized by an indefinite $\Pi_{,ij}$. The transitional state from a stable to an unstable configuration or vice versa is marked by a singular $\Pi_{,ij}$ and it is called *critical state.* The corresponding point on the equilibrium path is called *singular point* or *critical point.*

In the following, the general theory of the stability of equilibrium of discrete conservative systems is used for an approach that features a natural parameter, such as the applied loading of a system, as the independent variable: all results are thus conveniently established without recourse to any artificial parameters. In section 5.2 the criteria for identifying singular (critical) points, which include bifurcation points and limit points, and determining their stability are obtained in a simple matrix form suitable for computation in the form of so-called stability coefficients. Note that section 5.2 is based on a report by Bangemann [Ban92] which itself is based on a paper by Allman [All89b]. Section 5.3 is based on a report by Morley [Mor94] and provides an alternative equivalent formulation for computing the above mentioned stability coefficients by making direct use of higher order directional derivatives.

5.2 Matrix interpretation of the general theory of the stability of equilibrium of discrete conservative systems

5.2.1 Introduction

A derivation of the theory of the stability of equilibrium of discrete conservative systems is given which conveniently establishes all results in a simple matrix form suitable for finite element computation. First, the criteria for identifying the type of a singular point are obtained by an application of the differential calculus to the equilibrium equations of a system. The stability of equilibrium of a singular point is then determined by consideration of an increment of the total potential energy

expressed as a Taylor series expansion in terms of differentials of energy, instead of the equivalent series expansion in terms of displacements and their derivatives proposed by Koiter.

Critical points can be either limit points or bifurcation points. They are marked by a singular tangent stiffness matrix. Limit points occur when the tangent to the load-deflection curve becomes horizontal. Bifurcation points are points on the solution path from which the solution may proceed along several paths, some stable and the others unstable.

The results obtained for singular points using the differential theory are, of course, essentially the same as those of Koiter and other authors; but the present analysis displays all the basic features by a direct, unified formulation which should prove useful for practical calculations.

5.2.2 Singular points in discrete conservative systems

The potential energy function of a discrete conservative system is assumed to be a continuously differentiable form

$$\Pi = \Pi(\mathbf{a}, \lambda) = \Pi(a_1, ..., a_n, \lambda) \tag{5.2.1}$$

where the variables a_i describe the degrees of freedom and λ is the intensity of applied loading. An equilibrium state of such a system, for a specified value of λ, is associated with a stationary value of the potential energy function Π; the corresponding a_i are then functions of the independent variable λ which are determined implicitly by the nonlinear equations of equilibrium from

$$\delta\Pi = 0 \tag{5.2.2}$$

where

$$\delta\Pi = \sum_{i=1}^{n} \frac{\partial \Pi}{\partial a_i} \delta a_i \ . \tag{5.2.3}$$

Consider

$$\Pi = \Pi_s + \Pi_\lambda \tag{5.2.4}$$

with the strain energy Π_s given by

$$\Pi_s = \frac{1}{2} \mathbf{a}^T \mathbf{K_{SE}} \mathbf{a} \ , \tag{5.2.5}$$

$\mathbf{K_{SE}}$ being the appropriate $(n \times n)$-matrix in the finite element context. The loading is contained in

$$\Pi_\lambda = -\mathrm{A}\,\lambda\,(\mathbf{p}^*)^T\,\mathbf{a} \tag{5.2.6}$$

where A is the area considered, λ is the loading intensity and $\mathbf{p}^*$ is the constant reference load vector.

Altogether we thus get

$$\Pi = \frac{1}{2}\mathbf{a}^T\,\mathbf{K_{SE}}\,\mathbf{a} + L^\lambda\,(\mathbf{p}^*)^T\,\mathbf{a} \tag{5.2.7}$$

with

$$L^\lambda = -\mathrm{A}\,\lambda\ . \tag{5.2.8}$$

The first variation $\delta\Pi$ then becomes

$$\delta\Pi = \delta\mathbf{a}^T\,\mathbf{K}\,\mathbf{a} + L^\lambda\,(\mathbf{p}^*)^T\,\delta\mathbf{a} \tag{5.2.9}$$

with the appropriate stiffness matrix K, yielding the nonlinear equilibrium equations

$$\Pi_{,a_i} = \mathbf{K}\,\mathbf{a} + L^\lambda\,\mathbf{p}^* = \mathbf{0}\ . \tag{5.2.10}$$

The second variation $\delta^2\Pi$ is given by

$$\delta^2\Pi = \delta\mathbf{a}^T\,\mathbf{K}_T\,\delta\mathbf{a} \tag{5.2.11}$$

where the symmetric tangent stiffness matrix $\mathbf{K}_T$ has eigenvalues $\theta^{(r)}$ and corresponding eigenvectors $\xi^{(r)}$ defined relative to an (arbitrary) positive definite symmetric matrix T by the equations

$$\begin{aligned} \mathbf{K}_T\,\xi^{(r)} &= \theta^{(r)}\,\mathbf{T}\,\xi^{(r)} \quad (\text{no sum on } r)\ , \\ (\xi^{(r)})^T\,\mathbf{T}\,\xi^{(r)} &= 1\ . \end{aligned} \tag{5.2.12}$$

A minimum point of Π corresponds to a state of stable equilibrium of the system and the associated positive definite matrix $\mathbf{K}_T$ has all positive eigenvalues $\theta^{(r)}$. If the matrix $\mathbf{K}_T$, evaluated at an equilibrium point, has any negative eigenvalues then the potential energy function attains local maxima in the directions of the corresponding eigenvectors and this state of the system is one of unstable equilibrium. The transition from stable to unstable equilibrium occurs when at least one eigenvalue,

say $\theta^{(1)}$, becomes zero; the matrix $\mathbf{K}_T$ is then singular and this point on an equilibrium path is accordingly termed a *singular point* or *critical point.* Singular points indicate either that there is a bifurcation of the equilibrium path into alternative, stable or unstable, branches or that a limit point has been reached. It is therefore important to detect and calculate singular points in addition to stable points on an equilibrium path. Attention is restricted here to 'simple' singular points on a stable equilibrium path, *i.e.* where just one eigenvalue of the matrix $\mathbf{K}_T$ is equal to zero, so that the eigenvalues $\theta^{(r)}$ are given by

$$\theta^{(n)} \geq \ldots \geq \theta^{(2)} > \theta^{(1)} = 0 \ . \tag{5.2.13}$$

Consider a differential change $d\lambda$ in the parameter λ which produces a differential change $\mathbf{da}$ in the dependent variable $\mathbf{a}$; from equation (5.2.2) the total differentials $d(\delta\Pi)$ of the equilibrium equations in equation (5.2.10) of a system vanish, so that $d\lambda$ and $\mathbf{da}$ satisfy

$$d(\delta\Pi) = 0 \tag{5.2.14}$$

entailing

$$\mathbf{K}_T \, \mathbf{da} + L \, \mathbf{p}^* \, d\lambda = \mathbf{0} \tag{5.2.15}$$

with

$$L = \frac{\partial L^\lambda}{\partial \lambda} = -\mathrm{A} \tag{5.2.16}$$

and

$$\mathbf{da} = (da_1, \ldots, da_n)^T \ . \tag{5.2.17}$$

If $\mathbf{K}_T$ is nonsingular, equation (5.2.15) can be solved for the differential $\mathbf{da}$, but a simple estimate $(a_i + da_i)$ of the coordinates of a neighbouring point on the equilibrium path is a good approximation only if $d\lambda$ is sufficiently small. Practical calculation of points on an equilibrium path requires more sophisticated methods than merely repeated solutions of equation (5.2.15). At a singular point, however, equation (5.2.15) cannot be solved, but the nature of the point can be investigated by forming the components of $d(\Pi_{,a_i})$ in the directions of each eigenvector $\xi^{(r)}$ of equations (5.2.12) to obtain a new system of equations

$$\theta^{(r)} \, (\xi^{(r)})^T \, \mathbf{T} \, \mathbf{da} + (\xi^{(r)})^T \, L \, \mathbf{p}^* \, d\lambda = 0 \ . \tag{5.2.18}$$

Directing attention at the first of these equations, with $r = 1$ and $\theta^{(1)} = 0$, and defining the *first order stability coefficient* μ as

$$\mu = (\xi^{(1)})^T (\frac{\partial(\Pi_{,a_i})}{\partial\lambda}) \tag{5.2.19}$$

or, equivalently,

$$\mu = (\xi^{(1)})^T L\, \mathbf{p}^* \tag{5.2.20}$$

shows that

$$\begin{aligned} &\text{either} \quad \mu \neq 0 \quad \text{and} \quad d\lambda = 0 \\ &\text{or} \quad \mu = 0 \quad \text{and} \quad d\lambda \text{ indeterminate} . \end{aligned} \tag{5.2.21}$$

The first of equations (5.2.21) is the condition for a limit point. Since $d\lambda = 0$, but $\theta^{(r)} \neq 0$ for $r > 1$ in the remaining $(n-1)$ equations, it follows that

$$(\xi^{(r)})^T \mathbf{T}\, \mathbf{da} = 0 \quad \text{for all} \quad r > 1 \tag{5.2.22}$$

whence it is deduced that the differential changes in the dependent variables at a limit point are proportional to the eigenvector $\xi^{(1)}$, *i.e.*

$$\mathbf{da} = \xi^{(1)}\, ds \tag{5.2.23}$$

where ds is a differential amplitude which has, as yet, an unspecified magnitude. The second of equations (5.2.21) is the condition for a bifurcation point. Now it follows from equation (5.2.18) that

$$(\xi^{(r)})^T \mathbf{T}\, \mathbf{da} = -\frac{1}{\theta^{(r)}} (\xi^{(r)})^T (\frac{\partial(\Pi_{,a_i})}{\partial\lambda})\, d\lambda \quad \text{for all } r > 1 \tag{5.2.24}$$

which implies that the differential **da** at a bifurcation point takes a more general form than that given in equation (5.2.23) for a limit point, namely

$$\mathbf{da} = \xi^{(1)}\, ds + \mathbf{b}\, d\lambda \tag{5.2.25}$$

where the components of the vector $\mathbf{b} = (b_1, b_2, ..., b_n)^T$ are

$$b_i = \sum_{r=2}^{n} \beta^{(r)}\, \xi_i^{(r)} \quad \text{for } i = 1, ..., n , \tag{5.2.26}$$

i.e.

$$\mathbf{b} = \mathbf{E}\boldsymbol{\beta} , \tag{5.2.27}$$

where

$$\mathbf{E} = \begin{bmatrix} 0 & \xi_1^{(2)} & -- & \xi_1^{(n)} \\ 0 & \xi_2^{(2)} & -- & \xi_2^{(n)} \\ 0 & \xi_3^{(2)} & -- & \xi_3^{(n)} \\ | & | & | & | \\ | & | & | & | \\ 0 & \xi_n^{(2)} & -- & \xi_n^{(n)} \end{bmatrix} , \; \boldsymbol{\beta} = \begin{pmatrix} 0 \\ \beta^{(2)} \\ \beta^{(3)} \\ | \\ | \\ \beta^{(n)} \end{pmatrix} . \tag{5.2.28}$$

The coefficients $\beta^{(r)}$ are calculated by substituting equation (5.2.25) and equation (5.2.26) into equation (5.2.24) to obtain, using the second of equations (5.2.12),

$$\beta^{(r)} = -\frac{1}{\theta^{(r)}} (\xi^{(r)})^T (\frac{\partial(\Pi_{,a_i})}{\delta\lambda}) \tag{5.2.29}$$

or, in matrix notation,

$$\boldsymbol{\beta} = \Theta \, \mathbf{E}^T (\frac{\partial(\Pi_{,a_i})}{\delta\lambda}) \tag{5.2.30}$$

where $\mathbf{E}$ is as in equations (5.2.28) and the diagonal matrix Θ contains the eigenvalues in the form

$$\Theta = \begin{bmatrix} 0 & 0 & 0 & 0 & -- & 0 \\ 0 & -\frac{1}{\theta^{(2)}} & 0 & 0 & -- & 0 \\ 0 & 0 & -\frac{1}{\theta^{(3)}} & 0 & -- & 0 \\ | & | & | & | & | & | \\ | & | & | & | & | & | \\ 0 & 0 & 0 & 0 & -- & -\frac{1}{\theta^{(n)}} \end{bmatrix} . \tag{5.2.31}$$

Therefore, the vector $\mathbf{b}$ can be written as

$$\mathbf{b} = \mathbf{E} \, \Theta \, \mathbf{E}^T (\frac{\partial(\Pi_{,a_i})}{\partial\lambda}) \, . \tag{5.2.32}$$

It is necessary to employ a higher order approximation for further investigation of the bifurcation point and the limit point. This is accomplished by generating the second total differential $d^2(\delta\Pi)$ of equation (5.2.14) and by stipulating that

$$d^2(\delta\Pi) = 0 \tag{5.2.33}$$

in order to then get, *c.f.* equation (5.2.15) and equation (5.2.19),

$$d\{\mathbf{K}_T \, \mathbf{da} + (\frac{\partial(\Pi_{,a_i})}{\partial\lambda}) d\lambda\} = 0 \tag{5.2.34}$$

revealing

$$\mathbf{K}_T(\mathbf{d}^2\mathbf{a}) + (\frac{\partial(\Pi_{,a_i})}{\partial\lambda})(d^2\lambda) + (\partial\mathbf{K}_T(\mathbf{da}))\,\mathbf{da} + 2\,\delta(\frac{\partial(\Pi_{,a_i})}{\partial\lambda})\,\mathbf{da}\,d\lambda + (\frac{\partial^2(\Pi_{a_i})}{\partial\lambda^2})(d\lambda)^2 = 0\ . \tag{5.2.35}$$

Here, the term $(\partial\mathbf{K}_T(\mathbf{da}))$ in equation (5.2.35) is defined by

$$(\partial\mathbf{K}_T(\mathbf{da})) := \begin{bmatrix} (\frac{\partial\{(\mathbf{K}_T)_{11}\}}{\partial a_1},...,\frac{\partial\{(\mathbf{K}_T)_{11}\}}{\partial a_n})\,\mathbf{da} & - - - & (\frac{\partial\{(\mathbf{K}_T)_{1n}\}}{\partial a_1},...,\frac{\partial\{(\mathbf{K}_T)_{1n}\}}{\partial a_n})\,\mathbf{da} \\ | & - - - & | \\ | & - - - & | \\ (\frac{\partial\{(\mathbf{K}_T)_{n1}\}}{\partial a_1},...,\frac{\partial\{(\mathbf{K}_T)_{n1}\}}{\partial a_n})\,\mathbf{da} & - - - & (\frac{\partial\{(\mathbf{K}_T)_{nn}\}}{\partial a_1},...,\frac{\partial\{(\mathbf{K}_T)_{nn}\}}{\partial a_n})\,\mathbf{da} \end{bmatrix} \tag{5.2.36}$$

where $\mathbf{K}_T$ has entries

$$\mathbf{K}_T = [\mathbf{K}_T]_{ij} \quad , \quad i,j = 1,..,n\ . \tag{5.2.37}$$

Forming now the components of $d^2(\Pi_{,a_i})$ in the directions of the eigenvectors $\boldsymbol{\xi}^{(r)}$ and using equations (5.2.12) provides the result, *c.f.* equation (5.2.35),

$$\begin{aligned} (\boldsymbol{\xi}^{(r)})^T\,d^2(\Pi_{,a_i}) &= \theta^{(r)}\,(\boldsymbol{\xi}^{(r)})^T\,\mathbf{T}\,(\mathbf{d}^2\mathbf{a}) \\ &\quad + (\boldsymbol{\xi}^{(r)})^T\,(\frac{\partial(\Pi_{,a_i})}{\partial\lambda})(d^2\lambda) \\ &\quad + (\boldsymbol{\xi}^{(r)})^T\,(\partial\mathbf{K}_T(\mathbf{da}))\,\mathbf{da} \\ &\quad + 2\,(\boldsymbol{\xi}^{(r)})^T\,\delta(\frac{\partial(\Pi_{,a_i})}{\partial\lambda})\,\mathbf{da}\,d\lambda \\ &\quad + (\boldsymbol{\xi}^{(r)})^T\,(\frac{\partial^2(\Pi_{,a_i})}{\partial\lambda^2})(d\lambda)^2 \\ &= 0\ . \end{aligned} \tag{5.2.38}$$

Directing attention, again, at the first of these equations, with $r = 1$ and $\theta^{(1)} = 0$, and substituting equation (5.2.25) for **da** gives a quadratic equation for calculating the differential amplitude ds in terms of known quantities $d\lambda$ and $(d^2\lambda)$, namely

$$A\,(ds)^2 + 2\,B\,ds\,d\lambda + C\,(d\lambda)^2 = -\,\mu\,(d^2\lambda) \tag{5.2.39}$$

where μ is defined in equation (5.2.19) and the *second order stability coefficients* A, B and C are

$$\begin{aligned} A &= (\boldsymbol{\xi}^{(1)})^T\,(\partial\mathbf{K}_T(\boldsymbol{\xi}^{(1)}))\,\boldsymbol{\xi}^{(1)}\ , \\ B &= (\boldsymbol{\xi}^{(1)})^T\,(\partial\mathbf{K}_T(\mathbf{b}))\,\boldsymbol{\xi}^{(1)} + (\boldsymbol{\xi}^{(1)})^T\,(\frac{\partial\mathbf{K}_T}{\partial\lambda})\,\boldsymbol{\xi}^{(1)}\ , \\ C &= (\boldsymbol{\xi}^{(1)})^T\,(\partial\mathbf{K}_T(\mathbf{b}))\,\mathbf{b} + 2(\boldsymbol{\xi}^{(1)})^T\,(\frac{\partial\mathbf{K}_T}{\partial\lambda})\,\mathbf{b} + (\boldsymbol{\xi}^{(1)})^T\,(\frac{\partial^2(\Pi_{,a_i})}{\partial\lambda^2})\ . \end{aligned} \tag{5.2.40}$$

A proof is given in Appendix A.1 that the stability coefficient A as given in the first of the equations (5.2.40) coincides with A as in Allman's notation, *c.f.* [All89b]. It is prudent to note also that the coefficient A is identical with the *third directional derivative* $d^{(ppp)}\Pi$ (when taken in the same direction $\xi^{(1)}$) as introduced by Morley [Mor91],

$$A = d^{(ppp)}\Pi \ , \tag{5.2.41}$$

c.f. Appendix A.2.

The right hand side of equation (5.2.39) vanishes, of course, for a bifurcation point, since $\mu = 0$, but it plays an important role in the analysis of a limit point as seen later. There are, in general, two real solutions of equation (5.2.39), provided $B^2 > AC$, at a simple singular point; one corresponds to a primary 'fundamental' path and the other corresponds to a secondary 'bifurcation' path. But degenerate forms of equation (5.2.39) also correspond to types of singular points which often occur in physical systems.

The three most common types of singular points are

1. an asymmetric bifurcation point, where $\mu = 0$, $A \neq 0$, $B^2 > AC$, giving two distinct solutions for ds,

$$ds = \frac{1}{A}(-B \pm \sqrt{B^2 - AC}\,)\,d\lambda \tag{5.2.42}$$

which are substituted into equation (5.2.25) to obtain the differential **da**;

2. a symmetric bifurcation point, where $\mu = 0$, $A = 0$, $B \neq 0$, giving a degenerate form of equation (5.2.39)

$$(2B\,ds + C\,d\lambda)\,d\lambda = 0 \tag{5.2.43}$$

but there are still two distinct solutions

$$\begin{aligned} ds &= -\frac{1}{2}\left(\frac{C}{B}\right)d\lambda \ , \\ d\lambda &= 0 \ . \end{aligned} \tag{5.2.44}$$

The second of equations (5.2.44) means that $d\lambda = 0$ in the direction of the bifurcation path at a symmetric bifurcation point and hence equation (5.2.25) for the differential **da** reduces to equation (5.2.23) for the limit point, with

ds **indeterminate at this level of approximation. The differential da for the fundamental path is obtained by substituting the first of equations (5.2.44) into equation (5.2.25);**

3. **a limit point, where $\mu \neq 0$, $A \neq 0$, $d\lambda = 0$ (from the first of equations (5.2.21)) giving another degenerate form of equation (5.2.39)**

$$(ds)^2 = -(\frac{\mu}{A})(d^2\lambda) \ . \qquad (5.2.45)$$

The two solutions of this equation for *ds* are equal but opposite in sign; they correspond to points lying on the unique equilibrium path, which closely bracket the limit point. Note that the existence of real values for *ds* requires an appropriate (positive or negative) second order change ($d^2\lambda$) to make the right hand side of equation (5.2.45) positive.

For convenience of reference the above results are recorded here as the following criteria for identifying the type of a singular point:

$$\begin{aligned} &\text{(a) an asymmetric bifurcation point} && \mu = 0 \ , \ A \neq 0 \ ; \\ &\text{(b) a symmetric bifurcation point} && \mu = 0 \ , \ A = 0 \ ; \qquad (5.2.46) \\ &\text{(c) a limit point} && \mu \neq 0 \ , \ A \neq 0 \ . \end{aligned}$$

The symmetric bifurcation point, appearing as the second of the criteria in equations (5.2.46), occurs in two distinct types: stable symmetric and unstable symmetric. Additional criteria for identifying these singular points are derived in the following section.

5.2.3 Stability of equilibrium of singular points

The stability of equilibrium of a simple singular point $(\mathbf{a}, \lambda)$ is conditional upon the total potential energy function attaining a local minimum (stable equilibrium), a local maximum (unstable equilibrium) or a minimax point (unstable equilibrium). The natural condition that pertains can be determined by consideration of an increment $\Delta\Pi$ of the total potential energy expressed as a Taylor series expansion in terms of the differentials of Π, such that

$$\Delta\Pi = \Pi(\mathbf{a} + \mathbf{da}, \lambda) - \Pi(\mathbf{a}, \lambda)$$

$$= d\Pi(\mathbf{a},\lambda) + \frac{1}{2!}d^2\Pi(\mathbf{a},\lambda) + \frac{1}{3!}d^3\Pi(\mathbf{a},\lambda) + \frac{1}{4!}d^4\Pi(\mathbf{a},\lambda) + \ldots . \tag{5.2.47}$$

Here, the value of the natural parameter λ is considered to be fixed at the singular point, and consequently $d\lambda = 0$, $(d^2\lambda) = 0$, etc, but the dependent variable $\mathbf{a}$ is allowed a differential change $\mathbf{da}$, as specified by

$$\mathbf{da} = \boldsymbol{\xi}^{(1)}\, ds \tag{5.2.48}$$

and higher order differential changes $\mathbf{d^2a}$, $\mathbf{d^3a}$, $\mathbf{d^4a}$, etc as necessary. According to the reasoning of the previous section the choice of $\mathbf{da} = \boldsymbol{\xi}^{(1)} ds$ correctly applies to all types of singular points because equation (5.2.25) for bifurcation points reduces to equation (5.2.23) for limit points if $d\lambda = 0$. The differential change $\mathbf{da}$ is also considered to be limited in magnitude by putting

$$ds = \epsilon \tag{5.2.49}$$

in equation (5.2.48), where ϵ is a small disturbance parameter. Under these assumptions the differentials of energy $d\Pi$, $d^2\Pi$, etc which appear in equation (5.2.47) are given by

$$\begin{aligned}
d\Pi &= (\boldsymbol{\xi}^{(1)})^T \Pi_{,a_i}\, \epsilon \\
d^2\Pi &= (\mathbf{d^2a})^T \Pi_{,a_i} + (\boldsymbol{\xi}^{(1)})^T \mathbf{K}_T\, \boldsymbol{\xi}^{(1)}\, \epsilon^2 \\
d^3\Pi &= (\mathbf{d^3a})^T \Pi_{,a_i} + 3(\mathbf{d^2a})^T \mathbf{K}_T\, \boldsymbol{\xi}^{(1)}\, \epsilon \\
&\qquad + (\boldsymbol{\xi}^{(1)})^T (\partial \mathbf{K}_T(\boldsymbol{\xi}^{(1)}))\, \boldsymbol{\xi}^{(1)}\, \epsilon^3 \\
d^4\Pi &= (\mathbf{d^4a})^T \Pi_{,a_i} + 4(\mathbf{d^3a})^T \mathbf{K}_T\, \boldsymbol{\xi}^{(1)}\, \epsilon \\
&\qquad + 3(\mathbf{d^2a})^T \mathbf{K}_T\, (\mathbf{d^2a}) \\
&\qquad + 6(\mathbf{d^2a})^T (\partial \mathbf{K}_T(\boldsymbol{\xi}^{(1)}))\, \boldsymbol{\xi}^{(1)}\, \epsilon^2 \\
&\qquad + (\boldsymbol{\xi}^{(1)})^T (\partial(\partial \mathbf{K_T}(\boldsymbol{\xi}^{(1)}))(\boldsymbol{\xi}^{(1)}))\, \boldsymbol{\xi}^{(1)}\, \epsilon^4 \ .
\end{aligned} \tag{5.2.50}$$

Some of the terms in the expressions of equations (5.2.50) vanish in virtue of equation (5.2.10) and equations (5.2.12) and it is found that the first three differentials of energy evaluated at a singular point are

$$d\Pi = 0 \ ,$$

$$d^2\Pi = 0 , \qquad (5.2.51)$$
$$d^3\Pi = A\epsilon^3 ,$$

where the coefficient A is given in the first of equations (5.2.40).

At an asymmetric bifurcation point or a limit point $A \neq 0$ according to parts (a) and (c) of the criteria in equations (5.2.46), so equation (5.2.47) and equations (5.2.51) show that the increment of the total potential energy is given by

$$\Delta\Pi = \frac{1}{3!} A\epsilon^3 + O(\epsilon^4) . \qquad (5.2.52)$$

For a sufficiently small value of the disturbance parameter ϵ the increment $\Delta\Pi$ is seen to obey a cubic law close to those types of singular points and hence there is a point of inflexion of the total potential energy function in the direction of the eigenvector $\xi^{(1)}$. This means that $\Delta\Pi$ can decrease the total potential energy, so the asymmetric bifurcation point and the limit point are in a state of unstable equilibrium.

At a symmetric bifurcation point $A = 0$, according to part (b) of the criteria in equations (5.2.46), so equation (5.2.47) and equations (5.2.51) show that the increment $\Delta\Pi$ of the total potential energy depends principally on the fourth differential of energy $d^4\Pi$, given in the fourth of equations (5.2.50); using equation (5.2.10) and equations (5.2.12), this becomes

$$\begin{aligned} d^4\Pi = {} & 3(\mathbf{d^2a})^T \mathbf{K}_T (\mathbf{d^2a}) \\ & + 6(\mathbf{d^2a})^T (\partial \mathbf{K}_T(\xi^{(1)}))\, \xi^{(1)} \epsilon^2 \\ & + (\xi^{(1)})^T (\partial(\partial \mathbf{K_T}(\xi^{(1)}))(\xi^{(1)}))\, \xi^{(1)} \epsilon^4 . \end{aligned} \qquad (5.2.53)$$

This expression involves terms in $(\mathbf{d^2a})$ and these are calculated, using the second of equations (5.2.12) and equation (5.2.48), from

$$(\mathbf{da})^T \mathbf{T}\, \mathbf{da} = (ds)^2 \qquad (5.2.54)$$

whence, by differentiation,

$$(\mathbf{d^2a})^T \mathbf{T}\, \mathbf{da} = (ds)(d^2s) . \qquad (5.2.55)$$

Equation (5.2.55) read in conjunction with the second of equations (5.2.12) and equation (5.2.48) shows that $(\mathbf{d^2a})$ has the form

$$(\mathbf{d^2a}) = \xi^{(1)}(d^2s) + \sum_{r=2}^{n} c^{(r)} \xi^{(r)} \qquad (5.2.56)$$

where the coefficients $c^{(r)}$ are determined by substituting equation (5.2.56) into equation (5.2.35) (with $d\lambda = 0$, $(d^2\lambda) = 0$) and using equation (5.2.12) and equation (5.2.48), with $ds = \epsilon$, to obtain, *c.f.* Appendix A.3,

$$c^{(r)} = -\frac{1}{\theta(r)} (\xi^{(r)})^T (\partial \mathbf{K}_T(\xi^{(1)})) \xi^{(1)} \epsilon^2 \ . \tag{5.2.57}$$

In matrix/vector notation we hence have with

$$\mathbf{c} = (0, c^{(2)}, c^{(3)}, ..., c^{(n)})^T \tag{5.2.58}$$

the form

$$\mathbf{c} = \Theta \mathbf{E}^T (\partial \mathbf{K}_T(\xi^{(1)})) \xi^{(1)} \epsilon^2 \tag{5.2.59}$$

where Θ and $\mathbf{E}$ are defined in equation (5.2.31) and equation (5.2.28), respectively. Thus, equation (5.2.59) can be written as

$$(\mathrm{d}^2\mathbf{a}) = \xi^{(1)} (d^2 s) + \mathbf{E} \Theta \mathbf{E}^T (\partial \mathbf{K}_T(\xi^{(1)})) \xi^{(1)} \epsilon^2 \ . \tag{5.2.60}$$

Substituting now equation (5.2.60) into equation (5.2.53) gives the fourth differential of energy as

$$d^4\Pi = D \epsilon^4 \tag{5.2.61}$$

where the coefficient D is found to be, *c.f.* Appendix A.4,

$$\begin{aligned} D = \ & (\xi^{(1)})^T (\partial (\partial \mathbf{K_T}(\xi^{(1)})) (\xi^{(1)})) \xi^{(1)} \\ & + 3 (\xi^{(1)})^T (\partial \mathbf{K}_T(\xi^{(1)}))^T \mathbf{E} \Theta \mathbf{E}^T (\partial \mathbf{K}_T(\xi^{(1)})) \xi^{(1)} \ . \end{aligned} \tag{5.2.62}$$

A proof is given in Appendix A.5 that the stability coefficient D as given in equation (5.2.62) coincides with the stability coefficient D as in Allman's notation, *c.f.* [All89b]. It is prudent to note also that the first term of equation (5.2.62) is identical with the *fourth directional derivative* $d^{(pppp)}\Pi$ (when taken in the same direction $\xi^{(1)}$) as introduced by Morley [Mor91],

$$(\xi^{(1)})^T (\partial (\partial \mathbf{K_T}(\xi^{(1)})) (\xi^{(1)})) \xi^{(1)} = d^{(pppp)}\Pi \ , \tag{5.2.63}$$

c.f. Appendix A.6.

The increment $\Delta\Pi$ of the total potential energy is obtained from equation (5.2.47), with $d\Pi = d^2\Pi = d^3\Pi = 0$, and equation (5.2.62), namely

$$\Delta\Pi = \frac{1}{4!} D \epsilon^4 + O(\epsilon^5) \ . \tag{5.2.64}$$

Considering a sufficiently small value of the disturbance parameter ϵ now shows that the increment $\Delta\Pi$ obeys a quartic law close to a symmetric bifurcation point. This implies that the total potential energy function can attain either a local minimum (stable equilibrium), if $D > 0$, or a local maximum (unstable equilibrium), if $D < 0$, in the direction of the eigenvector $\boldsymbol{\xi}^{(1)}$. The following criteria for determining stability therefore apply

$$\begin{aligned} &\text{(a) a symmetric bifurcation point is stable if} \quad D > 0 \ ; \\ &\text{(b) a symmetric bifurcation point is unstable if} \, D < 0 \ . \end{aligned} \tag{5.2.65}$$

If the coefficients A and D in equations (5.2.40) and equation (5.2.62) are both zero, it is necessary to evaluate higher order differentials of energy in the expression for the increment $\Delta\Pi$ of the total potential energy in order to investigate the stability of equilibrium of a singular point.

A further observation, noted also by Koiter in his continuum analysis, may also be made regarding applications of the criteria in equations (5.2.65). It is often impractical to use more than a few of the eigenvalues and eigenvectors ($r = 2, ..., n$) to calculate an approximation to D in equation (5.2.62). Consequently, if this approximation to D is negative, the equilibrium of a singular point is certain to be unstable in reality. Conversely, a positive value of D, calculated without using a complete set of eigenvalues and eigenvectors, does not always mean that the equilibrium is actually stable. In the present work it is preferred to use the complete set of eigenvectors as for the computation of D the convenient matrix formulation as in equation (5.2.62) is derived.

5.2.4 Finite element formulation for the geometrically nonlinear constant moment triangle

The tangent stiffness matrix $\mathbf{K}_T$ for the geometrically nonlinear constant moment triangle is given in equation (4.5.50) as

$$\mathbf{K}_T = A \begin{bmatrix} \mathbf{B}^T\mathbf{D}\mathbf{B} & \mathbf{B}^T\mathbf{D}\mathbf{B}_w & \mathbf{B}^T\mathbf{D}\mathbf{B}_\kappa \\ & \mathbf{B}_w^T\mathbf{D}\mathbf{B}_w + \mathbf{B}_{Gw} & \mathbf{B}_w^T\mathbf{D}\mathbf{B}_\kappa \\ \text{sym} & & \mathbf{B}_\kappa^T\mathbf{D}\mathbf{B}_\kappa + \mathbf{B}_{G\kappa} + \frac{h^2}{12}\mathbf{D} \end{bmatrix} . \tag{5.2.66}$$

For the computation of the second order stability coefficients A, B and C the 'derivative' of $\mathbf{K}_T$, the matrix $(\partial \mathbf{K}_T(\boldsymbol{\xi}^{(1)}))$ (taken in the direction of $\boldsymbol{\xi}^{(1)}$) as defined in equation (5.2.36), is required. Equation (5.2.66) entails then that $(\partial \mathbf{K}_T(\boldsymbol{\xi}^{(1)}))$ becomes the symmetric matrix

$$(\partial \mathbf{K}_T(\mathbf{a})) = \frac{3}{2} A \begin{bmatrix} 0 & \mathbf{B}^T \mathbf{D} \hat{\mathbf{B}}_w & \hat{\mathbf{B}}^T \mathbf{D} \hat{\mathbf{B}}_\kappa \\ & \hat{\mathbf{B}}_w^T \mathbf{D} \mathbf{B}_w + \hat{\mathbf{B}}_w^T \mathbf{D} \hat{\mathbf{B}}_w & \hat{\mathbf{B}}_w^T \mathbf{D} \mathbf{B}_\kappa + \hat{\mathbf{B}}_w^T \mathbf{D} \hat{\mathbf{B}}_\kappa \\ \text{sym} & & \hat{\mathbf{B}}_\kappa^T \mathbf{D} \mathbf{B}_\kappa + \hat{\mathbf{B}}_\kappa^T \mathbf{D} \hat{\mathbf{B}}_\kappa \end{bmatrix} , \quad (5.2.67)$$

where the 'hatted' matrices are taken in the direction of $\boldsymbol{\xi}^{(1)}$ where $\boldsymbol{\xi}^{(1)} = (\mathbf{u}^T \mathbf{w}^T \boldsymbol{\kappa}^T)^T$, *c.f.* equation (4.5.21).

Note that the terms involving $(\frac{\partial \mathbf{K}_T}{\partial \lambda})$ and $(\frac{\partial^2 (\Pi_{,a_i})}{\partial \lambda^2})$ vanish as $\mathbf{K}_T$ is independent of λ and $\Pi_{,a_i}$ is linear in λ, respectively. Hence equations (5.2.40) for the second order stability coefficients reduce for the geometrically nonlinear constant moment triangle to

$$\begin{aligned} A &= (\boldsymbol{\xi}^{(1)})^T (\partial \mathbf{K}_T (\boldsymbol{\xi}^{(1)})) \boldsymbol{\xi}^{(1)} , \\ B &= (\boldsymbol{\xi}^{(1)})^T (\partial \mathbf{K}_T (\mathbf{b})) \boldsymbol{\xi}^{(1)} , \\ C &= (\boldsymbol{\xi}^{(1)})^T (\partial \mathbf{K}_T (\mathbf{b})) \mathbf{b} . \end{aligned} \quad (5.2.68)$$

For the computation of the stability coefficient D the 'derivative' of $(\partial \mathbf{K}_T(\boldsymbol{\xi}^{(1)}))$, the matrix $(\partial(\partial \mathbf{K}_T(\boldsymbol{\xi}^{(1)}))(\boldsymbol{\xi}^{(1)}))$ (taken twice in the direction of $\boldsymbol{\xi}^{(1)}$), is required. Equation (5.2.67) entails then that $(\partial(\partial \mathbf{K}_T(\boldsymbol{\xi}^{(1)}))(\boldsymbol{\xi}^{(1)}))$ becomes the symmetric matrix

$$(\partial(\partial \mathbf{K}_T(\boldsymbol{\xi}^{(1)}))(\boldsymbol{\xi}^{(1)})) = 3A \begin{bmatrix} 0 & 0 & 0 \\ & \hat{\mathbf{B}}_w^T \mathbf{D} \hat{\mathbf{B}}_w & \hat{\mathbf{B}}_w^T \mathbf{D} \hat{\mathbf{B}}_\kappa \\ \text{sym} & & \hat{\mathbf{B}}_\kappa^T \mathbf{D} \hat{\mathbf{B}}_\kappa \end{bmatrix} , \quad (5.2.69)$$

where, again, the hatted matrices are taken (twice) in the direction of $\boldsymbol{\xi}^{(1)}$.

The stability coefficient D is computed as in equation (5.2.62) by

$$\begin{aligned} D = {} & (\boldsymbol{\xi}^{(1)})^T (\partial(\partial \mathbf{K}_\mathbf{T}(\boldsymbol{\xi}^{(1)}))(\boldsymbol{\xi}^{(1)})) \boldsymbol{\xi}^{(1)} \\ & + 3 (\boldsymbol{\xi}^{(1)})^T (\partial \mathbf{K}_T(\boldsymbol{\xi}^{(1)}))^T \mathbf{E} \ominus \mathbf{E}^T (\partial \mathbf{K}_T(\boldsymbol{\xi}^{(1)})) \boldsymbol{\xi}^{(1)} . \end{aligned} \quad (5.2.70)$$

It is prudent to note that the second order stability coefficients A, B and C can be calculated element wise and the result is obtained by then summing up over

the element contributions, but the second term in the expression for D must be computed on the global level.

5.3 The geometrically nonlinear constant bending moment triangle and its repeated directional derivatives with respect to varied directions

5.3.1 Introduction

A formulation based on the paper by Morley [Mor91] is presented for the matrix evaluation of repeated directional derivatives with respect to varied directions for the geometrically nonlinear constant bending moment triangle. With the help of these directional derivatives the stability coefficients introduced earlier may be computed and, thus, an alternative way for determining the type and stability of critical points is provided.

5.3.2 The directional derivative

The *directional (Gateaux) derivative* $\mathrm{d}\mathbf{G} = \mathrm{d}\mathbf{G}(a;\hat{a})$ of the operator $\mathbf{G} = \mathbf{G}(a)$ in the direction of $\hat{a}$ is defined by

$$\mathrm{d}\mathbf{G} = \lim_{\lambda \to 0} \frac{\mathbf{G}(a + \lambda\hat{a}) - \mathbf{G}(a)}{\lambda} \tag{5.3.1}$$

where

$$a = a_1, a_2, \cdots, a_k, \qquad \hat{a} = \hat{a}_1, \hat{a}_2, \cdots, \hat{a}_k, \tag{5.3.2}$$

say. Introducing

$$\left.\begin{array}{rcl} \mathbf{a} & = & (a_1, \ a_2, \ \cdots, \ a_k)^{\mathrm{T}} = (\mathbf{u}^{\mathrm{T}} \ \ \mathbf{w}^{\mathrm{T}} \ \ \boldsymbol{\kappa}^{\mathrm{T}})^{\mathrm{T}} \\ \hat{\mathbf{a}} & = & (\hat{a}_1, \ \hat{a}_2, \ \cdots, \ \hat{a}_k)^{\mathrm{T}} = (\hat{\mathbf{u}}^{\mathrm{T}} \ \ \hat{\mathbf{w}}^{\mathrm{T}} \ \ \hat{\boldsymbol{\kappa}}^{\mathrm{T}})^{\mathrm{T}} \end{array}\right\}, \tag{5.3.3}$$

c.f. equation (4.5.21), the first scalar $g = g(a)$ with

$$g = c_0 + \mathbf{c}^{\mathrm{T}}\mathbf{a}\ , \qquad \mathbf{c} = (c_1, \ c_2, \ \ldots, \ c_k)^T \tag{5.3.4}$$

is considered, where $c_0, c_1, c_2, \ldots, c_k$ are fixed constants. Let $\hat{g} = \hat{g}(\hat{a})$ where[1]

$$\hat{g} = \mathbf{c}^{\mathrm{T}}\hat{\mathbf{a}} \ . \tag{5.3.5}$$

Equations (5.3.1), (5.3.4), (5.3.5) and (5.3.2) then show that the directional derivative $\mathrm{d}g = \mathrm{d}g(a;\hat{a})$ of g in the direction of $\hat{a}$ is

$$\mathrm{d}g = \hat{g} \ . \tag{5.3.6}$$

Consider next the matrix $\mathbf{G} = \mathbf{G}(a)$ with

$$\mathbf{G} = [g_{ij}] \ , \qquad i,j = 1,2,\ldots,k \tag{5.3.7}$$

where the coefficients $g_{ij} = g(a)_{ij}$ are defined similarly as for $g(a)$ in equation (5.3.4) and let

$$\hat{\mathbf{G}} = [\hat{g}_{ij}] \tag{5.3.8}$$

where the coefficients $\hat{g}_{ij} = \hat{g}(\hat{a})_{ij}$ are defined similarly as for $\hat{g}(\hat{a})$ in equation (5.3.5). The directional derivative $\mathrm{d}\mathbf{G} = \mathrm{d}\mathbf{G}(a;\hat{a})$ of the matrix $\mathbf{G}$ in the direction of $\hat{a}$ is then

$$\mathrm{d}\mathbf{G} = \hat{\mathbf{G}} \ . \tag{5.3.9}$$

Moreover, if say

$$\mathbf{F} = \mathbf{G}_1\mathbf{G}_2\mathbf{G}_3 \tag{5.3.10}$$

then the directional derivative is

$$\mathrm{d}\mathbf{F} = \hat{\mathbf{G}}_1\mathbf{G}_2\mathbf{G}_3 + \mathbf{G}_1\hat{\mathbf{G}}_2\mathbf{G}_3 + \mathbf{G}_1\mathbf{G}_2\hat{\mathbf{G}}_3 \ . \tag{5.3.11}$$

5.3.3 Repeated directional derivatives with respect to varied directions

In order to denote repeated directional derivatives with respect to varied directions, it is convenient to replace the second of equations (5.3.3) with

$$\hat{\mathbf{a}}^{(p)} = (\hat{a}_1^{(p)}, \ \hat{a}_2^{(p)}, \ \cdots, \ \hat{a}_k^{(p)})^{\mathrm{T}} = (\hat{\mathbf{u}}^{(p)\mathrm{T}} \ \ \hat{\mathbf{w}}^{(p)\mathrm{T}} \ \ \hat{\boldsymbol{\kappa}}^{(p)\mathrm{T}})^{\mathrm{T}} \tag{5.3.12}$$

[1] In the application of the present results to the calculation of stability coefficients as are expressed by Allman [All89b] it is worth noting that $\hat{g} \equiv g_{,a_i}\,\hat{a}_i$ where the comma denotes partial differentiation with respect to a_i and where the repeated index i denotes summation over the range $i = 1,\ldots,k$.

where p is a prescribed index.

The directional derivative $\mathrm{d}^{(p)}\mathbf{G}$ of $\mathbf{G}$ in the direction of $\hat{a}^{(p)}$ is then denoted by

$$\mathrm{d}^{(p)}\mathbf{G} = \hat{\mathbf{G}}^{(p)} \ . \tag{5.3.13}$$

The second directional derivative of *e.g.* equation (5.3.10) is

$$\mathrm{d}^{(pq)}\mathbf{F} = \hat{\mathbf{G}}_1^p\hat{\mathbf{G}}_2^q\mathbf{G}_3+\hat{\mathbf{G}}_1^p\mathbf{G}_2\hat{\mathbf{G}}_3^q+\hat{\mathbf{G}}_1^q\hat{\mathbf{G}}_2^p\mathbf{G}_3+\mathbf{G}_1\hat{\mathbf{G}}_2^p\hat{\mathbf{G}}_3^q+\hat{\mathbf{G}}_1^q\mathbf{G}_2\hat{\mathbf{G}}_3^p+\mathbf{G}_1\hat{\mathbf{G}}_2^q\hat{\mathbf{G}}_3^p \tag{5.3.14}$$

where it is evident that

$$\mathrm{d}^{(pq)}\mathbf{F} = \mathrm{d}^{(qp)}\mathbf{F} \ . \tag{5.3.15}$$

5.3.4 Repeated directional derivatives of the strain vector

The strain vector $\boldsymbol{\gamma}$ for the geometrically nonlinear constant moment triangle of equation (4.5.28) is written

$$\boldsymbol{\gamma} = \mathbf{B}\mathbf{u} + \tfrac{1}{2}\mathbf{B}_w\mathbf{w} + \tfrac{1}{2}\mathbf{B}_\kappa\boldsymbol{\kappa}. \tag{5.3.16}$$

Equations (4.5.26) and (4.5.27) then imply that

$$\mathbf{B}_w\hat{\mathbf{w}}^{(p)} = \hat{\mathbf{B}}_w^{(p)}\mathbf{w}, \qquad \mathbf{B}_\kappa\hat{\boldsymbol{\kappa}}^{(p)} = \hat{\mathbf{B}}_\kappa^{(p)}\boldsymbol{\kappa} \tag{5.3.17}$$

and the equations for repeated directional derivatives with respect to varied directions become

$$\begin{aligned}
\mathrm{d}^{(p)}\boldsymbol{\gamma} &= \mathbf{B}\hat{\mathbf{u}}^{(p)} + \mathbf{B}_w\hat{\mathbf{w}}^{(p)} + \mathbf{B}_\kappa\hat{\boldsymbol{\kappa}}^{(p)} \ , \\
\mathrm{d}^{(pq)}\boldsymbol{\gamma} &= \hat{\mathbf{B}}_w^{(q)}\hat{\mathbf{w}}^{(p)} + \hat{\mathbf{B}}_\kappa^{(q)}\hat{\boldsymbol{\kappa}}^{(p)} \ , \\
\mathrm{d}^{(pqr)}\boldsymbol{\gamma} &= 0 \ .
\end{aligned} \tag{5.3.18}$$

Note that equations (5.3.17) show that

$$\hat{\mathbf{B}}_w^{(q)}\hat{\mathbf{w}}^{(p)} = \hat{\mathbf{B}}_w^{(p)}\hat{\mathbf{w}}^{(q)}, \qquad \hat{\mathbf{B}}_\kappa^{(q)}\hat{\boldsymbol{\kappa}}^{(p)} = \hat{\mathbf{B}}_\kappa^{(p)}\hat{\boldsymbol{\kappa}}^{(q)}. \tag{5.3.19}$$

which confirms that the sequence of directional differentiation is immaterial, *i.e.*

$$\begin{aligned}
\mathrm{d}^{(p)}\boldsymbol{\gamma} &= \mathbf{B}\hat{\mathbf{u}}^{(p)} + \hat{\mathbf{B}}_w^{(p)}\mathbf{w} + \hat{\mathbf{B}}_\kappa^{(p)}\boldsymbol{\kappa} \\
\mathrm{d}^{(qp)}\boldsymbol{\gamma} &= \mathrm{d}^{(pq)}\boldsymbol{\gamma}.
\end{aligned} \tag{5.3.20}$$

5.3.5 Repeated directional derivatives of the strain energy

The strain energy Π as given in equation (4.5.40) is

$$\Pi = \frac{A}{2}\{\boldsymbol{\gamma}^{\mathrm{T}}\mathbf{D}\boldsymbol{\gamma} + \frac{h^2}{12}\boldsymbol{\kappa}^{\mathrm{T}}\mathbf{D}\boldsymbol{\kappa}\} \tag{5.3.21}$$

which has first directional derivative, *c.f.* equation (4.5.42),

$$\begin{aligned} \mathrm{d}^{(p)}\Pi &= A\{\mathrm{d}^{(p)}\boldsymbol{\gamma}^{\mathrm{T}}\mathbf{D}\boldsymbol{\gamma} + \frac{h^2}{12}\mathrm{d}^{(p)}\boldsymbol{\kappa}^{\mathrm{T}}\mathbf{D}\boldsymbol{\kappa}\} \\ &= \hat{\mathbf{a}}^{(p)}\mathbf{K}\mathbf{a} \end{aligned} \tag{5.3.22}$$

where $\mathbf{K}$ is the asymmetrical stiffness matrix

$$\mathbf{K} = A\begin{bmatrix} \mathbf{B}^{\mathrm{T}}\mathbf{D}\mathbf{B} & \frac{1}{2}\mathbf{B}^{\mathrm{T}}\mathbf{D}\mathbf{B}_w & \frac{1}{2}\mathbf{B}^{\mathrm{T}}\mathbf{D}\mathbf{B}_\kappa \\ \mathbf{B}_w^{\mathrm{T}}\mathbf{D}\mathbf{B} & \frac{1}{2}\mathbf{B}_w^{\mathrm{T}}\mathbf{D}\mathbf{B}_w & \frac{1}{2}\mathbf{B}_w^{\mathrm{T}}\mathbf{D}\mathbf{B}_\kappa \\ \mathbf{B}_\kappa^{\mathrm{T}}\mathbf{D}\mathbf{B} & \frac{1}{2}\mathbf{B}_\kappa^{\mathrm{T}}\mathbf{D}\mathbf{B}_w & \frac{1}{2}\mathbf{B}_\kappa^{\mathrm{T}}\mathbf{D}\mathbf{B}_\kappa + \frac{h^2}{12}\mathbf{D} \end{bmatrix} \tag{5.3.23}$$

as in equation (4.5.43).

The second directional derivative of Π, *c.f.* equation (4.5.48), becomes

$$\begin{aligned} \mathrm{d}^{(pq)}\Pi &= A\{\mathrm{d}^{(pq)}\boldsymbol{\gamma}^{\mathrm{T}}\mathbf{D}\boldsymbol{\gamma} + \mathrm{d}^{(q)}\boldsymbol{\gamma}^{\mathrm{T}}\mathbf{D}\mathrm{d}^{(p)}\boldsymbol{\gamma} + \frac{h^2}{12}\mathrm{d}^{(q)}\boldsymbol{\kappa}^{\mathrm{T}}\mathbf{D}\mathrm{d}^{(p)}\boldsymbol{\kappa}\} \\ &= \hat{\mathbf{a}}^{(p)\mathrm{T}}\mathbf{K}_{2j}\mathbf{a} + \hat{\mathbf{a}}^{(p)\mathrm{T}}\mathbf{K}_2\hat{\mathbf{a}}^{(q)\mathrm{T}} \end{aligned} \tag{5.3.24}$$

where the asymmetrical matrix $\mathbf{K}_{2j}$ is given by

$$\mathbf{K}_{2j} = A\begin{bmatrix} 0 & 0 & 0 \\ \hat{\mathbf{B}}_w^{(q)\mathrm{T}}\mathbf{D}\mathbf{B} & \frac{1}{2}\hat{\mathbf{B}}_w^{(q)\mathrm{T}}\mathbf{D}\mathbf{B}_w & \frac{1}{2}\hat{\mathbf{B}}_w^{(q)\mathrm{T}}\mathbf{D}\mathbf{B}_\kappa \\ \hat{\mathbf{B}}_\kappa^{(q)\mathrm{T}}\mathbf{D}\mathbf{B} & \frac{1}{2}\hat{\mathbf{B}}_\kappa^{(q)\mathrm{T}}\mathbf{D}\mathbf{B}_w & \frac{1}{2}\hat{\mathbf{B}}_\kappa^{(q)\mathrm{T}}\mathbf{D}\mathbf{B}_\kappa \end{bmatrix} \tag{5.3.25}$$

and the symmetrical matrix $\mathbf{K}_2$ is given by

$$\mathbf{K}_2 = A\begin{bmatrix} \mathbf{B}^{\mathrm{T}}\mathbf{D}\mathbf{B} & \mathbf{B}^{\mathrm{T}}\mathbf{D}\mathbf{B}_w & \mathbf{B}^{\mathrm{T}}\mathbf{D}\mathbf{B}_\kappa \\ \mathbf{B}_w^{\mathrm{T}}\mathbf{D}\mathbf{B} & \mathbf{B}_w^{\mathrm{T}}\mathbf{D}\mathbf{B}_w & \mathbf{B}_w^{\mathrm{T}}\mathbf{D}\mathbf{B}_\kappa \\ \mathbf{B}_\kappa^{\mathrm{T}}\mathbf{D}\mathbf{B} & \mathbf{B}_\kappa^{\mathrm{T}}\mathbf{D}\mathbf{B}_w & \mathbf{B}_\kappa^{\mathrm{T}}\mathbf{D}\mathbf{B}_\kappa + \frac{h^2}{12}\mathbf{D} \end{bmatrix}. \tag{5.3.26}$$

The rôle of the geometric stiffness matrices $\mathbf{B}_{G\boldsymbol{w}}$ and $\mathbf{B}_{G\boldsymbol{\kappa}}$ of equations (4.5.45) in the derivation of the directional derivatives is considered in Appendix A.7. Geometric stiffness matrices are introduced in computational structural analysis so as to achieve symmetry of the Hessian, *i.e.* of the tangent stiffness matrix $\mathbf{K}_{\mathrm{T}}$ of equations (4.5.48) and (4.5.49).

The third directional derivative Π, in a similar way, then becomes

$$\begin{aligned} \mathrm{d}^{(pqr)}\Pi &= A\{\mathrm{d}^{(qr)}\boldsymbol{\gamma}^{\mathrm{T}}\mathbf{D}\mathrm{d}^{(p)}\boldsymbol{\gamma} + \mathrm{d}^{(pr)}\boldsymbol{\gamma}^{\mathrm{T}}\mathbf{D}\mathrm{d}^{(q)}\boldsymbol{\gamma} + \mathrm{d}^{(r)}\boldsymbol{\gamma}^{\mathrm{T}}\mathbf{D}\mathrm{d}^{(pq)}\boldsymbol{\gamma}\} \\ &= \hat{\mathbf{a}}^{(p)\mathrm{T}}\mathbf{K}_{3q}\hat{\mathbf{a}}^{(r)} + \hat{\mathbf{a}}^{(q)\mathrm{T}}\mathbf{K}_{3r}\hat{\mathbf{a}}^{(p)} + \hat{\mathbf{a}}^{(r)\mathrm{T}}\mathbf{K}_{3p}\hat{\mathbf{a}}^{(q)} \end{aligned} \tag{5.3.27}$$

where $\mathbf{K}_{3q}$ is the asymmetrical matrix

$$\mathbf{K}_{3q} = A\begin{bmatrix} 0 & 0 & 0 \\ \hat{\mathbf{B}}_{w}^{(q)\mathrm{T}}\mathbf{D}\mathbf{B} & \hat{\mathbf{B}}_{w}^{(q)\mathrm{T}}\mathbf{D}\mathbf{B}_{w} & \hat{\mathbf{B}}_{w}^{(q)\mathrm{T}}\mathbf{D}\mathbf{B}_{\kappa} \\ \hat{\mathbf{B}}_{\kappa}^{(q)\mathrm{T}}\mathbf{D}\mathbf{B} & \hat{\mathbf{B}}_{\kappa}^{(q)\mathrm{T}}\mathbf{D}\mathbf{B}_{w} & \hat{\mathbf{B}}_{\kappa}^{(q)\mathrm{T}}\mathbf{D}\mathbf{B}_{\kappa} \end{bmatrix} \tag{5.3.28}$$

and the fourth directional derivative of Π becomes

$$\begin{aligned} \mathrm{d}^{(pqrs)}\Pi &= A\{\mathrm{d}^{(pq)}\boldsymbol{\gamma}^{\mathrm{T}}\mathbf{D}\mathrm{d}^{(rs)}\boldsymbol{\gamma} + \mathrm{d}^{(qr)}\boldsymbol{\gamma}^{\mathrm{T}}\mathbf{D}\mathrm{d}^{(ps)}\boldsymbol{\gamma} + \mathrm{d}^{(rs)}\boldsymbol{\gamma}^{\mathrm{T}}\mathbf{D}\mathrm{d}^{(qs)}\boldsymbol{\gamma}\} \\ &= \hat{\mathbf{a}}^{(p)\mathrm{T}}\hat{\mathbf{K}}_{3q}^{(s)}\hat{\mathbf{a}}^{(r)} + \hat{\mathbf{a}}^{(q)\mathrm{T}}\hat{\mathbf{K}}_{3r}^{(s)}\hat{\mathbf{a}}^{(p)} + \hat{\mathbf{a}}^{(r)\mathrm{T}}\hat{\mathbf{K}}_{3p}^{(s)}\hat{\mathbf{a}}^{(q)} \end{aligned} \tag{5.3.29}$$

where, for example, $\hat{\mathbf{K}}_{3q}^{(s)}$ is the asymmetrical matrix

$$\hat{\mathbf{K}}_{3q}^{(s)} = A\begin{bmatrix} 0 & 0 & 0 \\ 0 & \hat{\mathbf{B}}_{w}^{(q)\mathrm{T}}\mathbf{D}\hat{\mathbf{B}}_{w}^{(s)} & \hat{\mathbf{B}}_{w}^{(q)\mathrm{T}}\mathbf{D}\hat{\mathbf{B}}_{\kappa}^{(s)} \\ 0 & \hat{\mathbf{B}}_{\kappa}^{(q)\mathrm{T}}\mathbf{D}\hat{\mathbf{B}}_{w}^{(s)} & \hat{\mathbf{B}}_{\kappa}^{(q)\mathrm{T}}\mathbf{D}\hat{\mathbf{B}}_{\kappa}^{(s)} \end{bmatrix}. \tag{5.3.30}$$

An alternative formulation for the repeated directional derivatives of Π with respect to varied directions is given in Appendix A.8 where all matrices are symmetric.

5.3.6 Stability coefficients for Koiter's criteria

The stability coefficients A, B, C and D, as derived in the prequel and given in equations (5.2.40) and equation (5.2.62), can now be expressed in terms of the directional derivatives of the strain energy introduced above by substituting from equations (5.3.27) and (5.3.29) so that symbolically

$$\begin{aligned} A &= \mathrm{d}^{(ppp)}\Pi, \\ B &= \mathrm{d}^{(ppq)}\Pi, \\ C &= \mathrm{d}^{(pqq)}\Pi, \\ D &= \mathrm{d}^{(pppp)}\Pi - \sum_{q=2}^{n}\frac{3}{\theta^{(q)}}(\mathrm{d}^{(ppq)}\Pi)^2, \end{aligned} \tag{5.3.31}$$

with

$$
\begin{aligned}
\mathrm{d}^{(ppp)}\Pi &= 3\hat{\mathbf{a}}^{(p)\mathrm{T}}\mathbf{K}_{3p}\hat{\mathbf{a}}^{(p)}, \\
\mathrm{d}^{(ppq)}\Pi &= 2\hat{\mathbf{a}}^{(p)\mathrm{T}}\mathbf{K}_{3p}\hat{\mathbf{a}}^{(q)} + \hat{\mathbf{a}}^{(p)\mathrm{T}}\mathbf{K}_{3q}\hat{\mathbf{a}}^{(p)}, \\
\mathrm{d}^{(pqq)}\Pi &= 2\hat{\mathbf{a}}^{(p)\mathrm{T}}\mathbf{K}_{3q}\hat{\mathbf{a}}^{(q)} + \hat{\mathbf{a}}^{(q)\mathrm{T}}\mathbf{K}_{3p}\hat{\mathbf{a}}^{(q)}, \\
\mathrm{d}^{(pppp)}\Pi &= 3\hat{\mathbf{a}}^{(p)\mathrm{T}}\hat{\mathbf{K}}_{3p}^{(p)}\hat{\mathbf{a}}^{(p)},
\end{aligned}
\tag{5.3.32}
$$

where the appropriate substitutions for the $\hat{a}_i^{(p)}$ and $\hat{a}_i^{(q)}$ are ascertained from the previous section or the paper by Allman [All89b]. While the stability coefficients A, B and C can be calculated element by element and then summed, the summation term in the last of equations (5.3.31) for D must be calculated on a global basis.

Chapter 6

Calculation of stable equilibrium paths

6.1 Introduction

In this chapter the numerical solution of equilibrium equations is elaborated on. In general, there exist two methods, perturbation methods and continuation methods. Perturbation methods consist of computer adaptations of Koiter's work [Koi45] or numerical implementations of the analyses by Thompson [Tho63], [Tho70] and the equivalent results derived by other people. The main characteristic is that they rely on power series expansion techniques. Hence, perturbation methods yield results that approximate the equilibrium paths only around a pre-determined solution point at which the series is taken. Continuation methods do not have this drawback and are employed in most of the modern finite element codes. The key feature is the use of iterations to correct an initially predicted solution for a particular point of the solution space. Many solution points can be calculated by gradually varying an independent parameter (usually the intensity of the applied loads) and, in this way, enabling the tracing of the equilibrium path.

The emphasis of the present work lies in the investigation of bifurcation points (buckling phenomena) rather than limit points (snapping phenomena) as for the latter methods suitable for finite element computation already exist. Bifurcational buckling as well as limit points often exhibit huge structural changes and the compu-

tation of the required switch procedures between bifurcation paths in earlier works have not been implemented in a satisfactory manner into finite element codes.

In this chapter, after a note on linear bifurcation analysis, some of the commonly used continuation methods for the calculation of stable equilibrium paths are discussed. Thereafter, a solution technique developed by Allman is described, where stable equilibrium paths are located reliably by a generalization of Newton's method, *c.f.* [All84], which converges only to minima in applications to find stationary points of a function of several variables. Some important computational aspects are also considered such as reliably locating critical points. Then, a branch switching method, which has successfully been applied at bifurcation points in order to enter the post buckling regime on the stable equilibrium path, is presented.

6.2 Linear bifurcation analysis

Buckling takes place when a member or a structure converts membrane strain energy into strain energy of bending with no change in externally applied load. A critical condition, at which buckling occurs, exists when it is possible that the deformation state may change slightly in a way that makes a loss in membrane strain energy numerically equal to the gain in bending strain energy.

The effects of membrane forces are accounted for by a matrix $\mathbf{K}_G$ that augments the conventional stiffness matrix $\mathbf{K}_0$. The matrix $\mathbf{K}_G$ is called the geometric stiffness matrix and it is thus defined by the element's geometry, displacement field, and state of stress. For the geometrically nonlinear constant moment triangle the matrices $\mathbf{K}_0$ and $\mathbf{K}_G$ are given by

$$\mathbf{K}_0 = A \begin{bmatrix} \mathbf{B}^T\mathbf{D}\mathbf{B} & \mathbf{0} & \mathbf{0} \\ & \mathbf{0} & \mathbf{0} \\ \text{sym} & & \frac{h^2}{12}\mathbf{D} \end{bmatrix}, \tag{6.2.1}$$

$$\mathbf{K}_G = A \begin{bmatrix} \mathbf{0} & \mathbf{0} & \mathbf{0} \\ & \mathbf{B}_{G_w} & \mathbf{0} \\ \text{sym} & & \mathbf{B}_{G_\kappa} \end{bmatrix}, \tag{6.2.2}$$

c.f. equation (4.5.43) in the matrix formulation given in section 4.5.

A bifurcation buckling load is the load for which a reference configuration of the

structure and an infinitesimally close (buckled) configuration are both possible equilibrium configurations. As a buckling displacement **da** takes place from a reference configuration **a**, the load does not change. Accordingly,

$$(\mathbf{K}_0 + \mathbf{K}_G)\,\mathbf{da} = \mathbf{0}\ , \tag{6.2.3}$$

or, equivalently,

$$(\mathbf{K}_0 + \lambda_{cr}\,\mathbf{K}_G^*)\,\mathbf{da} = \mathbf{0}\ , \tag{6.2.4}$$

where $\mathbf{K}_G^*$ defines the reference state of $\mathbf{K}_G$. Note that here the so-called linear classical buckling analysis is followed where prebuckling rotations are either ignored or are zero. Equation (6.2.3) or equation (6.2.4) define a generalized eigenvalue problem the lowest eigenvalue of which, λ_{cr}, is associated with buckling. The critical load or buckling load **p** is then

$$\mathbf{p}_{cr} = \lambda_{cr}\,\mathbf{p}^*\ , \tag{6.2.5}$$

where $\mathbf{p}^*$ defines the reference state of the loading. The eigenvector **da** associated with λ_{cr} defines the buckling mode. The magnitude of **da** is indeterminate. Therefore, **da** identifies shape but not amplitude.

Thus, the linear bifurcation analysis provides an easy way for calculating critical loads at which elastic structures buckle. It is to be noted, however, that physically significant answers can be obtained only for a limited number of problems such as for perfect structures.

6.3 Commonly used continuation methods and branch switching

6.3.1 Introduction

There is a plethora of methods that can be employed for the iterative solution of nonlinear systems. Any of these techniques designed for the solution of nonlinear algebraic equations can be modified so that applicability in structural analysis in the form of a continuation method is obtained. This leads to the determination of a number of points that belong to the solution curve of interest, *e.g.* the stable

equilibrium path in the present work. Continuation methods are iterative methods requiring starting values from a point found on the solution curve in order to construct an approximation for another point sought on the same solution curve.

This must be done using a step-by-step procedure and, hence, continuation methods can be classified essentially as predictor-corrector methods where the initially constructed prediction is corrected by employing the iterative technique at hand.

6.3.2 The Newton-Raphson method

The most popular method for the iterative solution of nonlinear systems is undoubtedly the Newton-Raphson method. The equilibrium equations for the finite element model are as given in equation (3.2.7), $\mathbf{Ka} = \mathbf{p}$. This may be rewritten, assuming a fixed load value, as a set of functions for which the roots are sought,

$$\mathbf{f(a)} = \mathbf{Ka} - \mathbf{p} = \mathbf{0} \ . \tag{6.3.6}$$

Presume that for a given load value at the k'th iteration the approximate solution $\mathbf{a}_{k-1}$ is known and an approximation $(\mathbf{a}_{k-1} + \delta\mathbf{a}_k)$ closer to the true solution is sought.

Setting the first order Taylor series expansion at $(\mathbf{a}_{k-1} + \delta\mathbf{a}_k)$ equal to zero gives the system of linear equations

$$(\mathbf{K}_T)_{k-1}\, \delta\mathbf{a}_k = -(\mathbf{K}_{k-1}\, \mathbf{a}_{k-1} - \mathbf{p}) \ , \tag{6.3.7}$$

where the subscripts denote the iteration numbers. Equation (6.3.7) is then solved for the unknown $\delta\mathbf{a}_k$ and a new better approximation for $\mathbf{a}_k$ is obtained from

$$\mathbf{a}_k = \mathbf{a}_{k-1} + \delta\mathbf{a}_k \ . \tag{6.3.8}$$

The term $\mathbf{a}_k$ is then substituted into equation (6.3.7) for a further correction and the procedure carries on until a certain cut-off criterion is satisfied and a solution point $\mathbf{a}$ or $\mathbf{a}^m$ is obtained if it is assumed that the calculations were performed for the m'th increment. The $\mathbf{a}^m$ is then used as a first approximation for the $(m+1)$'th increment.

The initial starting vector $\mathbf{a}_0$ for the first iteration increment is ideally chosen close to the unknown true answer. A common step is to employ a solution vector

obtained from the linear theory as an initial first guess. This approach is also made use of in the present work.

The standard Newton-Raphson method as presented above has a quadratic rate of convergence, provided that the initial guess is close enough to the true solution and that the tangent stiffness matrix satisfies certain conditions as stated by Ortega and Rheinboldt [OR70]. The popularity of the Newton-Raphson method is due to its good convergence properties as well as it being easy to implement into a computer code. The drawbacks, however, can be severe in complex problems. Firstly, the tangent stiffness matrix $\mathbf{K}_T$ requires updating after each iteration, which is computationally extremely costly. The second drawback of the method is, that it may fail to converge due to numerical errors.

6.3.3 Modified Newton-Raphson methods and Quasi-Newton-Raphson methods

In order to overcome the drawback of the standard Newton-Raphson method of continuously having to update the tangent stiffness matrix the so-called *modified Newton-Raphson methods* have won popularity. The idea here is to update the tangent stiffness matrix after each increment only rather than after each iteration. Alternatively, the updating can take place after every s iterations or when convergence becomes too slow. An interesting recent suggestion was made by Forsgren and Ringertz [FR93] who use both descent directions and directions with negative curvature. In this way, the applicability is extended to nonconvex problems and the method seems to provide a useful complement to other existing Newton-Raphson-type techniques.

Following the same objective as the modified Newton-Raphson methods, the *quasi-Newton-Raphson methods* also try to avoid the costly computation of the inverse of the tangent stiffness matrix as well as the slow convergence, which is often the case with modified Newton-Raphson methods. The idea is the introduction of a matrix $\mathbf{B}$ which behaves in a 'similar' way to $\mathbf{K}_T$ but is easy to construct. The most common quasi-Newton-Raphson methods are Broyden's method, Davidon's method, the DFP method and the BFGS method. It is not the purpose of the present work to give detailed descriptions of these methods and, thus, it suf-

fices here to refer to the works by Dennis and Moré [JEDM77] for a survey and Matthies and Strang [MS79] for the first nonlinear finite element implementation of quasi-Newton-Raphson methods.

6.3.4 Constant arc-length method and its alternative forms

The constant arc-length method was first introduced independently by Riks [Rik72] and Wempner [Wem71], later developed by Riks [Rik79] and then modified to suit finite element computations by Crisfield [Cri81] and Ramm [Ram82]. The idea of the constant arc-length method is to add to the standard equilibrium equations a constraint that depends on the load. In this way, it aims to control both the displacement and load in order to follow the equilibrium path of the structure. The resulting main advantage of the method is that the extended system of equations does not become singular at limit points and, thus, the entry into the post critical regime of snapping phenomena is made feasible. At bifurcation points, however, the system becomes singular, this being of importance to the present work. A major disadvantage of the constant arc-length method is that through the introduction of an additional row and column the otherwise symmetrical $(n \times n)$-matrix loses its symmetry in the now $(n+1)$-dimensional space.

Presuming that it is intended to advance from the $(m-1)$'th equilibrium configuration to the m'th equilibrium configuration, the unknown load value $\delta\lambda_1$ to be added to the structure is approximated using the identity

$$\delta\mathbf{a}_1^T\delta\mathbf{a} + (\mu\delta\lambda_1)^2 = (ds)^2 \ . \tag{6.3.9}$$

Here, the scaling parameter μ is usually taken as $\mu = 1$ and $\delta a_1 = \delta\lambda_1\,\delta\mathbf{a}$ where $\delta\mathbf{a} = ((\mathbf{K}_T)^{m-1})^{-1}\mathbf{p}^*$ is the tangential displacement of unit loading $\mathbf{p}^*$ and ds fixes the length of the increment in $(n+1)$-dimensional space. The corrections are then made by employing the Newton-Raphson method. In the constant arc-length method as suggested by Ramm [Ram82] the iteration path is forced to follow a plane normal to the tangent $\mathbf{t}_1$, say, of the equilibrium path at the solution point and, therefore,

$$\delta\mathbf{a}_1^T\delta\mathbf{a}_i + \delta\lambda_1\delta\lambda_i = 0 \ , \ i = 2,3,\ldots \ . \tag{6.3.10}$$

Alternative forms of the constant arc-length method have been developed which either, instead of the standard Newton-Raphson method, make use of a modified

Newton-Raphson method or quasi-Newton-Raphson method, or for which equation (6.3.10) is different. The different Newton-Raphson type techniques are as described in the prequel and, *e.g.* , Chang [Cha91] has used the constant arc-length method in combination with quasi-Newton-Raphson iterations. In the latter case, instead of following the plane normal to the tangent $\mathbf{t}_1$ the method could be modified to follow the plane normal to $\mathbf{t}_{i-1}$. Another alternative is to force all iterates to lie at a fixed distance from the current solution point, *i.e.* on a sphere with radius *ds* and centre at the current solution point. This method was suggested by Crisfield [Cri81]. Batoz and Dhatt [BD79] came up with a different approach by introducing as the additional constraint one which is dependent on the dominant displacement rather than on the load.

The constant arc-length method and its alternatives hence provide a useful tool for problems where limit points are encountered but gives no advantages compared with other mentioned techniques when bifurcations occur. Another drawback of the constant arc-length method is that the solution procedure fails in cases for which $\mathbf{K}_T$ becomes singular.

A good survey of Newton-Raphson as well as the constant arc-length type techniques is given in the paper by Kouhia [Kou] and in the book by Crisfield [Cri91]. Riks [Rik84] and Kouhia and Mikkola [KM89] concentrate on the constant arc-length method and its alternative forms.

6.3.5 Convergence criteria

Convergence criteria are important for deciding when an approximate solution is close enough to the true equilibriating answer. They can be based on displacements such as the smallness of $\delta\mathbf{a}$, the sufficiently small magnitude of the residual forces $(\mathbf{K}_i\mathbf{a}_i - \mathbf{p})$, or the energy.

Usually, convergence criteria are based on a scalar norm such as, *e.g.* , the *2-norm* or *Euler norm* $\| \mathbf{a} \|_2 = (\sum_{i=1}^{n} | a_i |^2)^{\frac{1}{2}}$. In the present work a convergence criterion is used that has also been favoured by Bergan and Clough [BC72], [BC73] and Providas [Pro90] and is based on displacements. For each connector a_i, $i = 1, .., n$ the ratio

$$e_i = \left| \frac{\delta a_i}{a_{max(st)}} \right| , \quad i = 1, .., n , \tag{6.3.11}$$

is computed. Here, $a_{max(st)}$ denotes the largest magnitude total displacement of the same type as the current δa_i. The occurring types in the context of the present work are in-plane displacements, out-of-plane displacements and rotations in terms of cartesian components. The iterations are then terminated if

$$\| \mathbf{e} \|_\infty < \epsilon \tag{6.3.12}$$

where $\| \mathbf{e} \|_\infty = max_{1 \leq i \leq n} \mid e_i \mid$ and ϵ is taken such that desired accuracy is obtained. In the examples in the present work a value $\epsilon = 10^{-7}$ is common.

6.3.6 Branch switching

Up to this point, attention has been paid only to the following of the equilibrium path and the encountering of limit points. The task of entering into the post buckling regime beyond bifurcation points is a more complex problem and is discussed here. Although the underlying theory for the computation of intersecting branches is reasonably well established, *c.f.* the surveys by Mittelmann and Weber [MW80] and Allgower and Georg [AG92], the switch procedures which enable these computations have so far not been implemented successfully into finite element codes in a satisfactory manner. The reasons for this are evident, as all the methods described above result in singular systems at bifurcation points.

The pioneering work in this area was done by Thurston [Thu69] who used a modified Newton-Raphson method applied on the differential equations of the problem at hand. The main drawback of his approach is that for each application a different system needs to be derived from the underlying theory.

An idea would be to restart the whole iterative process at the critical point and with help of a good initial guess seek the equilibrium path beyond the singularity. This has also been suggested by Riks [Rik84] for use with the constant arc-length method. Practical implementations for this have been made by Kouhia and Mikkola [KM89] and Kouhia [Kou92] who have accomplished successful branch switchings. Their achievements, however, are diluted due to problems with regards to robustness, reliability and economy. The major disadvantage is that computations involve higher order derivatives of the potential energy functional, for both determining the type of critical point as well as for finding a suitable starting vector for the continuation from

the critical point, which are obtained only approximately. All results correspond to fairly simple problems such as columns and frames and it should be noted as well that the bifurcations occur to branches where a continuous movement onto the new equilibrium path is feasible, *i.e.* no 'jumps' take place.

A different approach for branch switching has been suggested by Fujii and Choong [FC92]. Here, the type of critical point is determined with help of determinants. The branch switching is accomplished by a line search method in the direction of the tangent of the curve. Successful practical computations are obtained for simple problems such as frames and trusses. Fujii and Choong achieve jumps from the critical point to post critical branches. It is prudent to note, however, that the applicability of the method is confined to problems where these jumps are of small magnitude. Another drawback is the need for the derivative of the tangent stiffness matrix as well as an unjustified exchange of a valid equilibrium equation with an equation determined through the method.

An approach has been suggested by Stein *et al.* [ESO94], whereby an adaptive finite element analysis is used for buckling problems . It is stated in the paper, however, that the employed adaptivity concept is not applicable directly at bifurcation points.

Argyris *et al.* [JHAS77] have accomplished a branch switching through adding to the solution vector at the critical point $\mathbf{a}_{old}$, say, an increment of the critical eigenmode ξ_{old} with the point at which the deflection is imposed held fixed, *i.e.* $\mathbf{a}_{new} = \mathbf{a}_{old} + \alpha\xi_{old}$. A new eigenvector ξ_{new} is then computed for this newly calculated $\mathbf{a}_{new}$ emerging $(\xi_{new})^T \mathbf{K}_T \xi_{new} < 0$. The updating of $\mathbf{a}_{new}$ is continued until the tangent stiffness matrix is no longer negative definite, *i.e.* $(\xi_{new})^T \mathbf{K}_T \xi_{new} \geq 0$. The method provides a limited facility for the treatment of critical points as the above mentioned procedure is only applicable for bifurcation points with a snap-through. Also, no proper justification is given with regard to the employment of the technique. The tangent stiffness matrix used by Argyris *et al.* is an approximation and it is noted in their paper that the method is not fully automated and, thus, needs thorough background knowledge of the derivation of the element used in order to obtain the best possible results.

6.4 Allman's solution technique

6.4.1 Introduction

Keeping the above in mind, the objective is to seek a method that follows reliably the stable equilibrium path and locates accurately the critical point. Once this is achieved, the critical point can be identified using the criteria derived in equations (5.2.46) and equations (5.2.65). With help of knowing the type of critical point a branch switching method is then sought for continuing on the stable equilibrium path beyond the critical point. A generalized Newton-Raphson method developed by Allman [All84] is presented, which converges to minima only. This is a most useful property as it is well known that points on the stable equilibrium path correspond to minima of the total potential energy. The aim of this section is to merely describe the method. Computational aspects such as locating the critical point precisely and continuing from the critical point are discussed in the sequel.

6.4.2 Calculation of stable equilibrium paths

Stable equilibrium paths of discrete conservative systems are the loci of minima of a potential energy function Π with

$$\Pi = \Pi(\mathbf{a}, \lambda) \tag{6.4.13}$$

where the vector argument $\mathbf{a}$

$$\mathbf{a} = (a_1, ..., a_n)^T \tag{6.4.14}$$

describes the geometry and deformation of the structure while λ is a parameter by which the deformation can be changed. The parameter λ is assumed to be representative of a loading which is induced either by external forces or by prescribed displacements or by a combination of both.

Accordingly, stable equilibrium paths are solutions of the n nonlinear equilibrium equations

$$\mathbf{f} = \mathbf{f}(\mathbf{a}, \lambda) = \{f_i\} = (f_1, ..., f_n)^T = \mathbf{0} \quad , \quad f_i = \Pi_{,a_i} \tag{6.4.15}$$

for which the symmetric positive definite Hessian $\mathbf{H}$, *i.e.* the tangent stiffness matrix

$\mathbf{K_T}$ in the finite element context, is given by

$$\mathbf{H} = \mathbf{H}(\mathbf{a},\lambda) = [h_{ij}] = \begin{bmatrix} h_{11} & \dots & h_{1n} \\ | & \dots & | \\ h_{n1} & \dots & h_{nn} \end{bmatrix}, \quad h_{ij} = \Pi_{,a_i a_j} = f_{i,a_j} \ . \tag{6.4.16}$$

The n eigenvalues $\theta^{(i)}$ and eigenvectors $\boldsymbol{\xi}^{(i)}$ of H are taken to satisfy

$$\begin{aligned} \mathbf{H}\,\boldsymbol{\xi}^{(i)} &= \theta^{(i)}\,\mathbf{T}\,\boldsymbol{\xi}^{(i)}, \quad \text{(no sum on } i\text{)} \\ (\boldsymbol{\xi}^{(i)})^T\,\mathbf{T}\,\boldsymbol{\xi}^{(i)} &= 1 \end{aligned} \tag{6.4.17}$$

for any positive definite symmetric matrix T. The eigenvalues are therefore all positive and are arranged such that

$$\theta_{max} = \theta^{(n)} \geq \theta^{(n-1)} \geq \dots \geq \theta^{(2)} \geq \theta^{(1)} = \theta_{min} > 0 \ , \tag{6.4.18}$$

where θ_{max} and θ_{min} denote respectively the largest and smallest eigenvalues. On an unstable path there exist some $\theta^{(i)} < 0$ and so the Hessian matrix is indefinite. At a simple critical point $\theta_{min} = 0$ the Hessian matrix is singular. This causes difficulties for the calculation of these points by the standard Newton method; convergence is often very slow or the method fails due to numerical errors in computation.

A modification of Newton's method has been presented by Allman [All84] which converges only to minima in applications to find stationary points of a continuously differentiable function of several variables. This property proves to be useful for the reliable calculation of stable equilibrium paths of discrete conservative systems because they correspond to minima of the potential energy function.

The iteration to calculate an improvement $\mathbf{a}^{(k+1)}$ in a known vector of n variables $\mathbf{a}^{(k)}$ is

$$\mathbf{a}^{(k+1)} = \mathbf{a}^{(k)} + \Delta\mathbf{a}^{(k)}, \quad k = 0, 1, \dots, \tag{6.4.19}$$

where the increment $\Delta\mathbf{a}^{(k)}$ is found by solving the system of linear equations

$$[\mathbf{H}(\mathbf{a}^{(k)},\lambda) + \sigma\,\mathbf{T}]\,\Delta\mathbf{a}^{(k)} = -\gamma\,\mathbf{f}(\mathbf{a}^{(k)},\lambda) \ . \tag{6.4.20}$$

In equation (6.4.20) the coefficients γ, σ and the positive definite matrix T are chosen, *c.f.* Allman [All84], as follows: putting $\gamma = 2$ ensures that the iterative

method converges to minima only; the linear convergence of the iteration is fastest if $\sigma = \sigma_0$, an optimum value dependent on the problem, which can be shown to be

$$\sigma_0 = \sqrt{\theta_{min}\theta_{max}} \; ; \tag{6.4.21}$$

the positive definite matrix T is initially chosen as the Hessian matrix at the current (known) solution point, then a matrix updating algorithm for T improves the basic linear convergence to superlinear convergence as the next solution point is approached, *i.e.* when $\Delta\mathbf{a}^{(k)}$ becomes small enough. Allman's criterion $\| \Delta\mathbf{a}^{(k)} \| \leq \epsilon_{abs} + \epsilon_{rel} \| \mathbf{a}^{(k)} \|$ is adopted also in the present work with $\epsilon_{abs} = 2 \times 10^{-t}$ the absolute accuracy on a machine of t bit word length and for the relative accuracy $\epsilon_{rel} = 10^{-2}$ is found satisfactory.

6.5 Computational aspects

6.5.1 Introduction

The success of the current work is based on the combination of two recent advances: the above described solution technique by Allman [All89a], and the development of the geometrically nonlinear constant moment triangle finite element by Morley [Mor91]. For the proper evaluation of critical points higher order derivatives of the potential energy function Π are essential, but for most finite elements even the computation of the Hessian $\Pi_{,ij}$ is an approximation. Using the geometrically nonlinear constant moment triangle, however, allows a ready and accurate calculation of all directional derivatives of the potential energy function Π.

In this section some computational aspects regarding the implementation of Allman's method into the MBFEATPS (Morley-Bangemann Finite Element Analysis of Thin Plates and Shells) finite element code, which has been employed for computing all the results for the present work, are described. Locating the critical point in a safe manner without overstepping another critical point is of importance. Also, an additional feature of the code, the step length adaption algorithm, is presented.

6.5.2 Step length adaption

6.5.2.1 Displacement control

Using displacement control, the displacements in the direction of compression are prescribed to be of equal magnitude at each point of the compressive edge(s). The adapted step length is determined by using the following adaption procedure:

1. Let ID denote the predefined value indicating the *IDeal number of iterations per increment*

2. Let $ITER$ denote the value indicating the *current number of ITERations per increment*

3. Let $STEP$ denote the value indicating the *current STEP length in use*

4. During the iteration process, if the current number of iterations exceeds the ideal number of iterations per increment, halve the step size, *i.e.*
   (STABLE POINT NOT FOUND AND $ITER > ID$) $\Rightarrow$ $STEP = \frac{1}{2}STEP$

5. After the iteration process (*i.e.* after having found a stable solution point), if the number of iterations used for the current increment is smaller than the ideal number of iterations per increment, the step length for the next increment is the previous step length, multiplied by the ideal number of iterations, divided by the actual number of iterations used for the current increment, *i.e.*
   (STABLE POINT FOUND AND $ITER < ID$) $\Rightarrow$ $STEP = \frac{ID}{ITER}STEP$

6.5.2.2 Load control

Using load control, the load is applied such that the resulting displacements in the direction of compression are of equal magnitude at each point along the compressive edge(s) (loading of a constrained boundary). The objective of this load control is to provide identical solutions as for displacement control excepting, of course, where 'jumps' occur. The equivalent load increment adaption procedure is then:

1. Let ID denote the predefined value indicating the *IDeal number of iterations per increment*

2. Let $ITER$ denote the value indicating the *current number of ITERations per increment*

3. Let $INCR$ denote the value indicating the *current load INCRement in use*

4. During the iteration process, if the current number of iterations exceeds the ideal number of iterations per increment, halve the load increment, *i.e.*
(STABLE POINT NOT FOUND AND $ITER > ID$) $\Rightarrow$ $INCR = \frac{1}{2} INCR$

5. After the iteration process (*i.e.* after having found a stable solution point), if the number of iterations used for the current increment is smaller than the ideal number of iterations per increment, the load increment for the next increment is the previous load increment, multiplied by the ideal number of iterations, divided by the actual number of iterations used for the current increment, *i.e.*
(STABLE POINT FOUND AND $ITER < ID$) $\Rightarrow$ $INCR = \frac{ID}{ITER} INCR$

6.5.3 The value of σ

Recall equation (6.4.21) where the σ-value for Allman's solution technique is given by

$$\sigma = \sqrt{\theta_{min}\theta_{max}} \ , \tag{6.5.22}$$

where θ_{min} and θ_{max} are the smallest and largest eigenvalues of the tangent stiffness matrix, respectively. Note here, that θ_{min} and θ_{max} are actually not known at the current point and can only be estimated. Instead of using the estimated values for θ_{min} and θ_{max}, as Allman [All89b] does, the MBFEATPS code uses the smallest and largest eigenvalues at the previous solution point - θ^{pr}_{min} and θ^{pr}_{max} - which are known exactly and, then, takes σ as

$$\sigma = \sqrt{\theta^{pr}_{min}\theta^{pr}_{max}} \ . \tag{6.5.23}$$

This, however, is not believed to deteriorate the performance of the method significantly, and it should also be noted here that it is often found that the value $\sigma = 1$ is quite adequate, *cf.* Allman [All89b] and Bartholomew [Bar83].

6.5.4 Locating the critical point

Unlike in the original method by Allman [All89b], where he makes use of a predictor to locate singular points, no predictor is used in the MBFEATPS code. Instead, adapted displacement step lengths or load increments, as described earlier, are applied as long as the Hessian (tangent stiffness matrix) remains positive definite. When the Hessian becomes indefinite, the applied step length / load increment is halved until an appropriate step length / load increment is found leading to a positive definite Hessian. Hence, checking the positive definiteness of the Hessian at each iteration prevents overstepping a singular point. This kind of *bisection method* for locating the critical point is found to be safe and effective, and the critical point can be located precisely without any difficulties. For checking the positive definiteness of the Hessian the NAG-library routine F01BXF is used. This routine performs the Cholesky factorization of a real symmetric positive definite matrix.

6.5.5 Identifying the critical point

Once the critical point has been located, it has to be identified. This is done as described in Chapter 5 where the different stability coefficients μ, A, B, C, and D are calculated using a convenient matrix formulation. For convenience, the criteria for identifying the type of a critical point as in equations (5.2.46) are repeated here:

$$\begin{aligned} &\text{(a) an asymmetric bifurcation point} && \mu = 0\,,\ A \neq 0\,; \\ &\text{(b) a symmetric bifurcation point} && \mu = 0\,,\ A = 0\,; \\ &\text{(c) a limit point} && \mu \neq 0\,,\ A \neq 0\,. \end{aligned} \tag{6.5.24}$$

The symmetric bifurcation point, appearing as the second criteria in equations (6.5.24) occurs in two distinct types: stable symmetric and unstable symmetric. The following criteria for determining stability apply:

$$\begin{aligned} &\text{(a) a symmetric bifurcation point is stable if} && D > 0\,; \\ &\text{(b) a symmetric bifurcation point is unstable if} && D < 0\,. \end{aligned} \tag{6.5.25}$$

6.6 Continuation from critical points

6.6.1 Introduction

Once a critical point has been located and identified the aim is to continue beyond the singularity. In the past, this has been a formidable task. As discussed earlier, although the underlying theory is reasonably well established, *c.f. e.g.* surveys by Mittelmann and Weber [MW80] and Allgower and Georg [AG92], the required switch procedures between bifurcation paths have not been implemented previously into finite element codes in a satisfactory manner.

A branch switching method, here called METHOD A, which has been implemented into the MBFEATPS code and used successfully for getting beyond critical points is presented. Two other branch switching methods, METHOD B and METHOD C, are given in Appendix B.1 and Appendix B.2, respectively. METHOD B is shown in order to present an alternative approach to the branch switching, whereas METHOD C is mainly of historical importance. The aim of the continuation methods is to produce vectors $\mathbf{a}_1^{(0)}$ and $\mathbf{a}_2^{(0)}$ which are then employed as starting values for continuing from the critical point using Allman's solution technique. The methods are presented in algorithmic step-by-step forms. Note that the generalized eigenvalue problem in the first step of the branch switching methods is solved by employing the NAG-library routine F02BJF which solves the problem $\mathbf{Ax} = \lambda\mathbf{Bx}$, where **A** and **B** are real square matrices, using the QZ-algorithm.

6.6.2 Branch switching method METHOD A

METHOD A

1. • **At the initial start (from the origin)**

   (a) Compute the solution vector $\mathbf{a}_{lin}^*$ of the linear problem with uniform displacement.

   (b) Solve the generalized eigenvalue problem $(\mathbf{K}_0 + \lambda\mathbf{K}_G)\,\delta\mathbf{a} = \mathbf{0}$ which gives the eigenvector $\xi_p^{(1)}$ corresponding to the smallest eigenvalue λ_{min} and determine $\mathbf{a}_p^* = \lambda_{min}\mathbf{a}_{lin}^*$. Here, $\mathbf{K}_0$ denotes the linear stiffness matrix and $\mathbf{K}_G$ is the geometric stiffness matrix.

- **At the start from a critical point** compute the solution vector $\mathbf{a}_p^*$ and the eigenvector $\boldsymbol{\xi}_p^{(1)}$ corresponding to the zero eigenvalue at the critical point using the employed nonlinear solution technique.

2. Determine the first starting vector $\mathbf{a}_1^{(0)}$ for the continuation procedure from the buckling point from

$$\mathbf{a}_1^{(0)} = \mathbf{a}_p^* + \alpha_1 \boldsymbol{\xi}_p^{(1)} \tag{6.6.26}$$

where the parameter α_1 determines the proportion of the normalized eigenvector ($(\boldsymbol{\xi}_p^{(1)})^T \boldsymbol{\xi}_p^{(1)} = 1$) to be used.

3. Determine the second starting vector $\mathbf{a}_2^{(0)}$ for the continuation procedure from the buckling point from

$$\mathbf{a}_2^{(0)} = \mathbf{a}_p^* + \alpha_1 \alpha_2 \boldsymbol{\xi}_p^{(1)} , \tag{6.6.27}$$

where the parameter α_2 determines the difference in the eigenvector to be used compared to the first starting vector.

4. Use $\mathbf{a}_1^{(0)}$ and $\mathbf{a}_2^{(0)}$ as starting vectors for the continuation procedure and solve in the first iteration the system

$$[\, \mathbf{H}(\mathbf{a}_1^{(0)}) + \mathbf{T}(\mathbf{a}_2^{(0)})\,]\, \Delta\mathbf{a} = -\gamma [\, \mathbf{K}(\mathbf{a}_1^{(0)})\mathbf{a}_1^{(0)} - \lambda \mathbf{p}^*] \tag{6.6.28}$$

where $\mathbf{T}(\mathbf{a}_2^{(0)})$ is the Hessian constructed using $\mathbf{a}_2^{(0)}$.

5. Continue in the ordinary fashion.

6.6.3 Notes on methods

6.6.3.1 On the second starting vector $\mathbf{a}_2^{(0)}$

The choice of the second starting vector $\mathbf{a}_2^{(0)}$ has been examined closely. The points to keep in mind are:

1. a bad choice of $\mathbf{a}_2^{(0)}$ results in divergence and the method does not perform successfully;

2. practically, it is not feasible to construct an *ideal* second starting vector.

Therefore, the importance of the second starting vector should be lessened. This is achieved by eliminating $\mathbf{a}_2^{(0)}$ after the first iteration, *i.e.* after the first iteration of the continuation method $\mathbf{a}_2^{(0)}$ is substituted by the first starting vector $\mathbf{a}_1^{(0)}$. Evidently, this suggests to choose $\mathbf{a}_2^{(0)} = \mathbf{a}_1^{(0)}$ in the continuation method, which also has proven to be a good choice, *i.e.* the first iteration for continuation is an ordinary Newton-Raphson iteration.

6.6.3.2 On the choice of the parameter α_1

Although the branch switching method described in the previous section has proved to be most powerful, questions regarding the suitable choices of the different parameters occurring still exist. Ideally, it is anticipated to present a method with the following features:

1. all parameters are calculated automatically using problem-dependent parameters only;

2. the choices (see 1. above) are *ideal* choices.

The parameter α_2 can be eliminated by keeping in mind the above thoughts regarding the second starting vector in the continuation method, hence leaving α_1 the only unknown parameter to be determined. During the course of the present work a successful choice for the α_1 parameter has been found by a trial-and-error approach while simultaneously monitoring the behaviour of the norm. In Chapter 8 it is suggested that the manually-performed norm-monitoring could be coded and, in this way, an automated procedure for determining a suitable parameter α_1 entailing successful continuation beyond bifurcation points can be set up.

Also, a *least squares fit* procedure has been incorporated into the code for use with METHOD A. The algorithm for this procedure is given in Appendix B.3. With help of this the *ideal* choice for the parameter α_1 in equation (6.6.26) is found. The drawback of this procedure is that the ideal *least squares fit*-value can only be computed once a successful first increment has been performed by the continuation method. Still, once this has been accomplished, a good idea regarding a suitable choice is given by the magnitude of the value found. Also, if the ideal *least squares fit*-value α_1^A has been established for a mesh A, say, the ideal value for another mesh

B, say, can be determined immediately using the empirical relationship

$$\alpha_1^A \, (\xi_p^{(1)})_{max}^A = \alpha_1^B \, (\xi_p^{(1)})_{max}^B \, . \tag{6.6.29}$$

It should be noted here, however, that the procedure only yields a unique ideal solution in case of a symmetric or antisymmetric mode shape of the structure. In case of an asymmetric mode shape a different initial choice for α_1 will give a different ideal α_1-value calculated using the *least squares fit*-procedure.

The sign of the initial choice of α_1 is of importance in the sense that, in this way, the direction of buckling may be controlled. If additional imperfections are employed and METHOD A is used, then positive/negative α_1 give load and deflection values greater/smaller in magnitude compared with the solution when no imperfections are applied. This kind of 'stiffness control' is discussed in more detail in Chapter 7 where the sign of α_1 is considered in the context of specimen numerical applications.

Chapter 7

Numerical applications

7.1 Introduction

For the computational work, a comprehensive Fortran 77 code, the *Morley-Bangemann Finite Element Analysis of Thin Plates and Shells* code (MBFEATPS), has been developed during the course of the current work. A program description is given in Appendix D.1. MBFEATPS has been tested against the MPFEAS (*Morley-Providas Finite Element Analysis of Shells*) code by solving different numerical examples examined by Providas, *c.f.* [Pro90], revealing identical results for these problems which, evidently, are of a less complex nature (limit point problems) than the ones examined in this chapter (bifurcation point problems). It should be noted here that the MBFEATPS code has been completely rewritten and is not based on the MPFEAS code. All calculations make use of double precision variables (accuracy 1.0×10^{-14}) and have been performed on Sun-machines on a Unix system.

7.2 Plate problem

7.2.1 Introduction

A square clamped plate under uniaxial compression is investigated. The plate lies in the x^1-x^2-plane with out-of-plane direction x^3 and is clamped along the boundaries, but the in-plane displacement is free along the unloaded edges, *c.f.* Figure 7.1, where also the material and geometrical data are given and the boundary conditions are

stated.

The main interest in this work is the physical behaviour of the initially perfectly flat plate or *perfect plate* in the sequel. Additional work has also been done on the use of initial geometrical imperfections. Comparison results are extracted from Carnoy and Hughes, *c.f.* [CH83]. It should be mentioned here that Carnoy and Hughes consider only plates with initial imperfections. Note that in this work the first critical/buckling point refers to the first nonlinear critical/buckling point and so forth, whereas the linear buckling is referred to as Euler buckling.

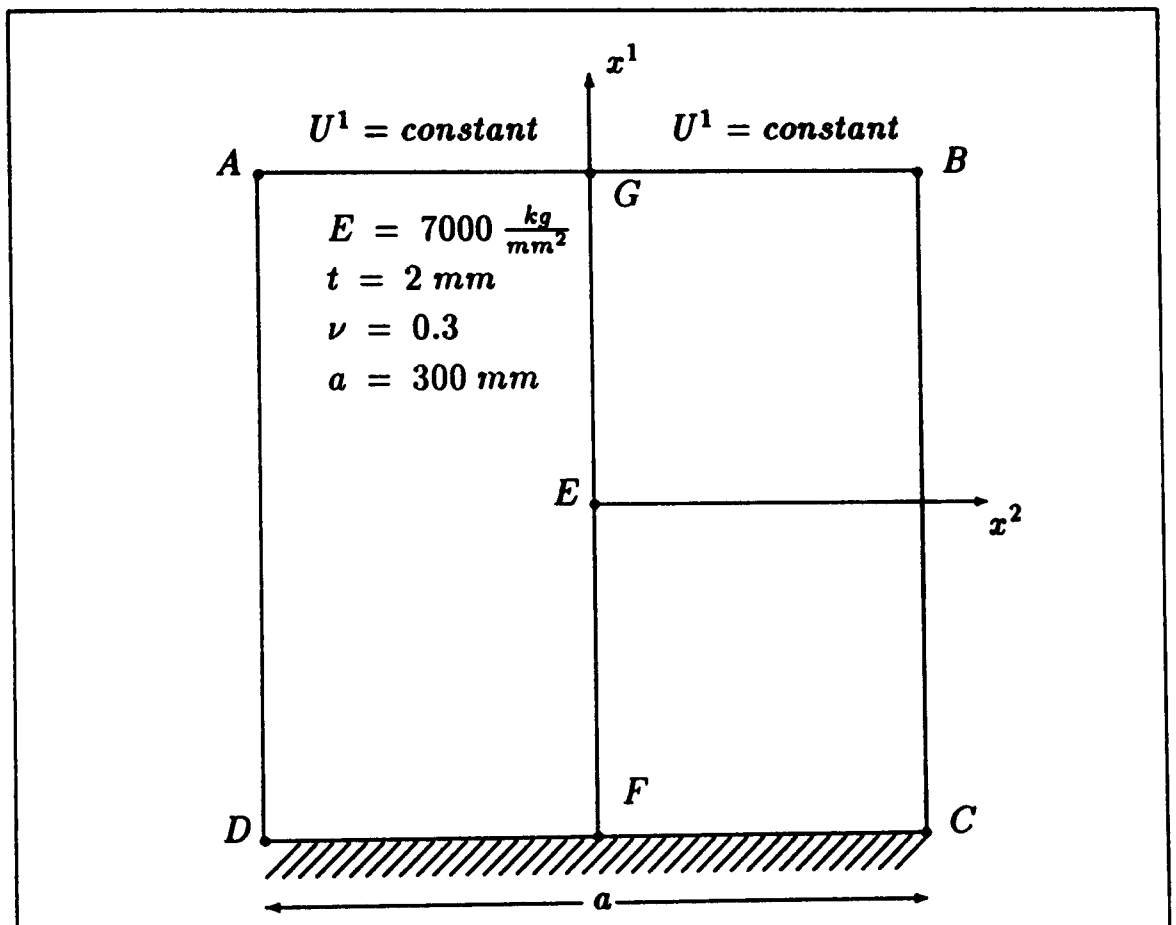

Boundary conditions:

$$AB \ : \ U^1 = constant\ ,\ U^2 = U^3 = \frac{\partial U^3}{\partial n} = 0$$

$$DC \ : \ U^1 = U^2 = U^3 = \frac{\partial U^3}{\partial n} = 0$$

$$BC\ ,\ AD \ : \ U^3 = \frac{\partial U^3}{\partial n} = 0$$

Figure 7.1. Square flat plate: material and geometrical data and boundary conditions.

As the interest lies in the symmetric buckling about the longitudinal line of compression $F - G$ only half a plate is modelled. Results given in this section

correspond to the 8×4 mesh as depicted in Figure 7.2 unless otherwise stated. Several meshes employed for the problem are shown in Appendix C.1.

For practical and verificational reasons, not only displacement control has been used for the calculations but also load control. In this context load control means that the load is applied such that the resulting displacements in the direction of compression are of equal magnitude at each point along the compressive edge (loading of a constrained boundary).

The continuation from critical points is accomplished by using the continuation method Method A as described in Chapter 6. Note that the sign of the parameter α_1 used in the method determines the sign of the waves obtained as results, *i.e.* the direction of buckling can be controlled in this way.

7.2.2 Perfect plate

7.2.2.1 Numerical results

All results presented in this section are obtained using displacement control unless otherwise stated. The emerging load - deflection curve, smallest eigenvalue - deflection curves, deflection - compression curve and curves for the mode shapes along the longitudinal and transverse axes are shown in Figures 7.3 - 7.8, respectively, with comparison results by Carnoy and Hughes, *c.f.* [CH83], for the load - deflection curve. In the context of the present work, deflection means the central deflection, *i.e.* the out-of-plane displacement at the centre point of the plate E, *c.f.* Figure 7.1. Note that the comparison results presented by Carnoy and Hughes are for non-perfect plates with initial symmetrical imperfections with an initial out-of-plane central deflection of $0.5mm$. The figures show the behaviour until well beyond the third critical point. It is emphasized that Carnoy and Hughes are able to treat the problem (even with imperfections) only up to the first critical point. The straight line at the start of the load - deflection curve (Figure 7.3) indicates the jump to the Euler buckling load from where the non-linear regime is entered. The non-dimensional load P is calculated here from $P = \frac{P_{tot}}{F}$ where P_{tot} is the total applied load and $F = \frac{\pi^2 D}{a}$ where $D = \frac{Et^3}{12(1-\nu^2)}$ is the flexural rigidity of the plate and $a = 300mm$ and $t = 2mm$ are the dimension and the thickness of the plate, re-

spectively, while E is Young's modulus and ν is Poisson's ratio. The marked points on the curves depict the found increment points on the stable equilibrium path. The notation $CPi-$ and $CPi+$ is used in the sequel where $CPi-$ corresponds to the last found solution point on the stable equilibrium path before the ith critical point, *i.e.* it represents the ith singular point, whereas $CPi+$ corresponds to the configuration immediately after the ith critical point. The first critical point $CP1-$ is found at increment number 40. Up to here the mode shape is symmetric. Then a jump takes place to increment number 41. A snap mode change occurs as the mode changes to be antisymmetric and remains as such until the second critical point $CP2-$ is found at increment number 92. Continuing from $CP2-$ involves a branch switching with no snap onto another path with an asymmetric two wave mode shape at increment number 93. The mode shape remains asymmetric all the way up to the third critical point $CP3-$ at increment number 134. Note that the change in load along this asymmetric path is small. Increasing the compression entails again a snap mode change to a fully antisymmetric four wave form at increment number 135. The mode shape remains antisymmetric and no further critical points are found. It should be noted here that at the last marked solution point at increment number 400 the compression is as large as $370\,mm$, *i.e.* with a plate dimension of $300\,mm$ this means that the plate has actually flipped over long before this. Recall that the plate theory employed in the present work is valid up to a maximum displacement of magnitude ≈ 6 times the plate thickness. The example is treated up to a maximum displacement of magnitude ≈ 20 times the plate thickness, *i.e.* $\approx 40mm$ with the example thickness $t = 2mm$, in order to underline the potential of the method employed. The point where the maximum displacement takes this value is marked in Figure 7.3 at increment number 225. Two smallest eigenvalue - deflection curves are presented. In the curve denoted 'with T-matrix' the T-matrix in equation (6.4.17) is taken as the Hessian at the previous increment or iteration point according to Allman's solution technique, whereas in the curve denoted 'without T-matrix' the T-matrix is taken as the identity matrix. To improve visualization, for the curves depicting mode shapes only a few curves are presented for chosen increment points. Note that all curves are obtained by simply connecting the found points, *i.e.* no attention is drawn *e.g.* to the fact that the slopes at the edges of the plate are supposed to be

zero. Also, the four wave form beyond $CP3-$ is not visible as along the centre line, where the connectors for the mode shapes are saved, the mesh is not able to exhibit this behaviour.

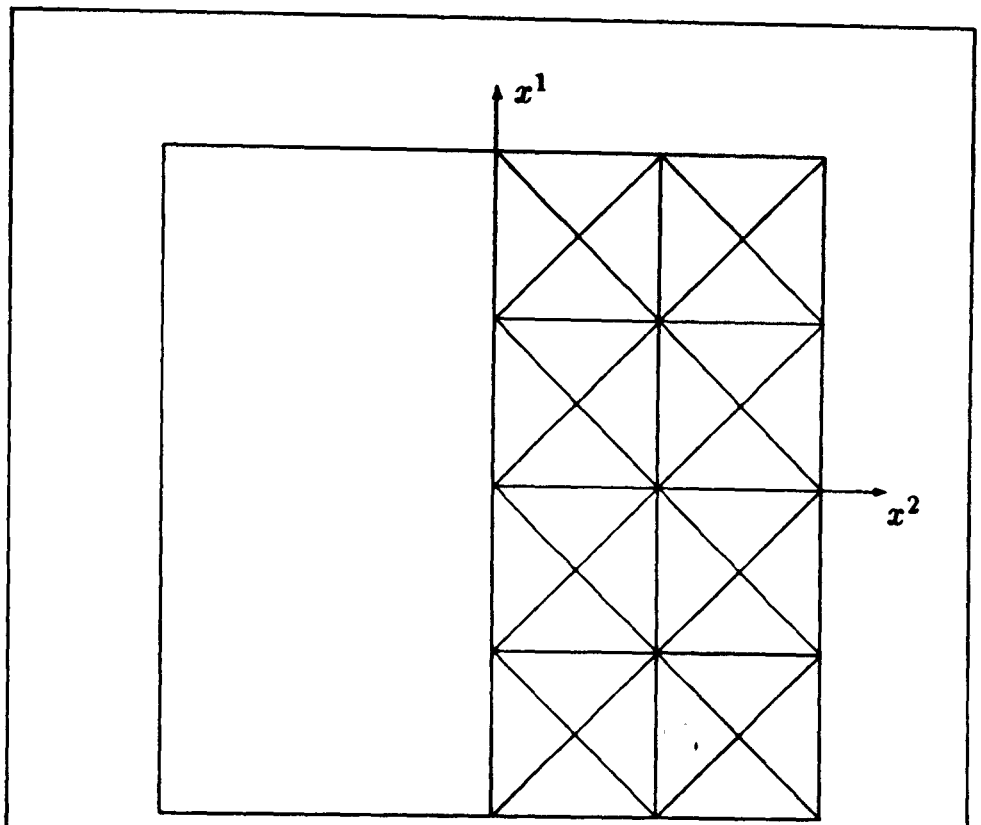

Figure 7.2. Half a plate modelled using the 8×4 mesh.

The stability coefficients at the critical points reveal that

- at $CP1-$:

$$\begin{aligned} \mu &= \pm 0.000 \times 10^{0} \quad i.e. \quad \mu = 0 \\ A &= -0.549 \times 10^{-8} \quad i.e. \quad A = 0 \\ D &= -0.576 \times 10^{5} \quad i.e. \quad D < 0 \ . \end{aligned} \tag{7.2.1}$$

Hence the critical point is identified as an *unstable symmetric bifurcation point* which is in agreement with the investigations performed by Carnoy and Hughes, *c.f.* [CH83]. It is called symmetric because the load - amplitude of the bifurcation eigenmode curve is symmetric with respect to a change of sign of the amplitude. Hence, an antisymmetric eigenmode is expected at this first critical point after snapping, which is also the case. [1]

[1] Recalling the linear theory it is expected that, if the mode shape at the i'th critical point is symmetric (antisymmetric) with i waves, then the eigenmode at this critical point reveals an antisymmetric (symmetric) shape with $(i+1)$ waves and the deformed configuration beyond the critical point also has an antisymmetric (symmetric) shape with $(i+1)$ waves.

The load at $CP1-$ is $P = 0.872 \times 10^1$, the central deflection $w_{cd} = 0.250 \times 10^1$ and the end displacement $U^1 = 0.138 \times 10^0$.

The mode shape between the linear buckling point and $CP1-$ is symmetric with one wave.

Successful continuation from the Euler buckling point is achieved with $\alpha_1 = 0.500 \times 10^1$. Successful continuation from $CP1-$ is achieved with $\alpha_1 = 0.100 \times 10^1$.

- at $CP2-$:

$$\begin{aligned} \mu &= \pm 0.000 \times 10^0 \quad i.e. \quad \mu = 0 \\ A &= -0.220 \times 10^{-8} \quad i.e. \quad A = 0 \\ D &= -0.160 \times 10^6 \quad i.e. \quad D < 0 \ . \end{aligned} \tag{7.2.2}$$

Hence the critical point is identified as an ***unstable symmetric bifurcation point.***

The load at $CP2-$ is $P = 0.106 \times 10^2$, the central deflection $w_{cd} = 0.506 \times 10^{-6}$ and the end displacement $U^1 = 0.329 \times 10^1$.

The mode shape between $CP1+$ and $CP2-$ is antisymmetric with two waves.

Successful continuation from $CP2-$ is achieved with $\alpha_1 = 0.010 \times 10^0$.

- at $CP3-$:

$$\begin{aligned} \mu &= \pm 0.000 \times 10^0 \quad i.e. \quad \mu = 0 \\ A &= +0.604 \times 10^0 \quad i.e. \quad A \neq 0 \ . \end{aligned} \tag{7.2.3}$$

Hence the critical point is identified as an ***asymmetric bifurcation point.*** It should be remembered here that the stability coefficient D has in the case where $A \neq 0$ no significance as all asymmetric bifurcation points are unstable.

The load at $CP3-$ is $P = 0.113 \times 10^2$, the central deflection $w_{cd} = 0.116 \times 10^1$ and the end displacement $U^1 = 0.732 \times 10^1$.

The mode shape between $CP2+$ and $CP3-$ is asymmetric with two waves.

Successful continuation from $CP3-$ is achieved with $\alpha_1 = -0.591 \times 10^1$.

For the justification, that the values obtained for the stability coefficient A at $CP1-$ and $CP2-$ can be interpreted as zero here and in other examples in the sequel, *c.f.* Appendix C.2.

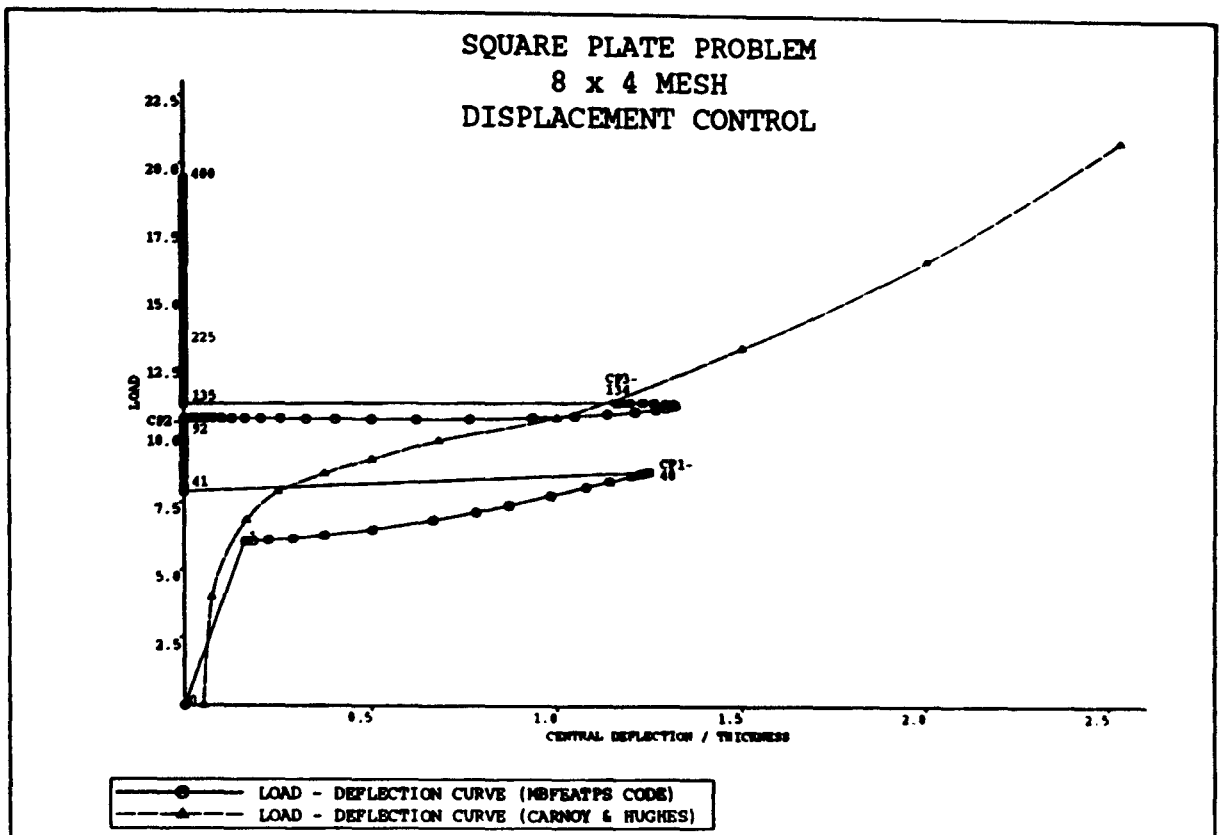

Figure 7.3. Load - deflection curve for the perfect plate using the 8 × 4 mesh.

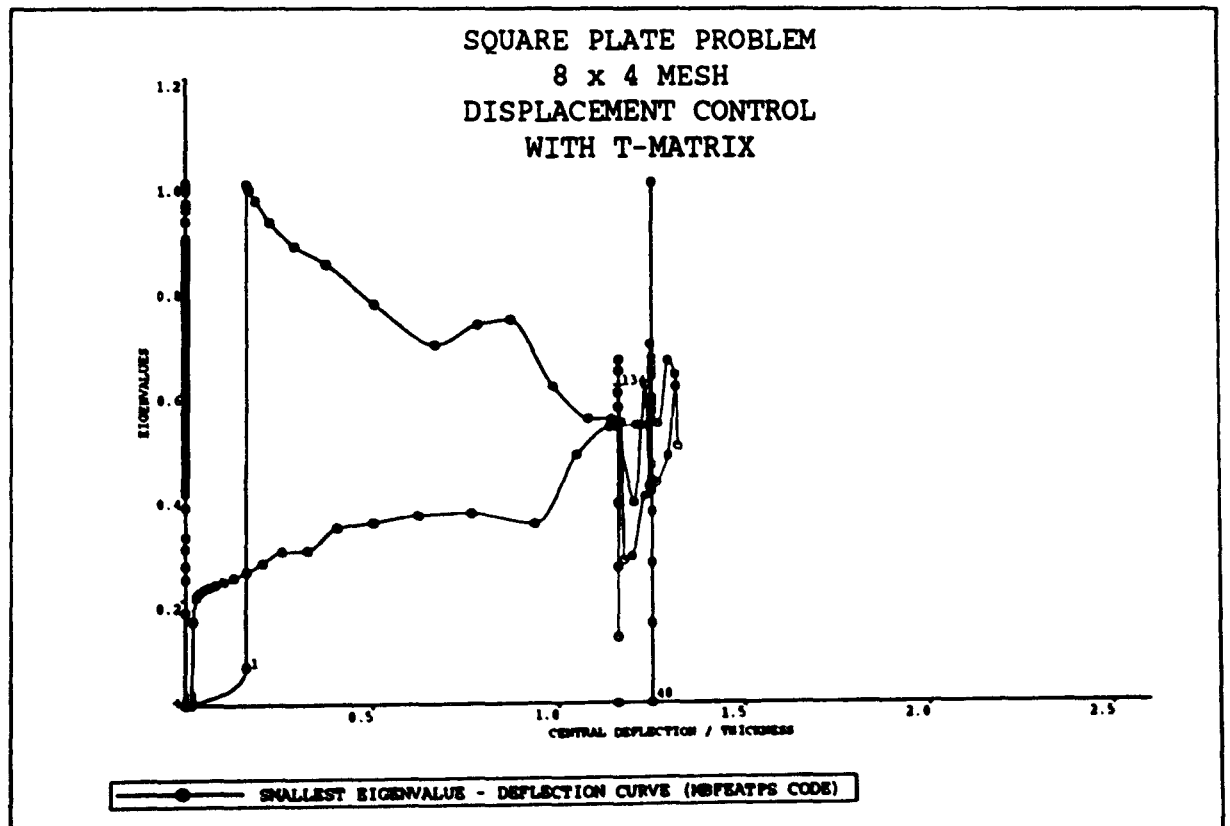

Figure 7.4. Smallest eigenvalue - deflection curve for the perfect plate using the 8 × 4 mesh (with T-matrix, *i.e.* eigenvalues $\theta^{(r)}$ calculated from $\mathbf{K_T}\boldsymbol{\xi}^{(r)} = \theta^{(r)}\mathbf{T}\boldsymbol{\xi}^{(r)}$ (no sum on r)).

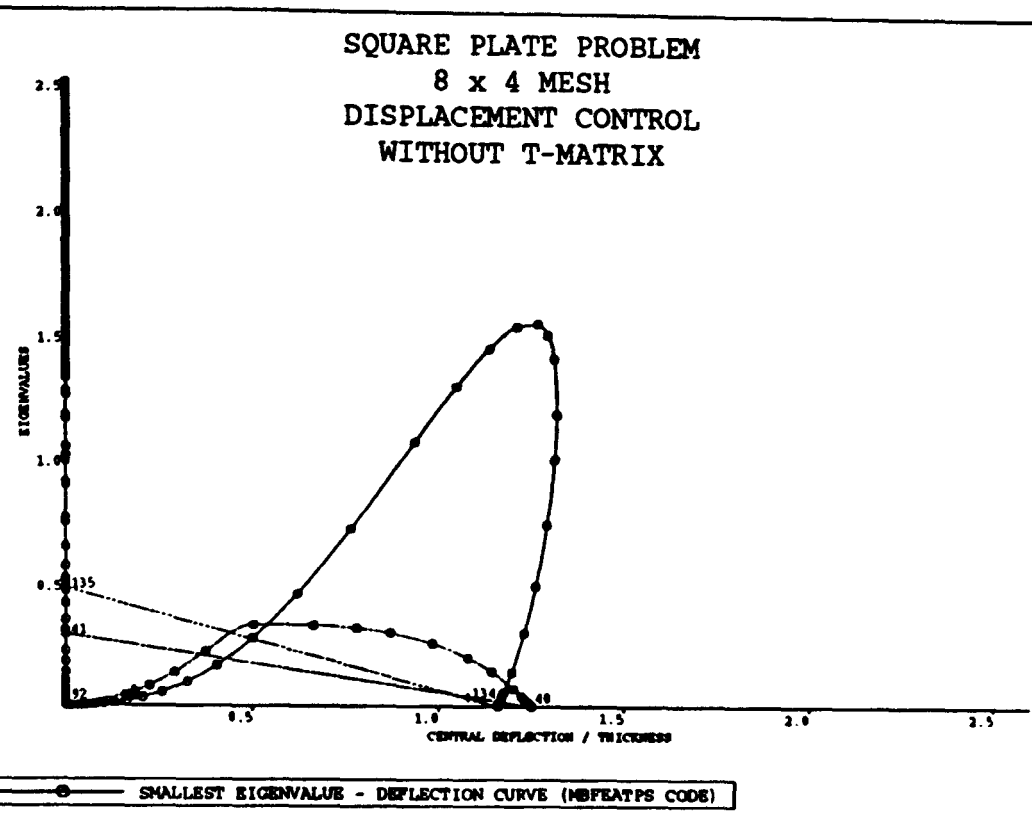

Figure 7.5. Smallest eigenvalue - deflection curve for the perfect plate using the 8×4 mesh (without T-matrix, *i.e.* eigenvalues $\theta^{(r)}$ calculated from $\mathbf{K_T}\boldsymbol{\xi}^{(r)} = \theta^{(r)}\boldsymbol{\xi}^{(r)}$ (no sum on r)).

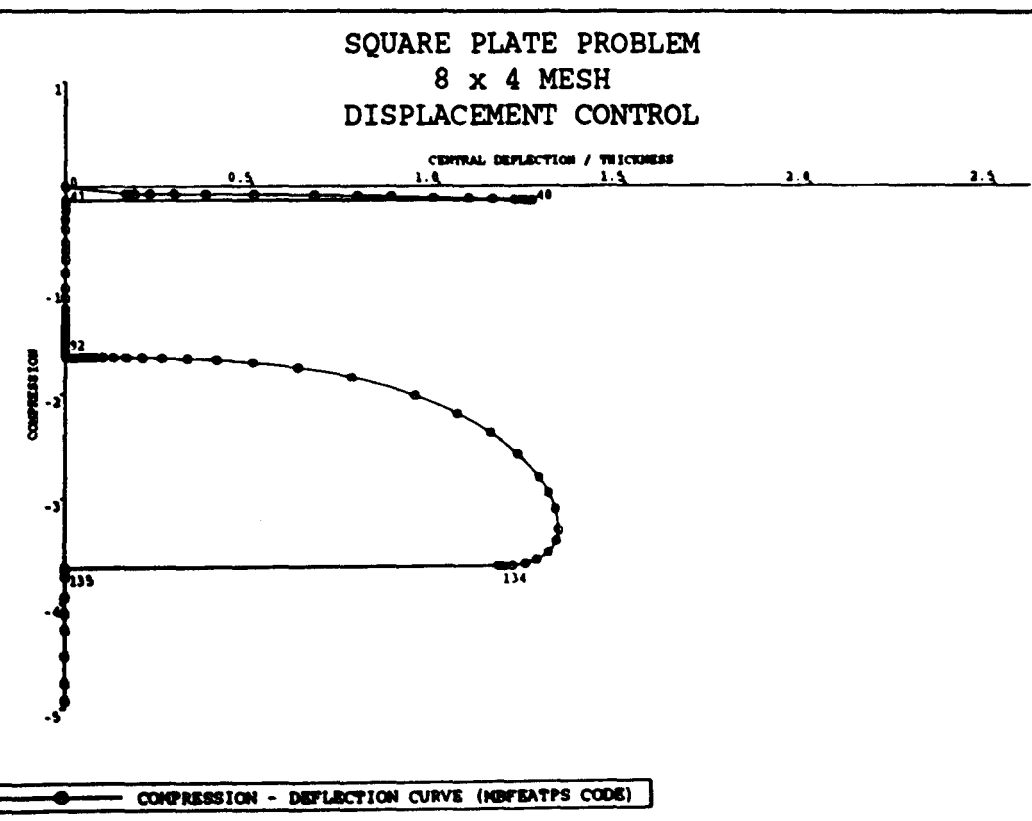

Figure 7.6. Compression - deflection curve for the perfect plate using the 8×4 mesh.

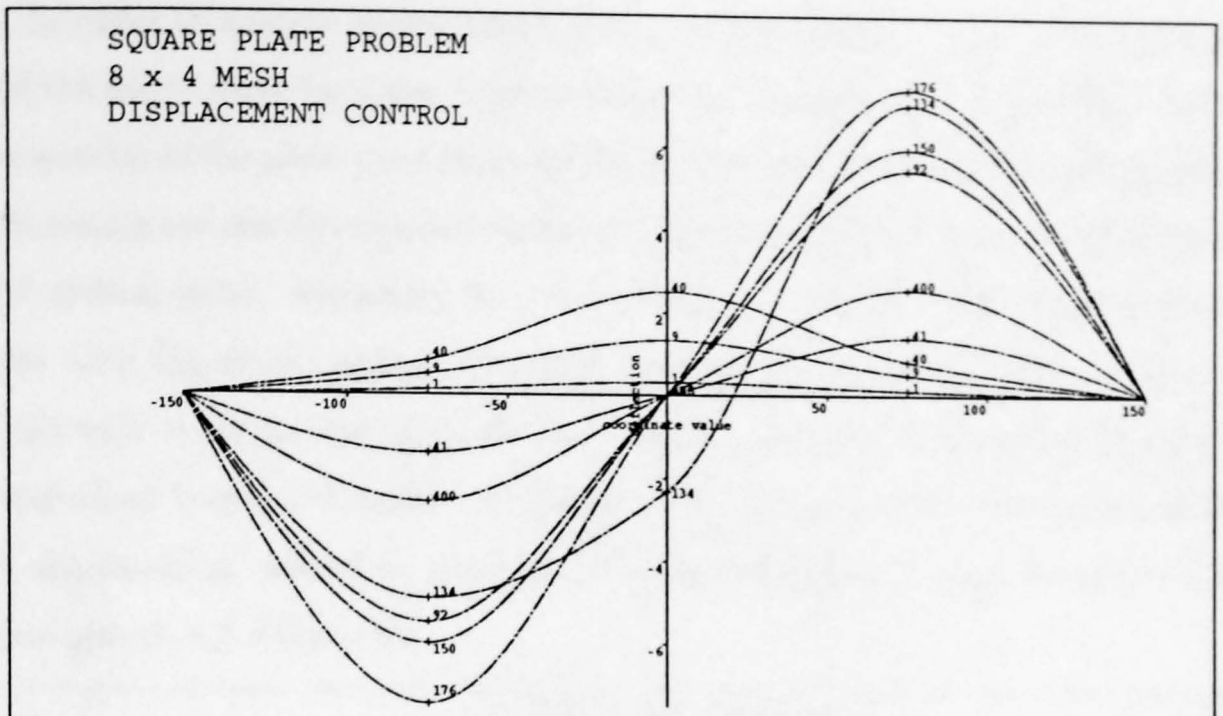

Figure 7.7. Mode shapes along the longitudinal axis of the perfect plate using the 8×4 mesh.

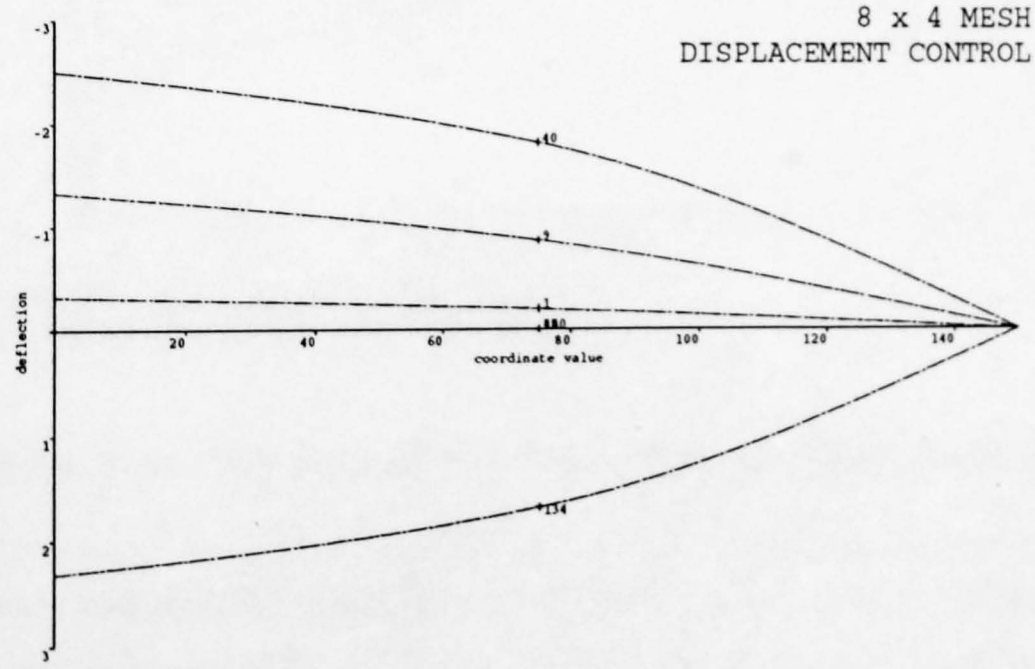

Figure 7.8. Mode shapes along the transverse axis of the perfect plate using the 8×4 mesh.

In order to achieve confirmation of the results obtained, a quarter of the plate and the whole plate have also been modelled for this example. Evidently, modelling the quarter of the plate constrains out the first critical point and, therefore, comparison results are merely obtained for load, deflection and compression values until the first critical point. Modelling the whole plate, *i.e.* modelling the other half of the plate with the mirror image of the half plate model, reveals identical results compared with those for the half plate. In addition, applying load control (loading of a constrained boundary) instead of displacement control verifies the results obtained for displacement control as identical solutions are found (except for where a snap takes place), *c.f.* Figure 7.9.

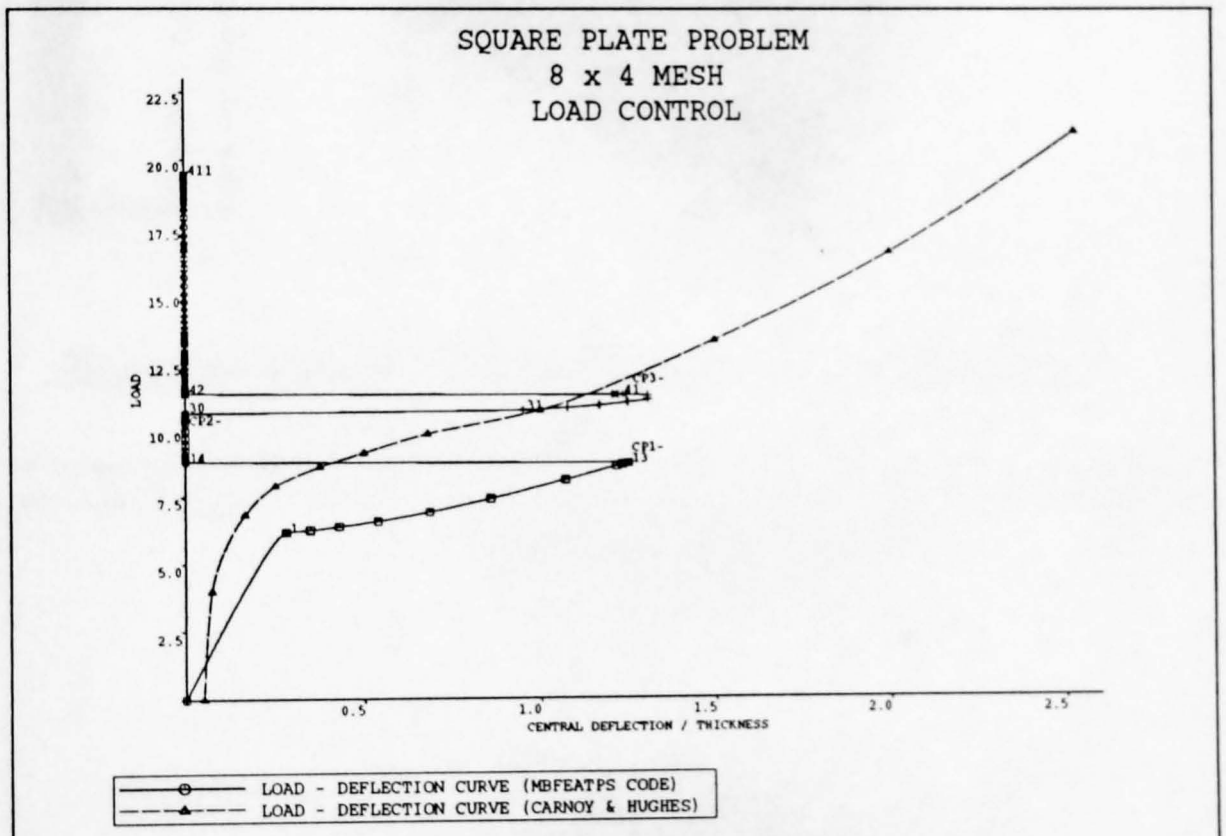

Figure 7.9. Load - deflection curve for the perfect plate using the 8×4 mesh.

For better visualization of the physical changes of the structure, Figures 7.10 - 7.12 show the deformed plate at the first, second and third critical points, respectively. Figure 7.13 shows the deformed plate at increment number 225 beyond the third critical point where the maximum displacement is of magnitude $\approx$ 20 times the plate thickness. Here, it is seen clearly that the mode shape is of a four wave antisymmetric form. For all of Figures 7.10 - 7.13, the whole plate is modelled. Note that in these figures the solution points obtained are connected using polyno-

mials and, hence, the edges within the figures may not be straight nor lying on the x^1-x^2-plane.

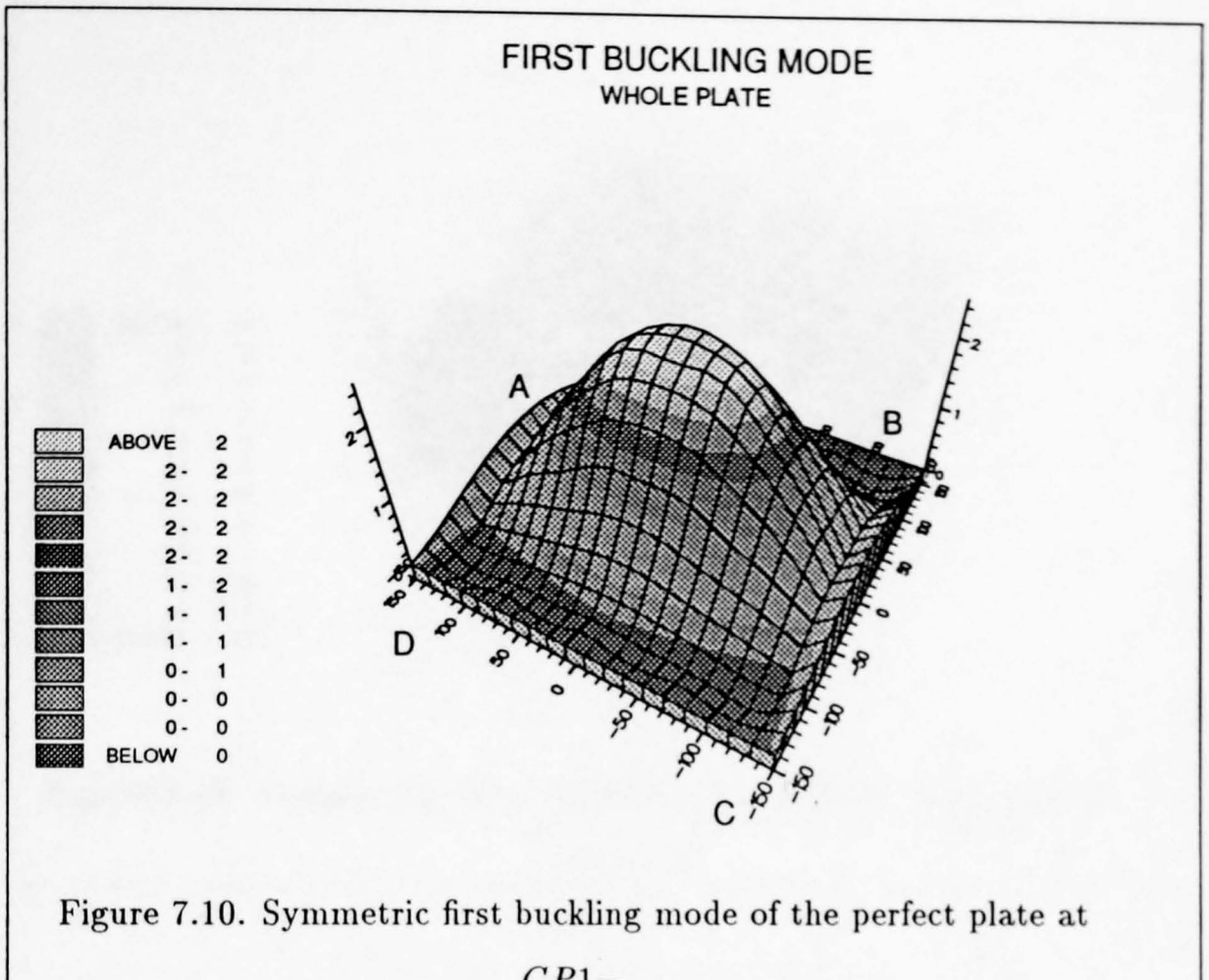

Figure 7.10. Symmetric first buckling mode of the perfect plate at $CP1-$.

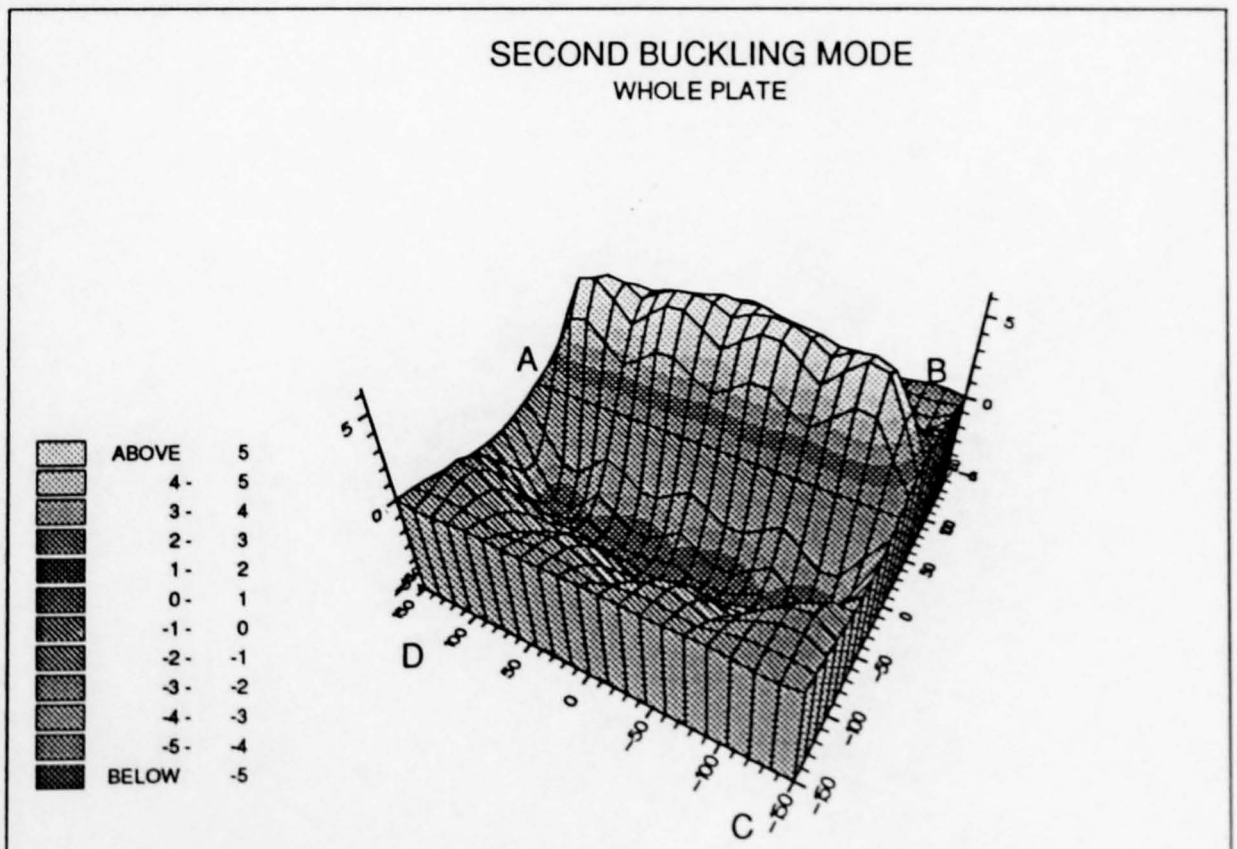

Figure 7.11. Antisymmetric second buckling mode of the perfect plate at $CP2-$.

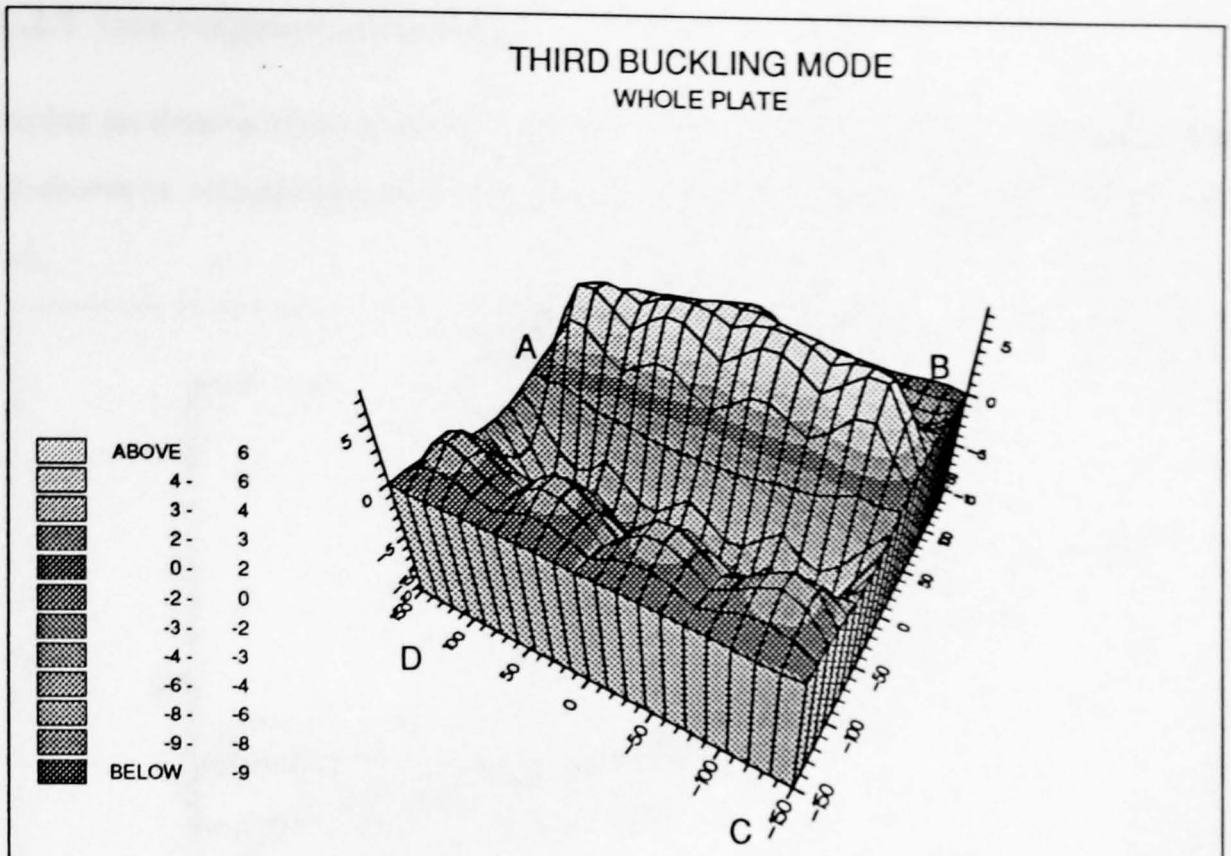

Figure 7.12. Asymmetric third buckling mode of the perfect plate at $CP3-$.

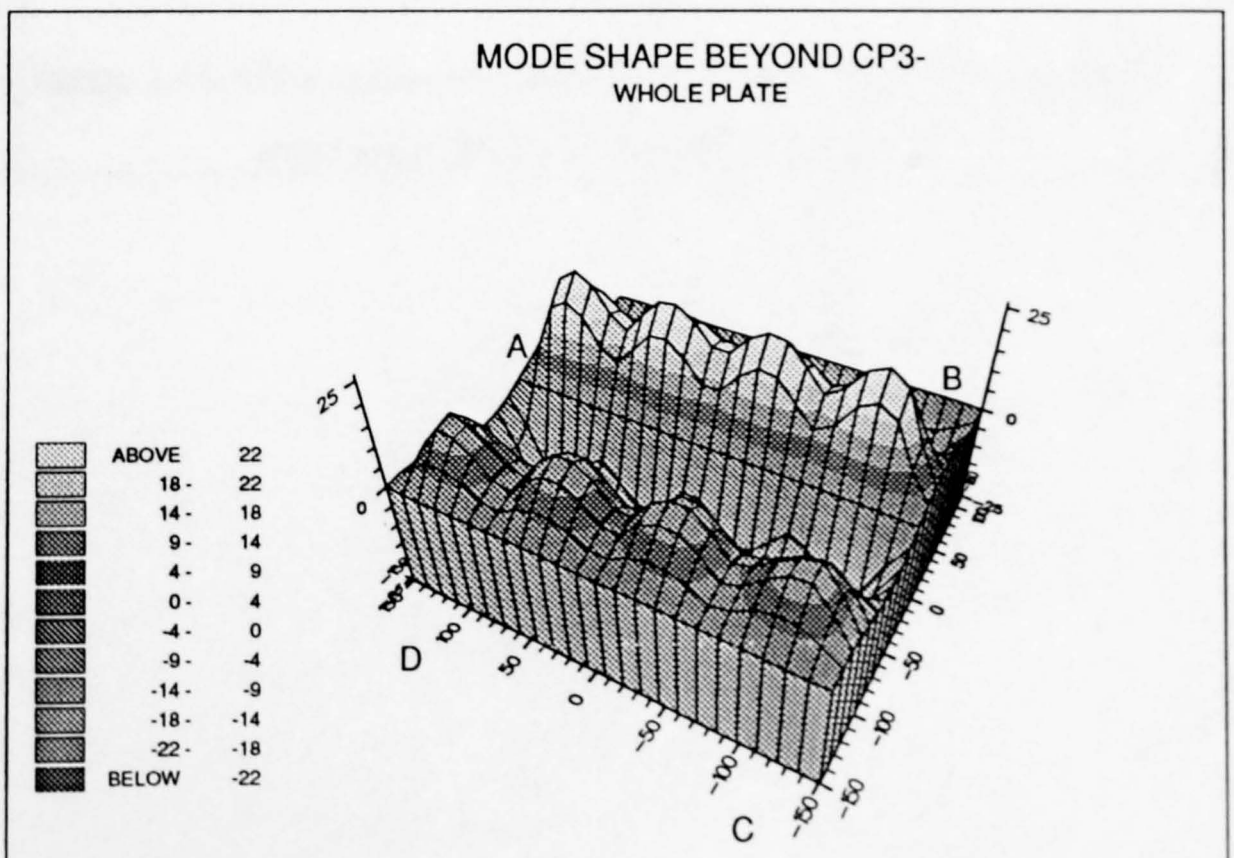

Figure 7.13. Antisymmetric mode shape of the perfect plate at increment point 225 beyond $CP3-$.

7.2.2.2 Convergence of results

In order to demonstrate that the results converge when the mesh is refined, Figure 7.14 shows in comparison load - deflection curves for the 8×4 mesh and the 16×8 mesh.

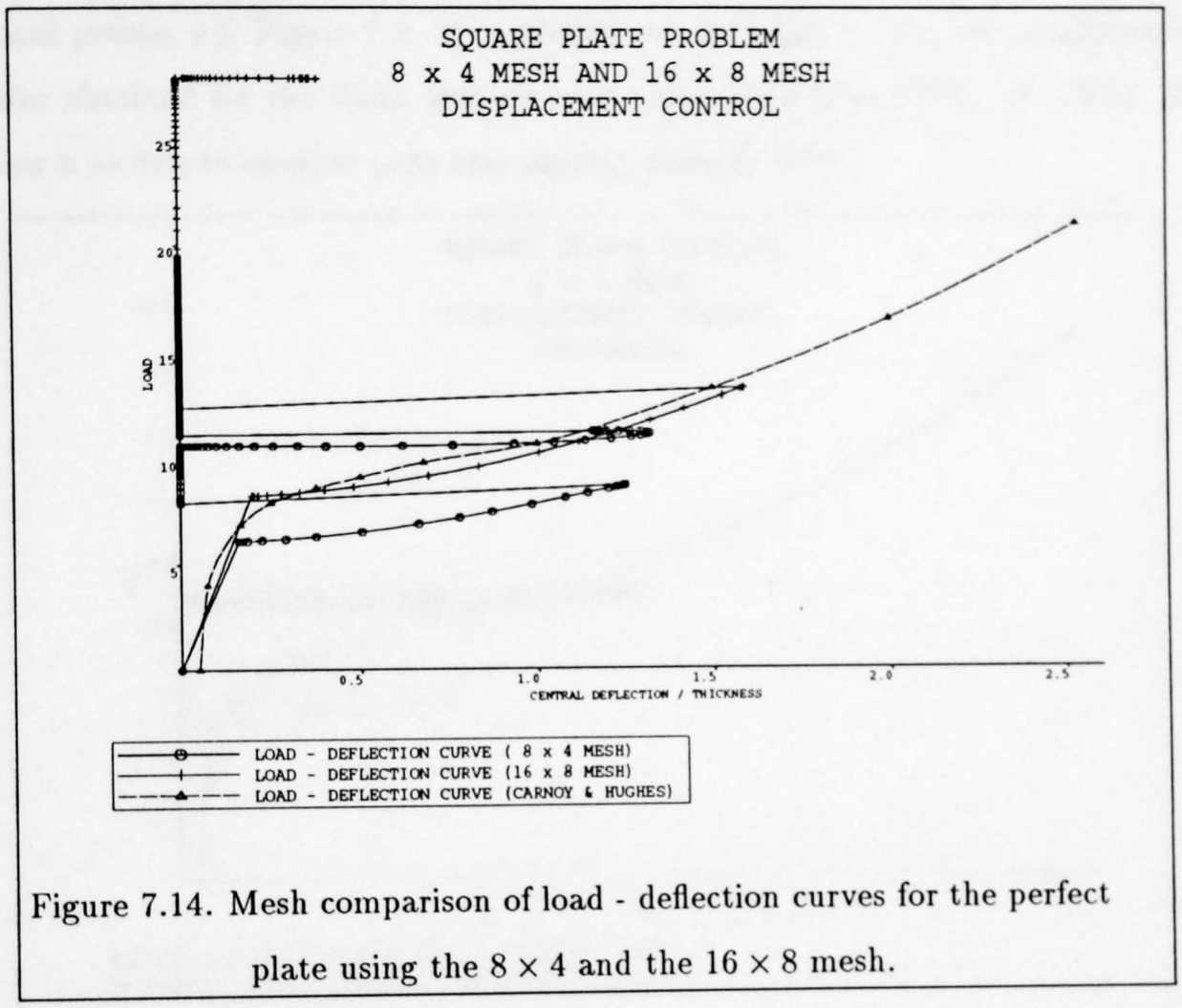

Figure 7.14. Mesh comparison of load - deflection curves for the perfect plate using the 8×4 and the 16×8 mesh.

7.2.2.3 Unloading

An unloading procedure is performed commencing at a point beyond $CP3-$. The resulting load - deflection curve is shown in Figure 7.15 and reveals identical results to those obtained by increasing the compression except in the neighbourhood of critical points, *c.f.* Figure 7.3. It is prudent to note that in this way confirmation is also obtained for the claim that no snap takes place from $CP2-$ to $CP2+$ but rather a switch to another path also passing through $CP2-$.

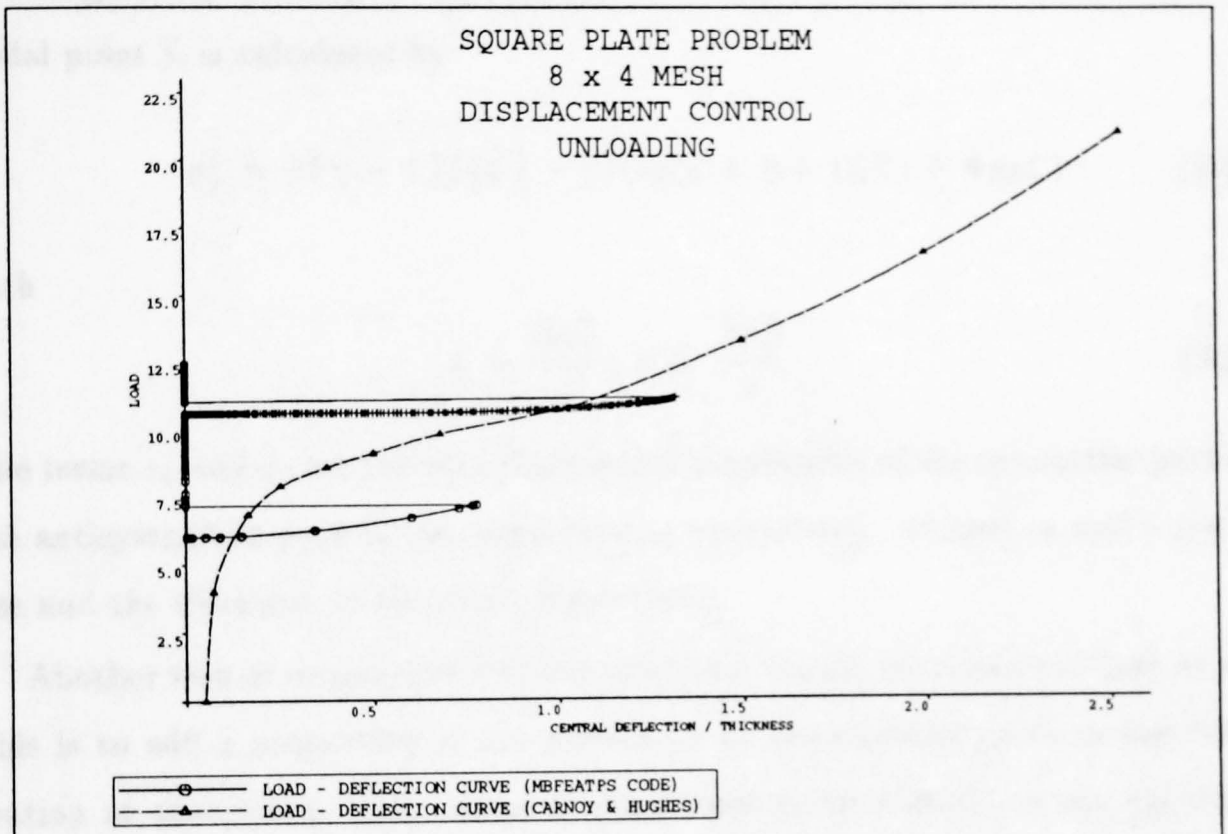

Figure 7.15. Load - deflection curve for the perfect plate using an unloading procedure for the 8×4 mesh.

7.2.3 Imperfect plate

7.2.3.1 Introduction

Initial geometrical imperfections can be used by giving nodes within the plate non-zero x^3-coordinates (out-of-plane coordinates), *i.e.* the plate will then not be flat anymore. Two different kinds of initial imperfections are examined, symmetrical and antisymmetrical. In particular, initial imperfections as employed by Carnoy and Hughes, *c.f.* [CH83], are prescribed in the way that x_j^3, the x^3-coordinate of a nodal point j, is calculated by

$$x_j^3 = t(\eta - 1)(|\zeta| - 1)(\varepsilon_1(1 + \eta + |\zeta|) + 4\varepsilon_2\zeta) \qquad (7.2.7)$$

with

$$\zeta = \frac{2x_j^1}{a}, \eta = \frac{2x_j^2}{a} . \qquad (7.2.8)$$

The terms ε_1 and ε_2 are the non-dimensional amplitudes of the symmetric part and the antisymmetric part of the imperfection, respectively, whereas a and t are the size and the thickness of the plate, respectively.

Another way of imposing initial imperfections should be mentioned here as well. This is to add a proportion of the eigenmode at the buckling point to the configuration at that point. This choice is considered to be suitable as the eigenmode approximates the shape of the deforming structure beyond the critical point, *c.f.* also branch switching method METHOD B in Appendix B.1.

7.2.3.2 Symmetrical initial imperfections

In this section there are no antisymmetrical imperfections, *i.e.* $\varepsilon_2 = 0.0$. Figure 7.16 shows comparison results for three levels of symmetrical initial imperfections, $\varepsilon_1 = 0.005$, $\varepsilon_1 = 0.050$ and $\varepsilon_1 = 0.500$, and the perfect plate as well as results by Carnoy and Hughes, *c.f.* [CH83], with $\varepsilon_1 = 0.050$ up to the first critical point. It is seen that the larger the initial imperfections used, the larger the load and deflection values at $CP1-$ and the further away from the perfect plate - curve they lie. If a set of different initial imperfections is used, an envelope of curves is obtained with the curve corresponding to the smallest initial imperfection being closest to that of

the perfect plate. Note, that curves with initial imperfections always remain below the perfect plate - curve.

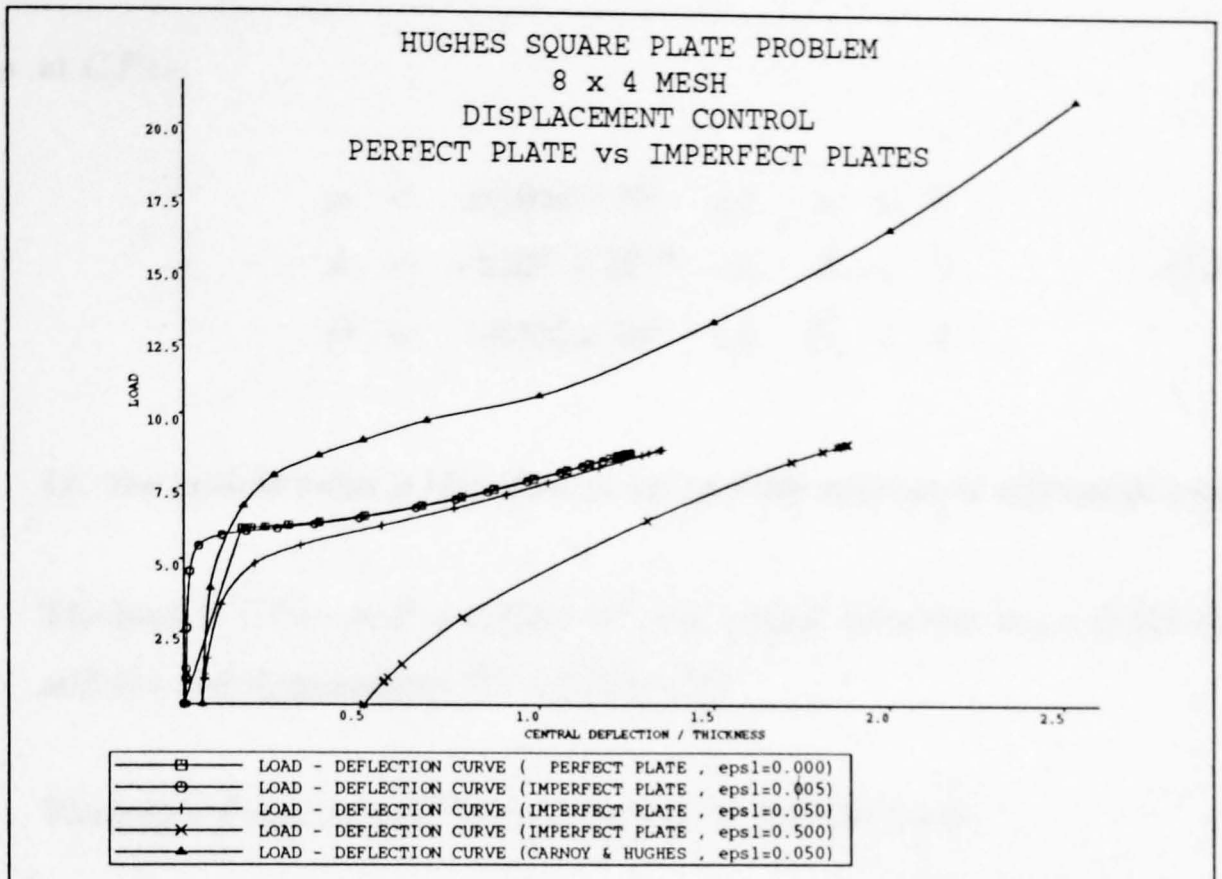

Figure 7.16. Perfect plate vs. imperfect plates load - deflection curves using symmetrical initial imperfections and the 8×4 mesh.

Figure 7.17 shows the load - deflection curve using the symmetrical initial imperfection $\varepsilon_1 = 0.005$ with comparison results by Carnoy and Hughes, *c.f.* [CH83], with $\varepsilon_1 = 0.050$. The first critical point $CP1-$ is found at increment number 43 from where a 'jump' follows to a point on the stable equilibrium path at increment number 44 where no fully antisymmetric mode with zero central deflection is obtained but an asymmetric two wave form. The closer the central deflection gets to zero, the closer the mode shape gets to a fully antisymmetric mode. The mode shape remains asymmetric and from increment number 88 on it distances itself from an antisymmetric mode shape with the central deflection also increasing in magnitude. The second critical point $CP2-$ is found at increment number 122. Increasing the compression entails again a snap mode change to an asymmetric mode shape close to an antisymmetric mode shape. No further critical points are found. The last marked point at increment number 170 corresponds to an end displacement of $20mm$ which is as far as the example has been investigated. Note the strong resemblance with the load - deflection curve for the perfect plate, *c.f.* Figure 7.3.

The stability coefficients at the critical points yield

- at $CP1-$

$$\begin{aligned} \mu &= \pm 0.000 \times 10^{0} \quad i.e. \quad \mu = 0 \\ A &= -0.327 \times 10^{-8} \quad i.e. \quad A = 0 \\ D &= -0.590 \times 10^{5} \quad i.e. \quad D < 0 \ , \end{aligned} \tag{7.2.9}$$

i.e. the critical point is identified as an ***unstable symmetric bifurcation point.***

The load at $CP1-$ is $P = 0.873 \times 10^{1}$, the central deflection $w_{cd} = 0.252 \times 10^{1}$ and the end displacement $U^{1} = 0.139 \times 10^{0}$.

The mode shape up to $CP1-$ is symmetric with one wave.

Successful continuation from $CP1-$ is achieved with $\alpha_1 = 0.30 \times 10^{1}$.

- at $CP2-$

$$\begin{aligned} \mu &= \pm 0.000 \times 10^{0} \quad i.e. \quad \mu = 0 \\ A &= +0.605 \times 10^{0} \quad i.e. \quad A \neq 0 \ , \end{aligned} \tag{7.2.10}$$

i.e. the critical point is identified as an ***asymmetric bifurcation point.***

The load at $CP2-$ is $P = 0.113 \times 10^{2}$, the central deflection $w_{cd} = 0.232 \times 10^{1}$ and the end displacement $U^{1} = \times 0.36510^{1}$.

The mode shape between $CP1-$ and $CP2-$ is asymmetric with two waves.

Successful continuation from $CP2-$ is achieved with $\alpha_1 = -0.30 \times 10^{1}$.

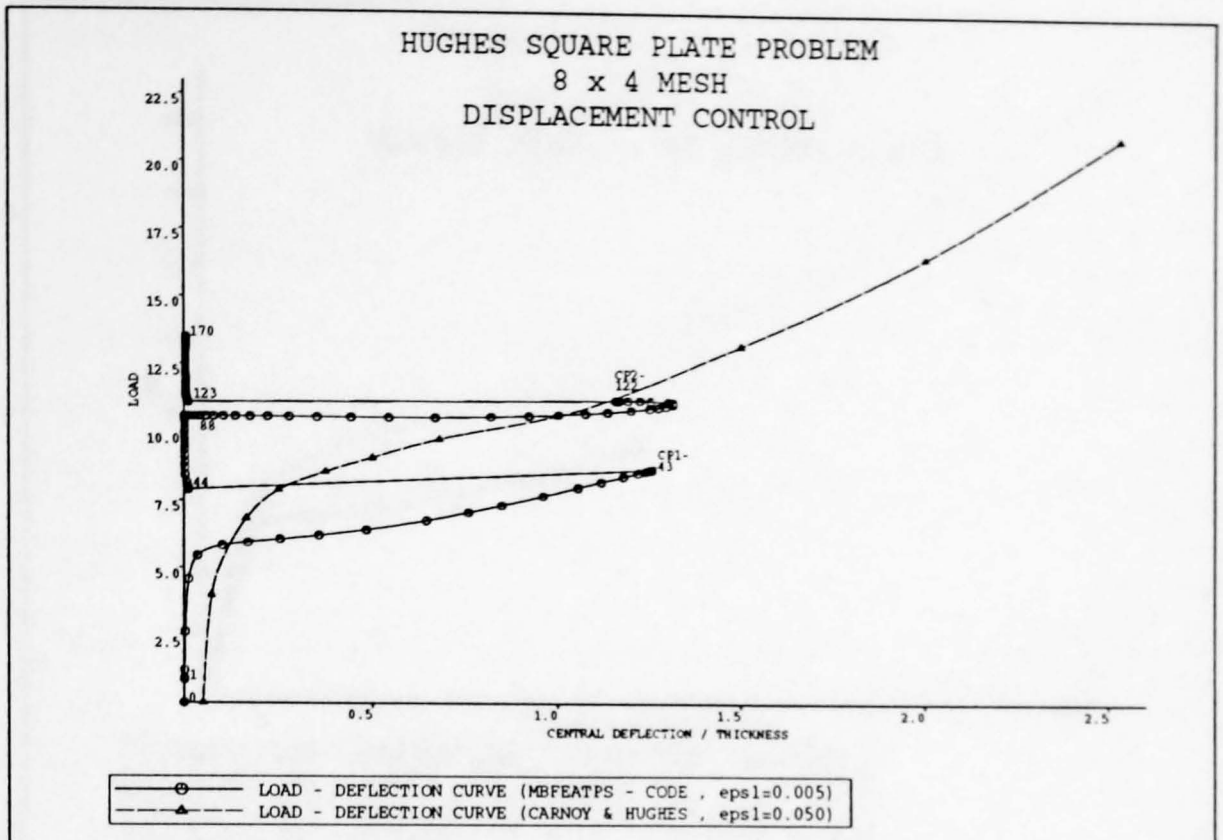

Figure 7.17. Load - deflection curve for an imperfect plate with symmetrical initial imperfection $\varepsilon_1 = 0.005$ (and $\varepsilon_2 = 0.000$) using the 8×4 mesh.

7.2.3.3 Antisymmetrical initial imperfections

In this section there are no symmetrical imperfections, *i.e.* $\varepsilon_1 = 0.0$. Figure 7.18 shows comparison results for three kinds of antisymmetrical initial imperfections, $\varepsilon_2 = 0.005$, $\varepsilon_2 = 0.050$ and $\varepsilon_2 = 0.500$, and the perfect plate as well as results by Carnoy and Hughes, *c.f.* [CH83], which are for symmetrical imperfections $\varepsilon_1 = 0.050$, up to the first critical point. Only for the smallest applied imperfection $\varepsilon_2 = 0.005$ is it feasible to break away from the zero central deflection value. The curve obtained for $\varepsilon_2 = 0.005$ is very close to the one for the perfect plate but lies below it indicating smaller load and deflection values in magnitude at the critical point found.

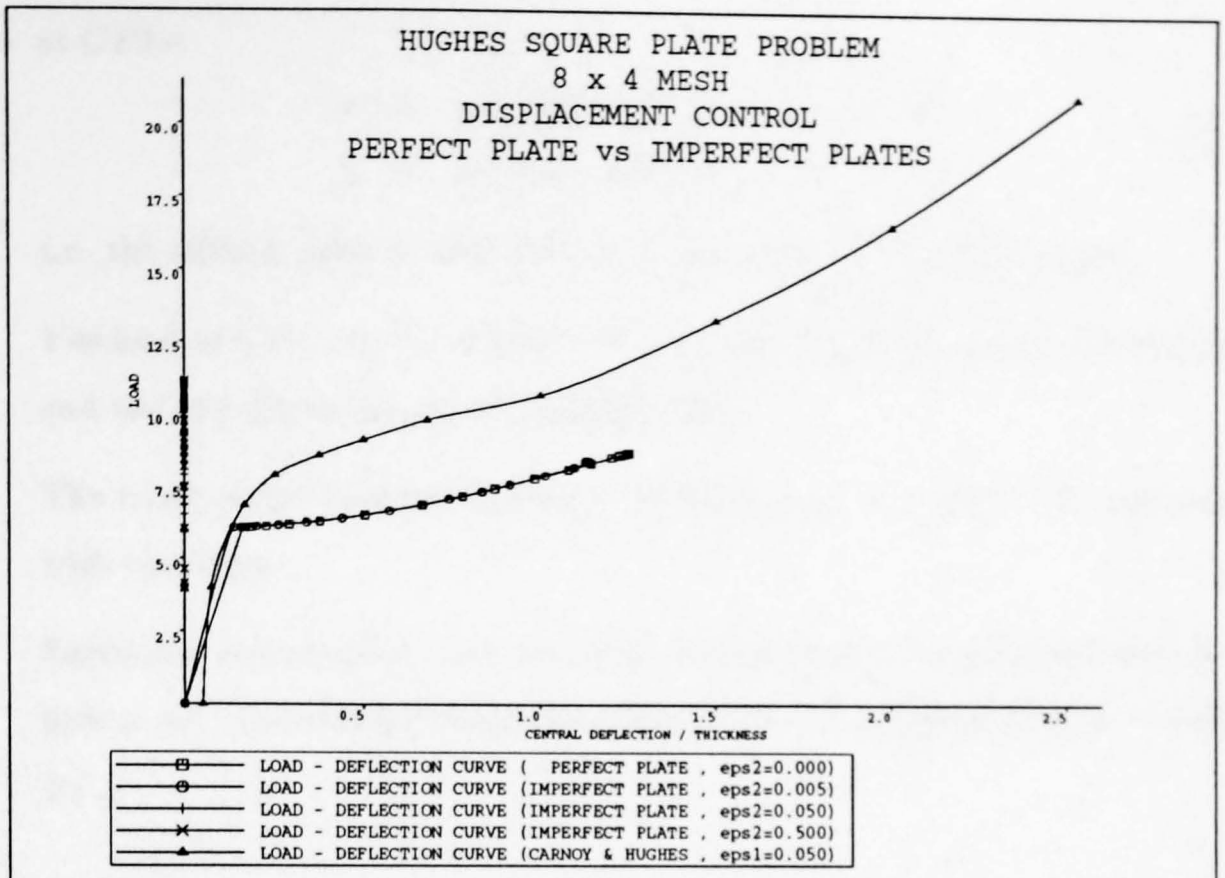

Figure 7.18. Perfect plate vs. imperfect plates load - deflection curves using antisymmetrical initial imperfections and the 8×4 mesh.

Figure 7.19 shows the load - deflection curve using the antisymmetrical initial imperfection $\varepsilon_2 = 0.005$ with comparison results by Carnoy and Hughes, *c.f.* [CH83], with symmetrical imperfections $\varepsilon_1 = 0.050$. The mode shape from the first found solution point (increment number 1) on up to the first critical point $CP1-$ is an asymmetric one wave buckled form. $CP1-$ is found at increment number 25 where a snap mode change follows to a point on the stable equilibrium path at increment number 26 where a fully antisymmetric mode with zero central deflection is obtained. The mode shape remains antisymmetric up to the second critical point $CP2-$ at increment point 77. Continuing from $CP2-$ involves again a change in the mode shape and from increment number 78 on the mode is asymmetric all the way up to the third critical point $CP3-$ at increment number 117. Increasing the compression entails again a snap mode change to an asymmetric mode shape to a fully antisymmetric mode shape. No further critical points are found. The last marked point at increment number 164 corresponds to an end displacement of $20mm$ which is as far as the example has been investigated. Note the strong resemblance with the load - deflection curve for the perfect plate, *c.f.* Figure 7.3.

The stability coefficients at the critical points yield

- at $CP1-$

$$\begin{aligned} \mu &= \pm 0.000 \times 10^{0} \quad i.e. \quad \mu = 0 \\ A &= +0.192 \times 10^{0} \quad i.e. \quad A \neq 0 \ , \end{aligned} \tag{7.2.11}$$

i.e. the critical point is identified as an ***asymmetric bifurcation point.***

The load at $CP1-$ is $P = 0.843 \times 10^{1}$, the central deflection $w_{cd} = 0.226 \times 10^{1}$ and the end displacement $U^1 = 0.129 \times 10^{0}$.

The mode shape between the linear buckling point and $CP1-$ is asymmetric with one wave.

Successful continuation from the Euler buckling point is achieved with $\alpha_1 = 0.70 \times 10^{1}$. Successful continuation from $CP1-$ is achieved with $\alpha_1 = 0.50 \times 10^{1}$.

- at $CP2-$

$$\begin{aligned} \mu &= \pm 0.000 \times 10^{0} \quad i.e. \quad \mu = 0 \\ A &= +0.674 \times 10^{-7} \quad i.e. \quad A = 0 \\ D &= -0.159 \times 10^{6} \quad i.e. \quad D < 0 \ , \end{aligned} \tag{7.2.12}$$

i.e. the critical point is identified as an ***unstable symmetric bifurcation point.***

The load at $CP2-$ is $P = 0.106 \times 10^{2}$, the central deflection $w_{cd} = 0.149 \times 10^{-6}$ and the end displacement $U^1 = 0.165 \times 10^{1}$.

The mode shape between $CP1+$ and $CP2-$ is antisymmetric with two waves.

Successful continuation from $CP2-$ is achieved with $\alpha_1 = 0.10 \times 10^{1}$.

- at $CP3-$

$$\begin{aligned} \mu &= \pm 0.000 \times 10^{0} \quad i.e. \quad \mu = 0 \\ A &= +0.596 \times 10^{0} \quad i.e. \quad A \neq 0 \ , \end{aligned} \tag{7.2.13}$$

i.e. the critical point is identified as an ***asymmetric bifurcation point.***

The load at $CP3-$ is $P = 0.113 \times 10^{2}$, the central deflection $w_{cd} = 0.230 \times 10^{1}$ and the end displacement $U^1 = 0.363 \times 10^{1}$.

The mode shape between $CP2+$ and $CP3-$ is asymmetric with two waves.

Successful continuation from $CP3-$ is achieved with $\alpha_1 = -0.30 \times 10^{1}$.

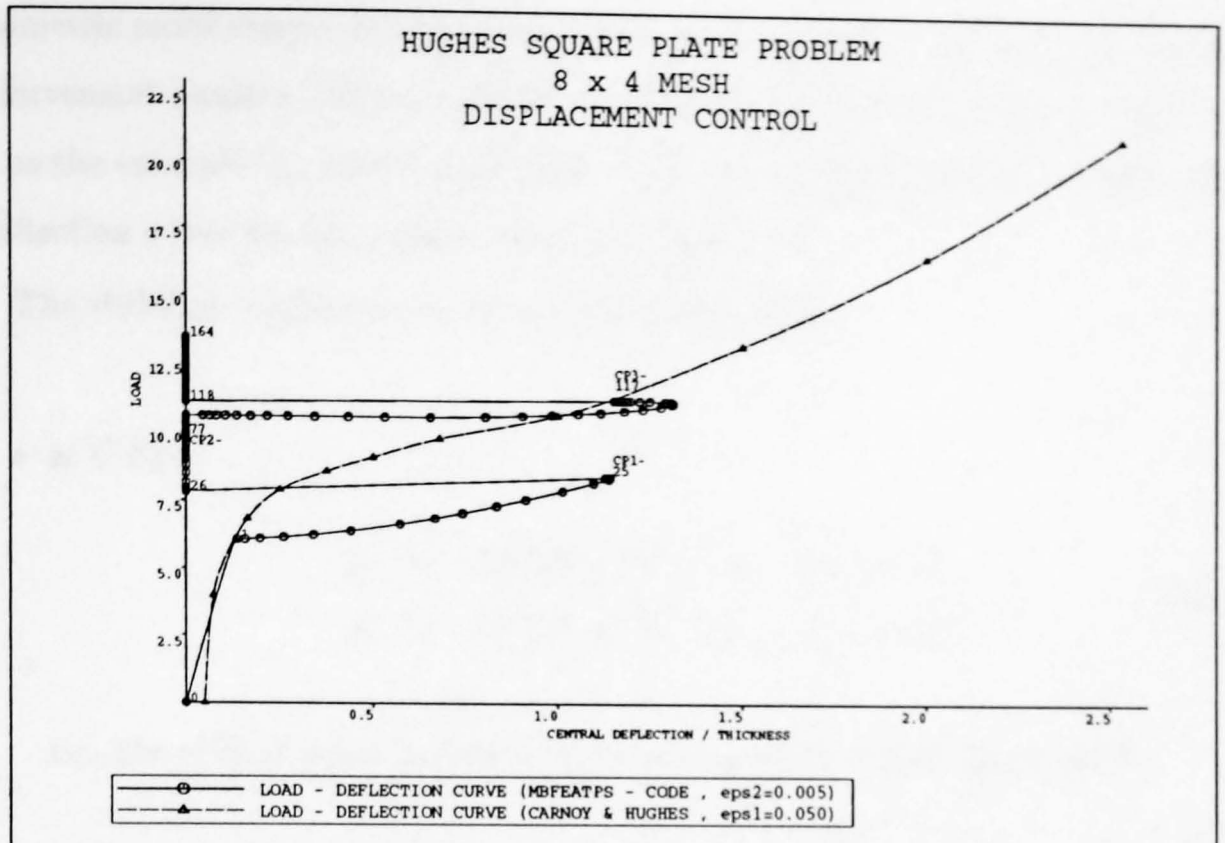

Figure 7.19. Load - deflection curve for an imperfect plate with antisymmetrical initial imperfection $\varepsilon_1 = 0.005$ (and $\varepsilon_2 = 0.000$) using the 8×4 mesh.

7.2.3.4 Asymmetrical initial imperfections

Consider the asymmetrical initial imperfections obtained by combining the symmetrical imperfections $\varepsilon_1 = 0.005$ and the antisymmetrical imperfections $\varepsilon_2 = 0.005$. Figure 7.20 shows the load - deflection curve with comparison results by Carnoy and Hughes, *c.f.* [CH83], with $\varepsilon_1 = 0.050$ and $\varepsilon_2 = 0.000$. From the first found solution point on (increment number 1) the mode shape is an asymmetric one wave buckled form all the way up to the first critical point $CP1-$ at increment number 28. A snap mode change then follows to a point on the stable equilibrium path at increment number 29 where an asymmetric two wave buckled form is found with no zero central deflection. The closer the central deflection gets to zero, the closer the mode shape gets to a fully antisymmetric mode. The mode shape remains asymmetric and from around increment number 75 on it distances itself from an antisymmetric mode shape with the central deflection also increasing in magnitude. The second critical point $CP2-$ is found at increment number 97. Increasing the compression entails again a snap mode change to an asymmetric mode shape close to an anti-

symmetric mode shape. No further critical points are found. The last marked point at increment number 168 corresponds to an end displacement of $20mm$ which is as far as the example has been investigated. Note the strong resemblance with the load - deflection curve for the perfect plate, *c.f.* Figure 7.3.

The stability coefficients at the critical points yield

- at $CP1-$

$$\begin{aligned} \mu &= \pm 0.000 \times 10^0 \quad i.e. \quad \mu = 0 \\ A &= -0.187 \times 10^0 \quad i.e. \quad A \neq 0 \ , \end{aligned} \tag{7.2.14}$$

i.e. the critical point is identified as an *asymmetric bifurcation point.*

The load at $CP1-$ is $P = 0.846 \times 10^1$, the central deflection $w_{cd} = 0.228 \times 10^1$ and the end displacement $U^1 = 0.130 \times 10^0$.

The mode shape between the linear buckling point and $CP1-$ is asymmetric with one wave.

Successful continuation from $CP1-$ is achieved with $\alpha_1 = 0.10 \times 10^1$.

- at $CP2-$

$$\begin{aligned} \mu &= \pm 0.000 \times 10^0 \quad i.e. \quad \mu = 0 \\ A &= +0.614 \times 10^0 \quad i.e. \quad A \neq 0 \ , \end{aligned} \tag{7.2.15}$$

i.e. the critical point is identified as an *asymmetric bifurcation point.*

The load at $CP2-$ is $P = 0.113 \times 10^2$, the central deflection $w_{cd} = 0.233 \times 10^1$ and the end displacement $U^1 = 0.368 \times 10^1$.

The mode shape between $CP2-$ and $CP3-$ is asymmetric with two waves.

Successful continuation from $CP2-$ is achieved with $\alpha_1 = -0.60 \times 10^1$.

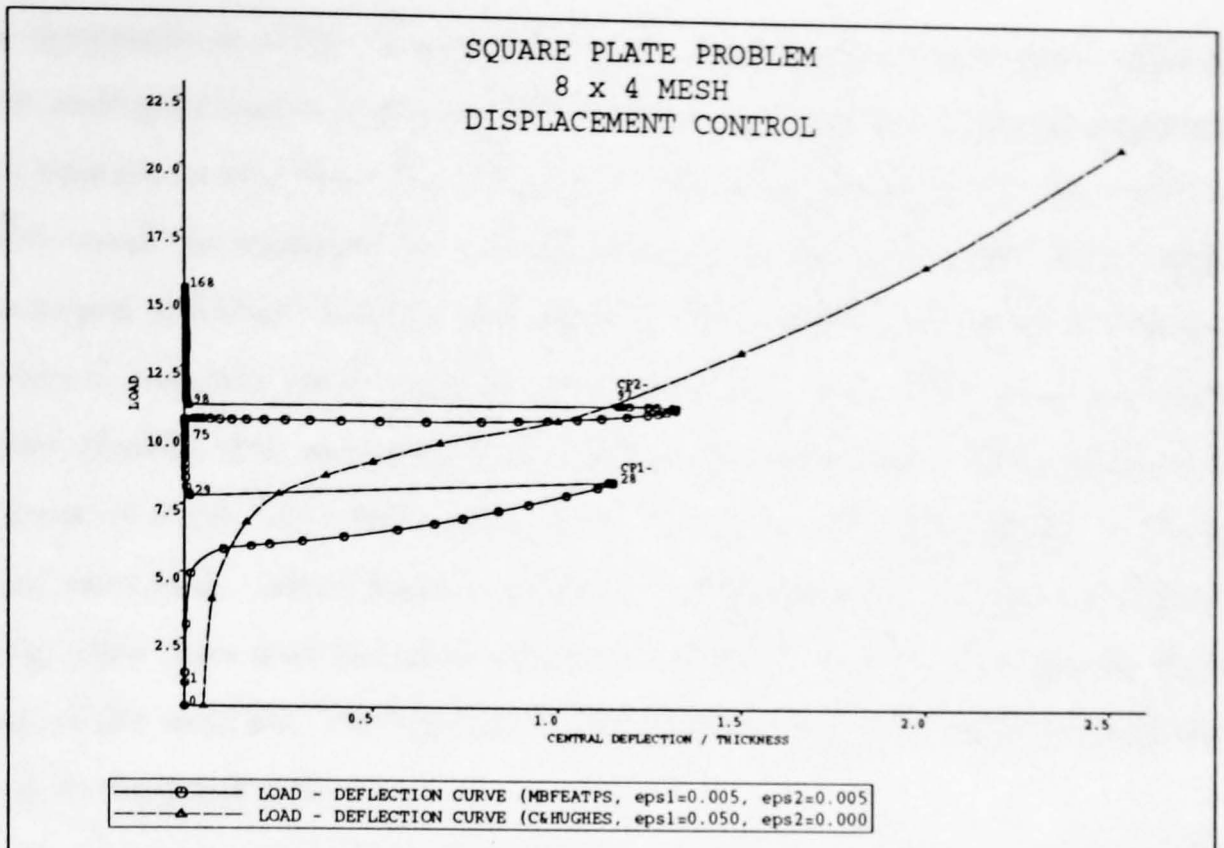

Figure 7.20. Load - deflection curve for symmetrical imperfection $\varepsilon_1 = 0.005$ and antisymmetrical imperfection $\varepsilon_2 = 0.005$ using the 8×4 mesh.

7.2.4 Conclusions

The results obtained are as expected up to the second critical point. The perfect plate, see Figure 7.3 and Figure 7.7, exhibits the anticipated symmetric one wave buckled shape of the plate at the first critical point (at increment point 40) and an antisymmetric two wave buckled shape at the second critical point (at increment point 92). A branch switching with no snap then takes place and the mode shape changes to be asymmetric after the second critical point and remains as such until the third critical point, during which the load changes only slightly. This is not in agreement with the suggestions made by the linear theory, where a symmetric three wave buckled mode is normally to be anticipated. It is thought within the linear theory that, if at the inception everything is perfect, then everything should remain perfect. This leads to expectations of having alternating mode shapes between symmetric and antisymmetric modes where at each new critical point the number of buckles is increased by one. As seen in the presented work, however, these assumptions are not correct within the employed nonlinear theory, although

the eigenmode at $CP2-$ reveals a symmetric three wave buckled mode. The plate then undergoes another snap at $CP3-$ and returns back to an antisymmetric mode, this time into a four wave form. The asymmetry along the path between $CP2+$ and $CP3-$ could be explained by the known fact from the bifurcation theory whereby the second and third buckling modes are not compatible under some circumstances [1], thus causing the mode shape not to be a pure one but rather a mixture of other modes [Fur95]. The reason that the asymmetric mode shape, which seems to be a mixture of a two wave form and a three wave form, is stable instead of the pure three wave form - which hence is unstable - is dependent on the physical behaviour of the plate (how does the plate absorb the energy?) as well as the specific material data of the example. For aspects of symmetry breaking, reference is made to the book by Seydel [Sey88].

No real comparison results exist for checking the results obtained as in the current work for the first time to the author's knowledge it has been feasible, by employing the finite element method within a nonlinear theory, to accomplish a successful branch switching into the post buckling regime and to continue there on the stable equilibrium path and even find further critical points. The following points are used for verifying the validity of the results obtained:

1. Several different meshes produce similar results with the same physical features, see *e.g.* Figure 7.3 and Figure 7.14.

2. Modelling the whole plate reveals identical solutions compared with the half plate model, *i.e.* the assertion that the asymmetry is caused by the plate wanting to deform into an antisymmetrical mode shape along the transverse axis after the second critical point is false.

3. Identical results are obtained for both load control and displacement control except for just after snaps, *c.f.* Figure 7.9.

4. Performing an unloading procedure from a point well beyond $CP3-$ produces identical results to those where the compression is increased except for in the neighbourhood of critical points, *c.f.* Figure 7.15. It should also be noted

[1] In general, the mode shapes are put together as a combination of several eigenmodes. Evidently, two and three are co-primes and, hence, the construction of these mode shapes may fail.

here that the fact that performing the unloading procedure by simply using negative increments underlines the potential of the method employed.

5. An analysis regarding the quality of the solution vector and the eigenvector revealing the eigenmode has been performed. Here, the computed quality values show that there is no difference in accuracy in the solution vector obtained and eigenvector between $CP1-$ and $CP2-$, *i.e.* the likely assumption that the quality of the solution vector and/or the eigenvector at the first critical point compared with the second critical point might be considerably better at $CP1-$ and, thus, allowing numerical inaccuracies to be blamed for the unexpected mode change, is unfounded.

The results obtained using the MBFEATPS code compare well with those given by Carnoy and Hughes, *c.f.* [CH83], up to the first critical point (Carnoy and Hughes only treat the problem up to this point), although different kinds of elements are applied for solving the problem. The geometrically nonlinear constant moment triangle by Morley [Mor91] used in the MBFEATPS code is known to be overflexible, whereas Carnoy and Hughes use overstiff shell elements.

With regards to the choice of a suitable parameter α_1 for continuation from the critical point it is left for future work to develop a method with the feature that it computes automatically a suitable parameter (*i.e.* leading to a successful continuation) and, if possible, such that this α_1 is also the *ideal* choice. A first step in this direction has been made, *c.f.* Appendix B.3, where a 'least squares fit' procedure is presented that is believed to compute the ideal choice for α_1 as long as the eigenmode at the critical point is not asymmetric and one suitable α_1 value is already known.

The 'up-and-down' movement of the smallest eigenvalue - deflection curve when using the T-matrix is due to the fact that the T-matrix converges towards the Hessian, when the step length is made smaller. This means that the smallest eigenvalue θ_{min} converges towards $\theta_{min} = 1$. Computing the smallest eigenvalue while employing the T-matrix is considered very useful in cases where the magnitude of the smallest eigenvalue decreases slowly towards zero, where it might be difficult to precisely locate a critical point. With the T-matrix, however, the smallest eigenvalue

(depending on the chosen step length) remains clearly non-zero until a critical point is in a very near vicinity.

Employing a hierarchy of meshes as in Figure 7.14 clearly shows that refining the mesh continuously leads to improved results with larger values for both the central deflection and the load, *i.e.* the results converge towards a specific solution.

Investigations have been made regarding mesh sensitivity revealing that the shape of the element triangles is decisive for the performance of the employed method. It is suggested that triangles be designed with angles such that no angle is smaller than 45 degrees and no angle is larger than 90 degrees. Here, the angles are extracted from a triangle of pyramidal shape with two corners on the transverse line of symmetry. No definitive agreement is found as to which mesh pattern is the most suitable. It is suggested here, however, that meshes with crosses across both diagonals in each square are to be preferred. It is emphasized that great care must be taken in the choice of the mesh so as not to exclude any symmetry or antisymmetry.

When initial geometrical imperfections are applied it is observed that in the case of 'small' imperfections the results obtained are close to those of the perfect plate, *i.e.* initial imperfections can be used relatively safely for approximating the behaviour of the perfect plate, see Figures 7.16 and 7.18 together with Figure 7.3. In the case where 'large' imperfections are applied on the plate the results obtained are further away from those of the perfect plate or even exhibit totally different physical behaviour, see Figure 7.16 and Figure 7.18. Thus it can be said that the precise measurement of initial imperfections is imperative for predicting accurate numerical results.

7.3 Cylindrical panel problem

7.3.1 Introduction

A shell problem is drawn attention to, *viz* that of a cylindrical panel under biaxial compression. The panel is fixed against rotation at all edges and free to move longitudinally at both loaded edges and the sides, *c.f.* Figure 7.21. This has proven to be an extremely difficult problem as has also been recognized by Argyris *et al.* [JHAS77] and Riks [Rik84].

Only symmetrical deformations about the longitudinal axis of compression are considered and, hence, half a panel is modelled. Results given in this section correspond to the 8×8 mesh the projection of which onto the x^1-x^2-plane is as depicted in Figure 7.22. Several meshes employed for the problem are shown in Appendix C.3.

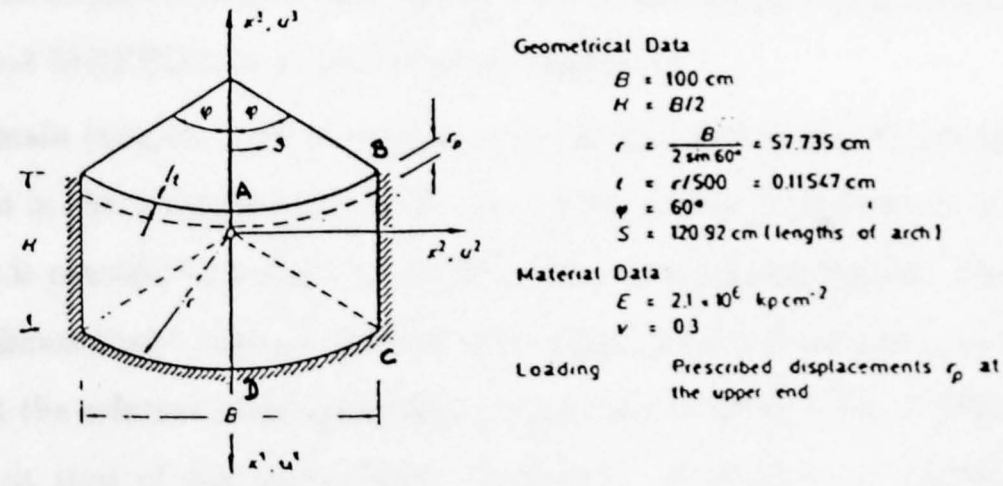

Figure 7.21 : Cylindrical panel: material and geometrical data and boundary conditions.

For practical and verificational reasons, in addition to displacement control load control has also been used. In analogy to the plate problem, load control here means that the load is applied such that the resulting displacements in the two opposite directions of compression are of equal magnitude at each point along the compressive edges (loading of constrained boundaries).

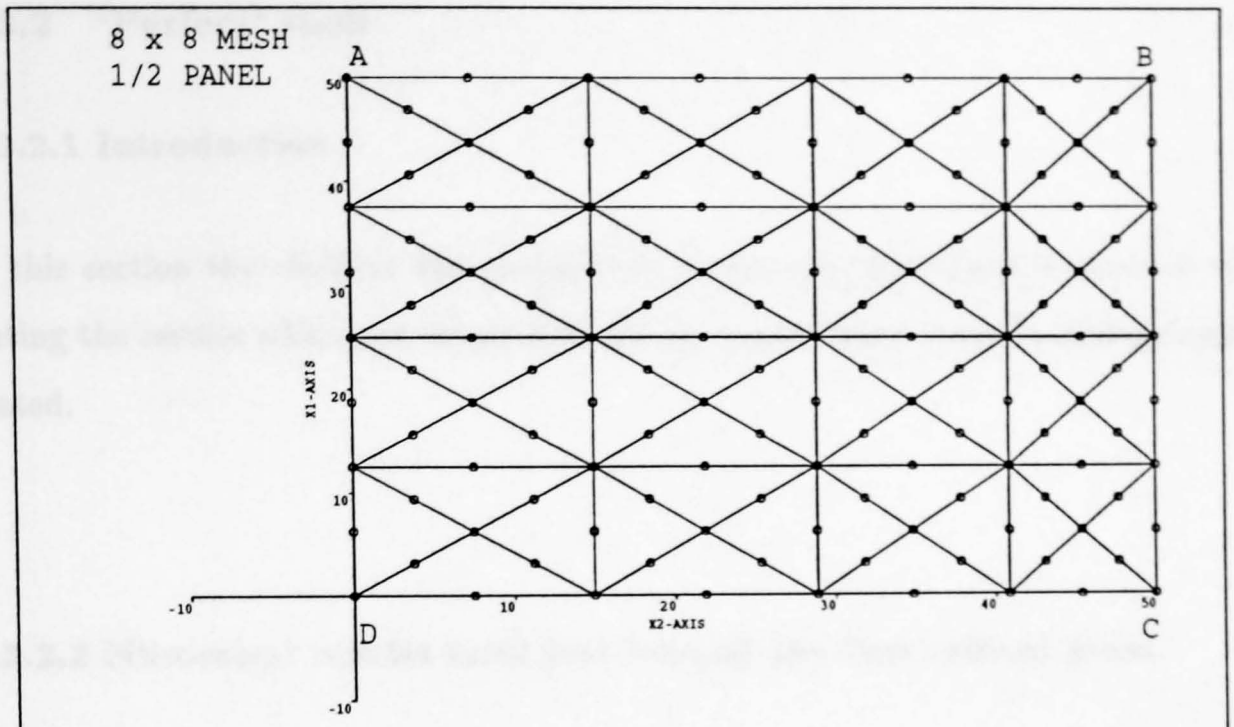

Figure 7.22. Half a panel modelled using the 8×8 mesh (projection on x^1-x^2-plane).

The continuation from critical points is accomplished by using the branch switching method METHOD A as described in Chapter 6.

The main interest is to investigate the physical behaviour of initially 'perfect' structures in the example at hand. In the context of the present work, as a 'perfect' structure is considered a *shell* (or *no-flat-plate-strips* approximation) when the shell is approximated such that all the (finite) element corner nodes lie on the shell surface. Note that the solution of the generalized eigenvalue problem $(\mathbf{K_0} + \lambda \mathbf{K_G})\,\delta\mathbf{a} = \mathbf{0}$ in the first step of the continuation method is of no physical significance when treating a shell.

It is noted also that additional imperfections can be prescribed. Details for this will be given in the sequel.

7.3.2 'Perfect' shell

7.3.2.1 Introduction

In this section the *shell* (or the *no-flat-plate-strips approximation*) is used for computing the results which are obtained by using displacement control unless otherwise stated.

7.3.2.2 Numerical results until just beyond the first critical point

The emerging load - compression curves and smallest eigenvalue - deflection curves as well as curves for the mode shapes along the longitudinal and transverse axes are shown in Figures 7.23 - 7.28.

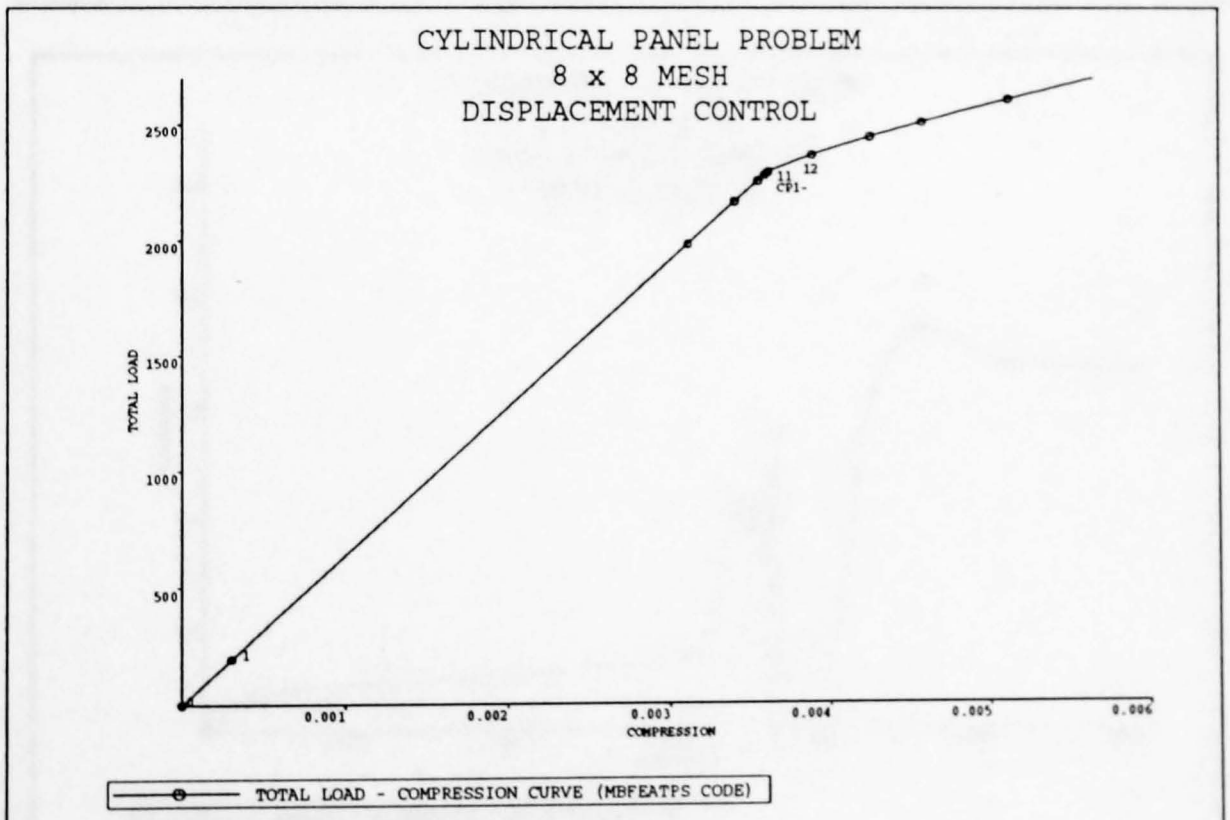

Figure 7.23. Total load - compression curve for the perfect shell using the 8×8 mesh.

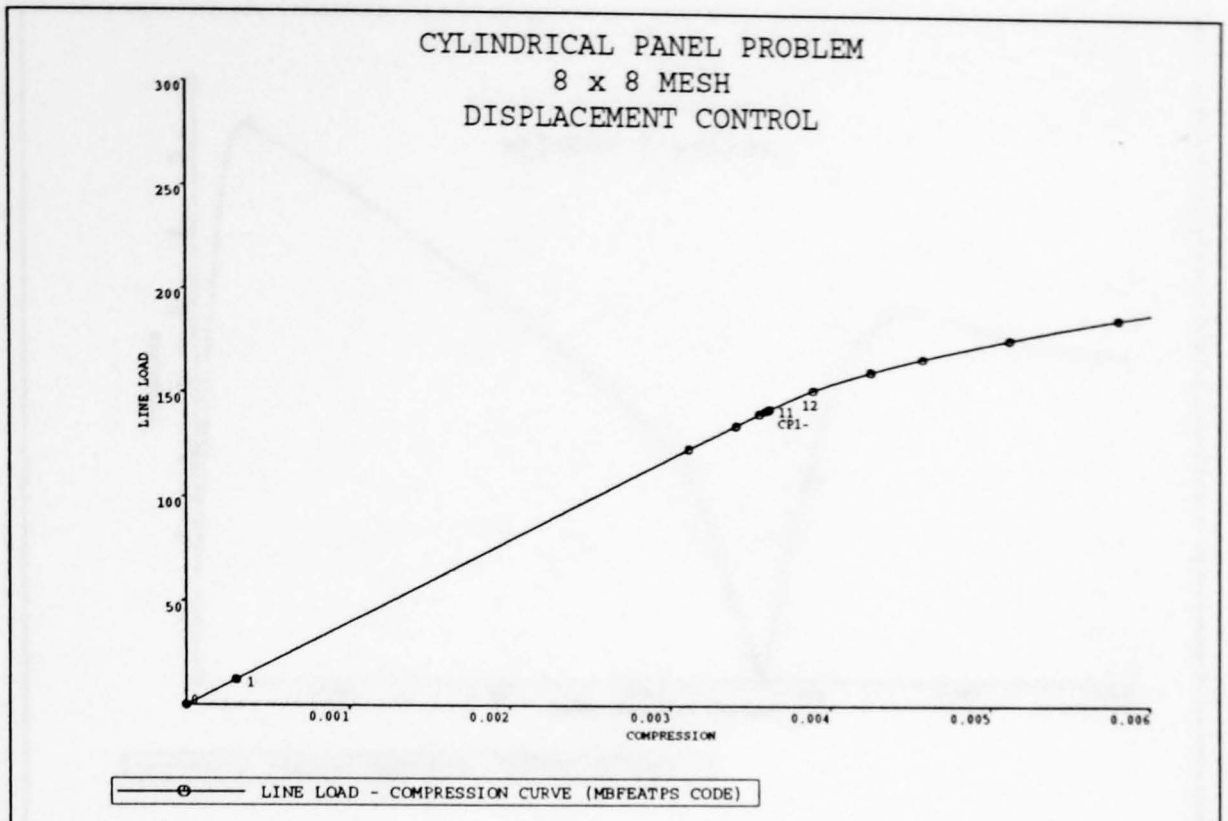

Figure 7.24. Line load - compression curve for the perfect shell using the 8×8 mesh.

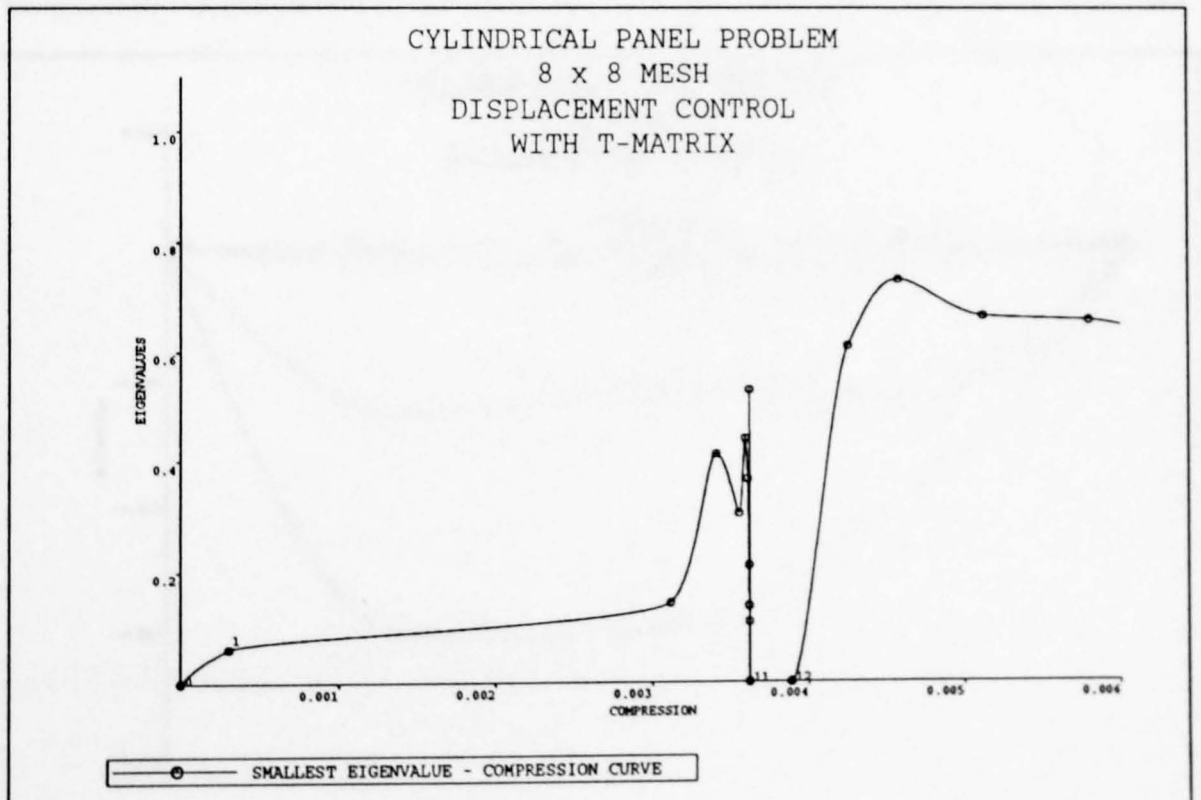

Figure 7.25. Smallest eigenvalue - compression curve for the perfect shell using the 8×8 mesh (with T-matrix, *i.e.* eigenvalues $\theta^{(r)}$ calculated from $\mathbf{K_T}\boldsymbol{\xi}^{(r)} = \theta^{(r)}\mathbf{T}\boldsymbol{\xi}^{(r)}$ (no sum on r))

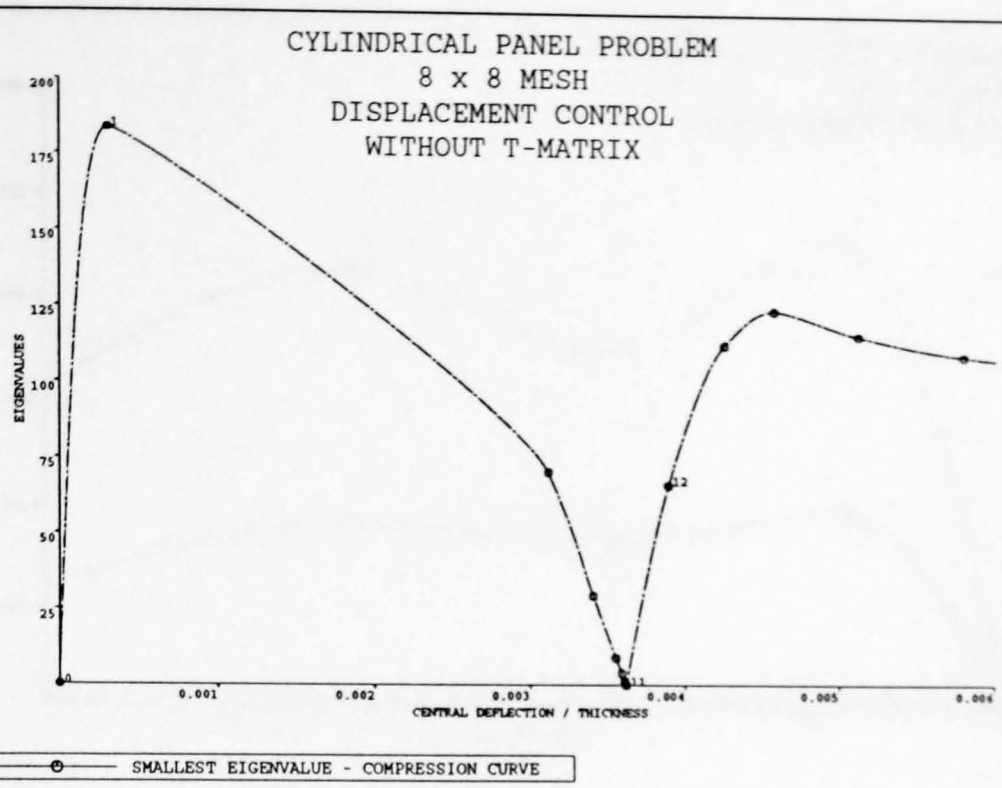

Figure 7.26. Smallest eigenvalue - compression curve for the perfect shell using the 8×8 mesh (without T-matrix, *i.e.* eigenvalues $\theta^{(r)}$ calculated from $\mathbf{K_T}\boldsymbol{\xi}^{(r)} = \theta^{(r)}\boldsymbol{\xi}^{(r)}$ (no sum on r))

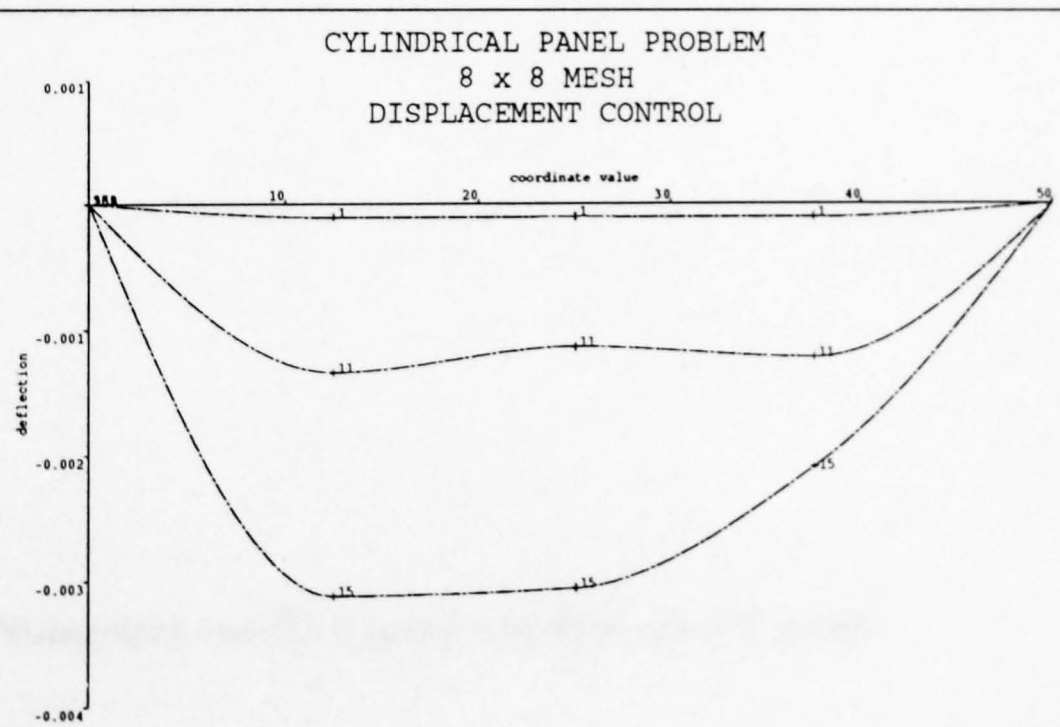

Figure 7.27. Mode shapes along the longitudinal axis for the perfect shell using the 8×8 mesh.

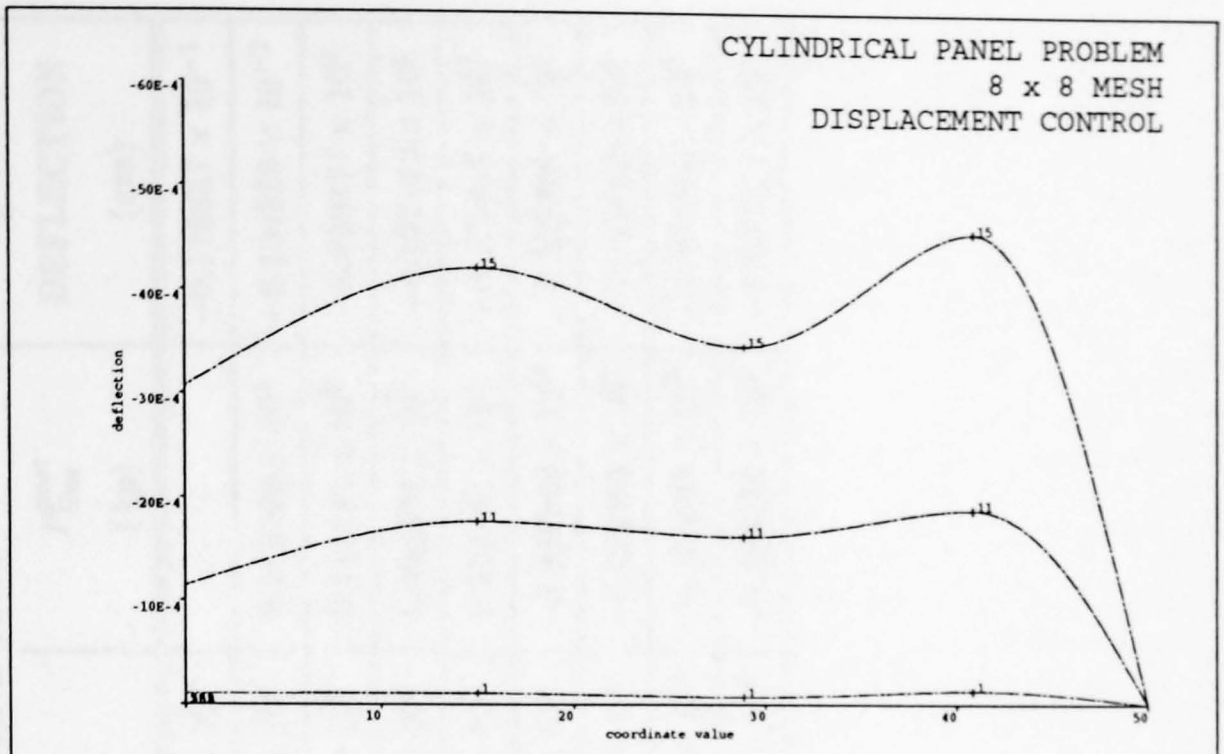

Figure 7.28. Mode shapes along the transverse axis for the perfect shell using the 8×8 mesh.

7.3.2.3 Numerical results beyond the first critical point

Table 7.1 shows results for the 8×8 mesh up to the eighth critical point. Table 7.2 gives the available comparison values by Argyris *et al.*, *c.f.* [JHAS77]. Note that these values in Table 7.2 are obtained using the eigenvalue-method as described in section 6.3.6 where the limitations of the technique are also explained.

CRITICAL POINT	COMPRESSION u^* (cm)	TOTAL LOAD P_{tot}^{pre} (kp)	TOTAL LOAD P_{tot}^{post} (kp)	LINE LOAD P_{line}^{pre} (kp)	LINE LOAD P_{line}^{post} (kp)	CENTRAL DEFLECTION (cm)
EULER	0.609321×10^{-1}	0.194806×10^{5}	–	0.988663×10^{3}	–	-0.119837×10^{-1}
$CP1-$	0.723886×10^{-2}	0.229366×10^{4}	0.236719×10^{4}	0.143336×10^{3}	0.152363×10^{3}	-0.124333×10^{-2}
$CP2-$	0.398216×10^{0}	0.953651×10^{4}	0.890378×10^{4}	0.770216×10^{2}	0.111681×10^{3}	-0.710477×10^{0}
$CP3-$	0.793240×10^{0}	0.114602×10^{5}	0.111061×10^{5}	0.138275×10^{3}	0.262601×10^{3}	-0.101170×10^{1}
$CP4-$	0.183301×10^{1}	0.140943×10^{5}	0.140321×10^{5}	0.160972×10^{3}	0.128131×10^{3}	-0.171647×10^{1}
$CP5-$	0.223302×10^{1}	0.146266×10^{5}	0.602045×10^{4}	0.908708×10^{2}	-0.937958×10^{3}	-0.193309×10^{1}
$CP6-$	0.235500×10^{1}	0.598561×10^{4}	0.551048×10^{4}	-0.105032×10^{4}	-0.850903×10^{3}	-0.188019×10^{1}
$CP7-$	0.309230×10^{1}	0.187256×10^{5}	0.186079×10^{5}	-0.163495×10^{4}	-0.166326×10^{4}	-0.467964×10^{1}
$CP8-$	0.315969×10^{1}	0.187618×10^{5}	0.179641×10^{5}	-0.164824×10^{4}	-0.154152×10^{4}	-0.507414×10^{1}

Table 7.1 : Results up to the eighth critical point for the 8×8 mesh.

CRITICAL POINT	COMPRESSION u^* (cm)	TOTAL LOAD P_{tot}^{pre} (kp)	TOTAL LOAD P_{tot}^{post} (kp)	LINE LOAD P_{line}^{pre} (kp)	LINE LOAD P_{line}^{post} (kp)
EULER	0.79317×10^{-1}	0.4616×10^5	–	–	–
$CP1-$	0.35061×10^{-1}	0.2044×10^5	0.1973×10^5	0.1097×10^4	0.9965×10^3
$CP2-$	0.60622×10^{-1}	0.3420×10^5	0.3365×10^5	0.1806×10^4	0.8629×10^3
$CP3-$	0.65000×10^{-1}	0.3544×10^5	0.3132×10^5	$\approx 0.900 \times 10^3$	$\approx 0.110 \times 10^4$
$CP4-$	0.84194×10^{-1}	0.3990×10^5	0.2211×10^5	$\approx 0.170 \times 10^4$	$\approx 0.550 \times 10^3$

Table 7.2 : Comparison values for different critical points by Argyris *et al.*.

In Table 7.1 and Table 7.2 the extreme left hand column denotes the buckling point under consideration in the corresponding row, *i.e.* EULER corresponds to the solution of the generalized eigenvalue problem $(\mathbf{K_0} + \lambda \mathbf{K_G})\,\delta\mathbf{a} = 0$. It is prudent to note that the EULER-solution is not the actual Euler buckling solution as the mesh under consideration is a *shell*-approximation for which the solution of the generalized eigenvalue problem is of no physical significance. The term 'Euler' is still used in the sequel due to the underlying mathematical relationship. $CPi-$ corre-

sponds to the i'th buckling point (critical point) found using nonlinear calculations. Hence for example $CP2-$ denotes the second critical point on the nonlinear equilibrium path. The Euler buckling mode, obtained from the solution of the generalized eigenvalue problem, is symmetric. The mode shape at $CP1-$ is symmetric with an antisymmetric eigenmode along the longitudinal line, although the connector positions with the largest magnitude entries do not lie on it. From $CP2-$ onwards all mode shapes and eigenmodes are asymmetric. Note also that the deformations in the direction of the compression (in x^1-direction) along the transverse middle line become different from one another. The P_{tot}^{pre} column gives the total applied load at the critical points ($CPi-$), whereas the P_{tot}^{post} column gives the total applied load immediately after the critical points ($CPi+$). Similarly, the P_{line}^{pre} column gives the line load at the critical points ($CPi-$), whereas the P_{line}^{post} column gives the line load immediately after the critical points ($CPi+$). In the context of the present work, line load means the nodal load at the compressive edge of the longitudinal axis.

The stability coefficients at the critical points reveal that

- at $CP1-$

$$\begin{aligned} \mu &= \pm 0.000 \times 10^{0} \quad i.e. \quad \mu = 0 \\ A &= +0.185 \times 10^{-4} \quad i.e. \quad A = 0 \\ D &= -0.138 \times 10^{12} \quad i.e. \quad D < 0 \ . \end{aligned} \tag{7.3.1}$$

Hence the critical point is identified as an *unstable symmetric bifurcation point.*

Successful continuation from the Euler buckling point is achieved with $\alpha_1 = 0.300 \times 10^{1}$. Successful continuation from $CP1-$ is achieved with $\alpha_1 = 0.100 \times 10^{0}$.

- at $CP2-$

$$\begin{aligned} \mu &= \pm 0.000 \times 10^{0} \quad i.e. \quad \mu = 0 \\ A &= -0.158 \times 10^{4} \quad i.e. \quad A \neq 0 \ . \end{aligned} \tag{7.3.2}$$

Hence the critical point is identified as an *asymmetric bifurcation point.*

Successful continuation from $CP2-$ is achieved with $\alpha_1 = 0.100 \times 10^{-2}$ and

- at $CP3-$

$$\begin{aligned} \mu &= \pm 0.000 \times 10^{0} \quad i.e. \quad \mu = 0 \\ A &= +0.140 \times 10^{4} \quad i.e. \quad A \neq 0 \ . \end{aligned} \tag{7.3.3}$$

Hence the critical point is identified as an *asymmetric bifurcation point.*

Successful continuation from $CP3-$ is achieved with $\alpha_1 = -0.120 \times 10^0$.

- at $CP4-$

$$\begin{aligned} \mu &= \pm 0.000 \times 10^0 \quad i.e. \quad \mu = 0 \\ A &= -0.346 \times 10^3 \quad i.e. \quad A \neq 0 \ . \end{aligned} \tag{7.3.4}$$

Hence the critical point is identified as an *asymmetric bifurcation point.*

Successful continuation from $CP4-$ is achieved with $\alpha_1 = 0.600 \times 10^{-1}$.

- at $CP5-$

$$\begin{aligned} \mu &= \pm 0.000 \times 10^0 \quad i.e. \quad \mu = 0 \\ A &= -0.201 \times 10^4 \quad i.e. \quad A \neq 0 \ . \end{aligned} \tag{7.3.5}$$

Hence the critical point is identified as an *asymmetric bifurcation point.*

Successful continuation from $CP5-$ is achieved with $\alpha_1 = -0.850 \times 10^{-1}$.

- at $CP6-$

$$\begin{aligned} \mu &= \pm 0.000 \times 10^0 \quad i.e. \quad \mu = 0 \\ A &= +0.395 \times 10^3 \quad i.e. \quad A \neq 0 \ . \end{aligned} \tag{7.3.6}$$

Hence the critical point is identified as an *asymmetric bifurcation point.*

Successful continuation from $CP6-$ is achieved with $\alpha_1 = -0.68 \times 10^{-1}$.

- at $CP7-$

$$\begin{aligned} \mu &= \pm 0.000 \times 10^0 \quad i.e. \quad \mu = 0 \\ A &= +0.999 \times 10^3 \quad i.e. \quad A \neq 0 \ . \end{aligned} \tag{7.3.7}$$

Hence the critical point is identified as an *asymmetric bifurcation point.*

Successful continuation from $CP7-$ is achieved with $\alpha_1 = 0.80 \times 10^{-1}$.

- at $CP8-$

$$\begin{aligned} \mu &= \pm 0.000 \times 10^0 \quad i.e. \quad \mu = 0 \\ A &= +0.481 \times 10^3 \quad i.e. \quad A \neq 0 \ . \end{aligned} \tag{7.3.8}$$

Hence the critical point is identified as an *asymmetric bifurcation point.*

Successful continuation from $CP8-$ is achieved with $\alpha_1 = -0.20 \times 10^{-1}$.

The emerging load - compression curves and smallest eigenvalue - deflection curves as well as curves for the mode shapes along the longitudinal and transverse

axes until a point beyond the eighth critical point $CP8-$ are shown in Figures 7.29 - 7.34.

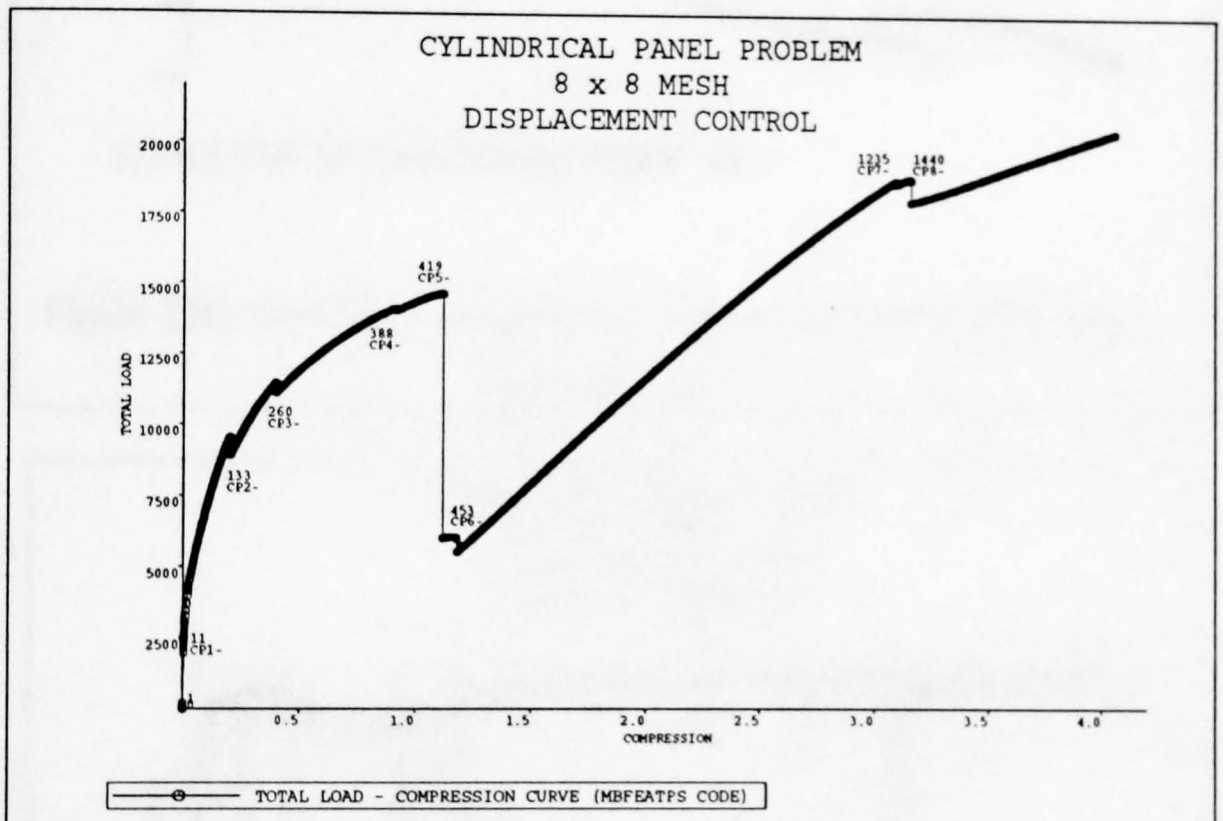

Figure 7.29. Total load - compression curve for the perfect shell using the 8×8 mesh.

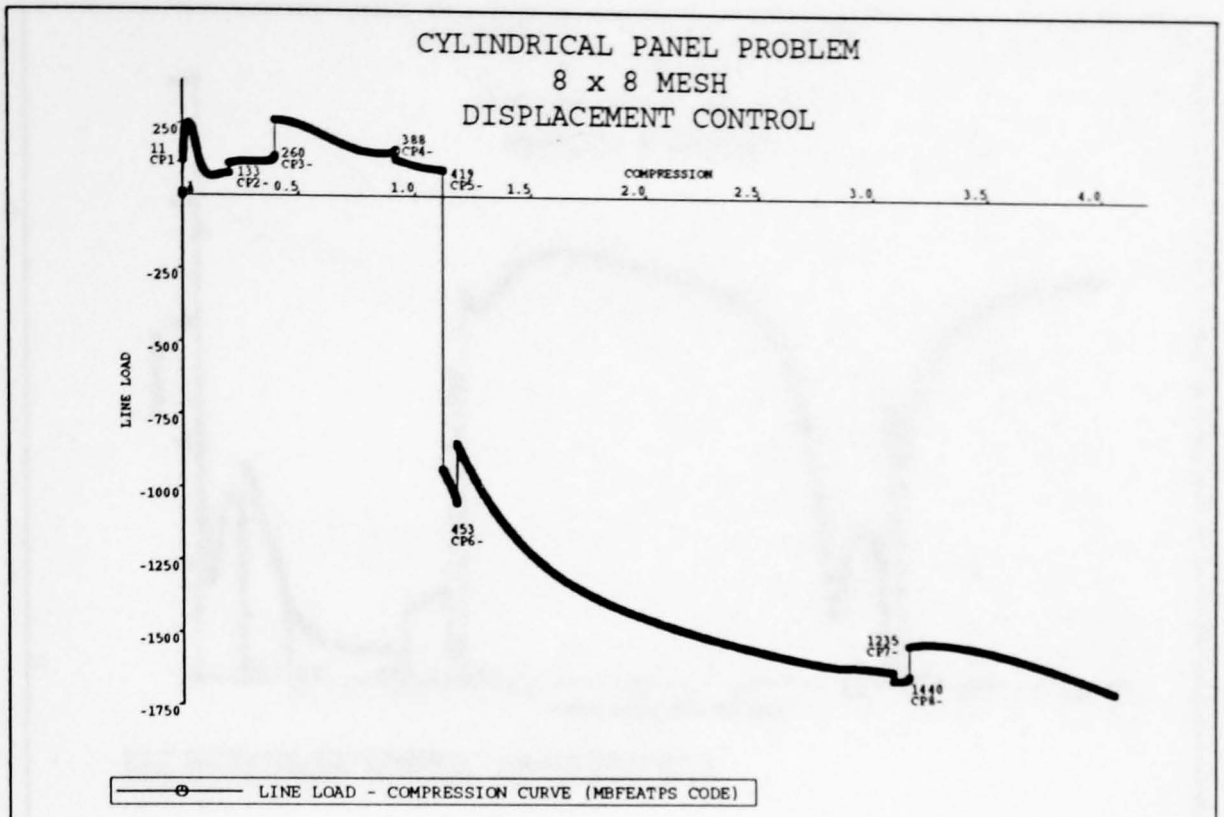

Figure 7.30. Line load - compression curve for the perfect shell using the 8×8 mesh.

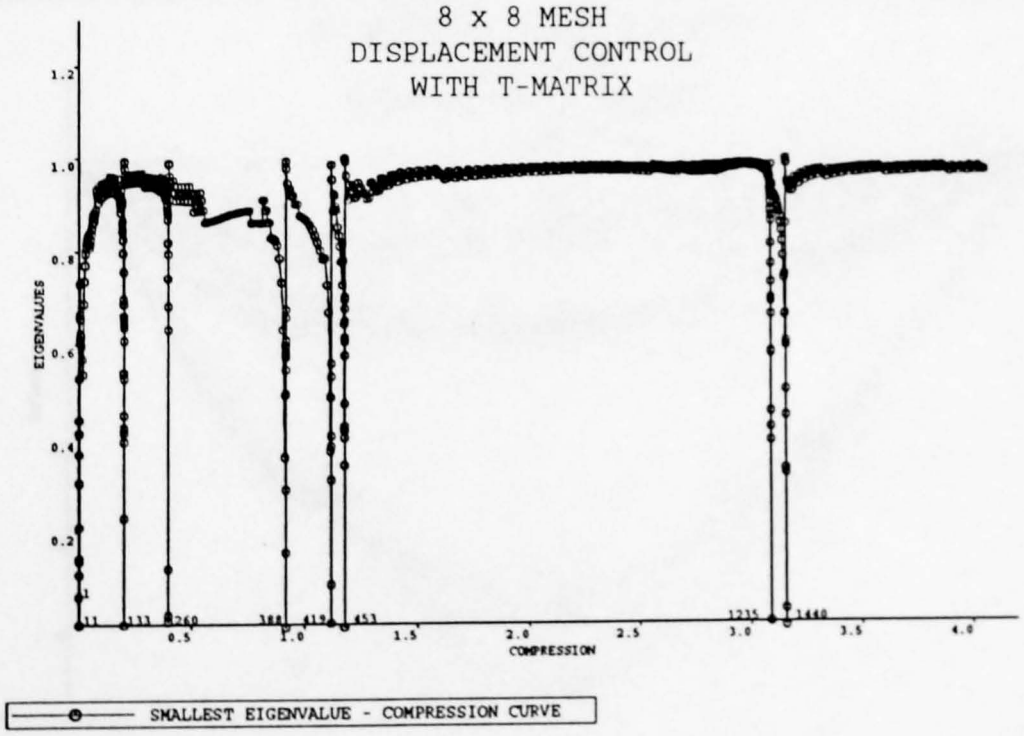

Figure 7.31. Smallest eigenvalue - compression curve for the perfect shell using the 8×8 mesh (with T-matrix, *i.e.* eigenvalues $\theta^{(r)}$ calculated from $\mathbf{K_T}\boldsymbol{\xi}^{(r)} = \theta^{(r)}\mathbf{T}\boldsymbol{\xi}^{(r)}$ (no sum on r))

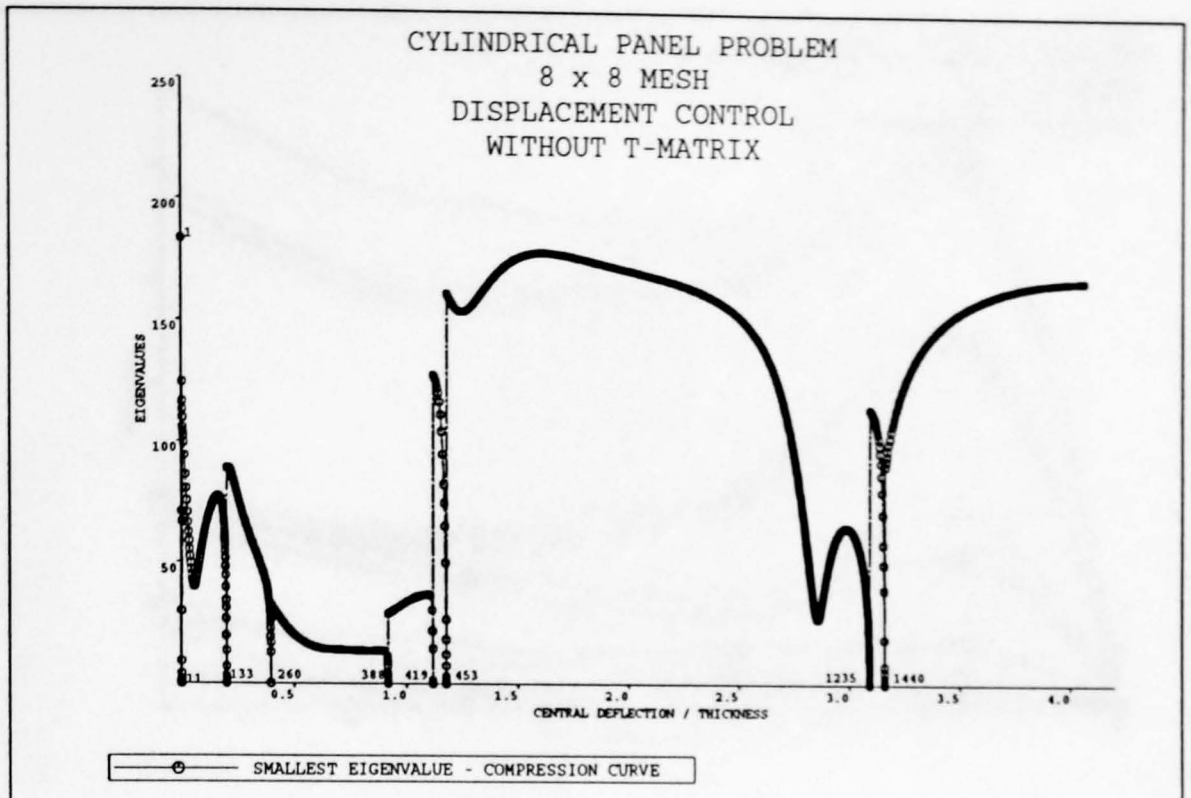

Figure 7.32. Smallest eigenvalue - compression curve for the perfect shell using the 8×8 mesh (without T-matrix, *i.e.* eigenvalues $\theta^{(r)}$ calculated from $\mathbf{K_T}\boldsymbol{\xi}^{(r)} = \theta^{(r)}\boldsymbol{\xi}^{(r)}$ (no sum on r))

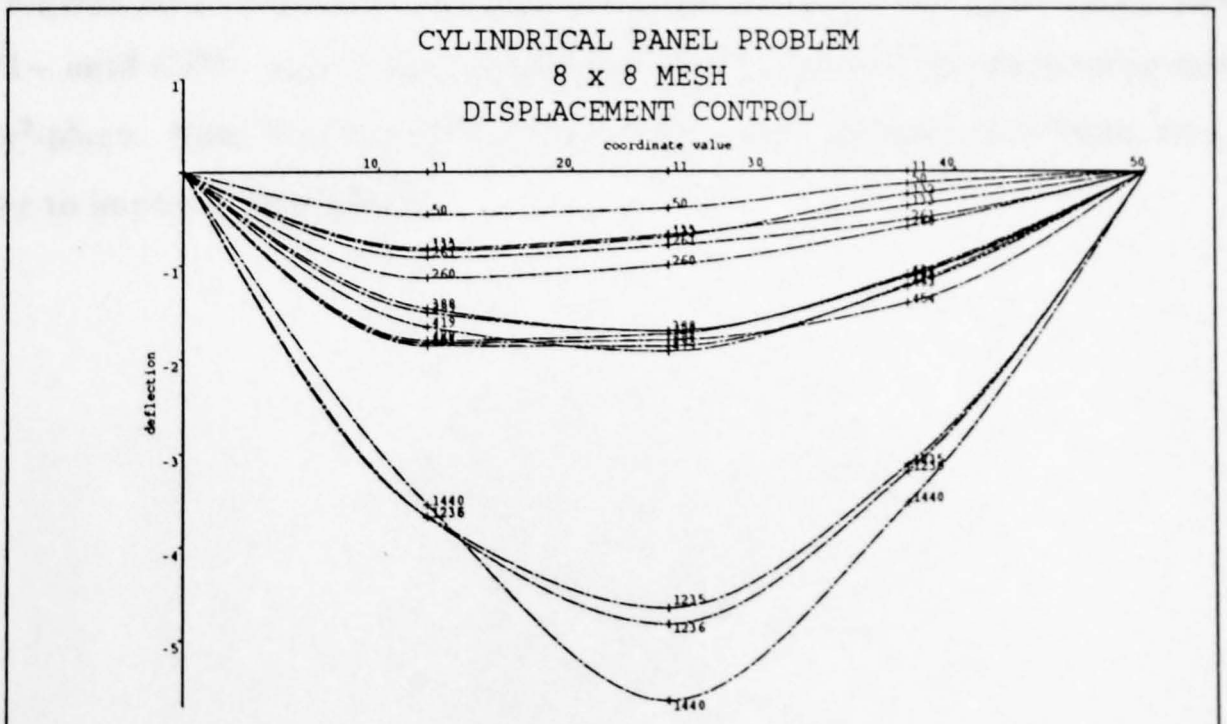

Figure 7.33. Mode shapes along the longitudinal axis for the perfect shell using the 8×8 mesh.

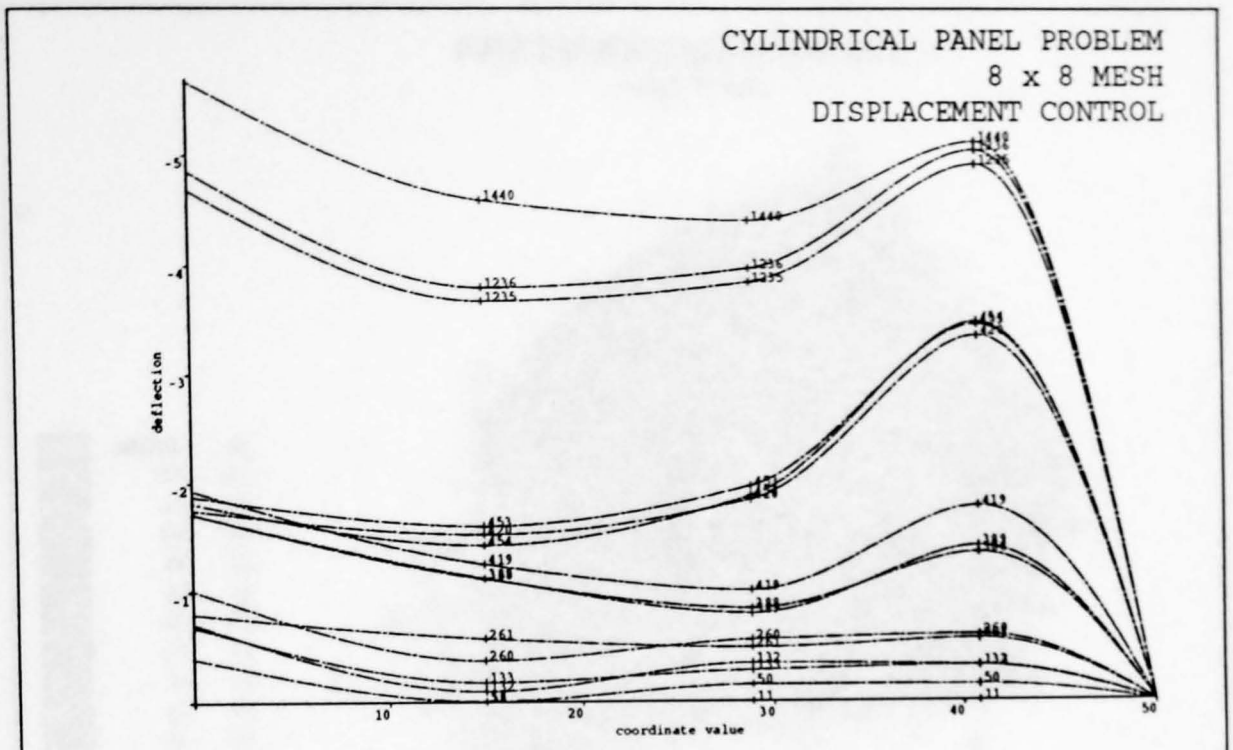

Figure 7.34. Mode shapes along the transverse axis for the perfect shell using the 8×8 mesh.

Figures 7.35 - 7.52 show the deformed configurations at the eight critical points $CP1-$ until $CP8-$ and at a point beyond $CP8-$ as well as their projections on the x^1-x^2-plane. Note that the deformations have been magnified by a factor of 5 in order to improve visualization.

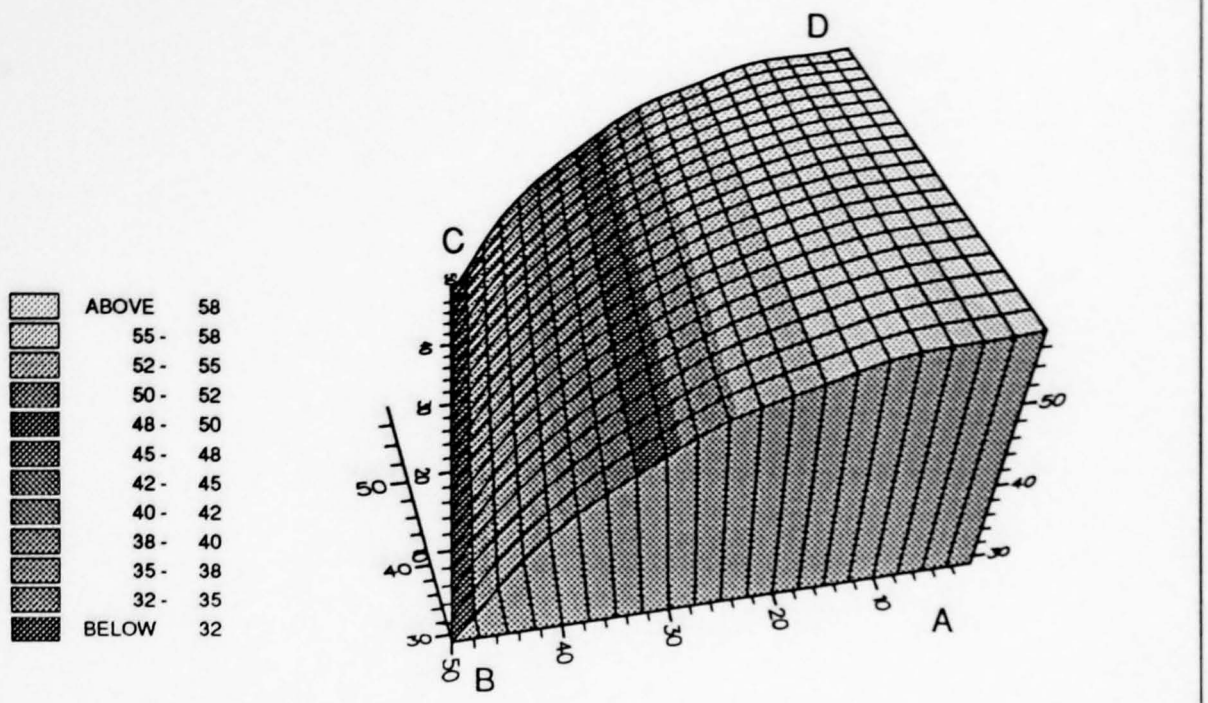

Figure 7.35 : Symmetric first buckling mode of the perfect shell at $CP1-$ for the 8×8 mesh (deformations magnified by factor 5).

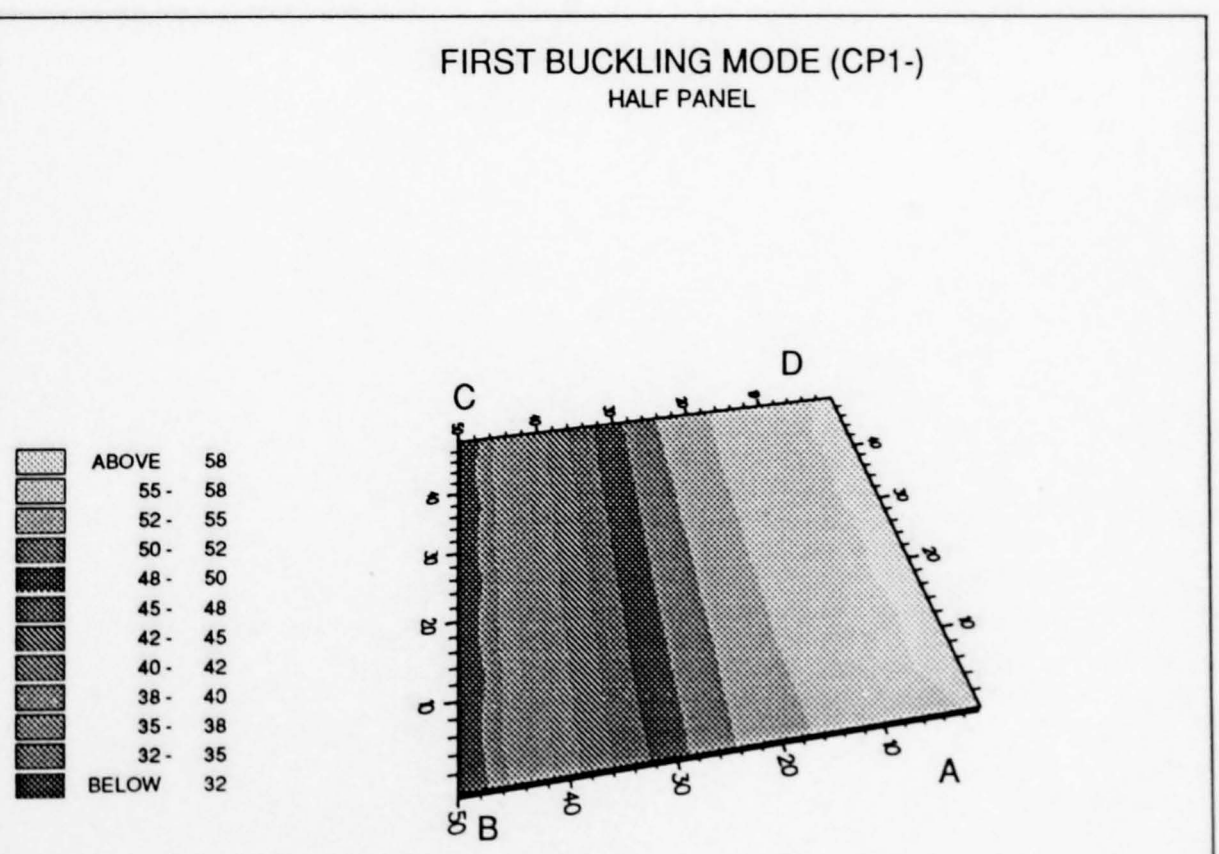

Figure 7.36 : Projection of the first buckling mode of the perfect shell at $CP1-$ for the 8×8 mesh (deformations magnified by factor 5).

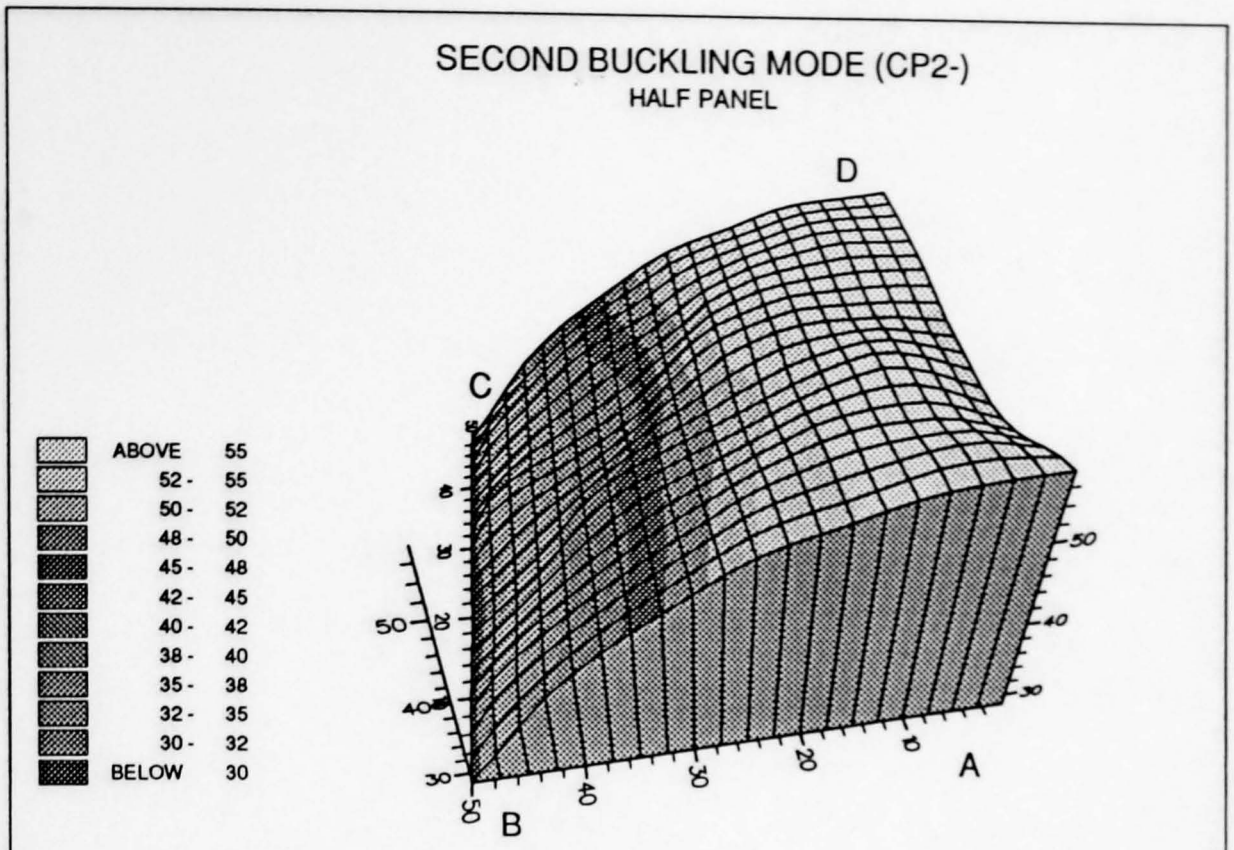

Figure 7.37 : Asymmetric second buckling mode of the perfect shell at $CP2-$ for the 8×8 mesh (deformations magnified by factor 5).

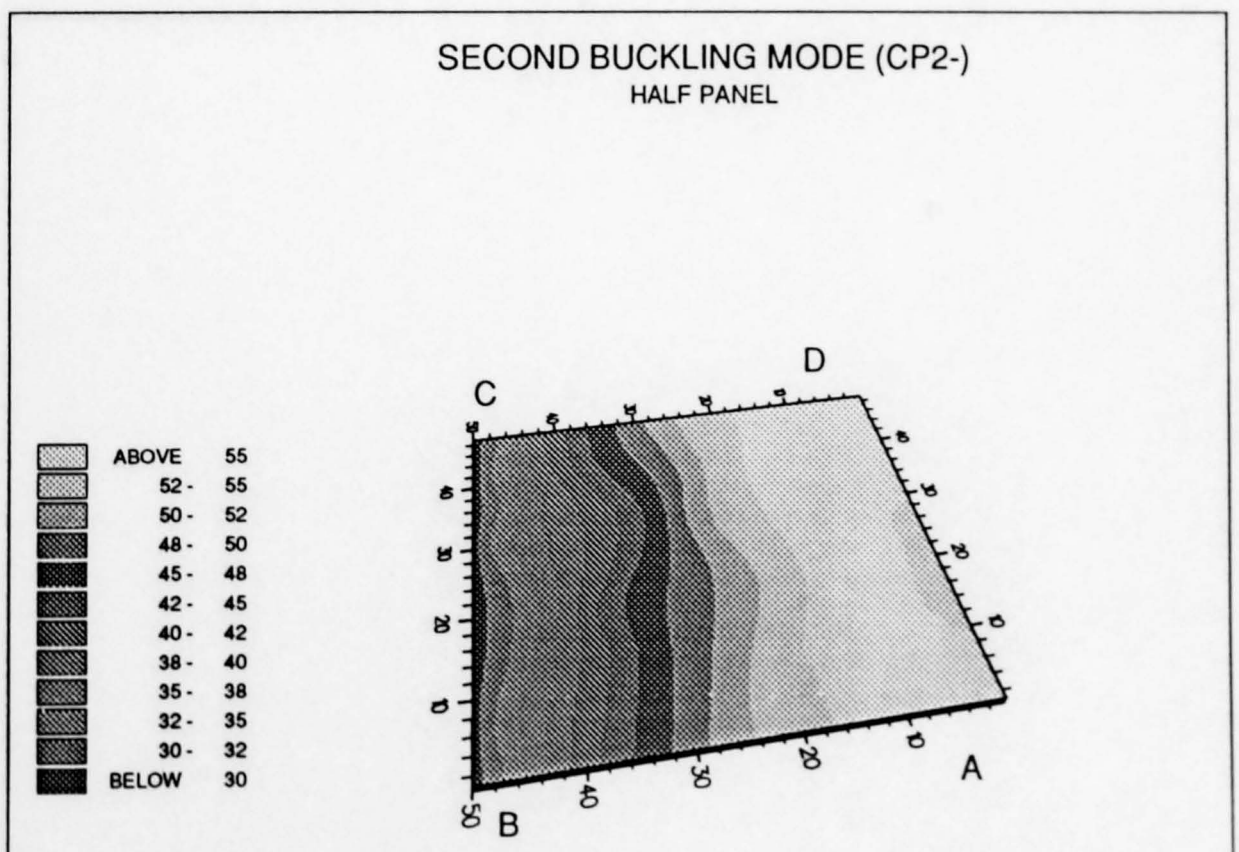

Figure 7.38 : Projection of the second buckling mode of the perfect shell at $CP2-$ for the 8×8 mesh (deformations magnified by factor 5).

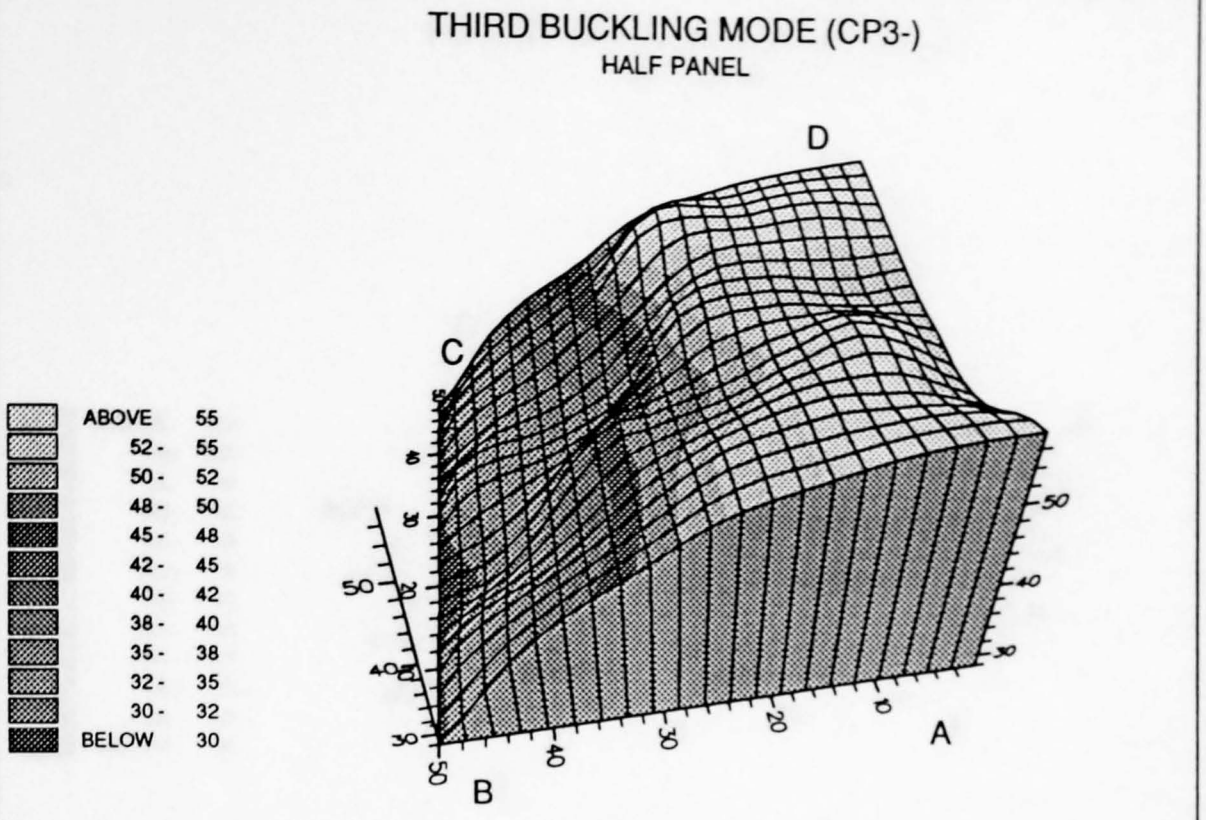

Figure 7.39 : Asymmetric third buckling mode of the perfect shell at $CP3-$ for the 8×8 mesh (deformations magnified by factor 5).

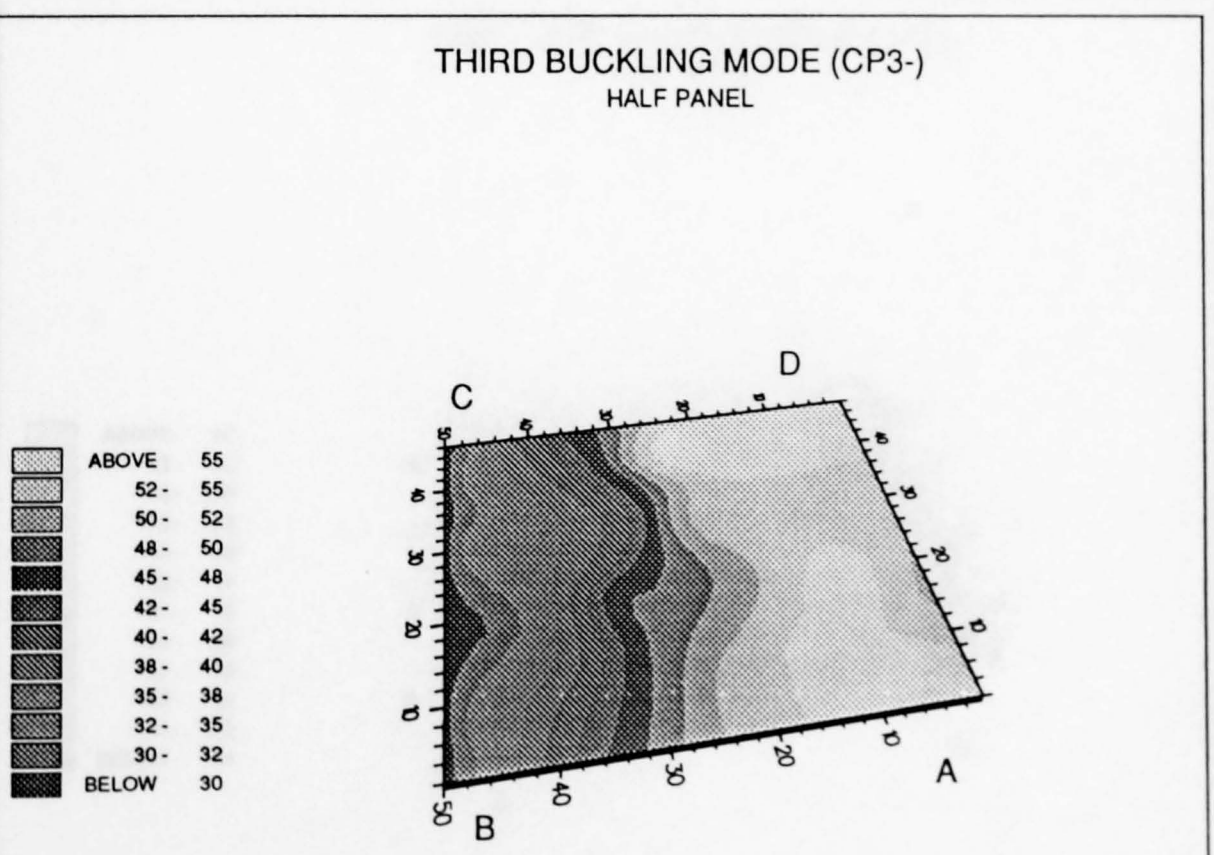

Figure 7.40 : Projection of the third buckling mode of the perfect shell at $CP3-$ for the 8×8 mesh (deformations magnified by factor 5).

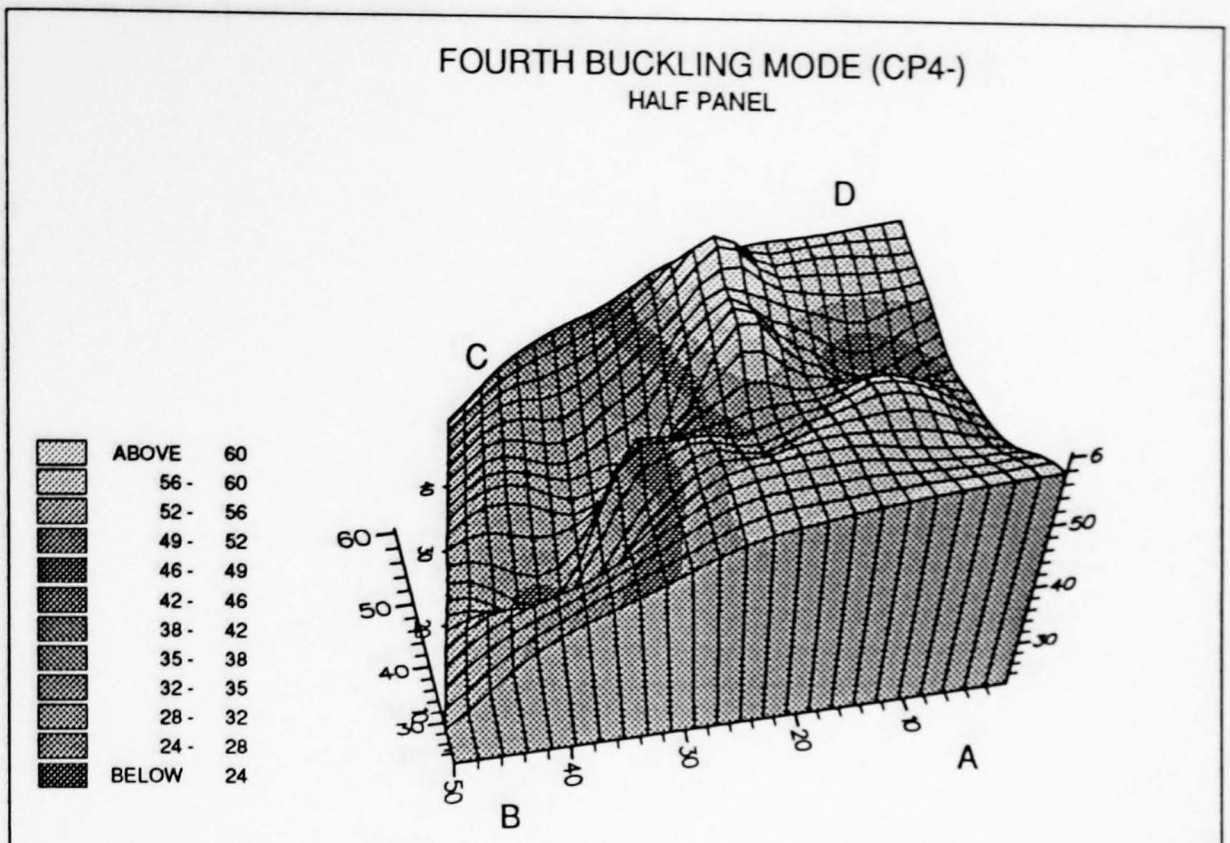

Figure 7.41 : Asymmetric fourth buckling mode of the perfect shell at $CP4-$ for the 8×8 mesh (deformations magnified by factor 5).

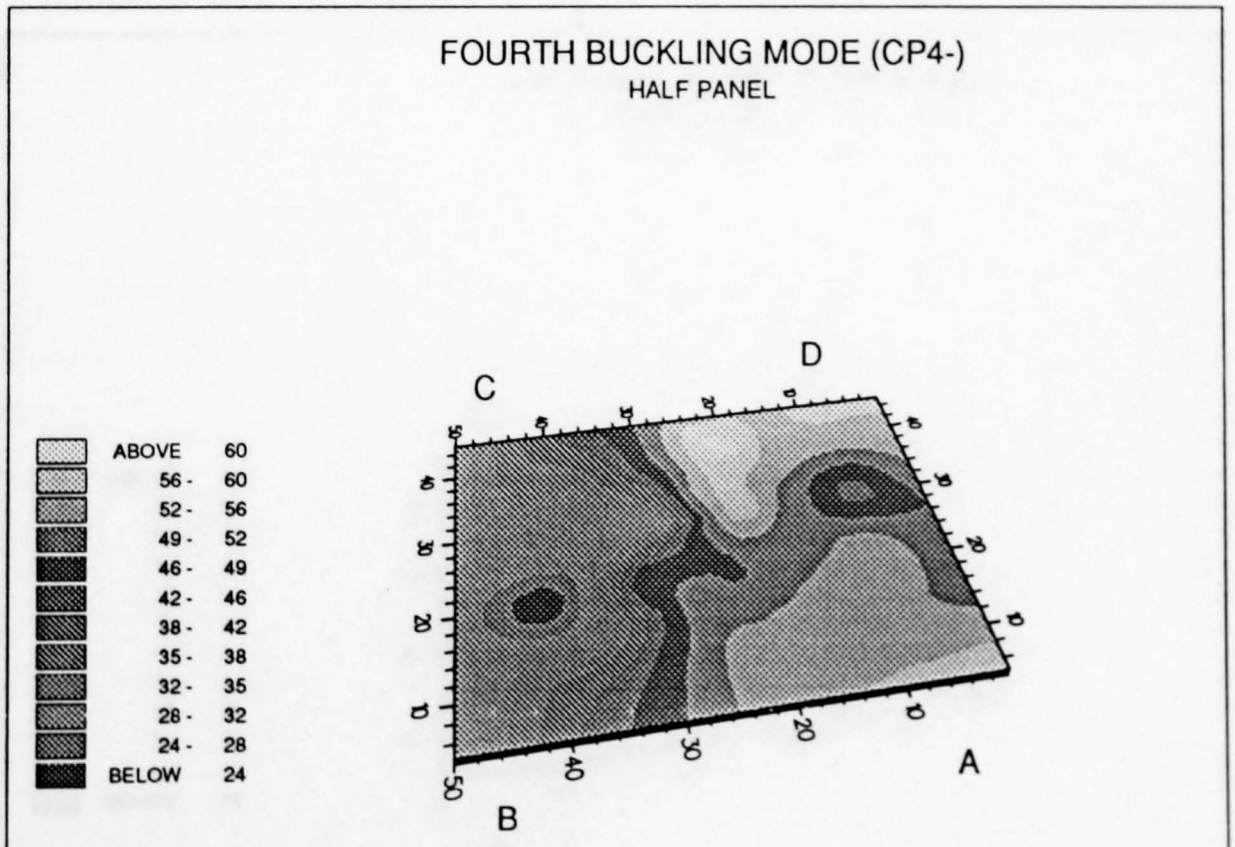

Figure 7.42 : Projection of the fourth buckling mode of the perfect shell at $CP4-$ for the 8×8 mesh (deformations magnified by factor 5).

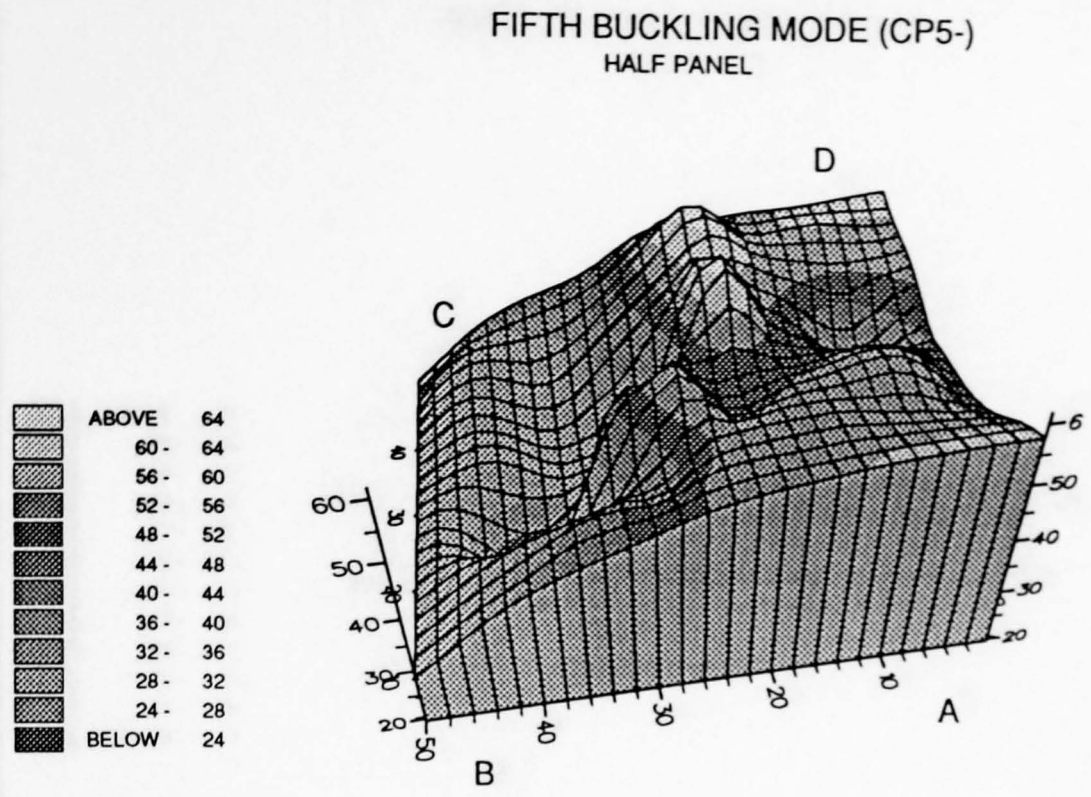

Figure 7.43 : Asymmetric fifth buckling mode of the perfect shell at $CP5-$ for the 8×8 mesh (deformations magnified by factor 5).

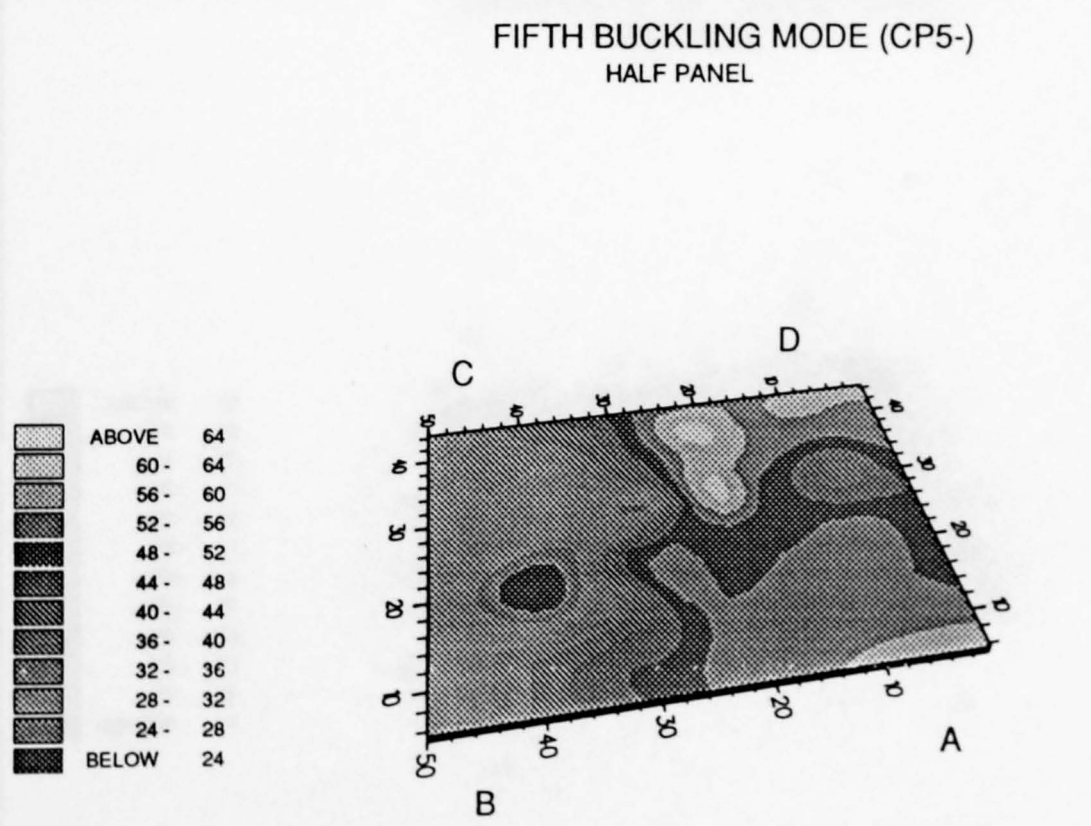

Figure 7.44 : Projection of the fifth buckling mode of the perfect shell at $CP5-$ for the 8×8 mesh (deformations magnified by factor 5).

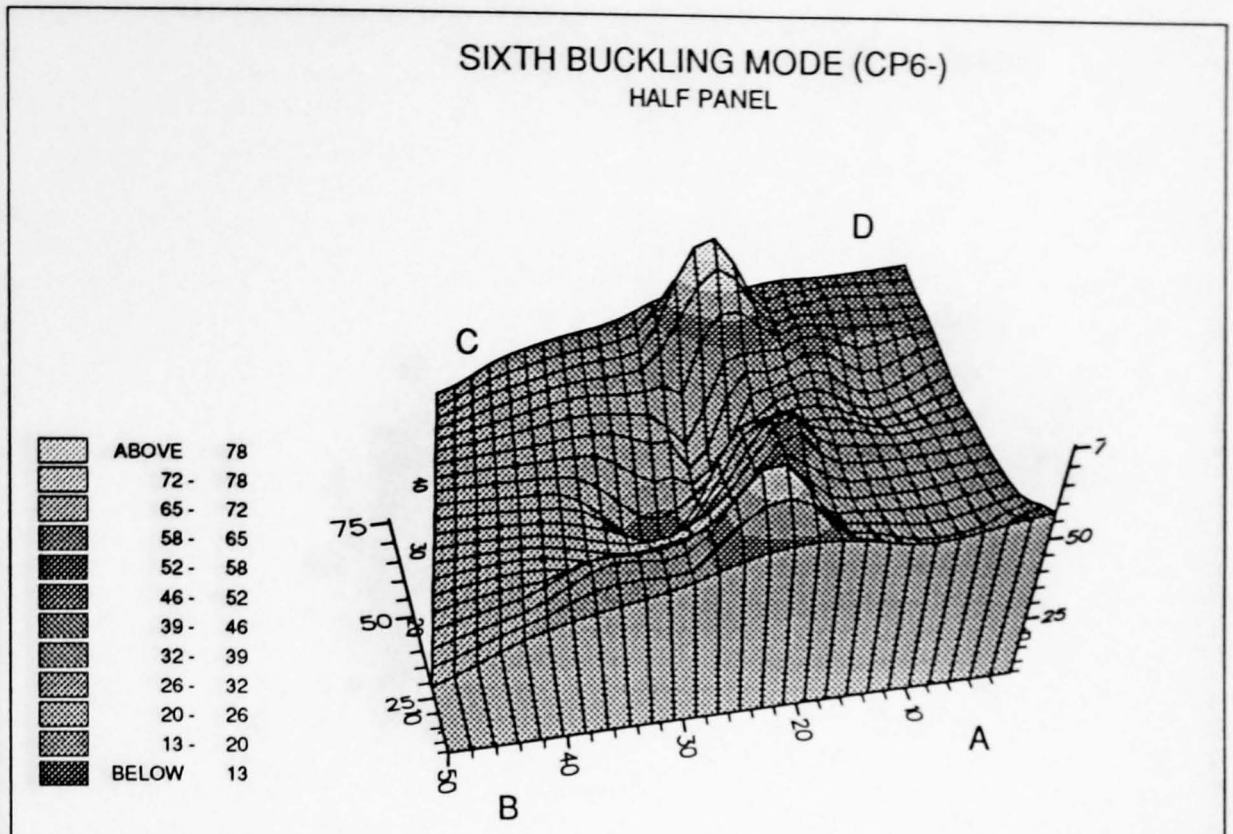

Figure 7.45 : Asymmetric sixth buckling mode of the perfect shell at $CP6-$ for the 8×8 mesh (deformations magnified by factor 5).

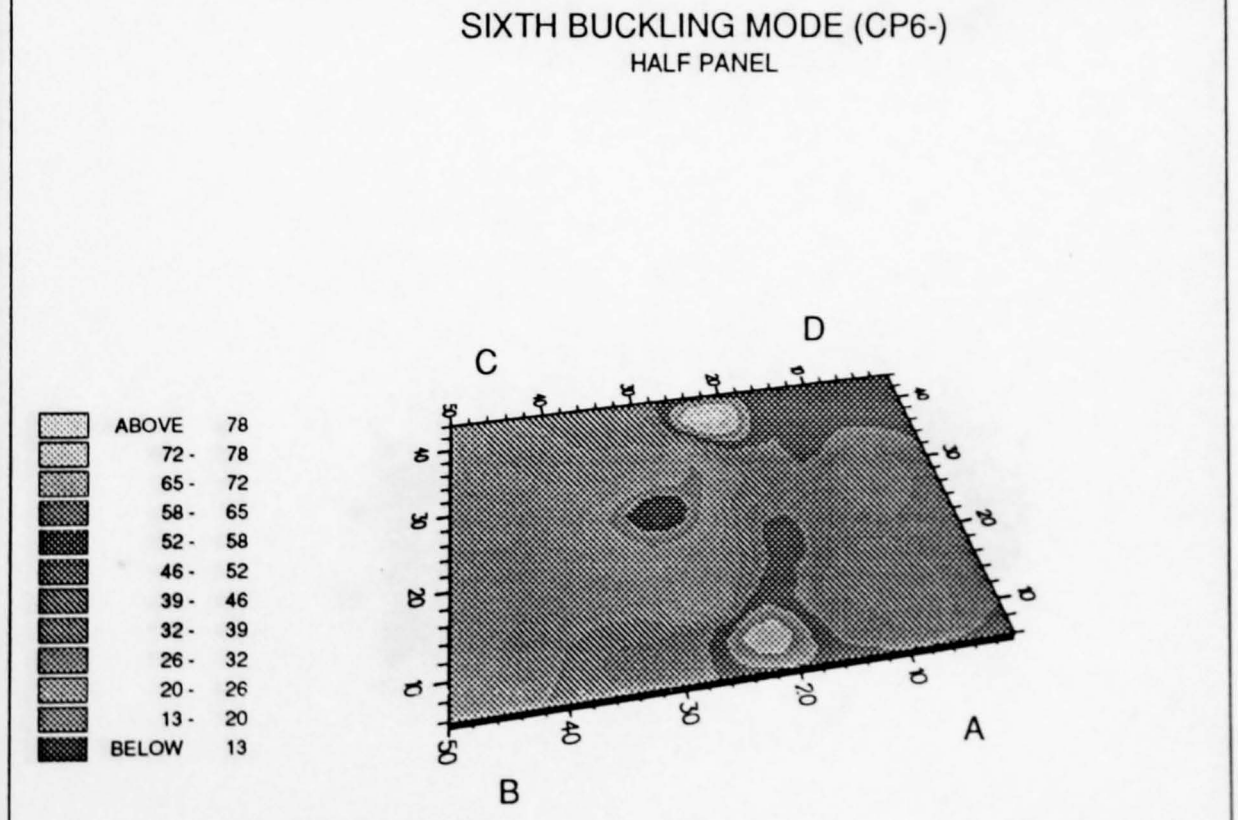

Figure 7.46 : Projection of the sixth buckling mode of the perfect shell at $CP6-$ for the 8×8 mesh (deformations magnified by factor 5).

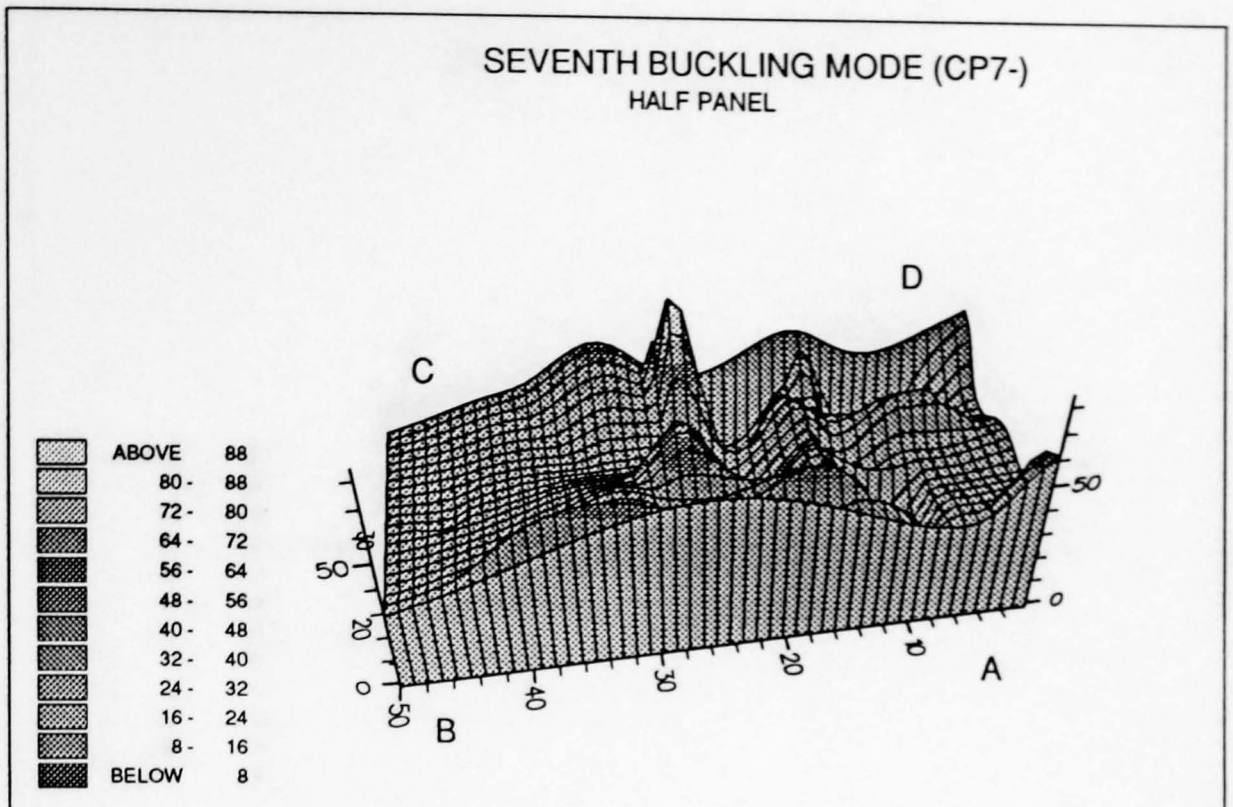

Figure 7.47 : Asymmetric seventh buckling mode of the perfect shell at $CP7-$ for the 8×8 mesh (deformations magnified by factor 5).

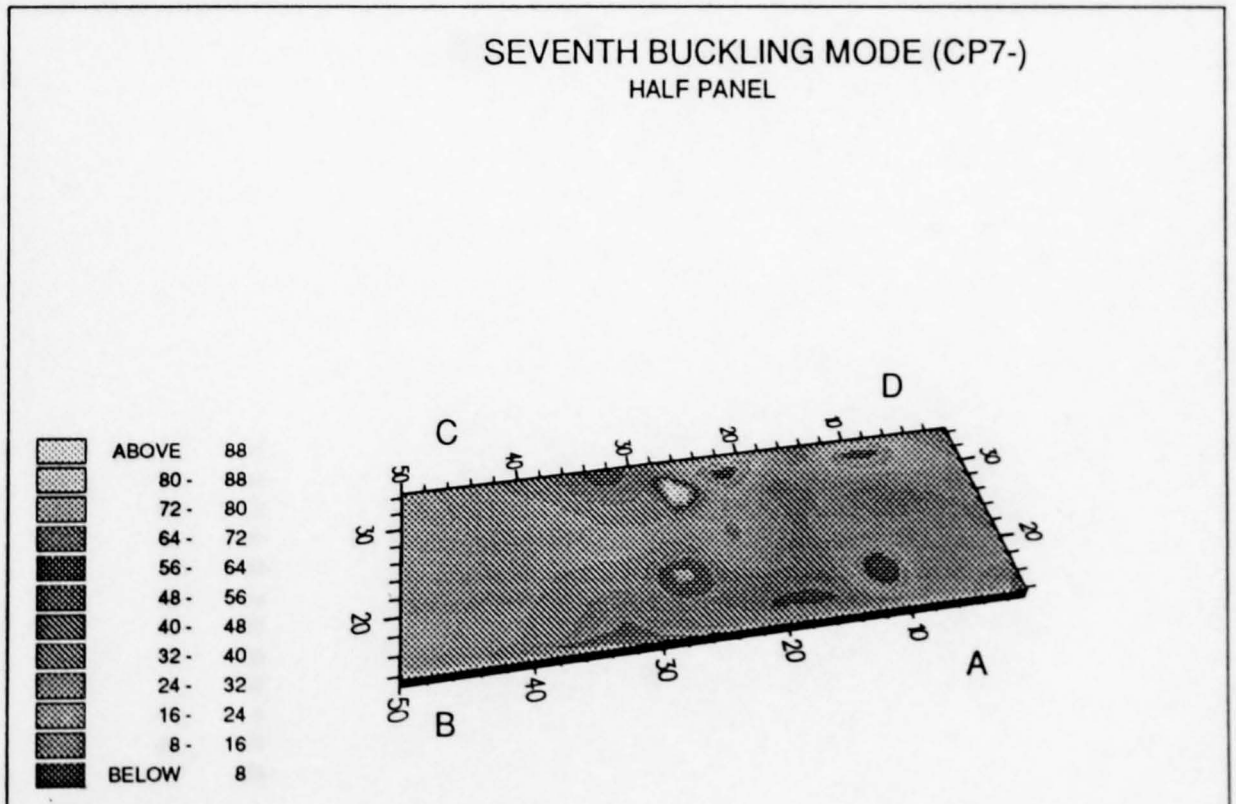

Figure 7.48 : Projection of the seventh buckling mode of the perfect shell at $CP7-$ for the 8×8 mesh (deformations magnified by factor 5).

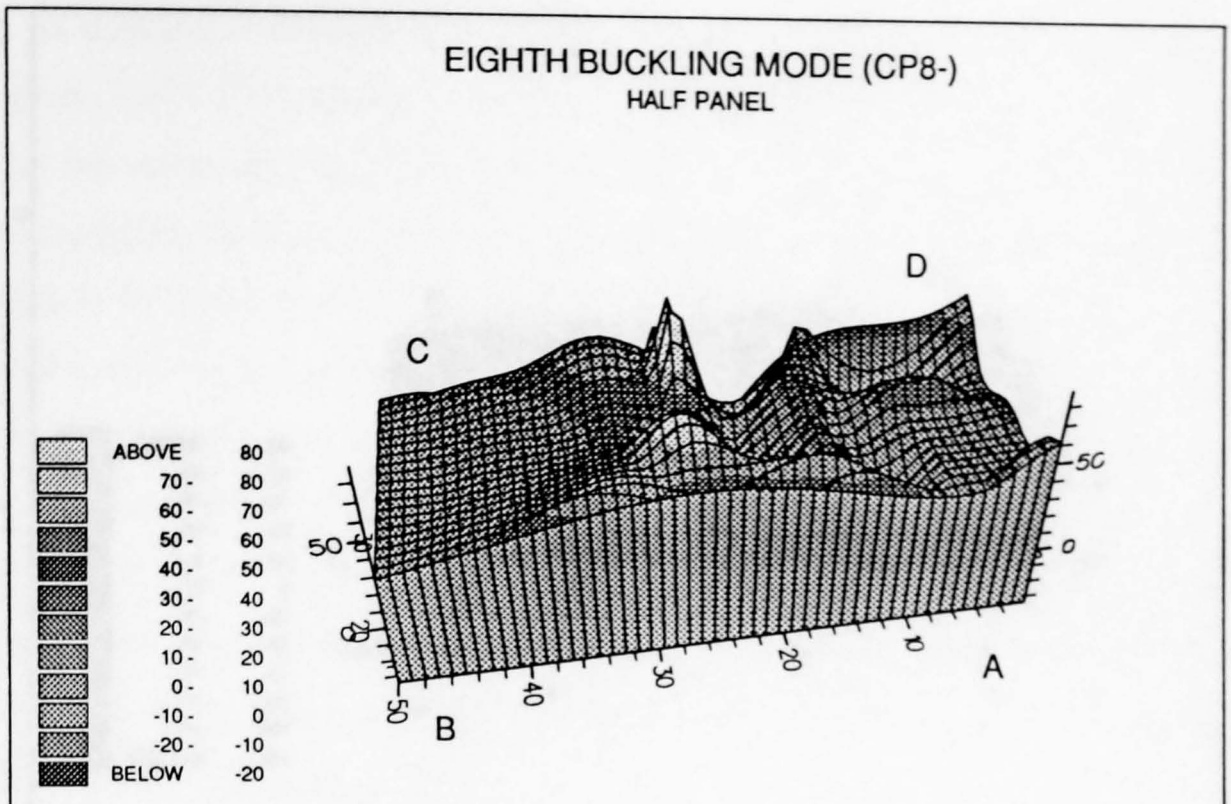

Figure 7.49 : Asymmetric eighth buckling mode of the perfect shell at $CP8-$ for the 8×8 mesh (deformations magnified by factor 5).

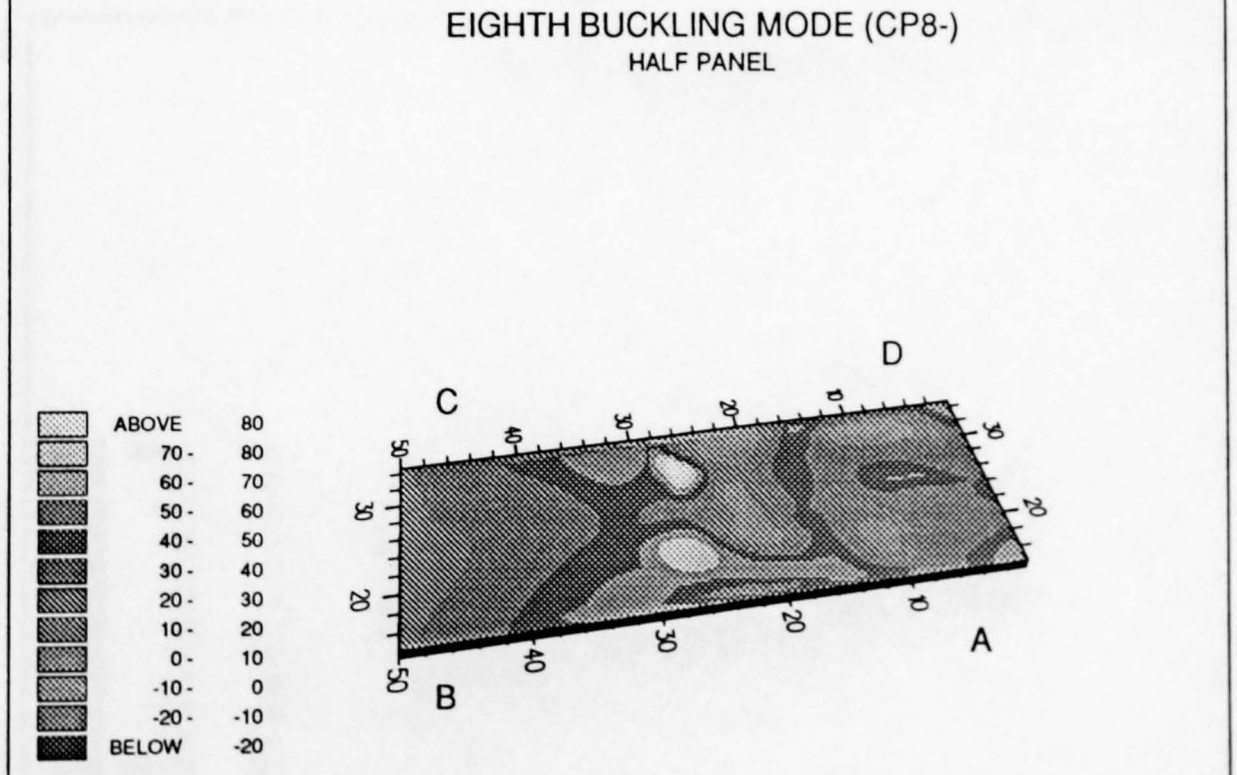

Figure 7.50 : Projection of the eighth buckling mode of the perfect shell at $CP8-$ for the 8×8 mesh (deformations magnified by factor 5).

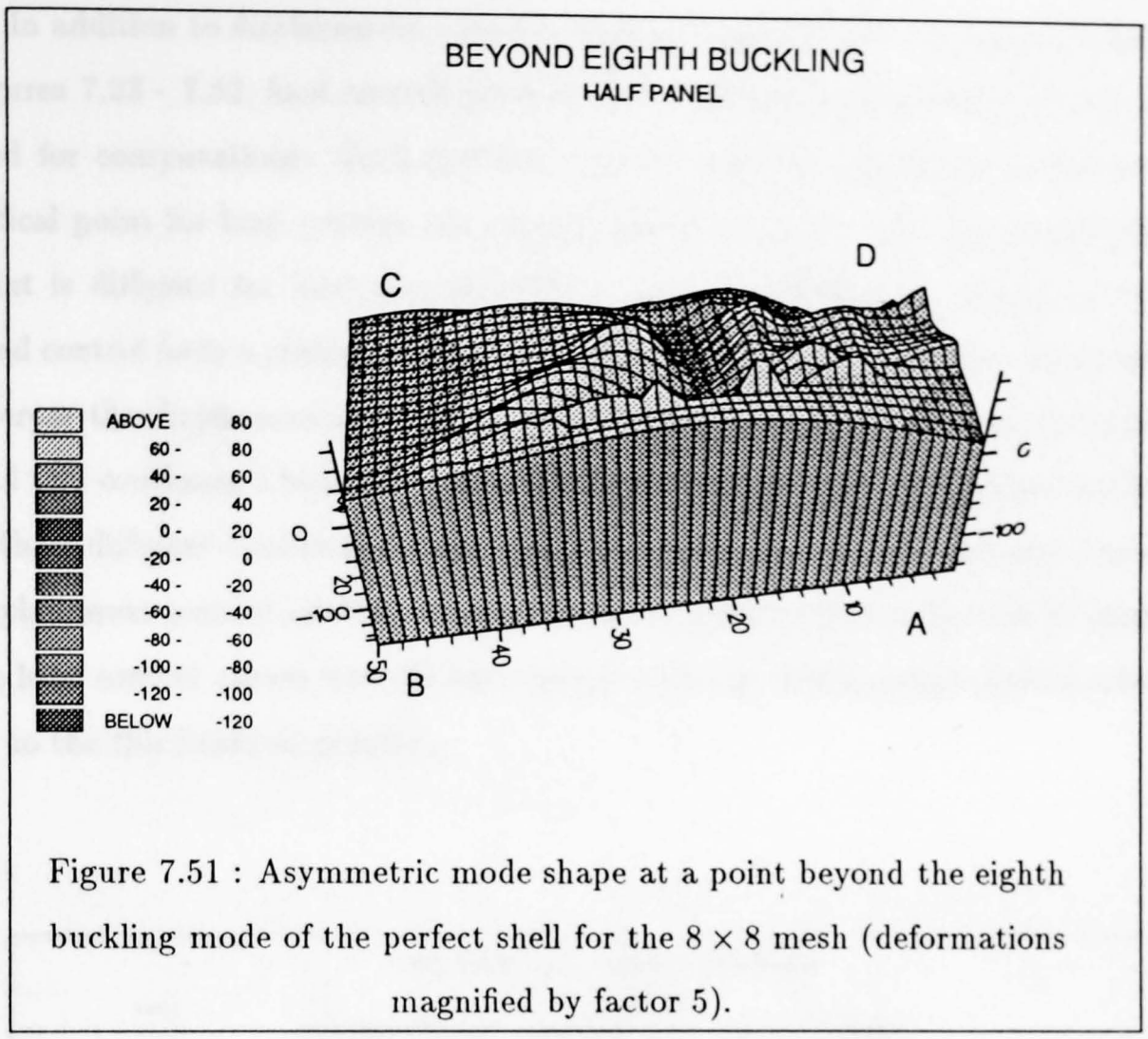

Figure 7.51 : Asymmetric mode shape at a point beyond the eighth buckling mode of the perfect shell for the 8×8 mesh (deformations magnified by factor 5).

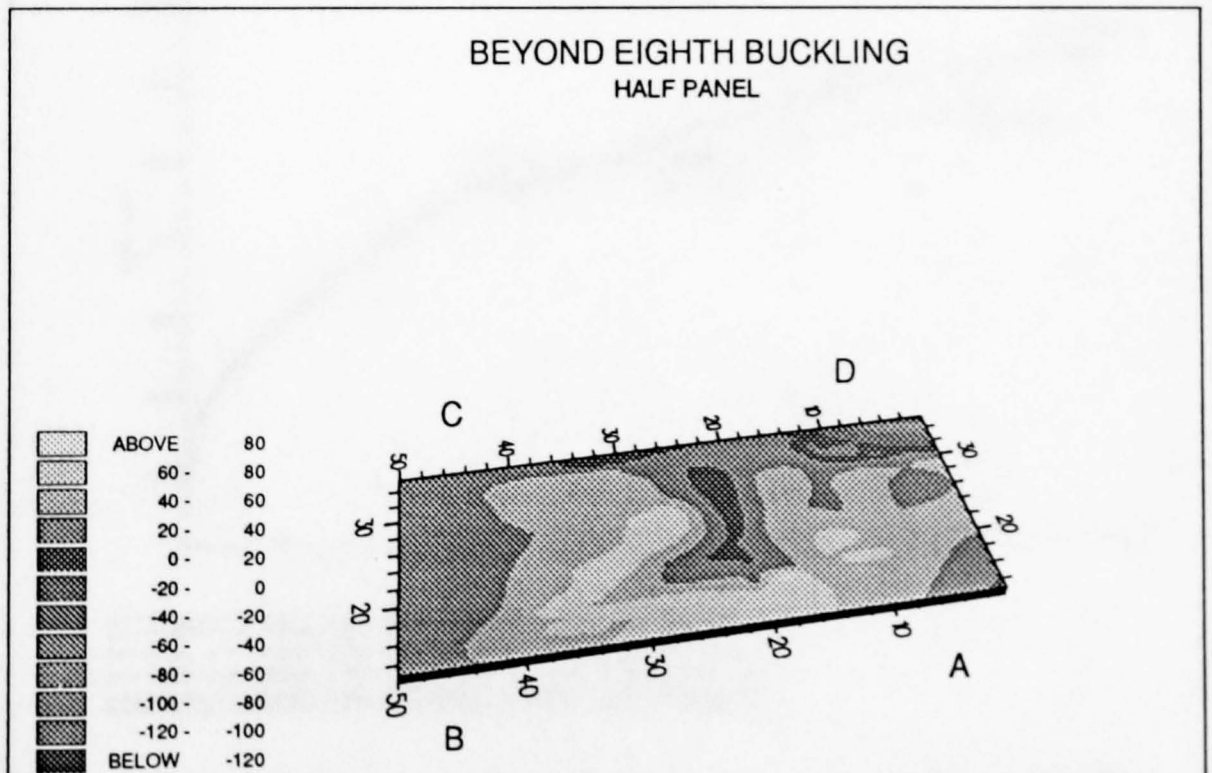

Figure 7.52 : Projection of the mode shape at a point beyond the eighth buckling mode of the perfect shell for the 8×8 mesh (deformations magnified by factor 5).

In addition to displacement control which has been discussed in detail so far, see Figures 7.23 - 7.52, load control (loading of constrained boundaries) has also been used for computations. Both techniques reveal identical results up to the second critical point for load control, see Figure 7.53 below. Note that the second critical point is different for load control ($CP2\text{-}_{load}$) and displacement control ($CP2-$). Load control finds a critical point where the tangent becomes horizontal (limit point) whereas the displacement control curve undergoes a hook with a slight decrease in load and continues a bit further until $CP2-$ is found. Employing load control leads to three different continuation solutions from $CP2\text{-}_{load}$, all being different from the displacement control solution. Figure 7.53 and Figure 7.54 visualize this by plotting the load control curves into the same graph with the displacement control solution up to the third critical point(s).

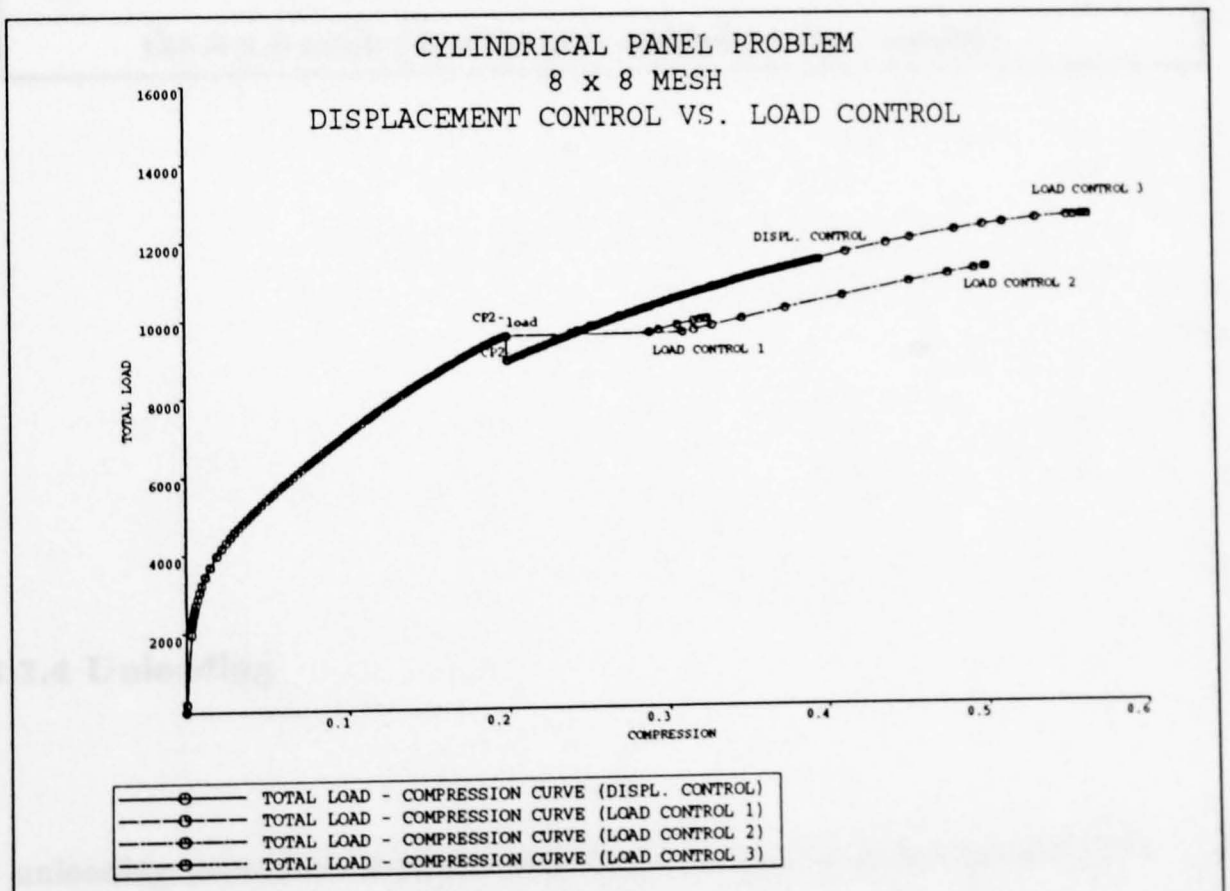

Figure 7.53 : Total load - compression curve for the perfect shell using the 8×8 mesh (displacement control vs. load control).

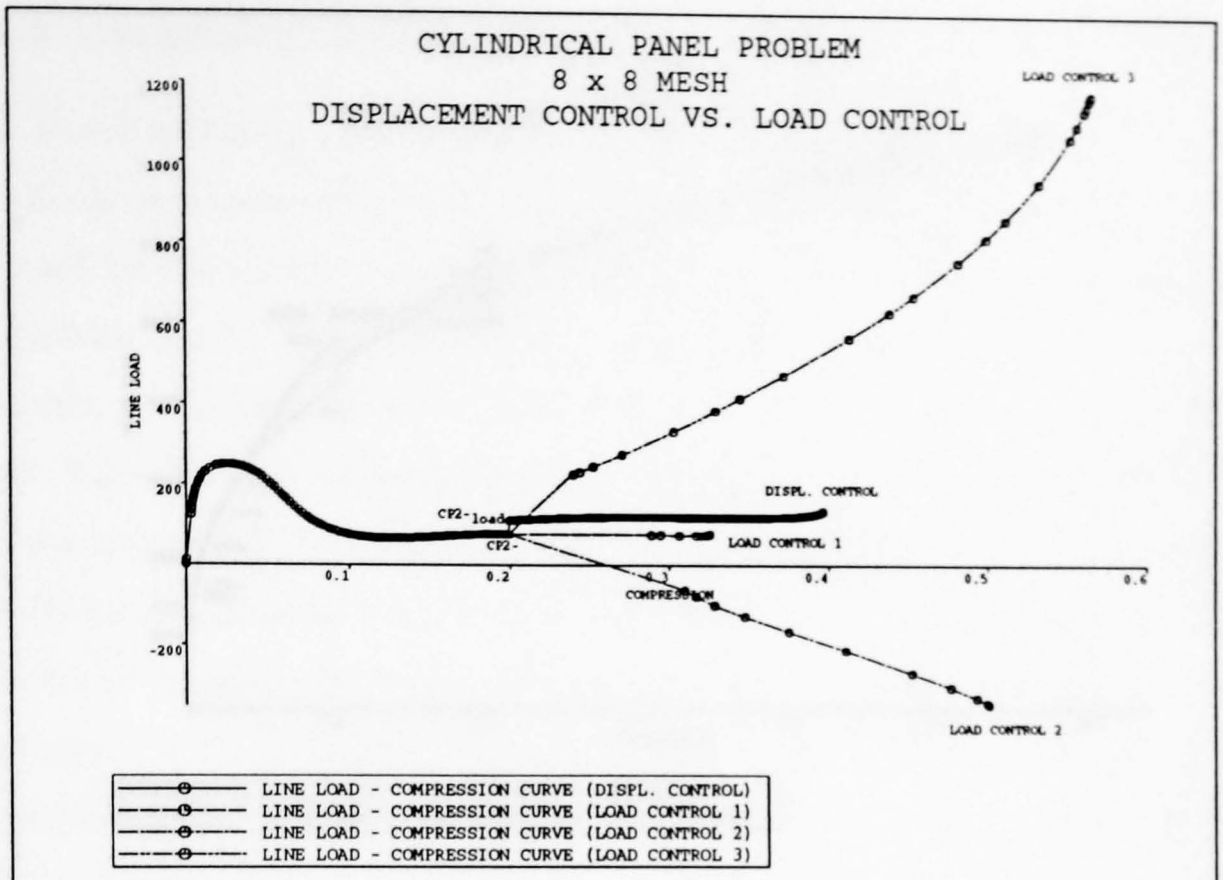

Figure 7.54 : Line load - compression curve for the perfect shell using the 8×8 mesh (displacement control vs. load control).

7.3.2.4 Unloading

An unloading procedure is performed commencing at a point beyond $CP4-$. The resulting load - deflection curves are shown in Figure 7.55 and Figure 7.56 where also the ordinary displacement control (increasing step size) curves are plotted for comparison. As is easily seen, the curves don't coincide. The critical points found using the unloading procedure are marked with $CPi+$, where i is the i'th critical point. Altogether for the unloading, 7 critical points are found.

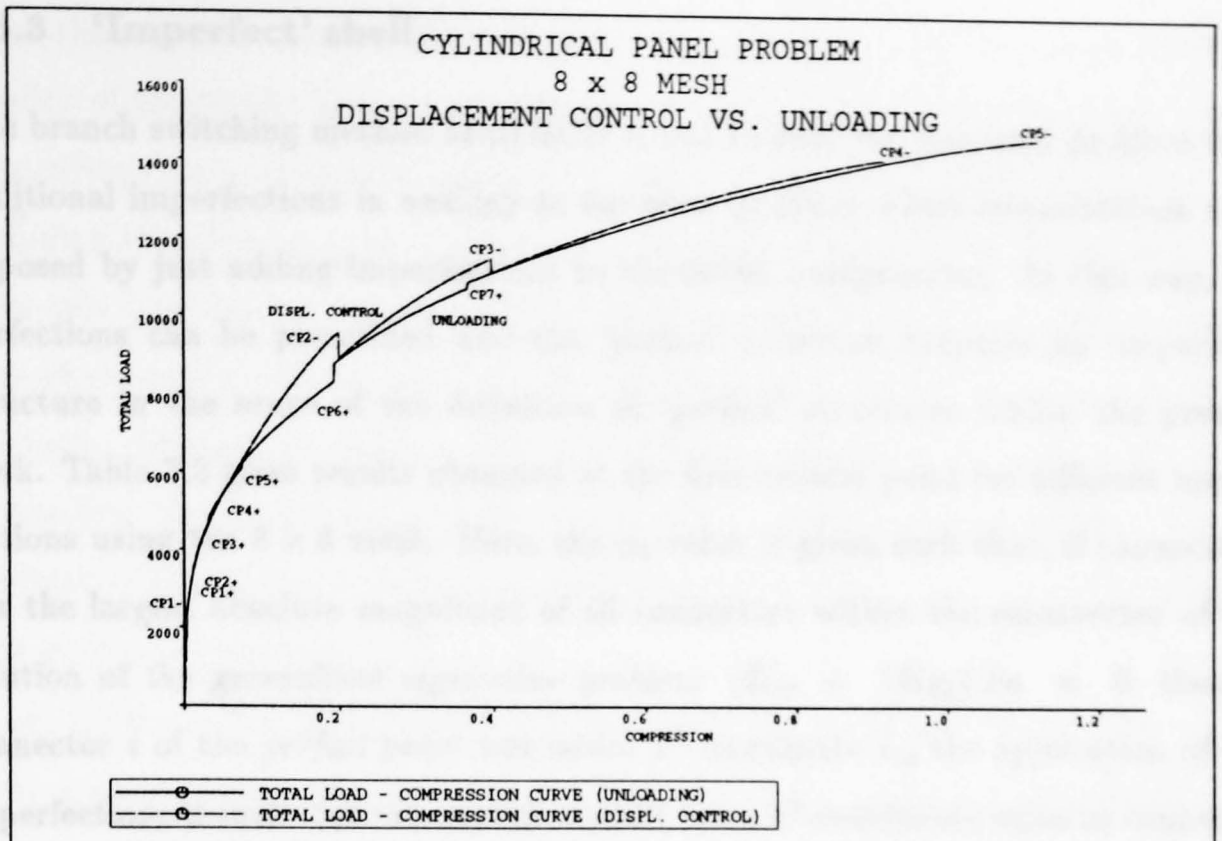

Figure 7.55 : Total load - compression curve for the perfect shell using the 8×8 mesh (displacement control vs. unloading).

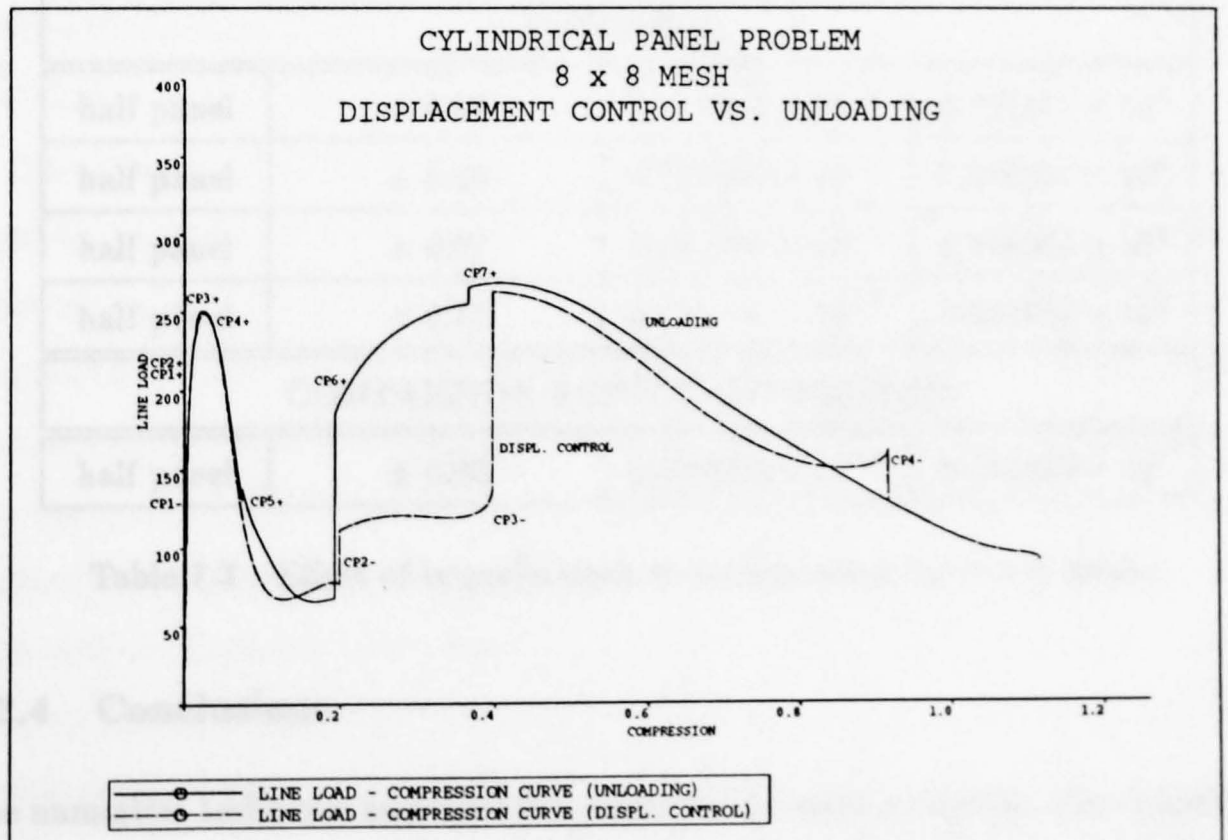

Figure 7.56 : Line load - compression curve for the perfect shell using the 8×8 mesh (displacement control vs. unloading).

7.3.3 'Imperfect' shell

The branch switching method METHOD A can be used for the panel problem with additional imperfections in analogy to the plate problem where imperfections were imposed by just adding imperfections to the initial configuration. In this way, imperfections can be prescribed and the 'perfect' structure becomes an 'imperfect' structure in the sense of the definition of 'perfect' structures within the present work. Table 7.3 gives results obtained at the first critical point for different imperfections using the 8×8 mesh. Here, the α_1-value is given such that, if connector i has the largest absolute magnitude of all connectors within the eigenvector of the solution of the generalized eigenvalue problem $(\mathbf{K_0} + \lambda \mathbf{K_G})\, \delta\mathbf{a} = \mathbf{0}$ then, if connector i of the *perfect* panel has initial x^3-coordinate i_3, the application of the imperfections is such that the *imperfect* panel has a x^3-coordinate value at connector i of $(i_3 + \alpha_1)$.

	IMPERFECTION	COMPRESSION	TOTAL LOAD
PROBLEM	α_1	u^*	P_{tot}^{pre}
8×8 MESH			
half panel	$-\ 0.10$	0.719068×10^{-2}	0.227471×10^{4}
half panel	$\pm\ 0.00$	0.723886×10^{-2}	0.229367×10^{4}
half panel	$+\ 0.01$	0.724398×10^{-2}	0.229560×10^{4}
half panel	$+\ 0.10$	0.729174×10^{-2}	0.231307×10^{4}
COMPARISON RESULTS BY ARGYRIS			
half panel	$\pm\ 0.00$	0.350610×10^{-1}	0.204400×10^{5}

Table 7.3 : Effect of imperfections on results using the 8×8 mesh.

7.3.4 Conclusions

The numerical technique employed has proved to be most powerful. The cylindrical panel is treated until beyond the eighth critical point without encountering any difficulties. It is believed that the investigations could easily be extended beyond the last presented solution point. Evidently, at the last solution point shown on the stable equilibrium path the end displacement is as large as $4.10cm$, *i.e.* about 35

times the panel thickness where $t = 0.11547cm$ and, hence, questions regarding the validity of the results have to be taken into consideration as well. The objective in computing the stable equilibrium path as shown *e.g.* in Figure 7.29 has not been the obtaining of realistic numerical results. A fine mesh would be required for this. The main aim has been to demonstrate the ability of the solution technique combined with the branch switching method to follow the stable equilibrium path throughout the load - deformation history. This has not been feasible in the past and, hence, for the first time to the author's knowledge, it has here been accomplished to follow the load - deformation path beyond bifurcation points for a most complex problem such as the one at hand.

At $CP1-$ a true bifurcation takes place with no snap, *c.f.* Figure 7.23. At all other critical points snaps occur with a decrease in the total load after the critical point, *c.f.* Figure 7.29. The line load, however, does not follow this pattern, *c.f.* Figure 7.30, which suggests rather large differences in the loading at the nodes along the compressive edges.

The first buckling takes place at a very early stage and it is suspected that $CP2-$ in the present calculations corresponds to Argyris's first critical point, *c.f.* Table 7.1 and Table 7.2, *i.e.* Argyris *et al.* are not able to identify $CP1-$ at all.

The differences in the magnitudes between the results of the present work and those by Argyris *et al.* are explained by recalling that the geometrically nonlinear constant moment triangle by Morley [Mor91] used in the MBFEATPS code is an overflexible element, *i.e.* it is expected to give lower load values for buckling, whereas the element employed by Argyris *et al.* is an overstiff element, *i.e.* it is expected to give higher buckling values. Note that Argyris *et al.* treat the problem only up to the fourth critical point and that their method only provides a limited technique as explained in Chapter 6. There seems to be a tendency that refining the mesh reveals buckling values for the panel which are larger in magnitude and, at the same time, getting closer to the comparison values by Argyris.

For the example, both displacement control and load control (loading of a constrained boundary) methods have been employed. Agreement is found in the solutions obtained up to the second critical point for load control $CP2-_{load}$ on noting that for displacement control the second critical point $CP2-$ occurs after a slight

decrease in load and further increase of the end displacement, *c.f.* Figure 7.53. Continuation from $CP2{-}_{load}$ yields three different solution curves, all being different from the curve obtained using displacement control, *c.f.* Figure 7.53 and Figure 7.54. This means that there is no unique solution to the problem. This non-uniqueness phenomenon is regarded as highly unconventional and can be explained by considering that, when load control is used, the total load along the compressive edges is prescribed and, thus, a huge amount of freedom is given to the actual nodal loads to develop, the only condition being that the sum of the nodal loads be equal to the prescribed total load. Questions still arise regarding the fact that the three different load control solutions all exhibit *stable* equilibrium paths, whereas the existence of *unstable* paths is more common.

The unloading procedure commencing from a point beyond $CP4-$ and presented in Figure 7.55 and Figure 7.56 shows, again, a stable equilibrium path emerging which is different to the one obtained using displacement control. It is known that the unloading procedure does not traverse exactly the same path as the ordinary displacement control with increasing step size. Still, a return to the same path is usually expected; this is not the case here, where the displacement control and unloading paths are virtually two different stable solutions.

As an overall conclusion it is hence suggested that no unique solution exists for a complex problem such as the one considered here, *i.e.* a cylindrical panel under biaxial compression. It should be kept in mind that the solution technique presented in the current work is a static one and, therefore, the real-world solution will depend decisively upon the time-dependent way the forces are applied on the structure.

By employing additional initial imperfections it is seen that applying a positive (negative) α_1-value for the imperfections reveals buckling values larger (smaller) in magnitude when compared with the perfect structure case ($\alpha_1 = 0$). This evidently suggests that the computational results can be controlled by employing imperfections. This kind of 'stiffness control' could prove to be a very useful tool for further applications.

Chapter 8

Conclusions and further developments

In this work a reliable and robust way of performing the steps

1. follow stable equilibrium path;
2. locate critical point precisely;
3. identify critical point;
4. continue from critical point;

is presented and proves to be most powerful. The success of the achievements is based on the combination of the following:

1. Allman's solution technique;
2. adaptive step size criteria;
3. rederivation of Koiter's work by Allman;
4. development of the geometrically nonlinear constant moment triangle finite element by Morley;
5. branch switching method.

The technique is applicable to all thin elastic plate and shell problems and hence does not entail any restrictions to specific examples. All kinds of critical points

can be handled, even though the present work only elaborates on bifurcation points (except for one limit point encountered using load control for the cylindrical panel problem). For realistic results, evidently, fine meshes should be used.

A major advantage of the presented work is that no change in technique is required when continuing into the post buckling regime. The continuation is merely based on finding suitable starting vectors for which a branch switching method with only one unknown parameter (α_1) is derived. Being able to perform the calculation of the tangent stiffness matrix exactly is considered of great importance as in this way symmetry and bandedness can be taken into account in the computation. The fact that the tangent stiffness matrix is no approximation provides a unique tool for engineering applications as to the author's knowledge no other finite element possesses this valuable feature.

The easy way of computing the so-called stability coefficients in the given matrix form makes the identification of critical points a straight-forward unproblematic task and, in this way, insight is given to how to continue from the critical point. The continuation is then achieved, even for very complex problems where huge structural changes occur, *i.e.* 'jumps' from the critical point on the stable equilibrium path into the post buckling regime is accomplished.

Future developments continuing the presented work should contain improving the presented universally applicable continuation method METHOD A for getting beyond critical points in the sense that automated procedures for computing the unknown parameter to be employed for successful continuation be developed. As mentioned in Chapter 6, suitable α_1 parameters to be used for the specimen problems were found by a trial-and-error basis while simultaneously monitoring the norm. It is suggested here that this kind of norm-monitoring could be made use of computationally, this implying a fully automated procedure for the continuation from critical (bifurcation) points. The suggested algorithm is as follows:

ALGORITHM FOR FINDING A SUITABLE α_1

1. Choose $(\alpha_1)_1$ as first try for α_1, *e.g.* $(\alpha_1)_1 = 0.1$.

2. Run program and monitor norm $\| \, . \, \|$.

3. When $\| \, . \, \| \geq TOL2$ then stop and store N_1 where N_1 is the number of iterations performed with $\| \, . \, \| < TOL1$. [1]

   In the present work values $TOL1 = 0.105$ and $TOL2 = 1.000$ have been used.

4. Choose $(\alpha_1)_2$ as second try for α_1, *e.g.* $(\alpha_1)_2 = 0.2$.

5. Run program and monitor norm $\| \, . \, \|$.

6. When $\| \, . \, \| \geq TOL2$ then stop and store N_2 where N_2 is the number of iterations performed with $\| \, . \, \| < TOL1$.

7. Let $N_{max} = max(N_1, N_2)$ and let $N_{min} = min(N_1, N_2)$.

   In case $N_1 = N_2$ use convention, *e.g.* if $N_1 = N_2$ then $N_{max} = N_1$ and $N_{min} = N_2$.

8. Calculate new α_1 from

$$\alpha_1 = \frac{(\alpha_1)(N_{min}) + \nu\,(\alpha_1)(N_{max})}{1 + \nu} \qquad (8.0.1)$$

   where ν is a predefined weighting factor with $1 < \nu < 2$, *e.g.* $\nu = \sqrt{3}$. $(\alpha_1)(N_{min})$ is the α_1 value corresponding to N_{min} and $(\alpha_1)(N_{max})$ is the α_1 value corresponding to N_{max}.

9. Run program and monitor norm $\| \, . \, \|$.

10. When $\| \, . \, \| \geq TOL2$ then stop and store N_i where N_i is the number of iterations performed for the i'th α_1-value with $\| \, . \, \| < TOL1$.

11. Let $N_{max} = max(N_i, N_{max})$ and let $N_{min} = min(N_i, N_{max})$.

12. If $(N_{max} - N_{min} < \varepsilon)$ then

    conclude that no suitable α_1-value exists in the chosen initial interval $[(\alpha_1)_1, (\alpha_1)_2]$ and try other choices for initial guesses;

    else

    go to step 8;

    end if.

---

[1] *Two* tolerance values are prescribed as the procedure might require some iterations to 'stabilise' itself and, hence, $\| \, . \, \| > TOL1$ might also occur for a suitable α_1.

An even more sophisticated technique could be set up by not only taking into account the eigenvector corresponding to the zero eigenvalue at the critical point but also other eigenvectors. Evidently, in this case, if k eigenvectors are considered, the modified branch switching method based on METHOD A requires k α_1-parameters to be determined.

Appendix A.1. Comparing notations for A

A proof is given that the second order stability coefficient A given in the present work in the first of equations (5.2.40) by

$$A = (\xi^{(1)})^T (\partial \mathrm{K}_T(\xi^{(1)}))\, \xi^{(1)} \tag{A.1.1}$$

coincides with Allman's [All89b] scalar notation where

$$A_{Allman} = V_{x_i x_j x_k}\, \xi_i^{(1)}\, \xi_j^{(1)}\, \xi_k^{(1)} \ . \tag{A.1.2}$$

Proof:

The proof is straight forward as follows:

$$\begin{aligned}
A_{Allman} &= V_{x_i x_j x_k}\, \xi_i^{(1)}\, \xi_j^{(1)}\, \xi_k^{(1)} \\
&= \sum_{i=1}^{n}\sum_{j=1}^{n}\sum_{k=1}^{n} V_{x_i x_j x_k}\, \xi_i^{(1)}\, \xi_j^{(1)}\, \xi_k^{(1)} \text{ (summation convention)} \\
&= \sum_{i=1}^{n}\sum_{j=1}^{n}\sum_{k=1}^{n} \frac{\partial\{(\mathrm{K}_T)_{ij}\}}{\partial a_k}\, \xi_i^{(1)}\, \xi_j^{(1)}\, \xi_k^{(1)} \text{ (consider } (\mathrm{K}_T)_{ij} = \mathrm{V}_{x_i x_j}) \\
&= \xi_1^{(1)} \sum_{j=1}^{n}\sum_{k=1}^{n} \frac{\partial\{(\mathrm{K}_T)_{1j}\}}{\partial a_k} \xi_j^{(1)} \xi_k^{(1)} + \ldots + \xi_n^{(1)} \sum_{j=1}^{n}\sum_{k=1}^{n} \frac{\partial\{(\mathrm{K}_T)_{nj}\}}{\partial a_k} \xi_j^{(1)} \xi_k^{(1)} \\
&= (\xi^{(1)})^T \begin{pmatrix} \sum_{j=1}^{n}\sum_{k=1}^{n} \frac{\partial\{(\mathrm{K}_T)_{1j}\}}{\partial a_k} \xi_j^{(1)} \xi_k^{(1)} \\ | \\ \sum_{j=1}^{n}\sum_{k=1}^{n} \frac{\partial\{(\mathrm{K}_T)_{nj}\}}{\partial a_k} \xi_j^{(1)} \xi_k^{(1)} \end{pmatrix} \text{ (with } (\xi^{(1)})^T = (\xi_1^{(1)}, \ldots, \xi_n^{(1)})) \\
&= (\xi^{(1)})^T \begin{pmatrix} \sum_{k=1}^{n} \frac{\partial\{(\mathrm{K}_T)_{11}\}}{\partial a_k} \xi_k^{(1)} \xi_1^{(1)} + \ldots + \sum_{k=1}^{n} \frac{\partial\{(\mathrm{K}_T)_{1n}\}}{\partial a_k} \xi_k^{(1)} \xi_n^{(1)} \\ \sum_{k=1}^{n} \frac{\partial\{(\mathrm{K}_T)_{n1}\}}{\partial a_k} \xi_k^{(1)} \xi_1^{(1)} + \ldots + \sum_{k=1}^{n} \frac{\partial\{(\mathrm{K}_T)_{nn}\}}{\partial a_k} \xi_k^{(1)} \xi_n^{(1)} \end{pmatrix} \\
&= (\xi^{(1)})^T \begin{pmatrix} \sum_{k=1}^{n} \frac{\partial\{(\mathrm{K}_T)_{11}\}}{\partial a_k} \xi_k^{(1)} & \cdots & \sum_{k=1}^{n} \frac{\partial\{(\mathrm{K}_T)_{1n}\}}{\partial a_k} \xi_k^{(1)} \\ \sum_{k=1}^{n} \frac{\partial\{(\mathrm{K}_T)_{n1}\}}{\partial a_k} \xi_k^{(1)} & \cdots & \sum_{k=1}^{n} \frac{\partial\{(\mathrm{K}_T)_{nn}\}}{\partial a_k} \xi_k^{(1)} \end{pmatrix} \xi^{(1)} \\
&= (\xi^{(1)})^T \begin{pmatrix} (\frac{\partial\{(\mathrm{K}_T)_{11}\}}{\partial a_1}, \ldots, \frac{\partial\{(\mathrm{K}_T)_{11}\}}{\partial a_n})\xi^{(1)} & - & (\frac{\partial\{(\mathrm{K}_T)_{1n}\}}{\partial a_1}, \ldots, \frac{\partial\{(\mathrm{K}_T)_{1n}\}}{\partial a_n})\xi^{(1)} \\ | & | & | \\ (\frac{\partial\{(\mathrm{K}_T)_{n1}\}}{\partial a_1}, \ldots, \frac{\partial\{(\mathrm{K}_T)_{n1}\}}{\partial a_n})\xi^{(1)} & - & (\frac{\partial\{(\mathrm{K}_T)_{nn}\}}{\partial a_1}, \ldots, \frac{\partial\{(\mathrm{K}_T)_{nn}\}}{\partial a_n})\xi^{(1)} \end{pmatrix} \xi^{(1)} \\
&= (\xi^{(1)})^T (\partial \mathrm{K}_T(\xi^{(1)}))\, \xi^{(1)} \\
&= A \ . \ \square
\end{aligned} \tag{A.1.3}$$

Appendix A.2. Proof of equation (5.2.41)

A proof is given that the second order stability coefficient A in the first of equations (5.2.40) where

$$A = (\boldsymbol{\xi}^{(1)})^T (\partial \mathbf{K}_T (\boldsymbol{\xi}^{(1)}))\, \boldsymbol{\xi}^{(1)} \tag{A.2.1}$$

coincides with the third directional derivative $d^{(ppp)}\Pi$ as introduced by Morley [Mor91] where

$$d^{(ppp)}\Pi = 3 (\hat{\mathbf{a}}^{(p)})^T \mathbf{K}_{3q}\, \hat{\mathbf{a}}^{(p)} , \tag{A.2.2}$$

c.f. the first of equations (5.3.32), and, hence, the validity of the first of equations (5.3.31) is also confirmed.

Proof:

Considering equation (A.2.2) with $\hat{\mathbf{a}}^{(p)} = \boldsymbol{\xi}^{(1)}$, it is evident that

$$d^{(ppp)}\Pi = 3 (\boldsymbol{\xi}^{(1)})^T \mathbf{K}_{3p}\, \boldsymbol{\xi}^{(1)} \tag{A.2.3}$$

where $\mathbf{K}_{3p}$ is also taken in the direction of $\boldsymbol{\xi}^{(1)}$. It is easily verified that

$$d^{(ppp)}\Pi = 3 (\boldsymbol{\xi}^{(1)})^T (\mathbf{K}_{3p})^T \boldsymbol{\xi}^{(1)} \tag{A.2.4}$$

as $(\boldsymbol{\xi}^{(1)})^T \mathbf{K}_{3p}\, \boldsymbol{\xi}^{(1)}$ represents a scalar value. Therefore, $d^{(ppp)}\Pi$ can be written as

$$\begin{aligned} d^{(ppp)}\Pi &= \frac{1}{2} \left(3 (\boldsymbol{\xi}^{(1)})^T \mathbf{K}_{3p}\, \boldsymbol{\xi}^{(1)} + 3 (\boldsymbol{\xi}^{(1)})^T (\mathbf{K}_{3p})^T \boldsymbol{\xi}^{(1)} \right) \\ &= \frac{3}{2} (\boldsymbol{\xi}^{(1)})^T \left(\mathbf{K}_{3p} + (\mathbf{K}_{3p})^T \right) \boldsymbol{\xi}^{(1)} . \end{aligned} \tag{A.2.5}$$

Recalling $\mathbf{K}_{3p}$ given in equation (5.3.28) as

$$\mathbf{K}_{3p} = A \begin{bmatrix} 0 & 0 & 0 \\ (\hat{\mathbf{B}}_w^{(p)})^T \mathbf{D}\mathbf{B} & (\hat{\mathbf{B}}_w^{(p)})^T \mathbf{D}\mathbf{B}_w & (\hat{\mathbf{B}}_w^{(p)})^T \mathbf{D}\mathbf{B}_\kappa \\ (\hat{\mathbf{B}}_\kappa^{(p)})^T \mathbf{D}\mathbf{B} & (\hat{\mathbf{B}}_\kappa^{(p)})^T \mathbf{D}\mathbf{B}_w & (\hat{\mathbf{B}}_\kappa^{(p)})^T \mathbf{D}\mathbf{B}_\kappa \end{bmatrix} , \tag{A.2.6}$$

i.e.

$$(\mathbf{K}_{3p})^T = A \begin{bmatrix} 0 & \mathbf{B}^T \mathbf{D}\mathbf{B}_w^{(p)} & \mathbf{B}^T \mathbf{D}\mathbf{B}_\kappa^{(p)} \\ 0 & \mathbf{B}_w^T \mathbf{D}\mathbf{B}_w^{(p)} & \mathbf{B}_w^T \mathbf{D}\mathbf{B}_\kappa^{(p)} \\ 0 & \mathbf{B}_\kappa^T \mathbf{D}\mathbf{B}_w^{(p)} & \mathbf{B}_\kappa^T \mathbf{D}\mathbf{B}_\kappa^{(p)} \end{bmatrix} , \tag{A.2.7}$$

thus

$$\mathbf{K}_{3p} + (\mathbf{K}_{3p})^T \tag{A.2.8}$$
$$= A \begin{bmatrix} 0 & \mathbf{B}^T\mathbf{D}\mathbf{B}_w^{(p)} & \mathbf{B}^T\mathbf{D}\mathbf{B}_\kappa^{(p)} \\ (\mathbf{B}_w^{(p)})^T\mathbf{D}\mathbf{B} & (\mathbf{B}_w^{(p)})^T\mathbf{D}\mathbf{B}_w + \mathbf{B}_w^T\mathbf{D}\mathbf{B}_w^{(p)} & (\mathbf{B}_w^{(p)})^T\mathbf{D}\mathbf{B}_\kappa + \mathbf{B}_w^T\mathbf{D}\mathbf{B}_\kappa^{(p)} \\ (\mathbf{B}_\kappa^{(p)})^T & (\mathbf{B}_\kappa^{(p)})^T\mathbf{D}\mathbf{B}_w + \mathbf{B}_\kappa^T\mathbf{D}\mathbf{B}_w^{(p)} & (\mathbf{B}_\kappa^{(p)})^T\mathbf{D}\mathbf{B}_\kappa + (\mathbf{B}_\kappa)^T\mathbf{D}\mathbf{B}_\kappa^{(p)} \end{bmatrix},$$

i.e.

$$\frac{3}{2}(\mathbf{K}_{3p} + (\mathbf{K}_{3p})^T) \tag{A.2.9}$$
$$= \frac{3}{2}A \begin{bmatrix} 0 & \mathbf{B}^T\mathbf{D}\mathbf{B}_w^{(p)} & \mathbf{B}^T\mathbf{D}\mathbf{B}_\kappa^{(p)} \\ (\mathbf{B}_w^{(p)})^T\mathbf{D}\mathbf{B} & (\mathbf{B}_w^{(p)})^T\mathbf{D}\mathbf{B}_w + \mathbf{B}_w^T\mathbf{D}\mathbf{B}_w^{(p)} & (\mathbf{B}_w^{(p)})^T\mathbf{D}\mathbf{B}_\kappa + \mathbf{B}_w^T\mathbf{D}\mathbf{B}_\kappa^{(p)} \\ (\mathbf{B}_\kappa^{(p)})^T & (\mathbf{B}_\kappa^{(p)})^T\mathbf{D}\mathbf{B}_w + \mathbf{B}_\kappa^T\mathbf{D}\mathbf{B}_w^{(p)} & (\mathbf{B}_\kappa^{(p)})^T\mathbf{D}\mathbf{B}_\kappa + (\mathbf{B}_\kappa)^T\mathbf{D}\mathbf{B}_\kappa^{(p)} \end{bmatrix}.$$

Recalling equation (5.2.67)

$$(\partial\mathbf{K}_T(\boldsymbol{\xi}^{(1)})) = \frac{3}{2}A \begin{bmatrix} 0 & \mathbf{B}^T\mathbf{D}\hat{\mathbf{B}}_w & \hat{\mathbf{B}}^T\mathbf{D}\hat{\mathbf{B}}_\kappa \\ & \hat{\mathbf{B}}_w^T\mathbf{D}\mathbf{B}_w + \hat{\mathbf{B}}_w^T\mathbf{D}\hat{\mathbf{B}}_w & \hat{\mathbf{B}}_w^T\mathbf{D}\mathbf{B}_\kappa + \hat{\mathbf{B}}_w^T\mathbf{D}\hat{\mathbf{B}}_\kappa \\ \text{sym} & & \hat{\mathbf{B}}_\kappa^T\mathbf{D}\mathbf{B}_\kappa + \hat{\mathbf{B}}_\kappa^T\mathbf{D}\hat{\mathbf{B}}_\kappa \end{bmatrix}, \tag{A.2.10}$$

where the 'hatted' matrices are taken in the direction of $\boldsymbol{\xi}^{(1)}$, it is evident that

$$(\partial\mathbf{K}_T(\boldsymbol{\xi}^{(1)})) = \frac{3}{2}(\mathbf{K}_{3p} + (\mathbf{K}_{3p})^T) \tag{A.2.11}$$

and, hence,

$$\begin{aligned} d^{(ppp)}\Pi &= \frac{3}{2}(\boldsymbol{\xi}^{(1)})^T(\mathbf{K}_{3p} + (\mathbf{K}_{3p})^T)\boldsymbol{\xi}^{(1)} \\ &= (\boldsymbol{\xi}^{(1)})^T(\partial\mathbf{K}_T(\boldsymbol{\xi}^{(1)}))\boldsymbol{\xi}^{(1)} \\ &= A \ . \ \square \end{aligned} \tag{A.2.12}$$

Appendix A.3. Proof of equation (5.2.57)

A proof is given of equation (5.2.57) where

$$c^{(r)} = -\frac{1}{\theta^{(r)}}(\xi^{(r)})^T(\partial \mathbf{K}_T(\xi^{(1)}))\,\xi^{(1)}\epsilon^2 \ . \tag{A.3.1}$$

Proof:

Start by substituting equations (5.2.56) and (5.2.48) into equation (5.2.35) (with $d\lambda = 0, (d^2\lambda) = 0$) giving

$$\begin{aligned} &\mathbf{K}_T[\,\xi^{(1)}(d^2s) + \sum_{r=2}^{n} c^{(r)}\xi^{(r)}\,] \\ &\qquad + (\partial \mathbf{K}_T(\xi^{(1)}ds))(\,\xi^{(1)}ds\,) = 0 \\ \Longleftrightarrow\ &\mathbf{K}_T\,\xi^{(1)}(d^2s) + \sum_{r=2}^{n} c^{(r)}\mathbf{K}_T\,\xi^{(r)} \\ &\qquad + (\partial \mathbf{K}_T(\xi^{(1)}))(\,\xi^{(1)})(ds)^2 = 0 \ . \end{aligned} \tag{A.3.2}$$

Making use of equations (5.2.12) and (5.2.49) gives

$$\begin{aligned} &\sum_{r=2}^{n} c^{(r)}\theta^{(r)}\,\mathbf{T}\,\xi^{(r)} \\ &\qquad + (\partial \mathbf{K}_T(\xi^{(1)}))\,\xi^{(1)}\epsilon^2 = 0 \\ \Longleftrightarrow\ &\sum_{r=2}^{n} c^{(r)}\theta^{(r)}\,\mathbf{T}\,\xi^{(r)} \\ &\qquad = -(\partial \mathbf{K}_T(\xi^{(1)}))\,\xi^{(1)}\epsilon^2 \ . \end{aligned} \tag{A.3.3}$$

Remembering that

$$\begin{aligned} (\xi^{(r)})^T\,\mathbf{T}\,\xi^{(r)} &= 1 \ , \\ (\xi^{(r)})^T\,\mathbf{T}\,\xi^{(s)} &= 0 \quad \text{for } r \neq s \quad , \end{aligned} \tag{A.3.4}$$

and premultiplying both sides of the second of equations (A.3.3) by $(\xi^{(s)})^T$ gives

$$\begin{aligned} &(\xi^{(s)})^T \sum_{r=2}^{n} c^{(r)}\theta^{(r)}\,\mathbf{T}\,\xi^{(r)} \\ &\qquad = -(\xi^{(s)})^T(\partial \mathbf{K}_T(\xi^{(1)}))\,\xi^{(1)}\epsilon^2 \\ \Longrightarrow\ &c^{(s)}\theta^{(s)}(\xi^{(s)})^T\,\mathbf{T}\,\xi^{(s)} \\ &\qquad = -(\xi^{(s)})^T(\partial \mathbf{K}_T(\xi^{(1)}))\,\xi^{(1)}\epsilon^2 \\ \Longrightarrow\ &c^{(s)} = -\frac{1}{\theta^{(s)}}(\xi^{(s)})^T(\partial \mathbf{K}_T(\xi^{(1)}))\,\xi^{(1)}\epsilon^2 \ . \ \square \end{aligned} \tag{A.3.5}$$

Appendix A.4. Proof of equation (5.2.62)

A proof is given that the second order stability coefficient D in equation (5.2.62) takes the form

$$\begin{aligned} D &= (\xi^{(1)})^T (\partial(\partial \mathbf{K}_T(\xi^{(1)}))(\xi^{(1)}))\,\xi^{(1)} \\ &\quad + 3\,(\xi^{(1)})^T (\partial \mathbf{K}_T(\xi^{(1)}))^T \mathbf{E} \Theta \mathbf{E}^T (\partial \mathbf{K}_T(\xi^{(1)}))\,\xi^{(1)} \,. \end{aligned} \tag{A.4.1}$$

Proof:

Substitute equation (5.2.56) into equation (5.2.53); this gives

$$\begin{aligned} d^4\Pi &= 3\,(\,\xi^{(1)}(d^2 s) + \mathbf{E}\Theta\mathbf{E}^T(\partial \mathbf{K}_T(\xi^{(1)}))\,\xi^{(1)}\epsilon^2\,)^T \mathbf{K}_T \cdot \\ &\quad \cdot(\,\xi^{(1)}(d^2 s) + \mathbf{E}\Theta\mathbf{E}^T(\partial \mathbf{K}_T(\xi^{(1)}))\,\xi^{(1)}\epsilon^2\,) \\ &\quad + 6\,(\,\xi^{(1)}(d^2 s) + \mathbf{E}\Theta\mathbf{E}^T(\partial \mathbf{K}_T(\xi^{(1)}))\,\xi^{(1)}\epsilon^2\,)^T (\partial \mathbf{K}_T(\xi^{(1)}))\,\xi^{(1)}\epsilon^2 \\ &\quad + (\xi^{(1)})^T (\partial(\partial \mathbf{K}_T(\xi^{(1)}))(\xi^{(1)}))\,\xi^{(1)}\epsilon^4 \quad . \\ &= 3\,(\,\mathbf{E}\Theta\mathbf{E}^T(\partial \mathbf{K}_T(\xi^{(1)}))\,\xi^{(1)}\,)^T \mathbf{K}_T\,(\mathbf{E}\Theta\mathbf{E}^T(\partial \mathbf{K}_T(\xi^{(1)}))\,\xi^{(1)}\,)\,\epsilon^4 \\ &\quad + 6\,(\mathbf{E}\Theta\mathbf{E}^T(\partial \mathbf{K}_T(\xi^{(1)}))\,\xi^{(1)})^T (\partial \mathbf{K}_T(\xi^{(1)}))\,\xi^{(1)}(d^2 s)\,\epsilon^2 \\ &\quad + 6\,(\mathbf{E}\Theta\mathbf{E}^T(\partial \mathbf{K}_T(\xi^{(1)}))\,\xi^{(1)})^T (\partial \mathbf{K}_T(\xi^{(1)}))\,\xi^{(1)}\epsilon^4 \\ &\quad + (\xi^{(1)})^T (\partial(\partial \mathbf{K}_T(\xi^{(1)}))(\xi^{(1)}))\,\xi^{(1)}\epsilon^4 \\ &\qquad (\text{since } \mathbf{K}_T\,\xi^{(1)} = 0\,) \\ &= 3\,(\,\mathbf{E}\Theta\mathbf{E}^T(\partial \mathbf{K}_T(\xi^{(1)}))\,\xi^{(1)}\,)^T \mathbf{K}_T\,(\mathbf{E}\Theta\mathbf{E}^T(\partial \mathbf{K}_T(\xi^{(1)}))\,\xi^{(1)}\,)\,\epsilon^4 \\ &\quad + 6\,(\mathbf{E}\Theta\mathbf{E}^T(\partial \mathbf{K}_T(\xi^{(1)}))\,\xi^{(1)})^T (\partial \mathbf{K}_T(\xi^{(1)}))\,\xi^{(1)}\epsilon^4 \\ &\quad + (\xi^{(1)})^T (\partial(\partial \mathbf{K}_T(\xi^{(1)}))(\xi^{(1)}\xi^{(1)}))\,\xi^{(1)}\epsilon^4 \\ &\qquad (\text{since } A = (\xi^{(1)})^T (\partial \mathbf{K}_T(\xi^{(1)}))\,\xi^{(1)} = 0\,) \\ &= 3\,(\,\mathbf{E}\Theta\mathbf{E}^T(\partial \mathbf{K}_T(\xi^{(1)}))\,\xi^{(1)}\,)^T (-\Theta^{-1}\,\mathbf{T}\,\mathbf{E})\,\Theta\,\mathbf{E}^T(\partial \mathbf{K}_T(\xi^{(1)}))\,\xi^{(1)}\epsilon^4 \\ &\quad + 6\,(\mathbf{E}\Theta\mathbf{E}^T(\partial \mathbf{K}_T(\xi^{(1)}))\,\xi^{(1)})^T (\partial \mathbf{K}_T(\xi^{(1)}))\,\xi^{(1)}\epsilon^4 \\ &\quad + (\xi^{(1)})^T (\partial(\partial \mathbf{K}_T(\xi^{(1)}))(\xi^{(1)}))\,\xi^{(1)}\epsilon^4 \end{aligned} \tag{A.4.2}$$

by making use of $\mathbf{K}_T\mathbf{E} = -\Theta^{-1}\mathbf{T}\mathbf{E}$, *c.f.* equation (5.2.12) and the definitions of $\mathbf{E}$ and Θ in equations (5.2.28) and (5.2.31). It is to be noted here that the inverse Θ^{-1} of the matrix Θ does not exist as such, since the first row and the first column of Θ only contain zero entries. However, by considering the reduced matrix Θ_R

constructed by omitting the first row and the first column of Θ, the inverse Θ_R^{-1} exists. The matrix Θ^{-1} used in this proof is the matrix which is obtained by adding a zero first row and a zero first column to Θ_R^{-1}. Continuing the proof from here, it then follows that

$$\begin{aligned}
d^4\Pi &= -3\left((\partial \mathbf{K}_T(\xi^{(1)}))\,\xi^{(1)}\right)^T \mathbf{E}\,\Theta\,\mathbf{E}^T\,\Theta^{-1}\,\mathbf{T}\,\mathbf{E}\,\Theta\,\mathbf{E}^T\,(\partial \mathbf{K}_T(\xi^{(1)}))\,\xi^{(1)}\,\epsilon^4 \\
&\quad + 6\,(\mathbf{E}\,\Theta\,\mathbf{E}^T\,(\partial \mathbf{K}_T(\xi^{(1)}))\,\xi^{(1)})^T\,(\partial \mathbf{K}_T(\xi^{(1)}))\,\xi^{(1)}\,\epsilon^4 \\
&\quad + (\xi^{(1)})^T\,(\partial(\partial \mathbf{K}_T(\xi^{(1)}))(\xi^{(1)}))\,\xi^{(1)}\,\epsilon^4 \\
&= -3\left((\partial \mathbf{K}_T(\xi^{(1)}))\,\xi^{(1)}\right)^T \mathbf{E}\,(\Theta\,\Theta^{-1})\,(\mathbf{E}^T\,\mathbf{T}\,\mathbf{E})\,\Theta\,\mathbf{E}^T\,(\partial \mathbf{K}_T(\xi^{(1)}))\,\xi^{(1)}\,\epsilon^4 \\
&\quad + 6\,(\mathbf{E}\,\Theta\,\mathbf{E}^T\,(\partial \mathbf{K}_T(\xi^{(1)}))\,\xi^{(1)})^T\,(\partial \mathbf{K}_T(\xi^{(1)}))\,\xi^{(1)}\,\epsilon^4 \\
&\quad + (\xi^{(1)})^T\,(\partial(\partial \mathbf{K}_T(\xi^{(1)}))(\xi^{(1)}))\,\xi^{(1)}\,\epsilon^4 \\
&\qquad \text{(since } \Theta \text{ is a diagonal matrix} \Rightarrow \Theta^{-1}\,\mathbf{E} = \mathbf{E}\,\Theta^{-1}) \\
&= -3\left((\partial \mathbf{K}_T(\xi^{(1)}))\,\xi^{(1)}\right)^T \mathbf{E}\,\Theta\,\mathbf{E}^T\,(\partial \mathbf{K}_T(\xi^{(1)}))\,\xi^{(1)}\,\epsilon^4 \\
&\quad + 6\,(\mathbf{E}\,\Theta\,\mathbf{E}^T\,(\partial \mathbf{K}_T(\xi^{(1)}))\,\xi^{(1)})^T\,(\partial \mathbf{K}_T(\xi^{(1)}))\,\xi^{(1)}\,\epsilon^4 \\
&\quad + (\xi^{(1)})^T\,(\partial(\partial \mathbf{K}_T(\xi^{(1)}))(\xi^{(1)}))\,\xi^{(1)}\,\epsilon^4\ . \qquad \text{(A.4.3)}
\end{aligned}$$

Here, use is made of the identities $\Theta\,\Theta^{-1} = \mathbf{I}_R$ and $\mathbf{E}^T\,\mathbf{T}\,\mathbf{E} = \mathbf{I}_R$ where $\mathbf{I}_R$ is the identity matrix with the exception that the first row first column entry is zero. It is easily verified, however, that $(\Theta\,\Theta^{-1})\,(\mathbf{E}^T\,\mathbf{T}\,\mathbf{E})\,\Theta = \Theta$ and therefore the last line of the proof follows. Continuing from here, it now follows that

$$\begin{aligned}
d^4\Pi &= -3\,(\mathbf{E}\,\Theta\,\mathbf{E}^T\,(\partial \mathbf{K}_T(\xi^{(1)}))\,\xi^{(1)})^T\,(\partial \mathbf{K}_T(\xi^{(1)}))\,\xi^{(1)}\,\epsilon^4 \\
&\quad + 6\,(\mathbf{E}\,\Theta\,\mathbf{E}^T\,(\partial \mathbf{K}_T(\xi^{(1)}))\,\xi^{(1)})^T\,(\partial \mathbf{K}_T(\xi^{(1)}))\,\xi^{(1)}\,\epsilon^4 \\
&\quad + (\xi^{(1)})^T\,(\partial(\partial \mathbf{K}_T(\xi^{(1)}))(\xi^{(1)}))\,\xi^{(1)}\,\epsilon^4 \\
&= 3\,(\mathbf{E}\,\Theta\,\mathbf{E}^T\,(\partial \mathbf{K}_T(\xi^{(1)}))\,\xi^{(1)})^T\,(\partial \mathbf{K}_T(\xi^{(1)}))\,\xi^{(1)}\,\epsilon^4 \\
&\quad + (\xi^{(1)})^T\,(\partial(\partial \mathbf{K}_T(\xi^{(1)}))(\xi^{(1)}))\,\xi^{(1)}\,\epsilon^4 \\
&= 3\,((\partial \mathbf{K}_T(\xi^{(1)}))\,\xi^{(1)})^T\,\mathbf{E}\,\Theta\,\mathbf{E}^T\,(\partial \mathbf{K}_T(\xi^{(1)}))\,\xi^{(1)}\,\epsilon^4 \\
&\quad + (\xi^{(1)})^T\,(\partial(\partial \mathbf{K}_T(\xi^{(1)}))(\xi^{(1)}))\,\xi^{(1)}\,\epsilon^4 \\
&\qquad \text{(since } \Theta = \Theta^T) \\
&= D\,\epsilon^4\ .\ \square \qquad \text{(A.4.4)}
\end{aligned}$$

Appendix A.5 : Comparing notations for D

A proof is given that the stability coefficient D given in the present work in equation (5.2.62) by

$$\begin{aligned} D \;=\; & (\xi^{(1)})^T\,(\partial(\partial \mathbf{K}_T(\xi^{(1)}))(\xi^{(1)}))\,\xi^{(1)} \\ & + 3\,(\xi^{(1)})^T\,(\partial \mathbf{K}_T(\xi^{(1)}))^T\,\mathbf{E}\,\Theta\,\mathbf{E}^T\,(\partial \mathbf{K}_T(\xi^{(1)}))\,\xi^{(1)} \end{aligned} \qquad \text{(A.5.1)}$$

coincides with Allman's [All89b] notation where

$$D_{Allman} \;=\; V_{x_i x_j x_k x_l}\,\xi_i^{(1)}\,\xi_j^{(1)}\,\xi_k^{(1)}\,\xi_l^{(1)} \;-\; \sum_{r=2}^{n} \frac{3}{\theta^{(r)}}\,(\,V_{x_i x_j x_k}\,\xi_i^{(1)}\,\xi_j^{(1)}\,\xi_k^{(r)}\,)^2\;. \qquad \text{(A.5.2)}$$

Proof:

First it is noted that the first terms of the equations (A.5.1) and (A.5.2) can be shown to coincide following a similar proof to the one given in Appendix A.1. Therefore, this need not be done here. A proof that the second terms are the same is straight forward as follows:

$$\begin{aligned} & -\sum_{r=2}^{n} \frac{3}{\theta^{(r)}}\,(\,V_{x_i x_j x_k}\,\xi_i^{(1)}\,\xi_j^{(1)}\,\xi_k^{(r)}\,)^2 \\ & \quad = \;-\sum_{r=2}^{n} \frac{3}{\theta^{(r)}}\,(\,V_{x_i x_j x_k}\,\xi_i^{(1)}\,\xi_j^{(1)}\,\xi_k^{(r)}\,)\,(\,V_{x_i x_j x_k}\,\xi_i^{(1)}\,\xi_j^{(1)}\,\xi_k^{(r)}\,) \\ & \quad = \;-\sum_{r=2}^{n} \frac{3}{\theta^{(r)}}\,(\xi^{(r)})^T\,(\partial \mathbf{K}_T\,(\xi^{(1)}))\,\xi^{(1)}\,(\xi^{(r)})^T\,(\partial \mathbf{K}_T(\xi^{(1)}))\,\xi^{(1)} \\ & \qquad \text{(using the result of Appendix A.1)} \\ & \quad = \;-\sum_{r=2}^{n} \frac{3}{\theta^{(r)}}\,(\xi^{(1)})^T\,(\partial \mathbf{K}_T\,(\xi^{(1)}))^T\,\xi^{(r)}\,(\xi^{(r)})^T\,(\partial \mathbf{K}_T(\xi^{(1)}))\,\xi^{(1)} \\ & \qquad \text{(since } (\xi^{(1)})^T\,(\partial \mathbf{K}_T(\xi^{(1)}))^T\,\xi^{(r)} \;=\; (\xi^{(r)})^T\;(\partial \mathbf{K}_T(\xi^{(1)}))\,\xi^{(1)}\;; \\ & \qquad \text{scalar quantities)} \\ & \quad = \;3\,(\xi^{(1)})^T\,(\partial \mathbf{K}_T(\xi^{(1)}))^T\,(\sum_{r=2}^{n} \frac{-1}{\theta^{(r)}}\,\xi^{(r)}\,(\xi^{(r)})^T\,)\,(\partial \mathbf{K}_T(\xi^{(1)}))\,\xi^{(1)} \\ & \quad = \;3\,(\xi^{(1)})^T\,(\partial \mathbf{K}_T(\xi^{(1)}))^T\,\Theta\,\mathbf{E}\,\mathbf{E}^T\,(\partial \mathbf{K}_T(\xi^{(1)}))\,\xi^{(1)} \\ & \qquad \text{(with } \Theta \text{ and } \mathbf{E} \text{ as in equations (5.2.31) and (5.2.28), respectively)} \\ & \quad = \;3\,(\xi^{(1)})^T\,(\partial \mathbf{K}_T(\xi^{(1)}))^T\,\mathbf{E}\,\Theta\,\mathbf{E}^T\,(\partial \mathbf{K}_T(\xi^{(1)}))\,\xi^{(1)} \\ & \qquad \text{(since } \Theta \text{ is a diagonal matrix} \Rightarrow \Theta\mathbf{E} = \mathbf{E}\Theta)\;. \;\square \end{aligned} \qquad \text{(A.5.3)}$$

Appendix A.6. Proof of equation (5.2.63)

A proof is given that the first term of the stability coefficient D of equation (5.2.62), D_1, where

$$D_1 = (\boldsymbol{\xi}^{(1)})^T (\partial(\partial \mathbf{K_T}(\boldsymbol{\xi}^{(1)}))(\boldsymbol{\xi}^{(1)}))\, \boldsymbol{\xi}^{(1)} \tag{A.6.1}$$

coincides with the fourth directional derivatives $d^{(pppp)}\Pi$ as introduced by Morley [Mor91] where

$$d^{(pppp)}\Pi = 3(\hat{\mathbf{a}}^{(p)})^T \hat{\mathbf{K}}_{3p}^{(p)} \hat{\mathbf{a}}^{(p)} , \tag{A.6.2}$$

c.f. the last of equation (5.3.32), and, hence, the validity of the first part of the last of equations (5.3.31) is also confirmed.

Proof:

Considering equation (A.6.2) with $\hat{\mathbf{a}}^{(p)} = \boldsymbol{\xi}^{(1)}$, it is evident that

$$d^{(pppp)}\Pi = 3(\boldsymbol{\xi}^{(1)})^T \hat{\mathbf{K}}_{3p}^{(p)} \boldsymbol{\xi}^{(1)} , \tag{A.6.3}$$

where $\hat{\mathbf{K}}_{3p}^{(p)}$ is also taken (twice) in the direction of $\boldsymbol{\xi}^{(1)}$. Then,

$$\hat{\mathbf{K}}_{3p}^{(p)} = A \begin{bmatrix} 0 & 0 & 0 \\ 0 & \hat{\mathbf{B}}_w^{(q)\mathrm{T}} \mathbf{D} \hat{\mathbf{B}}_w^{(s)} & \hat{\mathbf{B}}_w^{(q)\mathrm{T}} \mathbf{D} \hat{\mathbf{B}}_\kappa^{(s)} \\ 0 & \hat{\mathbf{B}}_\kappa^{(q)\mathrm{T}} \mathbf{D} \hat{\mathbf{B}}_w^{(s)} & \hat{\mathbf{B}}_\kappa^{(q)\mathrm{T}} \mathbf{D} \hat{\mathbf{B}}_\kappa^{(s)} \end{bmatrix} = A \begin{bmatrix} 0 & 0 & 0 \\ 0 & \hat{\mathbf{B}}_w^T \mathbf{D} \hat{\mathbf{B}}_w & \hat{\mathbf{B}}_w^T \mathbf{D} \hat{\mathbf{B}}_\kappa \\ 0 & \hat{\mathbf{B}}_\kappa \mathbf{D} \hat{\mathbf{B}}_w^T & \hat{\mathbf{B}}_\kappa^T \mathbf{D} \hat{\mathbf{B}}_\kappa \end{bmatrix} , \tag{A.6.4}$$

i.e. the matrix is identical to the one appearing in equation (5.2.69) for the calculation of $(\partial(\partial \mathbf{K}_T(\boldsymbol{\xi}^{(1)}))(\boldsymbol{\xi}^{(1)}))$. Therefore,

$$\begin{aligned} d^{(pppp)}\Pi &= 3(\boldsymbol{\xi}^{(1)})^T \hat{\mathbf{K}}_{3p}^{(p)} \boldsymbol{\xi}^{(1)} \\ &= 3A(\boldsymbol{\xi}^{(1)})^T \begin{bmatrix} 0 & 0 & 0 \\ 0 & \hat{\mathbf{B}}_w^{(q)\mathrm{T}} \mathbf{D} \hat{\mathbf{B}}_w^{(s)} & \hat{\mathbf{B}}_w^{(q)\mathrm{T}} \mathbf{D} \hat{\mathbf{B}}_\kappa^{(s)} \\ 0 & \hat{\mathbf{B}}_\kappa^{(q)\mathrm{T}} \mathbf{D} \hat{\mathbf{B}}_w^{(s)} & \hat{\mathbf{B}}_\kappa^{(q)\mathrm{T}} \mathbf{D} \hat{\mathbf{B}}_\kappa^{(s)} \end{bmatrix} \boldsymbol{\xi}^{(1)} \\ &= 3A(\boldsymbol{\xi}^{(1)})^T \begin{bmatrix} 0 & 0 & 0 \\ 0 & \hat{\mathbf{B}}_w^T \mathbf{D} \hat{\mathbf{B}}_w & \hat{\mathbf{B}}_w^T \mathbf{D} \hat{\mathbf{B}}_\kappa \\ 0 & \hat{\mathbf{B}}_\kappa \mathbf{D} \hat{\mathbf{B}}_w^T & \hat{\mathbf{B}}_\kappa^T \mathbf{D} \hat{\mathbf{B}}_\kappa \end{bmatrix} \boldsymbol{\xi}^{(1)} \\ &= (\boldsymbol{\xi}^{(1)})^T \left(3A \begin{bmatrix} 0 & 0 & 0 \\ 0 & \hat{\mathbf{B}}_w^T \mathbf{D} \hat{\mathbf{B}}_w & \hat{\mathbf{B}}_w^T \mathbf{D} \hat{\mathbf{B}}_\kappa \\ 0 & \hat{\mathbf{B}}_\kappa \mathbf{D} \hat{\mathbf{B}}_w^T & \hat{\mathbf{B}}_\kappa^T \mathbf{D} \hat{\mathbf{B}}_\kappa \end{bmatrix} \right) \boldsymbol{\xi}^{(1)} \end{aligned}$$

$$= (\xi^{(1)})^T (\partial(\partial \mathbf{K}_T(\xi^{(1)}))(\xi^{(1)}))\, \xi^{(1)}$$

$$= D_1 \ . \ \square \qquad \text{(A.6.5)}$$

Appendix A.7 : Rôle of geometric stiffness matrices in the derivation of directional derivatives

The purpose here is to consider the rôle of the geometric stiffness matrices $\mathbf{B}_{G\mathbf{w}}$ and $\mathbf{B}_{G\kappa}$, see equations (4.5.45), in the derivation of the directional derivatives of the strain energy Π.

When deriving the tangent stiffness matrix $\mathbf{K}_T$ in preparation for computational structural analysis it is the practice to establish the following relationships

$$\mathbf{B}_w^T \mathbf{D}\gamma = \mathbf{B}_w^T \mathbf{N} = \mathbf{B}_{G\mathbf{w}}\mathbf{w} \quad \text{and} \quad \mathbf{B}_\kappa^T \mathbf{D}\gamma = \mathbf{B}_\kappa^T \mathbf{N} = \mathbf{B}_{G\kappa}\boldsymbol{\kappa} \tag{A.7.1}$$

in order to achieve symmetry of the matrix $\mathbf{K}_T$, see equations (4.5.48) and (4.5.49) and then equations (4.5.38), (4.5.45), (4.5.46) and (4.5.47). In equation (A.7.1) the matrices $\mathbf{B}_w$ and $\mathbf{B}_\kappa$ are defined in equations (4.5.26) as

$$\mathbf{B}_w = \frac{1}{2}\begin{bmatrix} 2(w_1 - w_3) & & -2(w_1 - w_3) \\ & 2(w_2 - w_3) & -2(w_2 - w_3) \\ w_2 - w_3 & w_1 - w_3 & -w_1 - w_2 + 2w_3 \end{bmatrix} \tag{A.7.2}$$

and

$$\mathbf{B}_\kappa = \frac{1}{12}\begin{bmatrix} \kappa_{11} + \kappa_{22} & \kappa_{11} & -2\kappa_{12} \\ \kappa_{22} & \kappa_{11} + \kappa_{22} & -2\kappa_{12} \\ \kappa_{12} & \kappa_{12} & \kappa_{11} + \kappa_{22} - 2\kappa_{12} \end{bmatrix} \tag{A.7.3}$$

while the geometric stiffness matrices $\mathbf{B}_{G\mathbf{w}}$ and $\mathbf{B}_{G\kappa}$ are defined in equation (4.5.46) as

$$\mathbf{B}_{G\mathbf{w}} = \begin{bmatrix} N^{11} & N^{12} & -(N^{11} + N^{12}) \\ & N^{22} & -(N^{22} + N^{12} \\ \text{sym} & & N^{11} + N^{22} + 2N^{12} \end{bmatrix} \tag{A.7.4}$$

and

$$\mathbf{B}_{G\kappa} = \frac{1}{12}\begin{bmatrix} N^{11} & N^{11} + N^{22} & 2N^{12} \\ & N^{22} & 2N^{12} \\ \text{sym} & & -2(N^{11} + N^{22} + 3N^{12} \end{bmatrix}. \tag{A.7.5}$$

The following relationships then exist

$$\begin{aligned} &\mathbf{B}_w \delta\mathbf{w} = \delta\mathbf{B}_w \mathbf{w} \quad \text{and} \quad \mathbf{B}_\kappa \delta\boldsymbol{\kappa} = \delta\mathbf{B}_\kappa \boldsymbol{\kappa}\ , \\ &\delta\mathbf{B}_w^T \mathbf{N} = \mathbf{B}_{G\mathbf{w}} \delta\mathbf{w} \quad \text{and} \quad \delta\mathbf{B}_\kappa^T \mathbf{N} = \mathbf{B}_{G\kappa} \delta\boldsymbol{\kappa}\ . \end{aligned} \tag{A.7.6}$$

Consider now the term

$$\mathrm{d}^{(pq)}\boldsymbol{\gamma}^{\mathrm{T}}\mathbf{D}\boldsymbol{\gamma} = (\hat{\mathbf{w}}^{(p)\mathrm{T}}\hat{\mathbf{B}}_{w}^{(q)\mathrm{T}} + \hat{\boldsymbol{\kappa}}^{(p)\mathrm{T}}\hat{\mathbf{B}}_{\kappa}^{(q)\mathrm{T}})\mathbf{N} \tag{A.7.7}$$

which occurs in equation (5.3.24) for the second directional derivative of Π, see also equations (5.3.16) and (5.3.17). Analogously with equation (A.7.6) it is permissible to write

$$\begin{aligned} \hat{\mathbf{B}}_{w}^{(q)}\hat{\mathbf{w}}^{(p)} = \hat{\mathbf{B}}_{w}^{(p)}\hat{\mathbf{w}}^{(q)} \quad &\text{and} \quad \hat{\mathbf{B}}_{\kappa}^{(q)}\hat{\boldsymbol{\kappa}}^{(p)} = \hat{\mathbf{B}}_{\kappa}^{(p)}\hat{\boldsymbol{\kappa}}^{(q)}, \\ \hat{\mathbf{B}}_{w}^{(q)\mathrm{T}}\mathbf{N} = \mathbf{B}_{\mathrm{G}w}\hat{\mathbf{w}}^{(q)} \quad &\text{and} \quad \hat{\mathbf{B}}_{\kappa}^{(q)\mathrm{T}}\mathbf{N} = \mathbf{B}_{\mathrm{G}\kappa}\hat{\boldsymbol{\kappa}}^{(q)}. \end{aligned} \tag{A.7.8}$$

Thus, the equation (A.7.7) can be rewritten

$$\mathrm{d}^{(pq)}\boldsymbol{\gamma}^{\mathrm{T}}\mathbf{D}\boldsymbol{\gamma} = \hat{\mathbf{w}}^{(p)\mathrm{T}}\mathbf{B}_{\mathrm{G}w}\hat{\mathbf{w}}^{(q)} + \hat{\boldsymbol{\kappa}}^{(p)\mathrm{T}}\mathbf{B}_{\mathrm{G}\kappa}\hat{\boldsymbol{\kappa}}^{(q)} \tag{A.7.9}$$

so that equation (5.3.24) for the second directional derivative of Π becomes

$$\mathrm{d}^{(pq)}\Pi = \hat{\mathbf{a}}^{(p)\mathrm{T}}\mathbf{K}_{\mathrm{T}}\hat{\mathbf{a}}^{(q)} \ , \tag{A.7.10}$$

c.f. equation (4.5.49). In equation (A.7.10) the tangent stiffness matrix $\mathbf{K}_{\mathrm{T}}$ is given by, see equation (4.5.50),

$$\mathbf{K}_{\mathrm{T}} = A\begin{bmatrix} \mathbf{B}^{\mathrm{T}}\mathbf{D}\mathbf{B} & \mathbf{B}^{\mathrm{T}}\mathbf{D}\mathbf{B}_{w} & \mathbf{B}^{\mathrm{T}}\mathbf{D}\mathbf{B}_{\kappa} \\ & \mathbf{B}_{w}^{\mathrm{T}}\mathbf{D}\mathbf{B}_{w} + \mathbf{B}_{\mathrm{G}w} & \mathbf{B}_{w}^{\mathrm{T}}\mathbf{D}\mathbf{B}_{\kappa} \\ \text{sym} & & \mathbf{B}_{\kappa}^{\mathrm{T}}\mathbf{D}\mathbf{B}_{\kappa} + \mathbf{B}_{\mathrm{G}\kappa} + \frac{h^2}{12}\mathbf{D} \end{bmatrix}. \tag{A.7.11}$$

Note, however, that there is no computational advantage in attempting to derive the higher directional derivatives of the strain energy, *e.g.* $\mathrm{d}^{(pqr)}\Pi$, directly from equation (A.7.10). Such derivation requires evaluation of $\mathrm{d}^{(r)}\mathbf{K}_{\mathrm{T}}$ and this in turn requires substitutions $\mathbf{B}_{\mathrm{G}w}\mathbf{w} = \mathbf{B}_{w}^{\mathrm{T}}\mathbf{D}(\mathbf{B}\mathbf{u} + \frac{1}{2}\mathbf{B}_{w}\mathbf{w} + \frac{1}{2}\mathbf{B}_{\kappa}\boldsymbol{\kappa})$ and $\mathbf{B}_{\mathrm{G}\kappa}\boldsymbol{\kappa} = \mathbf{B}_{\kappa}^{\mathrm{T}}\mathbf{D}(\mathbf{B}\mathbf{u} + \frac{1}{2}\mathbf{B}_{w}\mathbf{w} + \frac{1}{2}\mathbf{B}_{\kappa}\boldsymbol{\kappa})$ see equations (A.7.1) and (5.3.16) which effectively returns the calculation process to the state which exists at equations (5.3.24), (5.3.25) and (5.3.26) — see also section 5.2 of the present work and the technical report by Bangemann [Ban92b].

Appendix A.8. Symmetric matrix formulation for directional derivatives of the strain energy

The strain energy Π of equation (5.3.21) can be expressed in terms of the symmetrical matrix $\mathbf{E}$ as

$$\Pi = \mathbf{a}^{\mathrm{T}}\mathbf{E}\mathbf{a} \tag{A.8.1}$$

where $\mathbf{E}$ is given by

$$\mathbf{E} = \frac{A}{4}\begin{bmatrix} 2\mathbf{B}^{\mathrm{T}}\mathbf{D}\mathbf{B} & \mathbf{B}^{\mathrm{T}}\mathbf{D}\mathbf{B}_w & \mathbf{B}^{\mathrm{T}}\mathbf{D}\mathbf{B}_\kappa \\ & \tfrac{1}{2}\mathbf{B}_w^{\mathrm{T}}\mathbf{D}\mathbf{B}_w & \tfrac{1}{2}\mathbf{B}_w^{\mathrm{T}}\mathbf{D}\mathbf{B}_\kappa \\ \text{sym} & & \tfrac{1}{2}\mathbf{B}_\kappa^{\mathrm{T}}\mathbf{D}\mathbf{B}_\kappa + \frac{h^2}{6}\mathbf{D} \end{bmatrix}. \tag{A.8.2}$$

The first directional derivative can now be written in the form

$$\mathrm{d}^{(p)}\Pi = 2\hat{\mathbf{a}}^{(p)\mathrm{T}}\mathbf{E}\mathbf{a} + \mathbf{a}^{\mathrm{T}}\mathbf{E}_p\mathbf{a} \tag{A.8.3}$$

where $\mathbf{E}_p$ is the symmetrical matrix

$$\mathbf{E}_p = \frac{A}{4}\begin{bmatrix} 0 & \mathbf{B}^{\mathrm{T}}\mathbf{D}\hat{\mathbf{B}}_w^{(p)} & \mathbf{B}^{\mathrm{T}}\mathbf{D}\hat{\mathbf{B}}_\kappa^{(p)} \\ & \tfrac{1}{2}(\hat{\mathbf{B}}_w^{(p)\mathrm{T}}\mathbf{D}\mathbf{B}_w + \mathbf{B}_w^{\mathrm{T}}\mathbf{D}\hat{\mathbf{B}}_w^{(p)}) & \tfrac{1}{2}(\hat{\mathbf{B}}_w^{(p)\mathrm{T}}\mathbf{D}\mathbf{B}_\kappa + \mathbf{B}_w^{\mathrm{T}}\mathbf{D}\hat{\mathbf{B}}_\kappa^{(p)}) \\ \text{sym} & & \tfrac{1}{2}(\hat{\mathbf{B}}_\kappa^{(p)\mathrm{T}}\mathbf{D}\mathbf{B}_\kappa + \mathbf{B}_\kappa^{\mathrm{T}}\mathbf{D}\hat{\mathbf{B}}_\kappa^{(p)}) \end{bmatrix}. \tag{A.8.4}$$

The second directional derivative is given by

$$\mathrm{d}^{(pq)}\Pi = 2\hat{\mathbf{a}}^{(p)\mathrm{T}}\mathbf{E}\hat{\mathbf{a}}^{(q)} + 2\hat{\mathbf{a}}^{(q)\mathrm{T}}\mathbf{E}_p\mathbf{a} + \mathbf{a}^{\mathrm{T}}\hat{\mathbf{E}}_p^{(q)}\mathbf{a} \tag{A.8.5}$$

where $\hat{\mathbf{E}}_p^{(q)}$ is the symmetrical matrix

$$\hat{\mathbf{E}}_p^{(q)} = \frac{A}{4}\begin{bmatrix} 0 & 0 & 0 \\ & \tfrac{1}{2}(\hat{\mathbf{B}}_w^{(p)\mathrm{T}}\mathbf{D}\hat{\mathbf{B}}_w^{(q)} + \hat{\mathbf{B}}_w^{(q)\mathrm{T}}\mathbf{D}\hat{\mathbf{B}}_w^{(p)}) & \tfrac{1}{2}(\hat{\mathbf{B}}_w^{(p)\mathrm{T}}\mathbf{D}\hat{\mathbf{B}}_\kappa^{(q)} + \hat{\mathbf{B}}_w^{(q)\mathrm{T}}\mathbf{D}\hat{\mathbf{B}}_\kappa^{(p)}) \\ \text{sym} & & \tfrac{1}{2}(\hat{\mathbf{B}}_\kappa^{(p)\mathrm{T}}\mathbf{D}\hat{\mathbf{B}}_\kappa^{(q)} + \hat{\mathbf{B}}_\kappa^{(q)\mathrm{T}}\mathbf{D}\hat{\mathbf{B}}_\kappa^{(p)}) \end{bmatrix}. \tag{A.8.6}$$

The third directional derivative is

$$\mathrm{d}^{(pqr)}\Pi = 2(\hat{\mathbf{a}}^{(p)\mathrm{T}}\mathbf{E}_r\hat{\mathbf{a}}^{(q)} + \hat{\mathbf{a}}^{(q)\mathrm{T}}\hat{\mathbf{E}}_p^{(r)}\mathbf{a} + \hat{\mathbf{a}}^{(q)\mathrm{T}}\mathbf{E}_p\hat{\mathbf{a}}^{(r)} + \hat{\mathbf{a}}^{(r)\mathrm{T}}\hat{\mathbf{E}}_p^{(q)}\mathbf{a}) \tag{A.8.7}$$

while the fourth directional derivative is

$$\begin{aligned} \mathrm{d}^{(pqrs)}\Pi \;=\; & 2(\hat{\mathbf{a}}^{(p)\mathrm{T}}\hat{\mathbf{E}}_r^{(s)}\hat{\mathbf{a}}^{(q)} + \hat{\mathbf{a}}^{(q)\mathrm{T}}\hat{\mathbf{E}}_p^{(r)}\hat{\mathbf{a}}^{(s)} \\ & + \hat{\mathbf{a}}^{(q)\mathrm{T}}\hat{\mathbf{E}}_p^{(s)}\hat{\mathbf{a}}^{(r)} + \hat{\mathbf{a}}^{(r)\mathrm{T}}\hat{\mathbf{E}}_p^{(q)}\hat{\mathbf{a}}^{(s)}). \end{aligned} \tag{A.8.8}$$

Thus the equations in (5.3.32) can be replaced by equations containing only symmetrical matrices like $\mathbf{E}_p$ and $\hat{\mathbf{E}}_p^{(q)}$ as follows

$$
\begin{aligned}
\mathrm{d}^{(ppp)}\Pi &= 4(\hat{\mathbf{a}}^{(p)\mathrm{T}}\mathbf{E}_p\hat{\mathbf{a}}^{(p)} + \hat{\mathbf{a}}^{(p)\mathrm{T}}\hat{\mathbf{E}}_p^{(p)}\mathbf{a}),\\
\mathrm{d}^{(ppq)}\Pi &= 2(\hat{\mathbf{a}}^{(p)\mathrm{T}}\mathbf{E}_q\hat{\mathbf{a}}^{(p)} + \hat{\mathbf{a}}^{(p)\mathrm{T}}\hat{\mathbf{E}}_p^{(q)}\mathbf{a} + \hat{\mathbf{a}}^{(p)\mathrm{T}}\mathbf{E}_p\hat{\mathbf{a}}^{(q)} + \hat{\mathbf{a}}^{(q)\mathrm{T}}\hat{\mathbf{E}}_p^{(p)}\mathbf{a}),\\
\mathrm{d}^{(pqq)}\Pi &= 2(\hat{\mathbf{a}}^{(p)\mathrm{T}}\mathbf{E}_q\hat{\mathbf{a}}^{(q)} + \hat{\mathbf{a}}^{(q)\mathrm{T}}\hat{\mathbf{E}}_p^{(q)}\mathbf{a} + \hat{\mathbf{a}}^{(q)\mathrm{T}}\mathbf{E}_p\hat{\mathbf{a}}^{(q)} + \hat{\mathbf{a}}^{(q)\mathrm{T}}\hat{\mathbf{E}}_p^{(q)}\mathbf{a}),\\
\mathrm{d}^{(pppp)}\Pi &= 8\hat{\mathbf{a}}^{(p)\mathrm{T}}\hat{\mathbf{E}}_p^{(p)}\hat{\mathbf{a}}^{(p)}.
\end{aligned}
\tag{A.8.9}
$$

Appendix B.1. Branch switching method METHOD B

METHOD B

1. • **At the initial start (from the origin)**

   (a) Compute the solution vector $\mathbf{a}^*_{lin}$ of the linear problem with uniform displacement.

   (b) Solve the generalized eigenvalue problem $(\mathbf{K}_0 + \lambda \mathbf{K}_G)\,\delta\mathbf{a} = \mathbf{0}$ which gives the eigenvector $\boldsymbol{\xi}_p^{(1)}$ corresponding to the smallest eigenvalue λ_{min} and determine $\mathbf{a}^*_p = \lambda_{min}\mathbf{a}^*_{lin}$. Here, $\mathbf{K}_0$ denotes the linear stiffness matrix and $\mathbf{K}_G$ is the geometric stiffness matrix.

   • **At the start from a critical point** compute the solution vector $\mathbf{a}^*_p$ and the eigenvector $\boldsymbol{\xi}_p^{(1)}$ corresponding to the smallest eigenvalue at the critical point using the nonlinear solution technique.

2. Derive initial imperfections by using the eigenvector $\boldsymbol{\xi}_p^{(1)}$ such that the initial imperfections are given by the vector $\mathbf{a}_{imp}$ where

$$\mathbf{a}_{imp} = \alpha_1\, \boldsymbol{\xi}_p^{(1)} \,. \tag{B.1.1}$$

   Here, the parameter α_1 determines the proportion of the normalized eigenvector $((\boldsymbol{\xi}_p^{(1)})^T \boldsymbol{\xi}_p^{(1)} = 1)$ to be used as initial imperfections.

3. Using the imperfections as derived in 2., perform a linear step from the critical point using a predefined step-size α_2, giving the solution vector $\mathbf{a}^*_{imp-lin}$.

4. Let $\mathbf{a}_1^{(0)} = \alpha_3\, \mathbf{a}^*_{imp-lin}$ be the first starting vector for the continuation procedure from the critical point. Here, the parameter α_3 determines the proportion of the linear solution vector to be used for continuation.

5. Let $\mathbf{a}_2^{(0)} = \alpha_3\, \alpha_4\, \mathbf{a}^*_{imp-lin}$, *i.e.* $\mathbf{a}_2^{(0)} = \alpha_4\, \mathbf{a}_1^{(1)}$, be the second starting vector for the continuation procedure from the critical point.

6. Remove the in step 2. derived imperfections.

7. Use $\mathbf{a}_1^{(0)}$ and $\mathbf{a}_2^{(0)}$ as starting vectors for the continuation procedure and solve in the first iteration the system

$$[\ \mathbf{H}(\mathbf{a}_1^{(0)}) + \mathbf{T}(\mathbf{a}_2^{(0)})\ ]\ \Delta\mathbf{a} = -\gamma[\ \mathbf{K}(\mathbf{a}_1^{(0)})\,\mathbf{a}_1^{(0)} - \lambda\,\mathbf{p}^*\ ] \tag{B.1.2}$$

8. Continue in the ordinary fashion.

Appendix B.2. Branch switching method METHOD C

METHOD C

1. • **At the initial start (from the origin)**

   (a) Compute the solution vector $\mathbf{a}^*_{lin}$ of the linear problem with uniform displacement.

   (b) Solve the generalized eigenvalue problem $(\mathbf{K}_0 + \lambda \mathbf{K}_G)\,\delta\mathbf{a} = \mathbf{0}$ which gives the eigenvector $\boldsymbol{\xi}^{(1)}_p$ corresponding to the smallest eigenvalue λ_{min} and determine $\mathbf{a}^*_p = \lambda_{min}\mathbf{a}^*_{lin}$. Here, $\mathbf{K}_0$ denotes the linear stiffness matrix and $\mathbf{K}_G$ is the geometric stiffness matrix.

   • **At the start from a critical point** compute the solution vector $\mathbf{a}^*_p$ and the eigenvector $\boldsymbol{\xi}^{(1)}_p$ corresponding to the smallest eigenvalue at the critical point using the nonlinear solution technique.

2. Derive initial imperfections by using the eigenvector $\boldsymbol{\xi}^{(1)}_p$ corresponding to the smallest eigenvalue at the buckling point, such that the initial imperfections are given by the vector $\mathbf{a}_{imp}$ where

$$\mathbf{a}_{imp} = \alpha_1 \boldsymbol{\xi}^{(1)}_p \,. \tag{B.2.1}$$

   Here, the parameter α_1 determines the proportion of the normalized eigenvector $((\boldsymbol{\xi}^{(1)}_p)^T \boldsymbol{\xi}^{(1)}_p = 1)$ to be used as initial imperfections.

3. Compute a starting vector $\mathbf{a}_{start}$ for the nonlinear part with added imperfections from

$$\mathbf{a}_{start} = (1 + \alpha_2)(\mathbf{a}^* + \alpha_3 \boldsymbol{\xi}^*) \tag{B.2.2}$$

   where α_2 and α_3 are parameters used as scaling factors.

   The vectors $\mathbf{a}^*$ and $\boldsymbol{\xi}^*$ are given as follows:

   • **For the primary buckling point**

$$\mathbf{a}^* = \mathbf{a}^*_p \tag{B.2.3}$$

$$\boldsymbol{\xi}^* = \boldsymbol{\xi}^{(1)}_p \tag{B.2.4}$$

- **For any other buckling point**

$$\mathbf{a}^* = (\mathbf{a}_p^*)_{(-w)} \tag{B.2.5}$$

$$\boldsymbol{\xi}^* = (\boldsymbol{\xi}_p^{(1)})_{(+w)} \tag{B.2.6}$$

where $(\mathbf{a}_p^*)_{(-w)}$ is the vector $\mathbf{a}_p^*$ but with all w-connectors set to zero, and $(\boldsymbol{\xi}_p^{(1)})_{(+w)}$ is the vector $\boldsymbol{\xi}_p^{(1)}$ with all but the w-connectors set to zero.

4. Use $\mathbf{a}_{start}$ as the starting vector for computing the solution vector $\mathbf{a}_{start}^*$ with initial imperfections as derived in 2. Only one starting vector is needed, as

   - **For the primary buckling point** the T-matrix is taken equal to the tangent stiffness matrix, *i.e.* the second starting vector is also taken as $\mathbf{a}_{start}$,
   - **For any other buckling point** the second starting vector used for the T-matrix is taken as the zero vector.

5. Compute another solution point $\mathbf{a}_{start2}^*$ on the equilibrium path with imperfections by using the starting vector $\mathbf{a}_{start}^*$ and a step length determined by the step-length adaption procedure.

6. Let $\mathbf{a}_1^{(0)} = \mathbf{a}_{start2}^*$ be the first starting vector for the continuation procedure from the buckling point.

7. Let $\mathbf{a}_2^{(0)} = \mathbf{a}_{start}^*$ be the second starting vector for the continuation procedure from the buckling point.

8. Remove the in step 2. derived imperfections.

9. Use $\mathbf{a}_1^{(0)}$ and $\mathbf{a}_2^{(0)}$ as starting vectors for the continuation procedure and solve in the first iteration the system

$$[\ \mathbf{H}(\mathbf{a}_1^{(0)}) + \mathbf{T}(\mathbf{a}_2^{(0)})\ ]\ \Delta\mathbf{a} = -\gamma[\ \mathbf{K}(\mathbf{a}_1^{(0)})\,\mathbf{a}_1^{(0)} - \lambda\,\mathbf{p}^*\ ] \tag{B.2.7}$$

10. Continue in the ordinary fashion.

Appendix B.3. Least squares fit - procedure for determining the optimal α-value for the continuation from the critical point (for METHOD A)

1. Let $\mathbf{a}^*$ be the solution vector at the critical point.

2. Let $\mathbf{a}_1^{(0)}$ be the first starting vector from the critical point where

$$\mathbf{a}_1^{(0)} = \mathbf{a}^* + \alpha\, \xi^{(1)} \,. \tag{B.3.1}$$

AIM

Find the ideal value for α such that the next solution point beyond the critical point is found in as few iterations as possible.

3. Choose a value for α.

4. Use the nonlinear solution technique for finding the next solution point for the chosen value of α to obtain the corresponding solution vector $\mathbf{a}_1^*$.

5. Let $\mathbf{u}_{inc}$ be defined by

$$\mathbf{u}_{inc} = \mathbf{a}_1^* - \mathbf{a}^* \tag{B.3.2}$$

i.e. $\mathbf{u}_{inc}$ represents the change from the pre-critical solution point to the post-critical solution point.

6. Perform the *least squares fit*-procedure for finding the ideal value for α, *i.e.* try to minimize the difference between $\mathbf{u}_{inc}$ and $\alpha\xi^{(1)}$.

LEAST SQUARES FIT-**PROCEDURE**

$$\begin{aligned}
&(\mathbf{u}_{inc} - \alpha\xi^{(1)})^2 \longrightarrow min \\
\Leftrightarrow\ &(\mathbf{u}_{inc})^2 + \alpha^2 (\xi^{(1)})^2 - 2\,\alpha\, \mathbf{u}_{inc}\xi^{(1)} \longrightarrow min \\
\Leftrightarrow\ &\delta\alpha \,(\,2\,\alpha (\xi^{(1)})^2 - 2\,\mathbf{u}_{inc}\xi^{(1)} \,) = 0 \\
\Leftrightarrow\ &\alpha = \frac{\mathbf{u}_{inc} \cdot \xi^{(1)}}{\xi^{(1)} \cdot \xi^{(1)}}
\end{aligned} \tag{B.3.3}$$

7. Determine α from equation (B.3.3) giving the optimum value for α to be used in equation (B.3.1).

Appendix C.1. Meshes for the plate problem

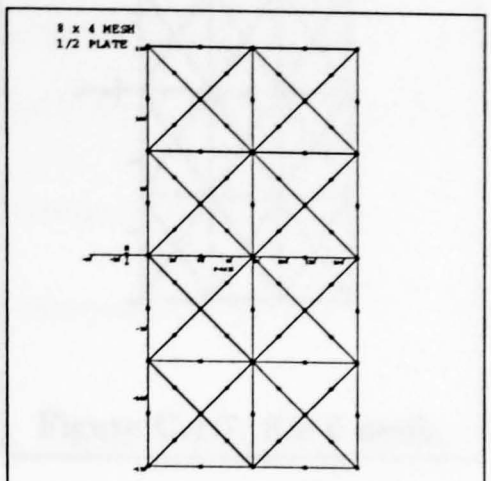

Figure C.1.1. 8×4 mesh.

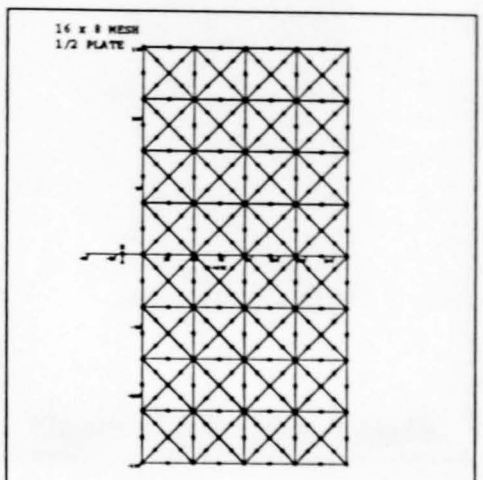

Figure C.1.2. 16×8 mesh.

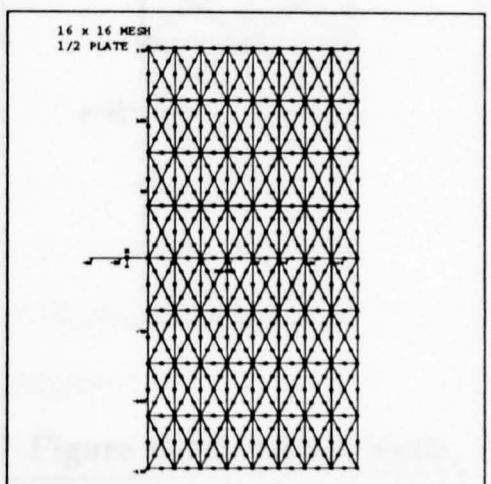

Figure C.1.3. 16×16 mesh.

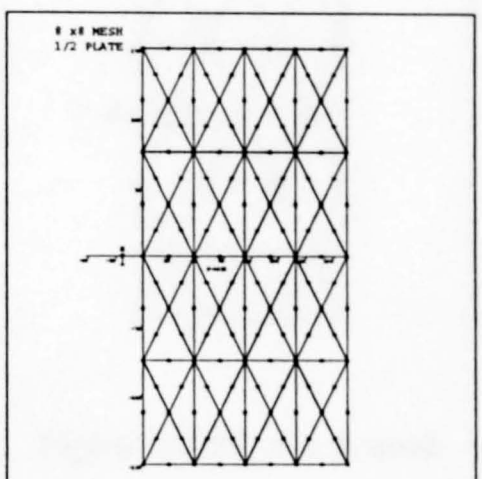

Figure C.1.4. 8×8 mesh.

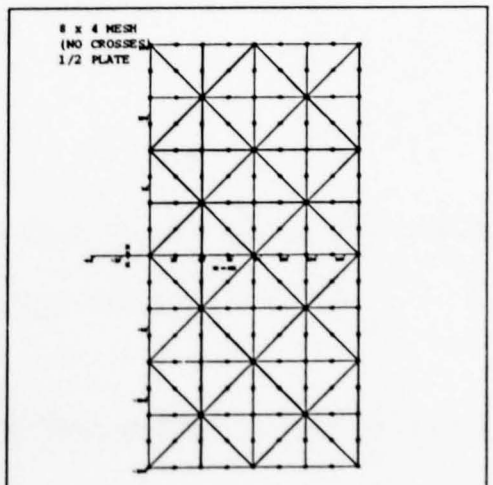

Figure C.1.5. 8×4 mesh (no crosses).

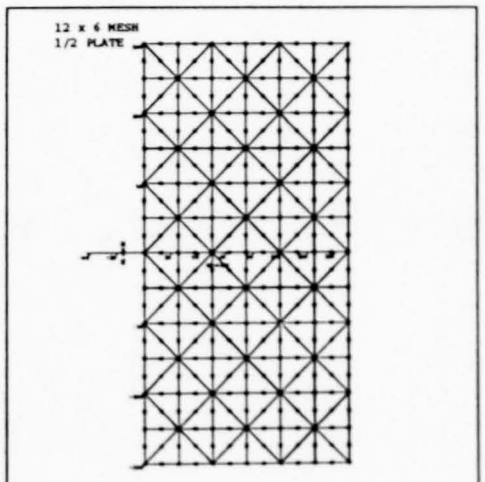

Figure C.1.6. 12×6 mesh (no crosses).

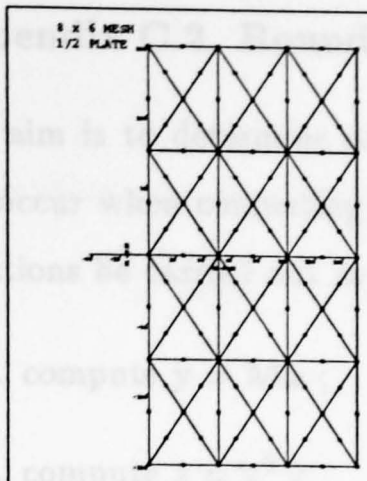

Figure C.1.7. 8×6 mesh.

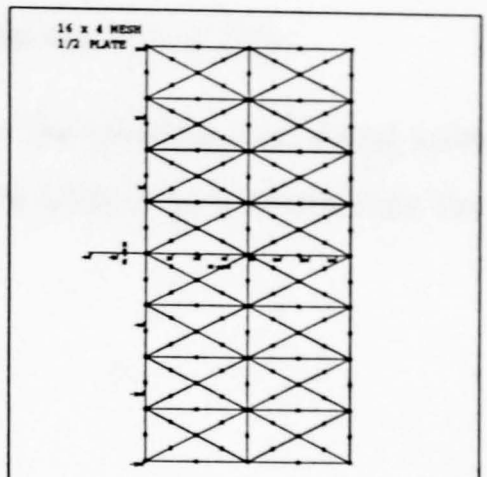

Figure C.1.8. 16×4 mesh.

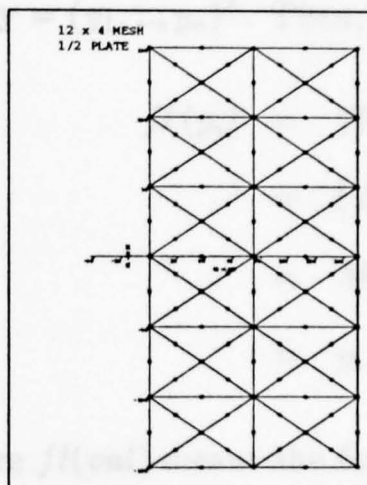

Figure C.1.9. 12×4 mesh.

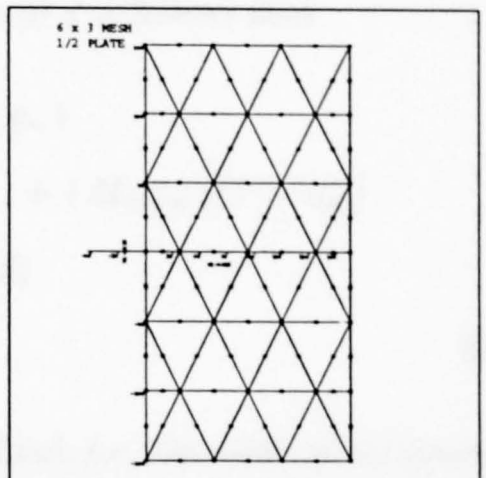

Figure C.1.10. 6×3 mesh (triangles).

Appendix C.2. Rounding error analysis on $z = \mathbf{x}^T\mathbf{M}\mathbf{x}$

The aim is to determine an approximation for the maximum rounding error that can occur when computing an expression $\mathbf{x}^T\mathbf{M}\mathbf{x}$ while it is assumed that the computations be carried out as follows:

1. compute $\mathbf{y} = \mathbf{M}\mathbf{x}$;
2. compute $z = \mathbf{x}^T\mathbf{y}$.

C.2.1 Rounding errors in $\mathbf{y} = \mathbf{M}\mathbf{x}$

Let $\mathbf{y} = (y_1, .., y_n)^T$. Then, for the i'th position of $\mathbf{y}$ it follows that

$$\begin{aligned} fl(y_i) &= fl(\, M_{i1}x_1 + .. + M_{in}x_n \,) \\ &= (\, M_{i1}x_1 \,)(1 + \epsilon_{i1}\,) + .. + (\, M_{in}x_n \,)(1 + \epsilon_{in}\,) \\ &= M_{i1}x_1 + .. M_{in}x_n + E_i \\ &= y_i + E_i \end{aligned} \qquad \text{(C.2.1)}$$

where $fl(val)$ means the floating point value of *val*, *i.e.* the value of *val* rounded in the computations, the ϵ_{ij} , $j = 1, .., n$ are the individually occurring rounding errors and the total error E_i is bounded by

$$\begin{aligned} |\, E_i \,| &< 5 \times 10^{-t} \{ |\, M_{i1}x_1 \,| + .. + |\, M_{in}x_n \,| \} \\ &\leq 5 \times 10^{-t} \{ |\, M_{i1} \,||\, x_1 \,| + .. + |\, M_{in} \,||\, x_n \,| \} \\ &\leq 5 \times 10^{-t}\, n \,|\, M_i \,||\, x \,| \\ &\leq 5 \times 10^{-t}\, n \,|\, M \,||\, x \,| \ . \end{aligned} \qquad \text{(C.2.2)}$$

Note that in the above it is assumed that $\epsilon_{i1} = .. = \epsilon_{in} = 5 \times 10^{-t}$ in machine accuracy denary notation.

C.2.2 Rounding errors in $z = \mathbf{x}^T\mathbf{M}\mathbf{x} = \mathbf{x}^T\mathbf{y}$

With help of equation (C.2.1) above,

$$\begin{aligned} fl(z) &= fl(\, x_1 fl(y_1) + .. + x_n fl(y_n) \,) \\ &= \mathbf{x}^T fl(\mathbf{y}) + E^* \end{aligned} \qquad \text{(C.2.3)}$$

where

$$| E^* | = 5 \times 10^{-t} n \, | M | \, | \mathbf{x} | \tag{C.2.4}$$

by recalling equation (C.2.2) and

$$\begin{aligned} \mathbf{x}^T fl(\mathbf{y}) &= x_1 (y_1 + E_1) + .. + x_n (y_n + E_n) \\ &= (x_1 y_1 + .. + x_n y_n) + (x_1 E_1 + .. + x_n E_n) \\ &= \mathbf{x}^T \mathbf{y} + E^{**} \\ &= z + E^{**} \end{aligned} \tag{C.2.5}$$

where with the help of equation (C.2.2)

$$\begin{aligned} | E^{**} | &\leq | x_1 E_1 | + .. + | x_n E_n | \\ &\leq | x_1 | \, | E_1 | + .. + | x_n | \, | E_n | \\ &\leq n \, | E | \, | \mathbf{x} | \\ &< n 5 \times 10^{-t} n \, | M | \, | \mathbf{x} | \, | \mathbf{x} | \\ &= 5 \times 10^{-t} n^2 \, | M | \, | \mathbf{x} |^2 \end{aligned} \tag{C.2.6}$$

by defining $| E | = max_{i=1,..,n} | E_i |$. Hence, the total error for $z = \mathbf{x}^T \mathbf{M} \mathbf{x}$ is given by

$$E_{tot} = E^* + E^{**} \tag{C.2.7}$$

and an upper bound for the rounding error is obtained by

$$\begin{aligned} | E_{tot} | &\leq | E^* | + | E^{**} | \\ &< 5 \times 10^{-t} n \, | M | \, | \mathbf{x} | + 5 \times 10^{-t} n^2 \, | M | \, | \mathbf{x} |^2 \\ &= 5 \times 10^{-t} n \, | M | \, | \mathbf{x} | \, (1 + n \, | \mathbf{x} |) \, . \end{aligned} \tag{C.2.8}$$

C.2.3 Example values as for the plate problem

Considering

$$\begin{aligned} t &= 14 \, , \\ n &= 87 < 100 \, , \\ | M | &= 10^5 \, , \\ | \mathbf{x} | &= 1 \, , \end{aligned} \tag{C.2.9}$$

it follows for the upper bound for the rounding error

$$\begin{aligned} |\, E_{tot} \,| &< 5 \times 10^{-14} \times 10^{2} \times 10^{5} \times 10^{0} (1 \times 10^{2} \times 10^{0}) \\ &= 5 \times 10^{-14} \times 10^{7} (1.01 \times 10^{2}) \\ &= 5.05 \times 10^{-14} \times 10^{9} \\ &= 5.05 \times 10^{-5} \ . \end{aligned} \tag{C.2.10}$$

C.2.4 Justification of $A = 0$ for the plate problem

The maximum value for the stability coefficient A for which it is considered zero is

$$A = 0.674 \times 10^{-7} \tag{C.2.11}$$

where A is computed as

$$A = (\xi^{(1)})^{T} (\partial \mathrm{K}_{T}(\xi^{(1)})) \xi^{(1)} \tag{C.2.12}$$

i.e. in the form $A = \mathbf{x}^{T}\mathbf{M}\mathbf{x}$ as discussed above. Hence,

$$A < 5.05 \times 10^{-5} \tag{C.2.13}$$

and the interpretation of $A = 0$ can be justified.

Appendix C.3. Meshes for the cylindrical panel problem (projections on x^1-x^2-plane)

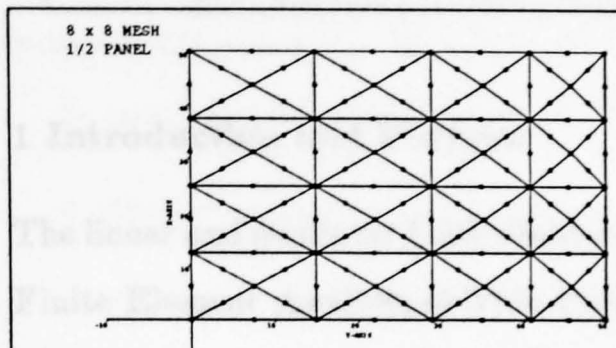

Figure C.3.1. 8×8 mesh.

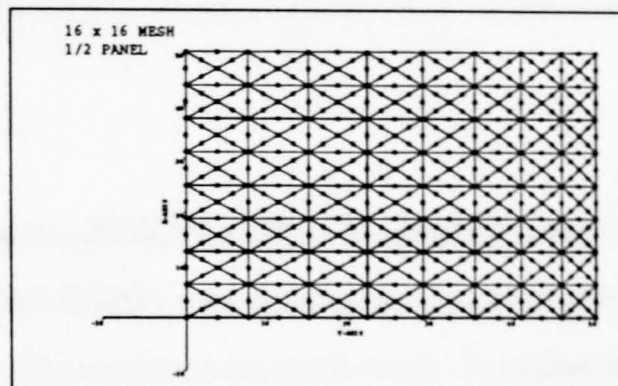

Figure C.3.2. 16×16 mesh.

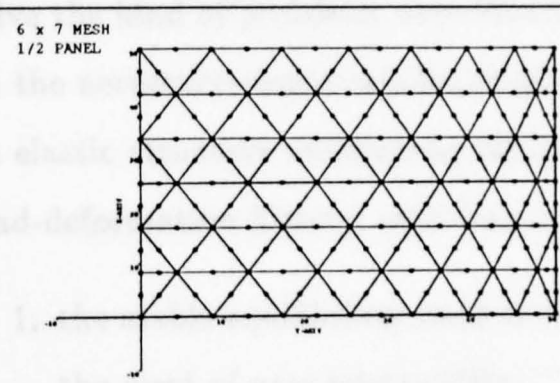

Figure C.3.3. 6×7 mesh (triangles).

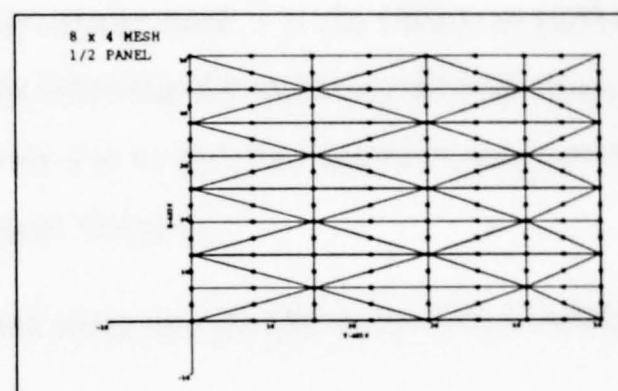

Figure C.3.4. 8×4 mesh (no crosses).

Appendix D.1. MBFEATPS program description

M B F E A T P S

Morley-Bangemann Finite Element Analysis of Thin Plates and Shells

1 Introduction and Purpose

The linear and nonlinear finite element program MBFEATPS (Morley-Bangemann Finite Element Analysis of Thin Plates and Shells) was written in standard FORTRAN 77 by the author during the course of the present research work. It makes use of the NAG-library. The intention was to develop a program for the nonlinear finite element analysis of thin plates and shells by using the *geometrically nonlinear constant moment triangle* by Morley [Mor91]. Of special interest was the feasibility to solve the kind of problems described in the current work, *i.e.* the ability to perform all the necessary computations required for following the stable equilibrium path of an elastic structure undergoing deformations due to specified forces throughout the load-deformation history with four important features:

1. the stable equilibrium path is followed using an automated procedure without the need of user intervention;
2. critical points are located precisely;
3. critical points are identified;
4. there is a facility for continuing from a critical point into the post critical regime.

An algorithm for the MBFEATPS code for solving problems of the above mentioned type is given in section 4 of this Appendix D.1.

In addition to the main characteristics described above, the program can also be used for

1. linear finite element analysis (including buckling analysis) of thin plates and shells;
2. inclusion of other linear or nonlinear flat triangular finite elements.

2 User's Manual

2.1 Introduction and Preparations

MBFEATPS is a user-friendly program with a menu selection system covering 69 incorporated problems. The code can be extended easily to handle more cases.

In order to use MBFEATPS, the following files are required:

- displacement control problems:
  1. **input-**** (contains main input data);
  2. **inc-**** (contains initial step size and maximum number of increments to be performed (currently a dummy));
- load control problems:
  1. **input-**** (contains main input data);
  2. **inc-**** (contains initial load magnitude, initial load increment and maximum number of increments to be performed (currently a dummy));
  3. **in-**-bc** (contains nodal load proportions).

Here, ** $\in \{01, 02, .., 69\}$ denotes the case number to be solved which corresponds to the one also appearing in the menu.

2.2 Running MBFEATPS

In order to run MBFEATPS, an executable file should be created by compiling and linking together the files listed in section 3 of this Appendix D.1.

It is prudent to note that some case parameter values have to be correctly set up for a successful MBFEATPS run. However, in case of an incorrect set up when trying to run the code, MBFEATPS comes up with a detailed error message explaining what values need to be changed. These changes are to be made in the pilot file **prog.f** in lines 137-148.

2.2.1 Start from origin

The α_1-value required for finding a first stable solution point should be inserted in **s-perf.f** on line 934

alpha = ...

2.2.1.1 User Interface and Cases

When executing the code, MBFEATPS presents a menu selection system as shown below:

```
FINITE ELEMENT PROGRAM
----------------------
FOR THIN PLATE AND THIN SHELL PROBLEMS
--------------------------------------

(A) Pyramid snap-through problems (01..04)
(B) Linear plate-buckling problem (05..06)
(C) Shell snap-through problem    (07..08)
(D) RAE plate problem             (09..20)
(E) Hughes plate problem          (21..45)
(F) Cylindrical panel problem     (46..69)

Please choose the problem type to be solved (A..F)
```

The user then follows the instructions by first choosing the problem type to be solved (A..F). A submenu then provides further case from which one is to be chosen.

2.2.2 Restart from a critical point

When restarting MBFEATPS from a critical point, the following additional files are required:

1. **displa** (contains displacement vector at critical point);
2. **displ2** (contains displacement vector at last point before critical point);
3. **restart** (contains case-dependent information for restart).

The α_1-value required for finding a first stable solution point should be inserted in **s-prf-bg.f** on line 934

alpha = ...

In case of a restart from a critical point restart carries the case number and, hence, no entry into the MBFEATPS menu takes place. The computations then commence immediately without the need for further user intervention.

2.3 Output of MBFEATPS

MBFEATPS automatically creates the following files (note that not all files are created for each problem / case number):

1. **outpt-**** : contains self-explanatory output information such as:

   (a) number of iterations;

   (b) number of increments;

   (c) norm;

   (d) nodal displacements and midside rotations;

   (e) nodal loads;

   (f) strain energy;

   (g) case-specific central deflection;

   (h) case-specific load value;

   (i) smallest eigenvalue (with and without T-matrix);

   (j) directional derivatives (only computed at a restart from a critical point);

   (k) stability coefficients (only computed at a restart from a critical point);

   (l) type of critical point (only at a restart from a critical point);

   (m) CPU time;

   (n) α_1-value computed using the *least squares fit*-procedure as described in Appendix B.3 (only computed after first increment);

2. **loads-**** : contains the case-specific loads vector;

3. **mode1-**** : contains values for the mode shapes along the line of compression;

4. **mode2-**** : contains values for the mode shapes along the transverse axis;

5. **emode** : contains eigenmode at critical point;

6. **displa** : contains displacement vector at last computed solution point;

7. **displ2** : contains displacement vector at last but first iteration;

8. **restart** : contains case-specific information required for the restart facility.

2.5 Running MBFEATPS in the background

MBFEATPS can also be run in the background. Section 3 below counts all the files required for running the code. In case a background run is wished for, the files in parentheses should be chosen. Also, the case number is to be set up in the file **s-st-bg.f** on line 25 in

itype = **

The α_1-parameter for continuation from a critical point (or for finding the first stable solution point when starting the program from the origin) should be inserted in the file **s-prf-bg.f** on line 934 in

alpha = ...

The same output files as described above are created.

3 Files

MBFEATPS consists of the following files (file names in parentheses to be chosen when running MBFEATPS in the background):

- **prog.f**
- **s-allman.f**
  (background start from origin: **s-al1-bg.f**)
  (background restart from critical point: **s-al2-bg.f**)
- **s-cont.f** (**s-contbg.f**)
- **s-disp.f**
- **s-iface.f**
- **s-load.f**

- **s-main-1.f**
- **s-main-2.f**
- **s-main-3.f**
- **s-plate.f (s-pl-bg.f)**
- **s-perf.f (s-prf-bg.f)**
- **s-pyrmd.f**
- **s-red245.f**
- **s-reduce.f**
- **s-start.f (s-st-bg.f)**
- **s-tract.f**
- **s-utilit.f**

prog.f is the pilot and drives the rest of the program. All subroutines are well documented with extensive comments.

4 Algorithm for MBFEATPS

An algorithm for the MBFEATPS code for solving problems as described in Chapter 7 of the present work is given. Main subroutines employed for solving different subtasks are also mentioned.

—— INPUT ——

1. Read information regarding restart facility
   (restif)
2. Read and check information regarding problem type
   (type)
3. Read input data, then apply and save traction boundary conditions
   (input, trbsav)

4. If restart facility needed go to (12)

—— COMPUTE LINEAR SOLUTION ——

5. Build up global linear stiffness matrix and global loads vector
   (genlin, loads2)

6. Apply kinematic boundary constraints
   (boucol)

7. Reduce system due to kinematic boundary constraints
   (reduce)

8. For load control cases: reduce system due to boundary constraints for the 'loading of a constrained boundary'
   (reduc2)

9. Solve system
   (solve1, postex)

10. Transfer reduced solution vector back to full size solution vector
    (postrv)

11. Output linear solution
    (outlin)

—— COMPUTE NONLINEAR SOLUTION ——

12. Read initial load intensity / initial displacement vector and increment size
    (dist3)

13. Determine new loads vector / displacement vector according to chosen/computed increment
    (dist4)

14. If restart facility was chosen and this is
    - first entry here, read displacement vector for last but one iteration point
    - second entry here, read displacement vector for last solution point

15. If maximum number of load increments has been exceeded or if the Hessian is indefinite, reduce displacement step size / load increment
    (toohi)

16. Build up global tangent stiffness matrix, global loads vector, global vector of generalized forces
    (gennon, comb3m)

17. Set up right hand side of system to be solved
    (dist5)

18. Apply kinematic boundary constraints
    (kinbcs)

19. If restart facility was chosen and this is
    - first entry here, read restart information, then go to (14)
    - second entry here, go to (26)

20. Reduce system due to kinematic boundary constraints
    (reduce)

21. For load control cases: reduce system due to boundary constraints for the 'loading of a constrained boundary'
    (reduc2)

22. If the Hessian is indefinite, go to (15)

23. Solve nonlinear system
    (solve2 (includes reductions))

24. Update solution vector
    (updata)

25. Check if cut-off criterion for current increment is satisfied
    (cutoff)

26. Check if criterion for superlinear convergence mode is satisfied
    (cutspr)

27. If criterion for superlinear convergence mode is satisfied,
    change into this mode
    (superc)

28. If cut-off criterion for current increment is not satisfied, go to (15)

—— CONVERGENCE ACHIEVED ——

29. Compute eigenvalues
    (eigenv)

30. Check mode shapes
    (modesh)

31. Compute directional derivatives and stability coefficients
    (values)

32. Predict eigenvalues for next increment (these predictions are currently not made use of in MBFEATPS)
    (eigprd)

33. Save information regarding current increment
    (saveta)

34. Output results
    - on screen (print1)
    - on file (print2)

35. Save information for plotting purposes
    (plot)

36. Compute new displacement step size / load increment according to the automated step size adaption technique

37. Save information for restart facility
    (restsv)

38. For next increment, go to (13)

5 Finally

The code has been tested extensively and is believed to be error-free. Some of the example problems (RAE plate problem) are the same as those solved by employing the MPFEAS code by Providas [Pro90]. The results for both codes coincide.

In case of encountering problems - and also otherwise - the author would appreciate comments and constructive criticism.

Bibliography

[AG92] E. L. Allgower and K. Georg. 'Continuation and path following'. *Acta Numerica*, pages 1–64, 1992.

[All81] E. L. Allgower. 'A survey of homotopy methods for smooth mappings'. In K. Glashof E. L. Allgower and H. O. Pether, editors, *Numerical Solution of Nonlinear Equations, Lecture Notes in Mathematics 878*. Springer, New York, 1981.

[All82] D. J. Allman. 'Improved finite element models for the large displacement bending and post buckling analysis of thin plates'. *Int. J. Solids. Structures*, 18:737–762, 1982.

[All84] D. J. Allman. 'An iterative method to locate minima of a function of several variables'. Technical Report 84038, Royal Aircraft Establishment, Farnborough, Hampshire, UK, 1984.

[All89a] D. J. Allman. 'Calculation of the stable equilibrium paths of discrete conservative systems with singular points'. *Comp. Struct.*, 32:1045–1054, 1989.

[All89b] D. J. Allman. 'On the general theory of the stability of equilibrium of discrete conservative systems'. *Aeronautical J.*, 93:29–35, 1989.

[Ban92a] T. R. Bangemann. 'Inextensional bending of a shell triangular element in quadratic parametric representation and finite element analysis'. Technical Report BICOM 92/5, Brunel University, BICOM, Uxbridge, Middlesex, UK, 1992.

[Ban92b] T. R. Bangemann. 'Matrix interpretation of the general theory of the stability of equilibrium of discrete conservative systems'. Technical Report BICOM 92/6, Brunel University, BICOM, Uxbridge, Middlesex, UK, 1992.

[Bar83] P. Bartholomew. 'A simple iterative method for the minimisation of an unconstrained function of many variables'. Technical Memorandum Mat/Str 1021, Royal Aircraft Establishment, Farnborough, Hampshire, UK, 1983.

[BC72] P. G. Bergan and R. W. Clough. 'Convergence criteria for iterative processes'. *AIAA J., Technical notes*, 10:1107–1108, 1972.

[BC73] P. G. Bergan and R. W. Clough. 'Large deflection analysis of plates and shallow shells using the finite element method'. *Int. J. Num. Meth. Engrg.*, 5:543–556, 1973.

[BCIZ65] G. P. Bazeley, Y. K. Cheung, B. M. Irons, and O. C. Zienkiewicz. 'Triangular elements in bending - conforming and non-conforming solutions'. In *Proc. Conf. on Matrix Methods in Structural Mechanics*, pages 547–576, Air Force Institute of Technology, Wright-Patterson Air Force Base, Ohio, 1965.

[BD79] J. L. Batoz and G. Dhatt. 'Incremental displacement algorithms for nonlinear problems'. *Int. J. Numer. Meth. Engng.*, 14:1262–1267, 1979.

[Ber77] M. S. Berger. *Nonlinearity and Functional Analysis.* Academic Press, New York, 1977.

[CH53] R. Courant and D. Hilbert. *Methods of mathematical physics. Vol. I.* Interscience Publishers, 1953.

[CH83] E. G. Carnoy and T. J. R. Hughes. 'Finite element analysis of the secondary buckling of a flat plate under uniaxial compression'. *Int. J. Non-Linear Mech. Eng.*, 18:167–175, 1983.

[Cha91] Ch.-Ch. Chang. 'Periodically restarted quasi-newton updates in constant arc-length method'. *Computers & Structures*, 41:963–972, 1991.

[Cia80] P. G. Ciarlet. 'A justification of the von Kármán equations'. *Archive for Rational Anal.*, 73:349–389, 1980.

[Coo81] R. D. Cook. *Concepts and applications of finite element analysis.* John Wiley, 2nd edition, 1981.

[Cri81] M. A. Crisfield. 'A fast incremental/iterative solution procedure that handles snap-through'. *Computers & Structures*, 13:55–62, 1981.

[Cri91] M. A. Crisfield. *Non-linear Finite Element Analysis of Solids and Structures, Vol. 1: Essentials.* John Wiley & Sons, 1991.

[Daw72] D. J. Dawe. 'Shell analysis using a simple facet element'. *J. Strain Anal.*, 7:266–270, 1972.

[ESO94] B. Seifert E. Stein and S. Ohnimus. 'Adaptive finite element analysis of geometrically non-linear plates and shells, especially buckling'. *Int. J. Numer. Meth. Engrg.*, 37:2631–2655, 1994.

[FC92] F. Fujii and K. K. Choong. 'Branch switching in bifurcation of structures'. *ASCE J. of Eng. Mech.*, 118(8):1578–1596, 1992.

[Flü72] W. Flügge. *Tensor analysis and continuum mechanics.* Springer-Verlag, Berlin, 1972.

[Flü73] W. Flügge. *Stresses in shells.* Springer-Verlag, Berlin, 1973.

[FR93] A. Forsgren and U. Ringertz. 'On the use of a modified Newton method for nonlinear finite element analysis'. *Comp. Meth. Appl. Mech. Engrg.*, 110:275–283, 1993.

[Fur95] J.-E. Furter. *Private communication.* Brunel University, West London, 1995.

[He92] E. Hinton (editor). *NAFEMS Introduction to Nonlinear Finite Element Analysis.* NAFEMS, 1992.

[Hel67] K. Hellan. 'Analysis of elastic plates in flexure by simplified finite element method'. In *Civ. Engrg. Bldg. Constructn. Ser. No. 46*, Acta Polytechnica Scandinavica, 1967.

[Her67] L. R. Herrmann. 'Finite element bending analysis of plates'. In *Proc. Am. Soc. Engrg.*, volume 93, EM5, 1967.

[IL83] B. Irons and M. Loikkanen. 'An engineer's defence of the patch test'. *Int. J. Num. Meth. Engrg.*, 19:1391–1401, 1983.

[JEDM77] Jr J. E. Dennis and J. J. Moré. 'Quasi-Newton methods, motivation and theory'. *SIAM Rev.*, 19:46–89, 1977.

[JHAS77] G. A. Malejannakis J. H. Argyris, P. C. Dunne and E. Schelkle. 'A simple triangular facet shell element with applications to linear and non-linear equilibrium and elastic stability problems'. *Comp. Meth. Appl. Mech. Engrg.*, 11:97–131, 1977.

[JHAS79] J. S. Doltsinis P. C. Dunne M. Haase M. Kleiber G. A. Malejannakis H. P. Mlejnek M. Müller J. H. Argyris, H. Balmer and D. W. Scharpf. 'Finite element method - the natural approach'. *Comp. Meth. Appl. Mech. Engrg.*, 19/20:1–106, 1979.

[Kik86] N. Kikuchi. *Finite element methods in mechanics.* Cambridge University Press, 1986.

[KJBW75] E. Ramm K. J. Bathe and E. L. Wilson. 'Finite element formulations for large deformation dynamic analysis'. *Int. J. Num. Meth. Engrg.*, 9:353–386, 1975.

[KM89] R. Kouhia and M. Mikkola. 'Tracing the equilibrium path beyond simple critical points'. *Int. J. Numer. Methods Eng.*, 28:2923–2941, 1989.

[Koi45] W. T. Koiter. *Over de Stabiliteit van het Elastisch Evenwicht.* H. J. Paris, 1945. [English translation: Technical Report AFFDL-TR-70-25. Air Force Flight Dynamics Laboratory, Wright-Patterson Air Force Base, Ohio].

[Koi60] W. T. Koiter. 'A consistent first approximation in the general theory of thin elastic shells'. In W. T. Koiter, editor, *Proc. of IUTAM Symposium on 'The theory of thin elastic shells'*, Amsterdam, 1960. North-Holland.

[Koi66] W. T. Koiter. 'On the nonlinear theory of elastic shells'. In *Proc. Koninklijke Nederlandse Akademie van Wetenschappen*, volume Ser. B, 69, pages 1–54, 1966.

[Kou] R. Kouhia. 'Generalized Newton-Raphson techniques'. In *Numerical Dynamics*, to be published.

[Kou92] R. Kouhia. 'On the solution of non-linear finite element equations'. *Comp. Struct.*, 44:243–254, 1992.

[Mal69] L. E. Malvern. *Introduction to the mechanics of a continuous medium.* Prentice Hall, 1969.

[Man89] E. H. Mansfield. *The Bending and Stretching of Plates.* Cambridge University Press, 2nd edition, 1989.

[Mat83] K. Mattiasson. *'On the co-rotational finite element formulation for large deflection problems'.* PhD thesis, Chalmers Tekniska Högskola, Göteborg, Sweden, 1983.

[McC31] A. J. McConnell. *Applications of the absolute differential calculus.* Blackie, Glasgow, 1931. [Reprinted under the title: 'Applications of tensor analysis', Dover, New York, 1957].

[MJTT56] H. C. Martin M. J. Turner, R. W. Clough and L. J. Topp. 'Stiffness and deflection analysis of complex structures'. *J. Aeronaut. Sci.*, 23:805–824, 1956.

[MM87] L. S. D. Morley and M. P. Mould. 'The role of bending in the finite element analysis of thin shells'. *Finite Elements in Analysis and Design*, 3:213–240, 1987.

[Mor71] L. S. D. Morley. 'The constant moment plate bending element'. *J. Strain Anal.*, 6:20–24, 1971.

[Mor87] L. S. D. Morley. '"Practical" components of vectors and tensors'. *Int. J. Eng. Sci.*, 25:37–53, 1987.

[Mor91] L. S. D. Morley. 'Geometrically non-linear constant moment triangle which passes the von Kármán patch test'. *Int. J. Numer. Methods Eng.*, 31:241–263, 1991.

[Mor94] L. S. D. Morley. 'Notes relating to: The geometrically nonlinear constant bending moment triangle'. Technical Report BICOM 94/1, Brunel University, BICOM, Uxbridge, Middlesex, UK, 1994.

[MS79] H. Matthies and G. Strang. 'The solution of nonlinear finite element equations'. *Int. J. Numer. Meth. Engng.*, 14:1613–1626, 1979.

[MW80] H. D. Mittelmann and H. Weber. 'Numerical methods for bifurcation problems, a survey and classification'. In H. D. Mittelmann and H. Weber, editors, *Bifurcation Problems and Their Numerical Solutions.* Birkhäuser, Basel, 1980.

[Nio85] F. I. Niordson. *Shell theory.* North-Holland, 1985.

[Nov53] V. V. Novozhilov. *Foundations of the nonlinear theory of elasticity.* Graylock Press, 1953.

[OR70] J. M. Ortega and W. C. Rheinboldt. *Iterative solution of nonlinear equations in several variables.* Academic Press, 1970.

[Pie84] W. Pietraszkiewicz. 'Lagrangian description and incremental formulation in the non-linear theory of thin shells'. *Int. J. Non-Linear Mech. Eng.*, 19(2):115–140, 1984.

[Pro90] E. D. Providas. *'On the geometrically nonlinear constant moment triangle (with a note on drilling rotations)'.* PhD thesis, Brunel University, BICOM, Uxbridge, Middlesex, UK, 1990.

[Ram82] E. Ramm. 'The Riks/Wempner approach - an extension of the displacement control method in nonlinear analysis'. In *Recent Advances in nonlinear computational mechanics (eds E. Hinton, D. R. J. Owen and C. Taylor)'*, Swansea, 1982. Pineridge Press.

[Rik72] E. Riks. 'The application of Newton's method to the problem of elastic stability'. *J. Appl. Mech.*, pages 1060–1065, 1972.

[Rik79] E. Riks. 'An incremental approach to the solution of snapping and buckling problems'. *Int. J. Solids Struct.*, 15:529–551, 1979.

[Rik84a] E. Riks. 'Bifurcation and stability, a numerical approach'. In T. Belytschko W. K. Liu and K. C. Pork, editors, *Innovative Methods For Nonlinear Problems.* Pineridge Press, 1984.

[Rik84b] E. Riks. 'Some computational aspects of the stability analysis of nonlinear structures'. *Comp. Meth. Appl. Mech. Engrg.*, 47:219–259, 1984.

[San63] J. L. Sanders. 'Nonlinear theories for thin shells'. *Q. Appl. Maths.*, 21:21–36, 1963.

[Sey88] R. Seydel. *From equilibrium to chaos - practical bifurcation and stability analysis.* Elsevier, 1988.

[TG61] S. P. Timoshenko and J. M. Gere. *Theory of elastic stability.* McGraw-Hill, 1961.

[Tho63] J. M. T. Thompson. 'Basic principles in the general theory of elastic stability'. *J. Mech. Phys. Solids*, 11:13–20, 1963.

[Tho70] J. M. T. Thompson. 'Basic theorems of elastic stability'. *Int. J. Engrg. Sci.*, 8:307–313, 1970.

[Thu69] G. A. Thurston. 'Continuation of Newton's method through bifurcation points'. *J. Appl. Mech.*, pages 425–430, 1969.

[Tru53] C. Truesdell. 'The physical components of vectors and tensors'. *Z. angew. Math. Mech.*, 33:345, 1953.

[TWK59] S. P. Timoshenko and S. Woinowsky-Krieger. *Theory of plates and shells.* McGraw-Hill, 1959.

[vK10] T. von Kármán. 'Festigkeitsprobleme im Maschinenbau'. *Encyklopädie der Mathematischen Wissenschaften*, IV/4(C):311–385, 1910.

[Was82] K. Washizu. *Variational methods in elasticity & plasticity.* Pergamon Press, 3rd edition, 1982.

[Wem71] G. A. Wempner. 'Discrete approximations related to nonlinear theories of solids'. *Int. J. Solids. Structures*, 7:1581–1599, 1971.

[Zie77] O. C. Zienkiewicz. *The finite element method.* McGraw-Hill, 3rd edition, 1977.